Commercial Adsorbents Modified to Remove Platinum Cytostatic Drugs at Trace Levels Some Synchrotron Exploration of Adsorption Mechanisms

Dong Han

UAB
Universitat Autònoma de Barcelona

Commercial Adsorbents Modified to Remove Platinum Cytostatic Drugs at Trace Levels

Some Synchrotron Exploration of Adsorption Mechanisms

Dong Han

Doctoral Thesis

Doctorate Program in Chemistry

Directors: Prof. Manuel Valiente

Assoc. Prof. Montserrat López-Mesas

Department of Chemistry

Faculty of Science

2023

UAB

Universitat Autònoma de Barcelona

Report submitted to aim for the Doctor Degree by

Dong Han

Approval:

Directors: Prof. Manuel Valiente Assoc. Prof. Montserrat López-Mesas

Bellaterra, 21/09/2023

Acknowledgement

Describing my current mood as I type these words is quite challenging, given its complexity. After several months of thesis writing, I'm experiencing a mix of emotions. There's a sense of relief and satisfaction, knowing I've reached this point, along with a bittersweet nostalgia when I reflect on the past four years. Additionally, there's a level of confusion about what lies ahead. As a PhD in Analytical Chemistry, I'm accustomed to precisely measuring and quantifying the components of my samples, regardless of their complexity. However, at this moment, I can't assign specific percentages to each of my feelings. Yet, one thing remains certain – the most overwhelming emotion I'm experiencing right now is profound gratitude towards all of you.

✧ **Manolo,** as my supervisor, your deep knowledge and extensive experience in scientific research, along with your four years of unwavering dedication, encouragement, and support, have played a crucial role in shaping my current position and achievements. I greatly admire your boundless enthusiasm for scientific research and your remarkable energy, which seems ageless. Without a doubt, you are my role model. I want to express my heartfelt gratitude for welcoming me into GTS, even after what might have been considered an imperfect interview at the start of our journey together. These past four years have been incredibly meaningful and transformative for me. We've created numerous cherished memories, and you've always been open to sharing not only insights about experiments and work but also about your family, friends, Spanish and Catalan culture, and, perhaps most importantly, your humor-filled lessons on Jamón. I will undoubtedly miss you a lot, much like I miss your Jamón, jajaja.

✧ **Montse,** it's really difficult to determine who has had a greater impact on me over the past four years, you or Manolo. You've been the "boss" with an ever-open office door, always ready for my questions. You've been the "professor" who stayed up late with me in the lab coat in Alba. And you've been the friend who's quick to say "good job" the first time around. Through you, I've come to recognize a profound sense of responsibility and attentiveness that defines a female scientist. This quality inspires trust and dependence. If I find myself becoming an educator in the future, I aspire to be someone like you. I want to express my gratitude for all the lessons you've imparted, both in science and in life.

✧ **Mon,** you are the one who taught me ICP, and I've lost count of the number of days you've been there for me in the ICP room. You used to joke that all these efforts deserved a reward in the form of chocolate, but I know they mean more to me than just

sweets. And in life, you are also a good friend to me. Thank you for leaving me so many fantastic memories (we have to admit most of them involving food). I have gained more kilograms but also heavy love.

✧ **Júlia,** thank you for being with me all the time. You think everything is “caca”, yet you're the one didn’t mind analyzing my urine. You are the one always asking me “what do you need and what can I do for you?” Today all I need is you to be happy forever. I appreciate your willingness to share everything with me. I feel trusted, and I believe you can sense the same from me.

✧ **Roberto,** I want to express my sincere gratitude for everything you've done for me. Like the XAS, from getting the proposal ready, to those 72-hour lab sessions, and all the way through data crunching. Whenever I reached out for assistance, you consistently made time for me, even beyond regular working hours. What I see is a dedicated scientist, a caring friend, and a reliable brother. I've learned so much from you, and I'm certain that this experience will have a significant impact on my career. Thank you.

✧ **Iris,** you're a trustworthy and sincere friend. Whenever I encounter problems, I know I can turn to you, and you'll always provide your best advice and assistance. I want to express my gratitude for all the times you've helped me over the past four years. Also, thanks for being my guide in Las Palmas; that experience during Los Reyes Magos will undoubtedly remain one of the most memorable moments.

✧ **Lucía,** I like you as much as I like your desserts. Days with you around are always relaxed and joyful. Your perpetual smile and boundless energy, always accompanied by a cheerful tune, are truly infectious. Your optimism has a knack for brightening my day. I genuinely look forward to the day when I can visit you in Argentina.

✧ **Marcia,** niña, Dziękuję! For a long time, the two of us were the only active PhDs in the lab. We know better what PhD life is like. During our time together in Urbino and Krakow, we shared numerous enjoyable moments, brimming with joy. I hope that you will successfully complete your PhD in the near future, and that all your diligent efforts will yield the desired rewards.

✧ **Mari,** my office neighbor, thank you for always being kind to me. I truly appreciated your warm invitations to BBQs and calçotadas at your home, I like your lovely family very much, and I am very grateful for your hospitality. You are a brilliant scientist and will be someone in future.

✧ **Sandra,** I miss the days with you in GTS very much, always joyful. You always come up with fantastic ideas and plans. You've got everything organized. It's hard to imagine how these past four years would have been without you; they might have been a bit

dull. And I haven't been home for four years, but during the days in Miranda, you and your parents made me feel like I was finally home again. I really value it, and I'm so thankful to you, Mar, and Alberto.

✧ **Lou,** you're the first person I contacted since I came to Spain, and we've kept in touch regularly up to this day. I appreciate all the advice and guidance you've given me; it has significantly eased the beginning of my life in a foreign country. Looking forward to seeing you again in China soon!

✧ **Tingting,** even though we only spent a year together at GTS, you've still become an important friend to me. It's a pretty cool that we're from the same hometown. Hopefully, I'll get to see you and Weiqiang again back there.

✧ **Jorge,** we haven't had those morning coffee sessions at GTS since you graduated. It's so sad, as I really miss you and the fun times and laughter you always brought to the place. Thanks for always smiling at me and being kind to me.

✧ **Manu (马乐),** I wish we would have made more trips to the Costa Brava with the inflatable ducks and eaten more croquetas at La Pizzarita and hotpot at Chinese restaurants. These memories are so funny. I hope you don't forget the Chinese words you have learned. One day you will use them when you travel to China to visit me, right?

✧ **Laia,** the pretty girl always with a warm smile, hope everything goes well for you on thesis, you almost did it. We had so many interesting conversations and I hope we will have more in the future.

✧ **My Cuban friends, Toky, Tania, Yula, Markel, Margarita and Mirella,** our cooperation was perfect. I respect you; you are full of wisdom, knowledge and experience, I have learned a lot from you during the days of your visit. We exchanged a lot of Cuban and Chinese culture, it was amazing.

✧ **My minions, Andreu (TFM), Raquel (TFG) and Alejandro (TFG),** thank you for participating in my thesis work, I am very impressed with your efforts. I also learned a lot from all of you. That was a great time.

✧ **Marilyn,** the strongest woman I have ever seen, handling work, thesis, and kid at the same time. I have great admiration for you and wish you the best of luck.

✧ **Uma,** although we have only known each other for a few months, we had so many interesting conversations. It's been surprising to discover how much we have in common. I hope we can stay in touch and become close friends.

✧ **Gus, Montse Fernández and Cristina,** you are very important members of GTS, your professionalism makes GTS work perfectly. Hope we could keep in touch and meet again someday somewhere.

✧ **Victor,** the charming guy, thank you for being always kind to me. I miss those days we spent together. I hope your career and life will always be perfect.

✧ **My Chinese friends in Spain, Songbai, Heting, Shunya, Fan Yang, Mingyue, Wenhai,** we've shared countless wonderful moments together. You have kept me from feeling alone even 10000 km away from hometown.

✧ **My friends (cerveceros), Elena, Albert, Clara, Javi, Marta and Mangi,** we have organized too many interesting activities together, these are my precious memories. I don't know if we will meet again, but I believe that when we meet again, we will still be as happy as before.

✧ **My Chinese friends in Netherlands, Xiang Wang, Jianwen Zhang, Kaisheng Peng, Ming Huang, Guanqun Xu (滚滚), Yifu Chen, and Wencan Wu,** we travelled a lot together, and there was always so much joy along the way. My days in Delft were lovely too. And thank you for accompanying Lala in Delft.

✧ **Last but definitely not least, I want to thank my family – my parents and Lala.** Your constant support has been crucial in helping me navigate through these four years that seemed to fly by but were far from easy. Countless calls always managed to lift my spirits when I was feeling down and gave me a boost when I was feeling defeated.

Certainly, acknowledgment is extended to the RECOPHARMA project (grant agreement #778266) funded by the European Community's H2020 Program H2020-MSCA-RISE 2017. Gratitude is also expressed for the financial support received from the China Scholarship Council (No. 201906450024). Appreciation is due to the ALBA synchrotron facility for the allocation of beamtime (No. 2022085922) at the BL22-CLÆSS beamline. Furthermore, appreciation is expressed to the COST action 18202, "Network for Equilibria and Chemical Thermodynamics Advanced Research" (NECTAR), for its support of a Short-Term Scientific Mission (STSM) undertaken in Udine, Italy.

Summary

Due to incomplete metabolism in chemotherapy patients, platinum-based cytostatic drugs (Pt-CDs) are discharged into the environment through urine excretion. The presence of these compounds at concentrations reaching several hundred μg L^{-1} in hospital and municipal wastewater matrices raises significant health and environmental apprehensions. The current thesis presents noteworthy discoveries concerning the effective removal of trace amounts of Pt-CDs from waters matrices, employing diverse functionalized adsorbents.

Initially, the adsorption of two commonly used Pt-CDs (cisplatin and carboplatin), onto three commercial adsorbents, MetalZorb® sponge (Sponge), 3-(diethylenetriamino)propyl-functionalized silica gel (Si-DETA) and cysteine-functionalized silica gel (Si-Cys), was investigated. The adsorption processes were compared with the adsorption of $PtCl_4^{2-}$ to elucidate potential underlying adsorption mechanisms. Si-Cys exhibited superior adsorption capabilities for both Pt-CDs compared to Sponge and Si-DETA, signifying the pronounced affinity of thiol functional groups in Pt complexation-dominated chemisorption. The adsorption of anionic $PtCl_4^{2-}$ exhibited pronounced pH dependence and generally demonstrated higher adsorption compared to both Pt-CDs. This difference can primarily be attributed to the involvement of protonated surfaces in electrostatic attraction towards the anionic species. The process of elimination of Pt(II) compounds occurs through an initial hydration of the complexes in solution followed by adsorption, favored by the ionic nature of the complex and chelation. The pseudo-second-order (PSO) kinetic model effectively characterized the rapid adsorption processes involving diffusion and chemisorption. Isotherm investigations exhibited conformity with the Langmuir model, affirming monolayer adsorption. The determined adsorption enthalpy values indicated endothermic processes during the complexation of both Pt-CDs with thiol groups, in contrast to the exothermic nature observed in the adsorption of $PtCl_4^{2-}$. At a temperature of 343 K, the removal efficiency achieved by Si-Cys was 98.5 ± 0.1% for cisplatin and 94.1 ± 0.1% for carboplatin, respectively.

Subsequently, the modification of Sponge involved functionalization with 3-

mercaptopropionic acid (MPA) and L-cysteine (Cys) as strategies to improve the removal efficacy for trace concentration of both Pt-CDs (235 μg L^{-1} of Pt). The resulting MPA@Sponge exhibited a maximum removal efficiency of 88.9 ± 0.5% and 85.2 ± 0.4% for cisplatin and carboplatin respectively, whereas the corresponding maximum removal efficiencies Cys@Sponge exhibited were 75 ± 2% and 59 ± 1%. In comparison, unmodified Sponge exhibited removal efficiencies of only 29 ± 4% for cisplatin and 4 ± 1% for carboplatin. This suggests that the introduction of thiol functional groups provided favorable binding sites for Pt complexation. Due to the limited rate of hydration, the adsorption of carboplatin is comparatively lower than that of cisplatin. However, facilitating hydration and promoting the generation of active carboplatin derivatives were achieved through the introduction of Cl^- into the stock solutions and elevating the temperature, thereby augmenting its adsorption. Pt L_3-edge X-ray absorption spectroscopy (XAS) analyses revealed a similar coordination environment for adsorbed Pt on both MPA@Sponge and Cys@Sponge, characterized by the establishment of four Pt−S bonds during the adsorption process.

Finally, the MPA@sponge was further optimized by introducing $Na_2S·9H_2O$ or $SnCl_2·2H_2O$ to reduce the disulfide formed due to the oxidation of thiol groups. The two generated thiol-functionalized sponges (TFSs), TFS_1 and Sn/SnO_2-coated TFS_2, achieved the maximum removal efficiencies of 95.5 ± 0.8% and 99.5 ± 0.1% towards trace cisplatin (235 μg L^{-1} of Pt), respectively, notably surpassing that of the initial MPA@Sponge (88.9 ± 0.5%). Characterization techniques including FTIR, elemental analysis, SEM-EDS, and XPS were employed to effectively delineate the porous morphology of TFS and the successful grafting of thiol groups. The introduced thiol groups acted as affinity sites for Pt−S coordination, thereby enhancing adsorption. Additionally, the presence of bubble-like Sn/SnO_2 coatings on TFS_2 further enhanced the adsorption. High temperatures facilitated the favorable formation of Pt−S bonds, significantly enhancing the adsorption process. However, for TFS_2, the elevated temperature of 343 K induced aggregation of Sn/SnO_2, compromising the adsorption efficacy.

Resumen

Debido al metabolismo incompleto en pacientes de quimioterapia, los fármacos citostáticos a base de platino (Pt-CDs) se descargan al medio ambiente a través de la excreción de orina. La presencia de estos compuestos en concentraciones que alcanzan varios cientos de μg L^{-1} en matrices de aguas residuales municipales y hospitalarias genera inquietudes sobre el efecto que pueda tener en la salud y el medio ambiente. La presente tesis presenta nuevos avances en la eliminación de trazas de Pt-CDs de matrices acuosas, empleando diversos adsorbentes funcionalizados.

Inicialmente, se estudió la adsorción de los compuestos citostáticos cisplatino y carboplatino sobre tres adsorbentes comerciales, gel de sílice funcionalizado con cisteína (Si-Cys), gel de sílice funcionalizado con 3-(dietilentriamina)propilo (Si-DETA) y una esponja de celulosa MetalZorb® (Sponge). Este estudio comparativo tuvo como objetivo dilucidar los mecanismos de adsorción respecto de la adsorción observada para $PtCl_4^{2-}$. Si-Cys exhibió capacidades de adsorción superiores para cisplatino y carboplatino en comparación con Si-DETA y Sponge, lo que manifiesta la pronunciada afinidad de los grupos funcionales tiol en la complejación de Pt(II) mediante un fenómeno dominante de quimisorción. Se ha observado una adsorción de $PtCl_4^{2-}$ aniónico dependiente notablemente del pH y generalmente superando a la del cisplatino y carboplatino debido a la contribución de la adsorción electrostática aniónica sobre las superficies protonadas. El proceso de eliminación de los compuestos de Pt (II) se produce mediante una sustitución inicial de los ligandos de los complejos por moléculas de agua, seguida de una adsorción, favorecida por la naturaleza iónica del complejo formado y la quelación. El proceso de adsorción se ajustó a un modelo cinético de pseudosegundo orden (PSO), implicando difusión y quimisorción. Los estudios de las isotermas se ajustaron al modelo de Langmuir , consistente con un proceso de adsorción monocapa. Los valores de entalpía de adsorción sugirieron reacciones endotérmicas para la quelación de cisplatino y carboplatino con grupos tiol, mientras que la adsorción de $PtCl_4^{2-}$ fue exotérmica. A 343 K, la eficiencia de eliminación de Si-Cys alcanzó el 98,5 ± 0,1% (cisplatino) y el 94,1 ± 0,1% (carboplatino).

Posteriormente, se llevó a cabo la funcionalización del material Sponge utilizando

ácido 3-mercaptopropiónico (MPA) y L-cisteína (Cys), llamadas MPA@Sponge y Cys@Sponge respectivamente, con el objetivo de mejorar la eficiencia de la eliminación de concentraciones traza de cisplatino y carboplatino (235 μg L^{-1} de Pt). El MPA@Sponge resultante logró una eficiencia de eliminación máxima de 88,9 ± 0,5 % para cisplatino y 85,2 ± 0,4 % para carboplatino, mientras que Cys@Sponge mostró eficiencias de eliminación máximas de 75 ± 2 % y 59 ± 1 %, respectivamente. Por el contrario, la esponja no modificada logró eliminar el 29 ± 4 % para el cisplatino y el 4 ± 1 % para el carboplatino. Esto sugiere que la introducción de grupos funcionales tiol proporcionó sitios de unión favorables para la complejación de Pt. Debido a la tasa de hidratación limitada del carboplatino, su adsorción es comparativamente menor que la del cisplatino. Sin embargo, se logró mejorar la hidratación y la formación de derivados activos de carboplatino mediante la introducción de Cl^- en las soluciones madre y elevando la temperatura, aumentando así su adsorción. Los resultados obtenidos mediante espectroscopía de absorción de rayos X (XAS) realizadas en el borde L_3 del Pt, mostraron un entorno de coordinación similar para ambos adsorbentes funcionalizados, observando la formación de cuatro enlaces Pt−S durante el proceso de adsorción.

Finalmente, el material MPA@Sponge se optimizó aún más mediante el uso de $Na_2S·9H_2O$ o $SnCl_2·2H_2O$ para reducir el disulfuro formado debido a la oxidación de los grupos tiol. Las dos esponjas funcionalizadas con tiol (TFS) generadas, TFS_1 y TFS_2, la segunda recubierta con Sn/SnO_2 como subproducto de la reacción, lograron eficiencias de eliminación máximas de 95,5 ± 0,8 % y 99,5 ± 0,1 % respectivamente, para trazas de cisplatino (235 μg L^{-1} de Pt), superando notablemente la de MPA@Sponge inicial (88,9 ± 0,5%). Utilizando técnicas como FTIR, análisis elemental, SEM-EDS y XPS se caracterizó eficazmente la morfología porosa de TFS, observando el anclaje de los grupos tiol que actuaron como sitios de afinidad para la coordinación de Pt−S, mejorando así la adsorción. Además, la presencia de recubrimientos de Sn/SnO_2 similares a burbujas en TFS_2 mejoró aún más la adsorción. Las altas temperaturas facilitaron la formación favorable de enlaces Pt−S, mejorando significativamente el proceso de adsorción. Sin embargo, para TFS_2, la temperatura elevada de 343 K indujo la agregación de Sn/SnO_2, comprometiendo la eficacia de la adsorción.

Glossary

AAS	Atomic absorption spectroscopy	**FT**	Fourier transformed
Ac_2O	Acetic anhydride	**FTIR**	Fourier transform infrared spectroscopy
AOP	Advanced oxidation process	**HPLC**	High-performance liquid chromatography
ATR	Attenuated total reflectance	**HSA**	Human serum albumin
BET	Brunauer-Emmett-Teller	**HSAB**	Hard-Soft Acid-Base
CBDCA	1,1-cyclobutanedicarboxylato	**ICP-MS**	Inductively coupled plasma mass spectrometry
Cys	L-cysteine	**LOD**	Limit of detection
Cys@ Sponge	L-cysteine functionalized sponge	**MBR**	Membrane bioreactor
DMF	*N,N*-dimethylformamide	**MPA or 3-MPA**	3-mercaptopropionic acid
D-R	Dubinin-Radushkevich	**MPA@ Sponge**	3-mercaptopropionic acid functionalized sponge
EA	Elemental analysis	**PFO**	Pseudo-first-order
EDS	Energy dispersive x-ray spectroscopy	**pHpzc**	Point of zero charge
EXAFS	Extended X-Ray absorption fine structure	**PSO**	Pseudo-second-order
FDA	Food and Drug Administration	**Pt-CDs**	Platinum-based cytostatic drugs
FE-SEM	Field emission-scanning electron microscope	**Si-Cys**	Cysteine-functionalized silica gel

Si-DETA	3-(diethylenetriamino)propyl-functionalized silica gel	**WWTPs**	wastewater treatment plants
Si-SH	3-Mercaptopropyl-functionalized silica gel	**XANES**	X-ray absorption near edge structure
Sponge	MetalZorb® sponge	**XAS**	X-ray absorption spectroscopy
TFSs	Thiol-functionalized sponges	**XPS**	X-ray photoelectron spectroscopy

Content

Chapter 1

Introduction

In the vast laboratory of existence, we are but curious observers.

1.1 Problem statement

Platinum-based cytostatic drugs (Pt-CDs) are extensively employed in chemotherapy treatments for various types of cancer [1]. Pt-CDs are capable of intervening in cellular DNA replication, triggering DNA responses and apoptosis, thereby eradicating rapidly proliferating cells, which are usually cancerous [2–6]. However, following intravenous administration, a significant portion of incompletely metabolized Pt-CDs is excreted through the kidneys [7,8], escaping into hospital wastewater via patient urine. Over the past two decades, substantial evidence has confirmed the presence of Pt-CDs in hospital wastewaters [9–12]. The residual presence of Pt-CDs in hospital wastewater, although typically maintained at low levels (from ng L^{-1} to μg L^{-1}) [13,14,23,15–22], poses a significant challenge for conventional wastewater treatment plants (WWTPs), which exhibit limited capacity to effectively remove these residues [23]. Consequently, these residuals inevitably find their way into freshwater and marine ecosystems, thereby introducing an emerging pollutant that poses environmental threats [23]. These Pt-CDs can readily exert harmful effects, such as cytotoxicity, neurotoxicity, genotoxicity, and oxidative stress, on vulnerable aquatic organisms inhabiting freshwater and marine ecosystems [24]. Addressing the emerging and progressively deteriorating environmental issues caused by Pt-CDs is of vital importance. Furthermore, it is imperative to develop, validate, and promptly adopt viable removal and disposal strategies in response to this pressing concern.

1.2 History of Pt-CDs

It all started from a serendipity in 1965, when Barnett Rosenberg observed that bacteria ceased to divide when subjected to an electric field, ultimately tracing the cause of this phenomenon to the platinum electrode he had employed [25] (see timeline in Fig. 1). In 1968, cisplatin was intraperitoneally administered to mice carrying a standard murine transplantable tumor known as sarcoma-180 and results indicated significant

regression of the tumor following cisplatin treatment [26]. Subsequently, in 1971, cisplatin was clinically utilized for the treatment of the first cancer patient [27], and approved by the US Food and Drug Administration (FDA) for treatment of testicular and bladder cancer in later 1978 [28]. Second-generation Pt-CDs, such as carboplatin (cisplatin analogue), have been subsequently developed and clinically validated for the first time in 1982 [29], and then also approved by FDA in 1989 for ovarian cancer therapy [30]. Similarly, oxaliplatin made its debut in 1992 and demonstrated potential for curing colorectal cancer when used in combination with 5-fluorouracil [31], and FDA granted approval for clinical utilization (specifically for the treatment of colorectal cancer) in the year 2002 [32]. Other Pt-CDs, such as Nedaplatin [33] (Japan), heptaplatin [34] (Korea), and lobaplatin [35] (China), have also been developed, but currently, they have only obtained regional approval for clinical use.

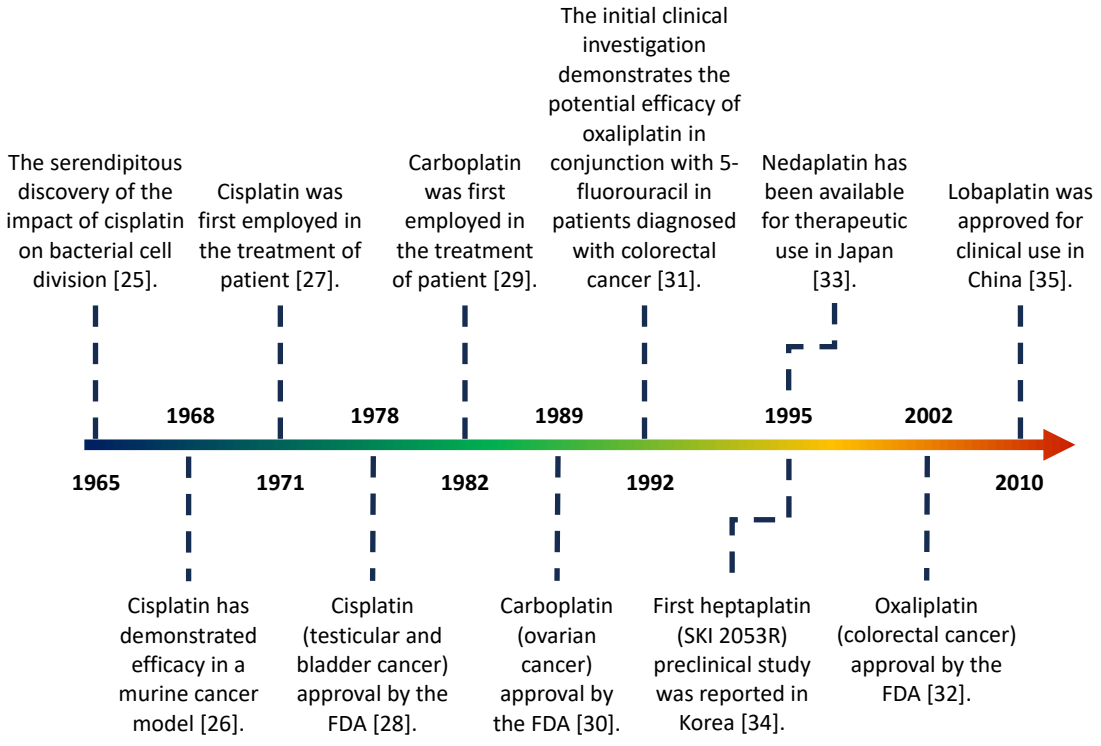

Fig. 1 Timeline of development of Pt-CDs for anticancer therapy.

The development of other Pt-CDs, analogues of cisplatin, based on its anti-cancer mechanism, has continued over the past fifty years. While a few of them have possibly

entered the international market as mentioned above, the majority of Pt-CDs are still in the early stages of 'bench' discovery. Some promising candidates have progressed to phase III trials like picoplatin or are still under consideration by the FDA like Satraplatin [6].

1.3 Action Mechanism of Pt-CDs

The chemical structures of the principal FDA-approved or regionally approved Pt-CDs are depicted in Fig. 2. Among them, cisplatin (cis-diamminedichloroplatinum(II)), carboplatin (cis-diammine(1,1-cyclobutanedicarboxylato)platinum(II)), and oxaliplatin (cis-oxalato-trans-l-1,2-diaminocyclohexaneplatinum(II)) represent the most frequently employed in clinical therapies and extensively investigated Pt-CDs.

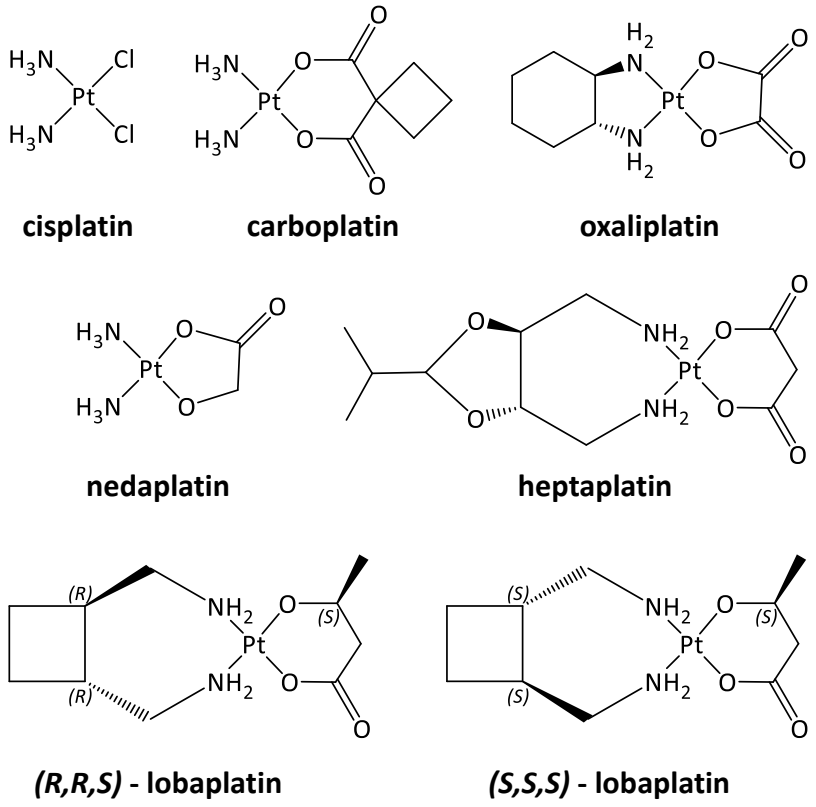

Fig. 2 FDA or regionally approved Pt-CDs.

The mechanism of action of Pt-CDs involves their interactions with DNA, leading to the inhibition of cancer cell proliferation and survival [5]. These cytostatic agents, such as cisplatin, carboplatin, and oxaliplatin, exert their effects through a common pathway

that involves the formation of covalent bonds with DNA, ultimately resulting in DNA damage and subsequent cellular responses [1]. Taking cisplatin as an example, the detailed process is described in Fig. 3. Upon entering the cancer cell, Pt cytostatics undergo hydration, where water molecules replace Cl ligand, forming hydrated Pt complexes [1]. These hydrated Pt complexes are highly reactive and can bind to nucleophilic sites on DNA, predominantly at the N^7 position of guanine residues [6]. The covalent binding of cisplatin to DNA leads to the formation of DNA adducts, including intra- and inter-strand crosslinks [6,23]. The formation of DNA adducts induced by cisplatin hampers DNA replication and transcription processes, thereby disrupting critical cellular functions [2]. This interference with DNA synthesis and repair triggers a cascade of cellular responses, including activation of DNA repair pathways, cell cycle arrest, and induction of apoptosis [1,2]. Additionally, cisplatin can generate reactive oxygen species, leading to oxidative stress and further contributing to the cytotoxic effects on cancer cells [36].

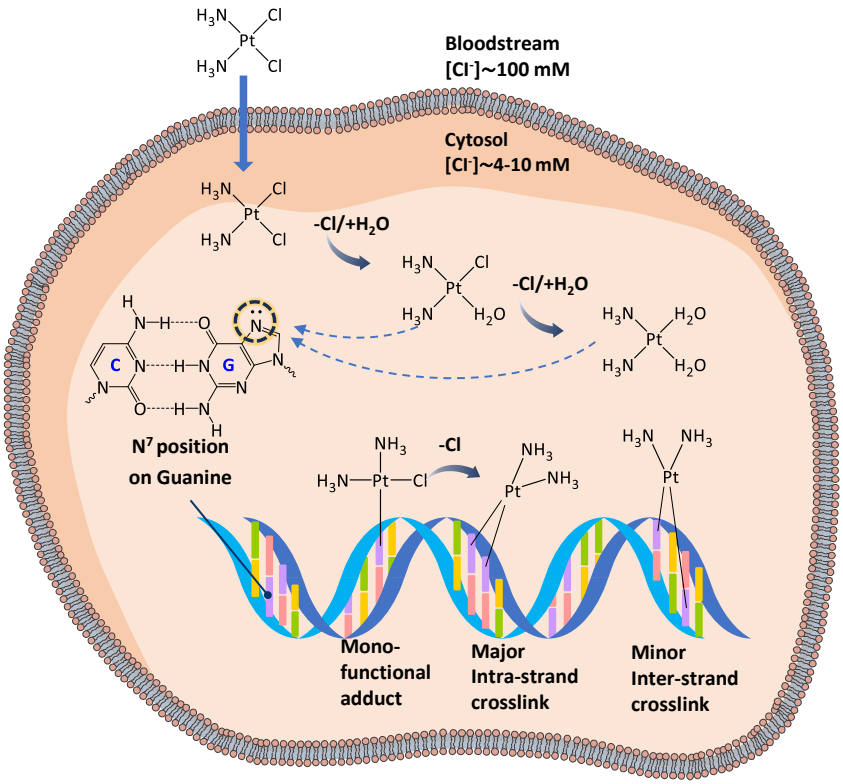

Fig. 3 Molecular mechanism of cisplatin action.

The mechanism of action of carboplatin is similar to that of cisplatin but exhibits some distinct differences. Like cisplatin, carboplatin exerts its cytotoxic effects by forming covalent DNA adducts, primarily at the N^7 position of guanine residues [37]. These DNA adducts interfere with DNA replication and transcription, leading to cellular dysfunction and ultimately inhibiting cancer cell proliferation [5]. However, the key difference lies in the reactivity and binding kinetics of carboplatin compared to cisplatin. Carboplatin has a lower reactivity due to the presence of a bidentate 1,1-cyclobutanedicarboxylato (CBDCA), which requires hydrolysis of the ligand to generate the active form capable of binding to DNA [38]. This slower activation process results in a delayed onset of DNA adduct formation compared to cisplatin [39].

Another important distinction between carboplatin and cisplatin is their binding selectivity. Carboplatin exhibits reduced affinity for DNA compared to cisplatin, resulting in a lower tendency for DNA crosslinking [40]. This difference in binding selectivity contributes to differences in their cytotoxicity profiles and potential side effects, being lower than cisplatin [41].

Oxaliplatin exerts its cytostatic effects through a mechanism like cisplatin [42]. However, there are notable differences in the way oxaliplatin and cisplatin interact with DNA, leading to distinct functional outcomes [43]. Like cisplatin, after hydration oxaliplatin covalently bind to DNA, forming DNA adducts [42]. However, oxaliplatin-induced DNA adducts are more flexible and less prone to repair compared to those formed by cisplatin [44]. Additionally, oxaliplatin can induce the formation of DNA inter-strand crosslinks more efficiently than cisplatin which compromise DNA function and contribute to the cytotoxic effects of oxaliplatin [44].

1.4 Occurrence of Pt-CDs in aquatic environment

1.4.1 Pt-CDs in urine

The incompletely metabolized Pt-CDs can be eliminated through renal clearance,

resulting in their excretion via urine [39,45–47]. Upon administration, the Pt-CDs undergo various metabolic processes, including biotransformation and binding to plasma proteins, before being filtered by the kidneys and excreted in urine [45,46,48,49]. However, a significant proportion of Pt-CDs, either in their intact form or as metabolites, can still be excreted within the subsequent 24 hours. It has been reported that approximately 28 ± 4% of cisplatin [50], 77 ± 5% of carboplatin [51], and 36 ± 8% of oxaliplatin [17] can be eliminated during this timeframe. The values obtained in these studies differ from those reported in other studies [9,20,48,52,53] but this still corroborates the urinary excretion of Pt-CDs. However, it is important to note that the accurate determination of urinary excretion rates is subject to various factors, including individual patient characteristics, drug formulation, dosage, and administration route. Additionally, differences in sampling time periods and sample handling can also contribute to observed discrepancies in the reported values. Generally, the presence of Pt-CDs in urine can be detected and quantified using analytical techniques such as high-performance liquid chromatography (HPLC) integrated with inductively coupled plasma mass spectrometry (ICP-MS) or atomic absorption spectroscopy (AAS) [54–59]. Table 1 provides a summary of selected studies investigating the detection of Pt compounds in the urine of cancer patients undergoing treatment with Pt-CDs. Although variations exist, there is reasonable evidence to believe that the presence of Pt-CDs or their derivatives in urine is common and substantial, reaching levels of up to mg L^{-1}. For instance, the concentration of cisplatin can reach up to as high as 115 mg L^{-1} [54].

1.4.2 Pt-CDs in hospital and municipal wastewaters

Unfortunately, there is no evidence to suggest that urine containing Pt-CDs has been subjected to special attention or additional treatment prior to its discharge into hospital wastewater. This directly contributes to the increasingly frequent detection of their residues in hospital wastewater [60]. A comprehensive literature review spanning over the past two decades was conducted in the present study to summarize the contamination

of Pt-CDs in wastewater, and it is presented in Table 2.

Table 1. A summary of the detection of Pt-CDs in the urine of patients undergoing chemotherapy.

Pt-CDs	Method	LOD	Result	Ref.
cisplatin	AAS	4 μg L^{-1} *	0.66-6.03 mg L^{-1} *	[57]
	Fluorescence	0.59 μg L^{-1} *	0.3-114.81 mg L^{-1} *	[54]
	HPLC	50 μg L^{-1}	up to 50 mg L^{-1}	[59]
carboplatin	LC-ICP-QMS**	1 ng g^{-1}	236 ug g^{-1}	[56]
	LC-ESI-TOFMS***	15 ng g^{-1}	250 ug g^{-1}	[56]
oxaliplatin	ICP-MS	0.39 μg L^{-1} *	0.01 - 41.10 mg L^{-1} *	[58]
	HPLC-ICP-MS	0.05 μg L^{-1}	11.1 mg L^{-1}	[55]

* Refers to the total Pt concentration.

** LC-ICP-QMS: liquid chromatography inductively coupled plasma quadrupole and sector field mass spectrometry.

*** LC-ESI-TOFMS: liquid chromatography electrospray ionization time-of-flight.

Table 2. A summary of the detection of Pt-CDs in the hospital and municipal wastewaters.

Pt-CDs	Method	concentration	sampling position	Country	Year	Ref.
cisplatin carboplatin	adsorptive voltammetry	10-601 ng L^{-1} (Total Pt)	hospital effluents	BE, IT, AT, DE, NL	1999	[19]
cisplatin carboplatin oxaliplatin	ICP-MS	4.7-145 μg L^{-1} (Total Pt)	hospital effluents of oncologic ward	AT	2005	[17]
cisplatin carboplatin	ICP-MS	3-250 μg L^{-1} 2-144 μg L^{-1} (Total Pt)	hospital effluents after treatment	AT	2007	[15]
cisplatin carboplatin oxaliplatin	ICP-MS	0.02-140 μg L^{-1} 0.03-100 μg L^{-1} (Total Pt)	oncology effluent the main drain of hospital	UK	2014	[13]
cisplatin	ICP-MS	226 ± 4 ng L^{-1} 352 ± 8 ng L^{-1} (Total Pt)	hospital wastewater (Collected in Jan.) hospital wastewater (Collected in Jun.)	SI	2016	[22]
cisplatin carboplatin	ICP-OES*	5-762 μg L^{-1}	oncology effluent (Shahid Beheshti Hospital)	IR	2018	[18]

Table 2. Continued.

Pt-CDs	Method	concentration	sampling position	Country	Year	Ref.
oxaliplatin		3-629 μg L^{-1} (Total Pt)	oncology effluent (Hazrat Masoumeh Hospital)			
cisplatin carboplatin oxaliplatin	ICP-MS	0.08-13.91 μg L^{-1} (Total Pt)	hospital wastewater	ES	2020	[21]
Total Pt	ICP-MS	27±3 ng L^{-1}	WWTP influent (Collected in Jan.)	SI	2016	[22]
		23±1 ng L^{-1}	WWTP influent (Collected in Jun.)			
		<LOQ	WWTP effluent (Collected in Jun.)			
cisplatin	SPE** + LC-MS/MS	0.52±0.20 μg L^{-1}	WWTP influent	IR	2018	[16]
carboplatin		0.94±0.36 μg L^{-1}				
oxaliplatin		0.27±0.16 μg L^{-1}				
cisplatin		0.24±0.07 μg L^{-1}	WWTP effluent			
carboplatin		0.28±0.05 μg L^{-1}				
oxaliplatin		0.11±0.01 μg L^{-1}				
Total Pt	ICP-MS	3.97-75.79 ng L^{-1}	WWTP	ES	2020	[21]

*OES: optical emission spectroscopy, **SPE: solid-phase extraction.

Based on the data presented in Table 2, it can be concluded that hospital wastewater serves as the primary source of Pt-CDs contamination, exhibiting a concentration range from 10 ng L^{-1} to several hundred μg L^{-1} [13,15,17–19,21,22]. The concentration of Pt-CDs not only varies spatially and temporally but also depends on the specific type of healthcare facility. For instance, the detected concentrations in dedicated oncology wards appear to be reasonably higher than those observed in general hospitals. Even within the same hospital setting, the Pt concentration of oncology effluent is typically higher compared to that of the main hospital drain [13]. Certainly, the concentration of Pt-CDs in wastewater is also influenced by various factors, including the number of hospital beds, local healthcare standards, preferred treatment regimens, regional demographic profiles, among others. However, it is important to note that research in this area remains limited. The explanation for this phenomenon can be attributed to two factors. Firstly, the levels

of Pt-CDs typically remain low, often below 1 mg L^{-1}, which distinguishes them from other common pollutants such as dyes and organic matter. Therefore, the detection and analysis of Pt-CDs require highly precise analytical techniques. Some residual Pt-CDs might elude detection. The second reason, which is also a cause for concern, indicates that this environmental issue has been overlooked or, at the very least, not given due attention in the past.

It is worth noting that, due to the increased frequency of outpatient treatments, domestic discharge has been emerging as another significant contributor to the discharge of Pt compounds into municipal wastewater. This problem has also attracted the attention of some researchers, and relying on advanced analytical methods, related studies have confirmed the emergence of platinum cytostatic compounds in different water matrixes due to their frequent use [23]. However, there is currently a scarcity of reports on the detection of Pt-CDs in urban wastewater, and comparative analysis reveals that the detected levels of Pt-CDs are significantly lower by several orders of magnitude than those found in hospital wastewater [16,21,22]. These compounds have been released into the environment without restrictions, primarily through hospital wastewater and municipal wastewater, Fig. 4 illustrates the pathways by which Pt-CDs enter and are transported in the environment. Despite their release, the total concentration of Pt in surface waters has maintained a consistently negligible presence, predominantly due to substantial dilution effects. Consequently, the concentration of Pt commonly remains beneath the limit of detection (LOD), leading to infrequent detection of these compounds [13,16,22,61]. However, according to research findings, the predicted environmental concentration range of Pt-CDs in various countries is reported to be between 0.1 and 0.8 ng L^{-1} [62]. These Pt-CDs are prone to adsorption and continuous accumulation by suspended solids and sewage sludge [63], and they progressively deposit into sediment, forming a reservoir of platinum in aquatic environments [64]. Eventually, resuspension of these sediments results in the sustained release of Pt into the water column [65].

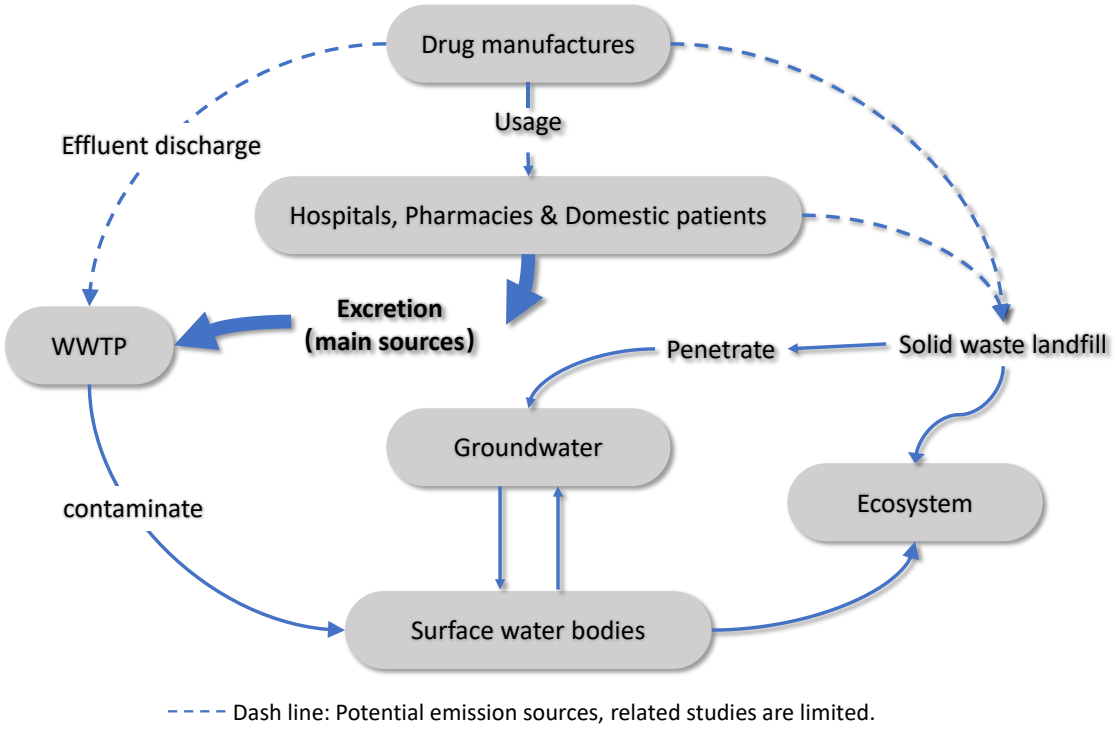

Fig. 4 The pathways by which Pt-CDs are introduced into the environment and transported.

However, the treatment of low-concentration Pt-CDs contaminated wastewater remains a challenging task. For example a case in Table 2 [15], a pilot membrane bioreactor system (MBR) was installed at a hospital in Vienna, with the influent sourced from the oncologic in-patient treatment ward. Pt concentrations were recorded during three monitoring periods, both in the influent (ranging from 3 to 250 μg L^{-1} Pt) and the effluent (ranging from 2 to 144 μg L^{-1} Pt) of the treatment plant, demonstrating elimination efficiencies ranging only between 51% and 63% [15]. Additionally, due to the significant challenges involved in treating low-concentration Pt-CDs, current WWTPs are not adequately equipped to effectively mitigate this environmental threat. For instance also presented in Table 2, a comparison of the concentrations of cisplatin, carboplatin, and oxaliplatin in the influent and effluent of a WWTP in Iran indicates that the removal efficiency of these Pt-CDs through the treatment process is limited [16].

1.5 Toxicity of Pt-CDs

Pt-CDs, such as cisplatin, carboplatin, and oxaliplatin, can have an impact on normal

cells in addition to their intended effects on cancer cells. While these cytostatic agents are designed to target rapidly proliferating cancerous cells, they can also inadvertently impact normal cells that undergo similarly high rates of cell division. This can lead to various side effects and toxicities [66].

1.5.1 Side effects to patients

Normal cells that are particularly susceptible to the effects of Pt-CDs include cells in the bone marrow (responsible for producing blood cells), hair follicles, gastrointestinal tract, and cells involved in sensory functions (such as hearing) [66]. These rapidly dividing cells can be affected by the cytotoxic effects of Pt-CDs, resulting in side effects such as myelosuppression (decreased production of blood cells) [46,48,49,66,67], hair loss (alopecia) [41,66], gastrointestinal disturbances (nausea, vomiting, diarrhea) [41,46,48,66,67], and hearing impairment (ototoxicity) [68–71]. Then, it is widely recognized that Pt-CDs have the potential to induce nephrotoxicity, which refers to the toxicity or damage to the kidneys [72]. Among Pt-CDs, cisplatin is known to exhibit a higher propensity for nephrotoxicity compared to carboplatin and oxaliplatin [66]. Nephrotoxicity is believed to occur as a result of direct cellular injury to the renal tubules and impairment of kidney function [73,74]. Cisplatin-induced nephrotoxicity is a complex process involving multiple mechanisms that are dependent on the dosage and cumulative exposure to the drug. In addition to the induction of DNA damage, several other factors contribute to the development of nephrotoxicity, including oxidative stress, mitochondrial dysfunction, inhibition of protein synthesis, and the activation of receptors associated with the tumor necrosis factor family, and notably, apoptosis of renal epithelial cells plays a crucial role in the pathogenesis of cisplatin-induced nephrotoxicity [75–78]. Similarly, neurotoxicity denotes the detrimental consequences experienced by the nervous system consequent to Pt-based chemotherapy, notably with the administration of Pt-CDs like cisplatin and oxaliplatin [67,79–81]. Specifically, oxaliplatin-induced neurotoxicity manifests as an acute form of peripheral neuropathy that is often elicited or

intensified by exposure to cold stimuli or objects. Clinical presentations encompass sensations of tingling or numbness in the extremities, including the hands, feet, or throat, along with occurrences of muscle cramps and impairment in fine motor skills [82,83]. However, it should be clarified that the acute clinical side effects associated with Pt-CDs do not appear to apply to populations exposed indirectly through environmental contact. As discussed in the previous section, the presence of Pt-CDs in the aquatic environment has consistently been reported to be low. Currently, limited evidence exists regarding the potential chronic adverse effects resulting from long-term, low-dose exposure to these Pt-CDs and/or their derivatives.

1.5.2 Ecotoxicity to aquatic invertebrates

However, the mere presence of trace levels of Pt-CDs does not imply their insignificance in terms of environmental risk. On the contrary, the potential for long-term exposure and bioaccumulation of these Pt-CDs raises concerns regarding their impact on aquatic organisms and ecosystems. Research has indicated that these Pt-CDs can have toxic effects on aquatic organisms, including fish, invertebrates, algae, and bacteria. Effects may include impaired growth and reproduction, changes in behavior, genotoxicity, and even mortality [24]. Taking cisplatin as an example, Table 3 provides a summary of ecotoxicity assessments conducted on aquatic invertebrate species concerning cisplatin or combinations of anticancer drugs containing cisplatin since 2007.

Table 3. Summary of the ecotoxicity of cisplatin (or other specified) in aquatic invertebrate species.

Species	Environment	Concentration ($\mu g\ L^{-1}$)	Time	End point	Ref
P. putida	soil	1200 [a]	16 h	growth-inhibition	[84]
P. subcapitata	freshwater	2300 [a]	96 h	growth-inhibition	
D. magna	freshwater	640 [a]	48 h	immobilization	
E. coli		90 [b]	2 h	genotoxicity	
S. cerevisiae		440 [b]	16 h	genotoxicity	
D. magna	freshwater	1.63 [a]	21 d	reproduction-inhibition	[85]

Table 3. Continued.

Species	Environment	Concentration (µg L^{-1})	Time	End point	Ref
C. dubia	freshwater	16.83 [a]	21 d	reproduction-inhibition	
T. platyurus	freshwater	440 [a]	21 d	growth-inhibition	
D. magna	freshwater	0.5-2.0	21 d	reproduction-inhibition	[86]
C. dubia	freshwater	12.3-125.3	7 d	reproduction-inhibition	
D. magna	freshwater	0.001-100	24 h	genotoxicity	[87]
C. dubia	freshwater	0.03-300	24 h	genotoxicity	
M. galloprovincialis	marine	0.1	14 d	oxidative stress genotoxicity neurotoxicity	[88]
U. pictorum	freshwater	1.2-1200	72 h	genotoxicity	[89]
U. tumidus	freshwater	1.2-1200	72 h	genotoxicity	
D. magna	freshwater	0.1-100	24 h	genotoxicity	[90]
C. dubia	freshwater	0.3-300	24 h	genotoxicity	
N. diversicolor	marine	0.0001-0.1	14 d	oxidative stress neurotoxicity genotoxicity behavioral impairment	[91]
D. magna	freshwater	0.01	24 h	genotoxicity	[92]
N. diversicolor	marine	0.01-1	14 d	oxidative stress neurotoxicity genotoxicity behavioral impairment	[93]
C. vulgaris	freshwater	106.2 (cisplatin) [c] 124.3 (carboplatin) [c] 153.9 (oxaliplatin) [c]	96 h	growth and reproduction inhibition	[36]

[a] Half maximal effective concentration (EC_{50})

[b] Minimum genotoxic concentrations

[c] Half maximal inhibitory concentration (IC_{50})

Results from these studies have demonstrated that cisplatin can exert toxic effects on aquatic invertebrates. The toxicity of cisplatin is influenced by factors such as exposure concentration, duration, and specific characteristics of the species under investigation. Even at a low concentration, it has been observed that cisplatin exposure

can lead to reduced survival rates, impaired reproductive capabilities, developmental abnormalities, and alterations in physiological and biochemical processes in aquatic invertebrates [24]. The mechanisms underlying cisplatin-induced toxicity in aquatic invertebrates are not fully elucidated but may involve oxidative stress, DNA damage, and disruption of cellular functions. Additionally, the bioaccumulation potential of cisplatin in aquatic organisms, particularly in long-lived species, has also been a subject of investigation [24].

1.5.3 Potential hazards to human health

The potential human health effects of exposure to Pt-CDs in the environment are a subject of ongoing research, research related to it is still very rare. While the concentrations of Pt-CDs found in the environment are generally low, long-term exposure or repeated exposure to these compounds could potentially lead to health concerns. Moreover, with the continuously aging population, increasing cancer incidence rates, and growing pharmaceutical consumption, the occurrence of Pt-CDs in the environment is expected to become more frequent and pronounced in the future. Studies have focused on evaluating the potential genotoxicity, carcinogenicity, and other adverse health effects associated with platinum cytostatic exposure in occupational settings, as well as potential exposure scenarios related to environmental contamination [12,94–96]. However, it is essential to note that the specific risks and effects may vary depending on factors such as the specific Pt-CDs, duration of exposure, route of exposure, individual susceptibility, and other contextual factors. To minimize potential risks to human health, efforts are being made to develop effective wastewater treatment methods that can remove these compounds from the environment and minimize human exposure. It is crucial for healthcare professionals, regulatory authorities, and individuals to be aware of the potential risks associated with Pt-CDs and to implement appropriate measures to mitigate those risks and ensure the safe use and disposal of these drugs.

1.6 Overview of Pt-CDs residues treatment

In summary, the environmental threat posed by Pt-CDs as an emerging pollutant has not received sufficient attention. Consequently, research reports on treatment strategies addressing this issue remain limited [23,97,98]. However, researchers are increasingly recognizing the urgency of this environmental problem and are actively exploring potential laboratory-scale treatment methods for Pt-CDs contaminated wastewater (by MBR, Advanced oxidation process (AOP), and adsorption), offering hope for future remediation efforts [23].

1.6.1 Non-adsorption methods

There are some studies where non-adsorption methods have been used to evaluate the elimination of Pt-CDs. For example, the treatment effects on the wastewater from an oncology in-patient treatment unit, using MBR system with or without combining with other treatments as activated carbon adsorption and UV-treatment have been evaluated, achieving a removal rates in the order to 50-60% [14,15]. This type of MBR system combines adsorption, biodegradation and filtration technology and shows a certain degree of wastewater treatment capacity, but it also has the disadvantage of long treatment period (weekly) which will probably limit the load and scale in practical industrial applications. Advanced oxidation process (AOP), a technology that could typically decompose a wild range of contaminants [96], was also selected as a competitive candidate to eliminate cisplatin. Hirose et al. [99] used electrolysis to inactivate multiple antineoplastics in clinical wastewater. The study found that the cytotoxicity of single cisplatin decreased by about 81.5% in two hours of electrolysis. Then a mixture containing cisplatin (89.3 μg mL^{-1}) and other agents like cyclophosphamide, mitomycin C, methotrexate and so on at their concentrations under practical conditions, was also electrolyzed, and eventually almost 99% cytotoxicity was successfully eliminated after 4 hours [99]. Kobayashi et al. [100] also studied the inactivation of antineoplastics residues in medical wastewater by

electrolysis technology. After a model wastewater containing a variety of antineoplastics such as cisplatin (10 mg L^{-1}) at concentrations under clinically practical conditions was subjected to electrolysis for two hours, 99% reduction of cytotoxicity was observed [100]. Subsequently, 26 real samples were treated under the same conditions, and the average reduction in cytotoxicity was 94% [100]. Another AOP strategy is ozonation, according to the study by Hernández et al., cisplatin (0.001 mol L^{-1}) is rapidly degraded in the first two minutes by ozone in aqueous samples [101]. It is undeniable that the scavenging effect and efficiency of AOPs are remarkable, however, by-product Pt still poses an environmental threat as a heavy metal ion after treatment, and although the authors stated that the cisplatin concentrations referred to the actual conditions, as proved by other studies above, the cisplatin concentration in real hospital wastewater often does not exceed 1 mg L^{-1}. Moreover, when considering economic costs and operational complexity, the competitiveness of these methods is diminished.

1.6.2 Adsorption methods

In comparison to the previously discussed treatment strategies, adsorption exhibits distinct merits in terms of the economic viability, operational simplicity, and treatment effectiveness. Furthermore, adsorption exhibits its suitability even at low concentrations of targets, its versatility in both continuous processing and batch modes, and the potential for adsorbates recovery and adsorbent regeneration [102].

Numerous adsorbents have undergone suitability for their efficacy in the removal of Pt-CDs. For instance, another study by Lenz et al. meticulously investigated the adsorption effect of cisplatin, carboplatin and oxaliplatin on suspended solids in real hospital wastewater and activated sludge [17]. In wastewater, cisplatin, carboplatin, and oxaliplatin were adsorbed by 88%, 26%, and 54%, respectively, after 24 hours of incubation. In comparison, activated sludge expressed better adsorption effect, 96% for cisplatin, 70% for carboplatin and 74% for oxaliplatin [17]. Then porous calcined gibbsite

was also prepared to remove cisplatin through adsorption [103]. 0.3 g of prepared calcined gibbsite adsorbent was added to 50 mL of cisplatin solution (10 mg L^{-1} Pt), after about 20 hours of stirring, the adsorption approached equilibrium, and the adsorption amount was 1.5 mg g^{-1}. In recent years, adsorbents derived from biomass sources, such as wood ash, biochar, chitosan and activated carbon were prepared to adsorb inorganic Pt(IV), cisplatin, carboplatin and oxaliplatin. The observed Pt adsorption capacities ranged from 0.23 to 0.97 mg g^{-1}, utilizing an adsorbent dose of 10 g L^{-1}. [104]. In a study published in 2020, cryogels were synthesized based on cryogelation polymerization of 2-hydroxyethyl metacrylate and methacrylic acid to capture cisplatin [105], similar methodologies were also employed in the synthesis of carriers intended for the delivery of cisplatin [106,107]. In this study, the initial concentrations investigated in batch adsorption experiments were 0.25 to 2 mg mL^{-1}, the dosage of the solid adsorbent was 10 mg mL^{-1}, the maximum adsorption capacity was found to be 150 mg g^{-1}, and the adsorption tended to equilibrium after 20 hours [105]. Recently, the latest research proposed another synthetic material (Pt(II)-imprinted mesoporous thiocyanato-functionalized silica) for adsorption of Pt in hospital wastewater, among these planar square Pt complexes, $PtCl_4^{2-}$, cisplatin, carboplatin, oxaliplatin were particularly investigated [108]. These ion-imprinted materials exhibited good adsorption performance in different matrices. Especially when adsorbing 153-206 μg L^{-1} of Pt(II) (concentrations in accordance with the Pt(II) concentration in actual hospital wastewater) from 10-folds diluted urine during seven days, the results demonstrated the potential of this adsorbent in future practical applications [108]. The recent study conducted by Fraguela et al. has introduced a cost-effective adsorbent known as Dithiocarbamate-Modified Silica [109]. This adsorbent has demonstrated successful removal of cisplatin under physiological conditions. However, it is important to note that the study primarily focused on concentration ranges exceeding 5 mg L^{-1}. The presence of low concentrations of Pt-CDs presents a hurdle for achieving efficient and rapid adsorption due to inadequate concentration gradients to propel Pt

compounds at the solid-liquid interface effectively. Furthermore, several studies [17,103,110] have reported that the adsorbents used for Pt compound adsorption often exhibit a prolonged equilibrium time of up to 24 hours. This slow kinetic performance poses challenges when attempting to scale up the adsorption system to a column configuration for field applications [17,103,110]. Additionally, several studies have commenced investigations into the adsorption properties by employing $PtCl_4^{2-}$ or $PtCl_6^{2-}$ as a preliminary model [108,110]. However, it should be noted that the adsorption mechanisms exhibited by these models might diverge from those originally intended for the target substances. This specific facet has not been given due consideration in the previously mentioned investigations. For instance, in the study where adsorbents such as granular activated carbon, chitosan, and biochar were employed to adsorb cisplatin, oxaliplatin, and carboplatin, respectively, substantial disparities in Pt recovery were already noted when compared to the template $PtCl_6^{2-}$ [110]. But these differences could not be adequately elucidated or comprehensively explained in detail.

Based on a literature review of Pt-CDs in wastewater, a systematic understanding and recognition of the environmental threat posed by these compounds has been established, encompassing their origins, current status, hazards, and existing disposal methods. However, it is evident that a knowledge gap exists, indicating insufficient research on the actual environmental risks associated with Pt-CDs contamination in wastewater and effective strategies for their practical disposal. This thesis focuses on the development of efficient adsorption systems based on various functionalized materials for the effective removal of trace amounts of Pt-CDs.

1.7 Objectives

The general objective of the present work is to study different adsorption systems based on various functionalized materials for the effective removal of trace amounts of Pt-CDs. To fulfill the primary aim, the subsequent objectives have been delineated:

1. To investigate the adsorption behaviors of cisplatin and carboplatin using three commercially available adsorbents: cysteine-functionalized silica gel (Si-Cys), 3-(diethylenetriamino)propyl-functionalized silica gel (Si-DETA), and a derivatized open-celled MetalZorb® sponge (Sponge). This investigation aims to conduct comparative analyses of the adsorption capabilities of these adsorbents, and compared to the adsorption of $PtCl_4^{2-}$ to gain a better understanding of the underlying adsorption mechanisms. The findings have been published and are presented in Chapter 2.
2. To functionalize Sponge using sulfur-containing compounds such as 3-mercaptopropionic acid (MPA) and L-cysteine (Cys) in order to enhance the adsorption of cisplatin and carboplatin on an inexpensive sponge substrate. Additionally, the aim is to elucidate the mechanism through the utilization of synchrotron-based X-ray absorption spectroscopy (XAS) techniques. The findings have been published and are presented in Chapter 2.
3. To enhance adsorption capabilities through the incorporation of a reduction step, further refining the functionalization process, as achieved by employing $Na_2S{\cdot}9H_2O$ and $SnCl_2{\cdot}2H2O$ for reduction. Additionally, the study aims to comprehensively elucidate the adsorption process through multiple characterizations including SEM-EDS, ATR-FTIR, XPS, and elemental analysis techniques. Related findings are presented in Chapter 3.

To achieve these objectives, effective international interdisciplinary and multidisciplinary collaborations have been established, which hold significant importance in the fields of environmental chemistry and environmental engineering. The dissemination of these findings to the society will raise awareness among readers regarding the escalating environmental risks associated with Pt cytostatics or other pharmaceutical pollutants. In turn, this will contribute to the development and enhancement of appropriate disposal procedures.

1.8 References

[1] D. Wang, S.J. Lippard, Cellular processing of platinum anticancer drugs, Nat. Rev. Drug Discov. 4 (2005) 307–320. https://doi.org/10.1038/nrd1691.

[2] Y. Jung, S.J. Lippard, Direct Cellular Responses to Platinum-Induced DNA Damage, Chem. Rev. 107 (2007) 1387–1407. https://doi.org/10.1021/cr068207j.

[3] E.R. Jamieson, S.J. Lippard, Structure, recognition, and processing of cisplatin-DNA adducts, Chem. Rev. 99 (1999) 2467–2498. https://doi.org/10.1021/cr980421n.

[4] Z.H. Siddik, Cisplatin: Mode of cytotoxic action and molecular basis of resistance, Oncogene. 22 (2003) 7265–7279. https://doi.org/10.1038/sj.onc.1206933.

[5] T.C. Johnstone, K. Suntharalingam, S.J. Lippard, The Next Generation of Platinum Drugs: Targeted Pt(II) Agents, Nanoparticle Delivery, and Pt(IV) Prodrugs, Chem. Rev. 116 (2016) 3436–3486. https://doi.org/10.1021/acs.chemrev.5b00597.

[6] L. Kelland, The resurgence of platinum-based cancer chemotherapy, Nat. Rev. Cancer. 7 (2007) 573–584. https://doi.org/10.1038/nrc2167.

[7] Pfizer, Product monograph: Cisplatin Injection BP, (2020). https://www.pfizer.ca/files/Cisplatin_PM_E_235278_2020-04-03.pdf (accessed April 3, 2020).

[8] Pfizer, Product monograph: carboplatin injection BP, (2022). https://www.pfizer.ca/files/Carboplatin_PM_EN_257501_29-Mar-2022.pdf (accessed March 29, 2022).

[9] S. Hann, G. Koellensperger, Z. Stefánka, G. Stingeder, M. Fürhacker, W. Buchberger, R.M. Mader, Application of HPLC-ICP-MS to speciation of cisplatin and its degradation products in water containing different chloride concentrations and in human urine, J. Anal. At. Spectrom. 18 (2003) 1391–1395. https://doi.org/10.1039/b309028k.

[10] K. Folens, S.T.F.C. Mortier, J. Baeten, K. Couvreur, R. Michelet, K. V. Gernaey, T. De Beer, G. Du Laing, I. Nopens, Modelling and sensitivity analysis of urinary platinum excretion in anticancer chemotherapy for the recovery of platinum, Sustain. Chem. Pharm. 4 (2016) 46–56. https://doi.org/10.1016/j.scp.2016.10.001.

[11] A. Turner, L. Mascorda, Particle–water interactions of platinum-based anticancer drugs in river water and estuarine water, Chemosphere. 119 (2015) 415–422. https://doi.org/10.1016/J.CHEMOSPHERE.2014.06.074.

[12] J. Zhang, V.W.C. Chang, A. Giannis, J.-Y. Wang, Removal of cytostatic drugs from aquatic environment: A review, Sci. Total Environ. 445–446 (2013) 281–298. https://doi.org/10.1016/J.SCITOTENV.2012.12.061.

[13] N. Vyas, A. Turner, G. Sewell, Platinum-based anticancer drugs in waste waters of a major UK hospital and predicted concentrations in recipient surface waters, Sci. Total Environ. 493 (2014) 324–329. https://doi.org/10.1016/j.scitotenv.2014.05.127.

[14] K. Lenz, S.N. Mahnik, N. Weissenbacher, R.M. Mader, P. Krenn, S. Hann, G. Koellensperger, M. Uhl, S. Knasmüller, F. Ferk, W. Bursch, M. Fuerhacker, Monitoring, removal and risk assessment of cytostatic drugs in hospital wastewater, Water Sci. Technol. 56 (2007) 141–149. https://doi.org/10.2166/wst.2007.828.

[15] K. Lenz, G. Koellensperger, S. Hann, N. Weissenbacher, S.N. Mahnik, M. Fuerhacker, Fate of cancerostatic platinum compounds in biological wastewater treatment of hospital effluents, Chemosphere. 69 (2007) 1765–1774. https://doi.org/10.1016/j.chemosphere.2007.05.062.

[16] Y. Ghafuri, M. Yunesian, R. Nabizadeh, A. Mesdaghinia, M.H. Dehghani, M. Alimohammadi, Platinum cytotoxic drugs in the municipal wastewater and drinking water, a validation method and health risk assessment, Hum. Ecol. Risk Assess. 24 (2018) 784–796. https://doi.org/10.1080/10807039.2017.1400372.

[17] K. Lenz, S. Hann, G. Koellensperger, Z. Stefanka, G. Stingeder, N. Weissenbacher, S.N. Mahnik, M. Fuerhacker, Presence of cancerostatic platinum compounds in hospital wastewater and possible elimination by adsorption to activated sludge, Sci. Total Environ. 345 (2005) 141–152. https://doi.org/10.1016/j.scitotenv.2004.11.007.

[18] Y. Ghafuria, M. Yunesian, R. Nabizadeh, A. Mesdaghinia, M.H. Dehghani, M. Alimohammadi, Environmental risk assessment of platinum cytotoxic drugs: a focus on toxicity characterization of hospital effluents, Int. J. Environ. Sci. Technol. 15 (2018) 1983–1990. https://doi.org/10.1007/s13762-017-1517-6.

[19] K. Kümmerer, E. Helmers, P. Hubner, G. Mascart, M. Milandri, F. Reinthaler, M. Zwakenberg, European hospitals as a source for platinum in the environment in comparison with other sources, Sci. Total Environ. 225 (1999) 155–165. https://doi.org/10.1016/S0048-9697(98)00341-6.

[20] A.C. Johnson, R. Oldenkamp, E. Dumont, J.P. Sumpter, Predicting concentrations of the cytostatic drugs cyclophosphamide, carboplatin, 5-fluorouracil, and capecitabine throughout the sewage effluents and surface waters of europe, Environ. Toxicol. Chem. 32 (2013) 1954–1961. https://doi.org/10.1002/etc.2311.

[21] S. Santana-Viera, M.E.T. Padrón, Z. Sosa-Ferrera, J.J. Santana-Rodríguez, Quantification of cytostatic platinum compounds in wastewater by inductively coupled plasma mass spectrometry after ion exchange extraction, Microchem. J. 157 (2020) 104862. https://doi.org/10.1016/j.microc.2020.104862.

[22] M. Isidori, M. Lavorgna, C. Russo, M. Kundi, B. Žegura, M. Novak, M. Filipič, M. Mišík, S. Knasmueller, M.L. de Alda, D. Barceló, B. Žonja, M. Česen, J. Ščančar, T. Kosjek, E. Heath, Chemical and toxicological characterisation of anticancer drugs in hospital and municipal wastewaters from Slovenia and Spain, Environ. Pollut. 219 (2016) 275–287. https://doi.org/10.1016/j.envpol.2016.10.039.

[23] Y. Roque-Diaz, M. Sanadar, D. Han, M. López-Mesas, M. Valiente, M. Tolazzi, A. Melchior, D. Veclani, The Dark Side of Platinum Based Cytostatic Drugs: From Detection to Removal, Processes. 9 (2021) 1873. https://doi.org/10.3390/pr9111873.

[24] V. Queirós, U.M. Azeiteiro, A.M.V.M. Soares, R. Freitas, The antineoplastic drugs cyclophosphamide and cisplatin in the aquatic environment – Review, J. Hazard. Mater. 412 (2021). https://doi.org/10.1016/j.jhazmat.2020.125028.

[25] B. ROSENBERG, L. VAN CAMP, T. KRIGAS, Inhibition of Cell Division in Escherichia coli by Electrolysis Products from a Platinum Electrode, Nature. 205 (1965) 698–699. https://doi.org/10.1038/205698a0.

[26] B. ROSENBERG, L. VANCAMP, J.E. TROSKO, V.H. MANSOUR, Platinum Compounds: a New Class of Potent Antitumour Agents, Nature. 222 (1969) 385–386. https://doi.org/10.1038/222385a0.

[27] D. Lebwohl, R. Canetta, Clinical development of platinum complexes in cancer therapy: An historical perspective and an update, Eur. J. Cancer. 34 (1998) 1522–1534. https://doi.org/10.1016/S0959-8049(98)00224-X.

[28] CISPLATIN for injection, for intravenous use.Initial U.S. Approval: 1978, (n.d.). https://www.accessdata.fda.gov/drugsatfda_docs/label/2019/018057s089lbl.pdf.

[29] A. Horwich, D.P. Dearnaley, G.M. Duchesne, M. Williams, M. Brada, M.J. Peckham, Simple nontoxic treatment of advanced metastatic seminoma with carboplatin, J. Clin. Oncol. 7 (1989) 1150–1156. https://doi.org/10.1200/JCO.1989.7.8.1150.

[30] D.E. Brenner, Liposomal encapsulation: Making old and new drugs do new tricks, J. Natl. Cancer Inst. 81 (1989) 1436–1438. https://doi.org/10.1093/jnci/81.19.1436.

[31] F. Levi, B. Perpoint, C. Garufi, C. Focan, P. Chollet, P. Depres-Brummer, R. Zidani, S. Brienza, M. Itzhaki, S. Iacobelli, F. Kunstlinger, J. Gastiaburu, J.L.

Misset, Oxaliplatin activity against metastatic colorectal cancer. A phase II study of 5-day continuous venous infusion at circadian rhythm modulated rate, Eur. J. Cancer. 29 (1993) 1280–1284. https://doi.org/10.1016/0959-8049(93)90073-O.

[32] Eloxatin (Oxaliplatin) Injection, (n.d.). https://www.accessdata.fda.gov/drugsatfda_docs/nda/2002/21-492_Eloxatin.cfm.

[33] G. Information, Platinum-containing cytostatic drugs, Meyler's Side Eff. Drugs. (2016) 810–833. https://doi.org/10.1016/b978-0-444-53717-1.01305-6.

[34] W.S. Hong, H.T. Kim, K.H. Kim, D.K. Kim, In vitro antitumor activity of a new platinum complex, cis-malonato [(4R,5R)-4,5-bis(aminomethyl)-2-isopropyl-1,3-dioxolane] platinum (II) (SKI 2053R), against human lung and stomach cancer cell lines, Anticancer Res. 15 (1995) 51—54. http://europepmc.org/abstract/MED/7733640.

[35] S.P. Vaidya, M. Patra, Platinum glycoconjugates: "Sweet bullets" for targeted cancer therapy?, Curr. Opin. Chem. Biol. 72 (2023) 102236. https://doi.org/10.1016/j.cbpa.2022.102236.

[36] S. Dehghanpour, H.R. Pourzamani, M.M. Amin, K. Ebrahimpour, Evaluation of toxic effects of platinum-based antineoplastic drugs (cisplatin, carboplatin and oxaliplatin) on green alga Chlorella vulgaris, Aquat. Toxicol. 223 (2020) 105495. https://doi.org/10.1016/j.aquatox.2020.105495.

[37] G.F. de Sousa, S.R. Wlodarczyk, G. Monteiro, Carboplatin: Molecular mechanisms of action associated with chemoresistance, Brazilian J. Pharm. Sci. 50 (2014) 693–702. https://doi.org/10.1590/S1984-82502014000400004.

[38] M. Pavelka, M.F.A. Lucas, N. Russo, On the hydrolysis mechanism of the second-generation anticancer drug carboplatin, Chem. - A Eur. J. 13 (2007) 10108–10116. https://doi.org/10.1002/chem.200700887.

[39] S. Dasari, P. Bernard Tchounwou, Cisplatin in cancer therapy: Molecular mechanisms of action, Eur. J. Pharmacol. 740 (2014) 364–378.

https://doi.org/10.1016/j.ejphar.2014.07.025.

[40] V. Brabec, J. Kasparkova, Modifications of DNA by platinum complexes: Relation to resistance of tumors to platinum antitumor drugs, Drug Resist. Updat. 8 (2005) 131–146. https://doi.org/10.1016/j.drup.2005.04.006.

[41] V.F. Vasconcellos, G.N. Marta, E.M.K. da Silva, A.F.T. Gois, T.B. de Castria, R. Riera, Cisplatin versus carboplatin in combination with third-generation drugs for advanced non-small cell lung cancer, Cochrane Database Syst. Rev. 2020 (2020). https://doi.org/10.1002/14651858.CD009256.pub3.

[42] T. Alcindor, N. Beauger, Oxaliplatin: A review in the era of molecularly targeted therapy, Curr. Oncol. 18 (2011) 18–25. https://doi.org/10.3747/co.v18i1.708.

[43] E. Raymond, S. Faivre, S. Chaney, J. Woynarowski, E. Cvitkovic, Cellular and molecular pharmacology of oxaliplatin, Mol. Cancer Ther. 1 (2002) 227–235.

[44] J.M. Woynarowski, W.G. Chapman, C. Napier, M.C.S. Herzig, P. Juniewicz, Sequence- and region-specificity of oxaliplatin adducts in naked and cellular DNA, Mol. Pharmacol. 54 (1998) 770–777. https://doi.org/10.1124/mol.54.5.770.

[45] M.A. Graham, G.F. Lockwood, D. Greenslade, S. Brienza, M. Bayssas, E. Gamelin, Clinical pharmacokinetics of oxaliplatin: A critical review, Clin. Cancer Res. 6 (2000) 1205–1218.

[46] A.J. Wagstaff, A. Ward, P. Benfield, R.C. Heel, Carboplatin: A Preliminary Review of its Pharmacodynamic and Pharmacokinetic Properties and Therapeutic Efficacy in the Treatment of Cancer, Drugs. 37 (1989) 162–190. https://doi.org/10.2165/00003495-198937020-00005.

[47] J.D. Blachley, J.B. Hill, Renal and electrolyte disturbances associated with cisplatin, Ann. Intern. Med. 95 (1981) 628–632. https://doi.org/10.7326/0003-4819-95-5-628.

[48] A.W. Prestayko, J.C. D'Aoust, B.F. Issell, S.T. Crooke, Cisplatin (cis-diamminedichloroplatinum II), Cancer Treat. Rev. 6 (1979) 17–39.

https://doi.org/10.1016/S0305-7372(79)80057-2.

[49] W.J.F. van der Vijgh, Clinical Pharmacokinetics of Carboplatin, Clin. Pharmacokinet. 21 (1991) 242–261. https://doi.org/10.2165/00003088-199121040-00002.

[50] J.B. Vermorken, W.J. van der Vijgh, I. Klein, A.A. Hart, H.E. Gall, H.M. Pinedo, Pharmacokinetics of free and total platinum species after short-term infusion of cisplatin, Cancer Treat. Rep. 68 (1984) 505—513. http://europepmc.org/abstract/MED/6538459.

[51] F. Elferink, W.J. van der Vijgh, I. Klein, J.B. Vermorken, H.E. Gall, H.M. Pinedo, Pharmacokinetics of carboplatin after i.v. administration, Cancer Treat. Rep. 71 (1987) 1231—1237. http://europepmc.org/abstract/MED/3319135.

[52] C.W.P. Schmidt, Pediatric Oncologic Pharmacy, Springer International Publishing, Cham, 2019. https://doi.org/10.1007/978-3-030-10988-2.

[53] P.J. LOEHRER, Cisplatin, Ann. Intern. Med. 100 (1984) 704. https://doi.org/10.7326/0003-4819-100-5-704.

[54] T. Jantarat, S. Chuaychob, C. Thammakhet-Buranachai, P. Thavarungkul, P. Kanatharana, W. Srisintorn, C. Buranachai, A Label-free DNA-based Fluorescent Sensor for Cisplatin Detection, Sensors Actuators, B Chem. 326 (2021) 128764. https://doi.org/10.1016/j.snb.2020.128764.

[55] G. Koellensperger, S. Hann, Ultra-fast HPLC-ICP-MS analysis of oxaliplatin in patient urine, Anal. Bioanal. Chem. 397 (2010) 401–406. https://doi.org/10.1007/s00216-010-3504-3.

[56] G. Koellensperger, Z. Stefanka, K. Meelich, M. Galanski, B.K. Keppler, G. Stingeder, S. Hann, Species specific IDMS for accurate quantification of carboplatin in urine by LC-ESI-TOFMS and LC-ICP-QMS, J. Anal. At. Spectrom. 23 (2008) 29–36. https://doi.org/10.1039/b708541a.

[57] A.C. Da Costa, M.A. Vieira, A.S. Luna, R.C. De Campos, Determination of

platinum originated from antitumoral drugs in human urine by atomic absorption spectrometric methods, Talanta. 82 (2010) 1647–1653. https://doi.org/10.1016/j.talanta.2010.07.029.

[58] L. Lemoine, E. Thijssen, J.P. Noben, P. Adriaensens, R. Carleer, K. Van der Speeten, A validated inductively coupled plasma mass spectrometry (ICP-MS) method for the quantification of total platinum content in plasma, plasma ultrafiltrate, urine and peritoneal fluid, J. Pharm. Biomed. Anal. 152 (2018) 39–46. https://doi.org/10.1016/j.jpba.2018.01.033.

[59] O.H. Drummer, A. Proudfoot, L. Howes, W.J. Louis, High-performance liquid chromatographic determination of platinum (II) in plasma ultrafiltrate and urine: comparison with a flameless atomic absorption spectrometric method, Clin. Chim. Acta. 136 (1984) 65–74. https://doi.org/10.1016/0009-8981(84)90248-1.

[60] T.I.A. Gouveia, A.M.T. Silva, M.G. Freire, A.C.A. Sousa, A. Alves, M.S.F. Santos, Multi-target analysis of cytostatics in hospital effluents over a 9-month period, J. Hazard. Mater. 448 (2023) 130883. https://doi.org/10.1016/j.jhazmat.2023.130883.

[61] J.-P.P. Besse, J.-F.F. Latour, J. Garric, Anticancer drugs in surface waters. What can we say about the occurrence and environmental significance of cytotoxic, cytostatic and endocrine therapy drugs?, Environ. Int. 39 (2012) 73–86. https://doi.org/10.1016/j.envint.2011.10.002.

[62] M. Mišík, M. Filipic, A. Nersesyan, M. Kundi, M. Isidori, S. Knasmueller, Environmental risk assessment of widely used anticancer drugs (5-fluorouracil, cisplatin, etoposide, imatinib mesylate), Water Res. 164 (2019) 114953. https://doi.org/10.1016/j.watres.2019.114953.

[63] R. Moreno-González, S. Rodriguez-Mozaz, M. Gros, D. Barceló, V.M. León, Seasonal distribution of pharmaceuticals in marine water and sediment from a mediterranean coastal lagoon (SE Spain), Environ. Res. 138 (2015) 326–344.

https://doi.org/10.1016/j.envres.2015.02.016.

[64] S.K. Rodrigues, D.M.S. Abessa, E.C. Machado, Geochemical and ecotoxicological assessment for estuarine surface sediments from Southern Brazil, Mar. Environ. Res. 91 (2013) 68–79. https://doi.org/10.1016/j.marenvres.2013.02.005.

[65] G.S. Araujo, L.B. Moreira, R.D. Morais, M.B. Davanso, T.F. Garcia, A.C.F. Cruz, D.M.S. Abessa, Ecotoxicological assessment of sediments from an urban marine protected area (Xixová-Japuí State Park, SP, Brazil), Mar. Pollut. Bull. 75 (2013) 62–68. https://doi.org/10.1016/j.marpolbul.2013.08.005.

[66] R. Oun, Y.E. Moussa, N.J. Wheate, The side effects of platinum-based chemotherapy drugs: A review for chemists, Dalt. Trans. 47 (2018) 6645–6653. https://doi.org/10.1039/c8dt00838h.

[67] M.R. Trendowski, O. El Charif, P.C. Dinh, L.B. Travis, M.E. Dolan, Genetic and Modifiable Risk Factors Contributing to Cisplatin-induced Toxicities, Clin. Cancer Res. 25 (2019) 1147–1155. https://doi.org/10.1158/1078-0432.CCR-18-2244.

[68] K.W. Chang, N. Chinosornvatana, Practical Grading System for Evaluating Cisplatin Ototoxicity in Children, J. Clin. Oncol. 28 (2010) 1788–1795. https://doi.org/10.1200/JCO.2009.24.4228.

[69] E. Tserga, T. Nandwani, N.K. Edvall, J. Bulla, P. Patel, B. Canlon, C.R. Cederroth, D.M. Baguley, The genetic vulnerability to cisplatin ototoxicity: a systematic review, Sci. Rep. 9 (2019) 3455. https://doi.org/10.1038/s41598-019-40138-z.

[70] J.H. van den Berg, J.H. Beijnen, A.J.M. Balm, J.H.M. Schellens, Future opportunities in preventing cisplatin induced ototoxicity, Cancer Treat. Rev. 32 (2006) 390–397. https://doi.org/10.1016/j.ctrv.2006.04.011.

[71] T. Langer, A. Am Zehnhoff-Dinnesen, S. Radtke, J. Meitert, O. Zolk, Understanding platinum-induced ototoxicity, Trends Pharmacol. Sci. 34 (2013)

458–469. https://doi.org/10.1016/j.tips.2013.05.006.

[72] T. Ludwig, C. Riethmüller, M. Gekle, G. Schwerdt, H. Oberleithner, Nephrotoxicity of platinum complexes is related to basolateral organic cation transport, Kidney Int. 66 (2004) 196–202. https://doi.org/10.1111/j.1523-1755.2004.00720.x.

[73] N. Pabla, Z. Dong, Cisplatin nephrotoxicity: Mechanisms and renoprotective strategies, Kidney Int. 73 (2008) 994–1007. https://doi.org/10.1038/sj.ki.5002786.

[74] A. Hamroun, R. Lenain, J.J. Bigna, E. Speyer, L. Bui, P. Chamley, N. Pottier, C. Cauffiez, E. Dewaeles, X. Dhalluin, A. Scherpereel, M. Hazzan, M. Maanaoui, F. Glowacki, Prevention of Cisplatin-Induced Acute Kidney Injury: A Systematic Review and Meta-Analysis, Drugs. 79 (2019) 1567–1582. https://doi.org/10.1007/s40265-019-01182-1.

[75] S.M. Somani, K. Husain, C. Whitworth, G.L. Trammell, M. Malafa, L.P. Rybak, Dose-dependent protection by lipoic acid against cisplatin-induced nephrotoxicity in rats: Antioxidant defense system, Pharmacol. Toxicol. 86 (2000) 234–241. https://doi.org/10.1034/j.1600-0773.2000.d01-41.x.

[76] H.R. Brady, B.C. Kone, M.E. Stromski, M.L. Zeidel, G. Giebisch, S.R. Gullans, Mitochondrial injury: an early event in cisplatin toxicity to renal proximal tubules, Am. J. Physiol. - Ren. Fluid Electrolyte Physiol. 258 (1990). https://doi.org/10.1152/ajprenal.1990.258.5.f1181.

[77] K. Tsuruya, T. Ninomiya, M. Tokumoto, M. Hirakawa, K. Masutani, M. Taniguchi, K. Fukuda, H. Kanai, K. Kishihara, H. Hirakata, M. Iida, Direct involvement of the receptor-mediated apoptotic pathways in cisplatin-induced renal tubular cell death, Kidney Int. 63 (2003) 72–82. https://doi.org/10.1046/j.1523-1755.2003.00709.x.

[78] M.S. Park, M. De Leon, P. Devarajan, Cisplatin Induces Apoptosis in LLC-PK1 Cells via Activation of Mitochondrial Pathways, J. Am. Soc. Nephrol. 13 (2002).

https://journals.lww.com/jasn/Fulltext/2002/04000/Cisplatin_Induces_Apoptosis_in_LLC_PK1_Cells_via.4.aspx.

[79] R.J. Cersosimo, Cisplatin neurotoxicity, Cancer Treat. Rev. 16 (1989) 195–211. https://doi.org/10.1016/0305-7372(89)90041-8.

[80] R.W. Gregg, J.M. Molepo, V.J.A. Monpetit, N.Z. Mikael, D. Redmond, M. Gadia, D.J. Stewart, Cisplatin neurotoxicity: The relationship between dosage, time, and platinum concentration in neurologic tissues, and morphologic evidence of toxicity, J. Clin. Oncol. 10 (1992) 795–803. https://doi.org/10.1200/JCO.1992.10.5.795.

[81] O. Kanat, H. Ertas, B. Caner, Platinum-induced neurotoxicity: A review of possible mechanisms, World J. Clin. Oncol. 8 (2017) 329–333. https://doi.org/10.5306/wjco.v8.i4.329.

[82] L.M. Pasetto, M.R. D'Andrea, E. Rossi, S. Monfardini, Oxaliplatin-related neurotoxicity: How and why?, Crit. Rev. Oncol. Hematol. 59 (2006) 159–168. https://doi.org/10.1016/j.critrevonc.2006.01.001.

[83] A. V. Krishnan, D. Goldstein, M. Friedlander, M.C. Kiernan, Oxaliplatin-induced neurotoxicity and the development of neuropathy, Muscle and Nerve. 32 (2005) 51–60. https://doi.org/10.1002/mus.20340.

[84] R. Zounková, P. Odráška, L. Doležalová, K. Hilscherová, B. Maršálek, L. Bláha, ECOTOXICITY AND GENOTOXICITY ASSESSMENT OF CYTOSTATIC PHARMACEUTICALS, Environ. Toxicol. Chem. 26 (2007) 2208. https://doi.org/10.1897/07-137R.1.

[85] A. Parrella, M. Lavorgna, E. Criscuolo, C. Russo, V. Fiumano, M. Isidori, Acute and chronic toxicity of six anticancer drugs on rotifers and crustaceans, Chemosphere. 115 (2014) 59–66. https://doi.org/10.1016/j.chemosphere.2014.01.013.

[86] A. Parrella, M. Kundi, M. Lavorgna, E. Criscuolo, C. Russo, M. Isidori, Toxicity

of exposure to binary mixtures of four anti-neoplastic drugs in Daphnia magna and Ceriodaphnia dubia, Aquat. Toxicol. 157 (2014) 41–46. https://doi.org/10.1016/j.aquatox.2014.09.012.

[87] A. Parrella, M. Lavorgna, E. Criscuolo, C. Russo, M. Isidori, Eco-genotoxicity of six anticancer drugs using comet assay in daphnids, J. Hazard. Mater. 286 (2015) 573–580. https://doi.org/10.1016/j.jhazmat.2015.01.012.

[88] C. Trombini, T. Garcia da Fonseca, M. Morais, T.L. Rocha, J. Blasco, M.J. Bebianno, Toxic effects of cisplatin cytostatic drug in mussel Mytilus galloprovincialis, Mar. Environ. Res. 119 (2016) 12–21. https://doi.org/10.1016/j.marenvres.2016.05.004.

[89] S. Kolarević, Z. Gačić, J. Kostić, K. Sunjog, M. Kračun-Kolarević, M. Paunović, J. Knežević-Vukčević, B. Vuković-Gačić, Impact of Common Cytostatics on DNA Damage in Freshwater Mussels Unio pictorum and Unio tumidus, Clean - Soil, Air, Water. 44 (2016) 1471–1476. https://doi.org/10.1002/clen.201500482.

[90] M. Kundi, A. Parrella, M. Lavorgna, E. Criscuolo, C. Russo, M. Isidori, Prediction and assessment of ecogenotoxicity of antineoplastic drugs in binary mixtures, Environ. Sci. Pollut. Res. 23 (2016) 14771–14779. https://doi.org/10.1007/s11356-015-4884-x.

[91] T.G. Fonseca, M.B. Morais, T. Rocha, D.M.S. Abessa, M. Aureliano, M.J. Bebianno, Ecotoxicological assessment of the anticancer drug cisplatin in the polychaete Nereis diversicolor, Sci. Total Environ. 575 (2017) 162–172. https://doi.org/10.1016/j.scitotenv.2016.09.185.

[92] C. Russo, M. Isidori, J.A. Deaver, H.C. Poynton, Toxicogenomic responses of low level anticancer drug exposures in Daphnia magna, Aquat. Toxicol. 203 (2018) 40–50. https://doi.org/10.1016/j.aquatox.2018.07.010.

[93] T.G. da Fonseca, D.M.S. Abessa, M.J. Bebianno, Effects of mixtures of anticancer drugs in the benthic polychaete Nereis diversicolor, Environ. Pollut. 252 (2019)

1180–1192. https://doi.org/10.1016/j.envpol.2019.05.095.

[94] G. Gajski, C. Ladeira, M. Gerić, V. Garaj-Vrhovac, S. Viegas, Genotoxicity assessment of a selected cytostatic drug mixture in human lymphocytes: A study based on concentrations relevant for occupational exposure, Environ. Res. 161 (2018) 26–34. https://doi.org/10.1016/J.ENVRES.2017.10.044.

[95] M. Villarini, V. Gianfredi, S. Levorato, S. Vannini, T. Salvatori, M. Moretti, Occupational exposure to cytostatic/antineoplastic drugs and cytogenetic damage measured using the lymphocyte cytokinesis-block micronucleus assay: A systematic review of the literature and meta-analysis, Mutat. Res. - Rev. Mutat. Res. 770 (2016) 35–45. https://doi.org/10.1016/j.mrrev.2016.05.001.

[96] A. Pieczyńska, A.F. Borzyszkowska, A. Ofiarska, E.M. Siedlecka, Removal of cytostatic drugs by AOPs: A review of applied processes in the context of green technology, Crit. Rev. Environ. Sci. Technol. 47 (2017) 1282–1335. https://doi.org/10.1080/10643389.2017.1370990.

[97] D. Han, M. López-Mesas, R. Boada, T. Farías, A.R. Lazo Fraga, M. Valiente, Trace cisplatin and carboplatin removal by 3-mercaptopropionic acid and l-cysteine functionalized sponges: adsorption behaviour and mechanism, Chem. Eng. J. 472 (2023) 144894. https://doi.org/10.1016/j.cej.2023.144894.

[98] D. Han, M. López-Mesas, M. Luaces, Y. Enamorado, M. Sanadar, A. Melchior, M. Valiente, Comparative study on removal of platinum cytostatic drugs at trace level by cysteine, diethylenetriamino functionalized Si-gels and polyethyleneimine functionalized sponge: Adsorption performance and mechanisms, Sci. Total Environ. 891 (2023) 164385. https://doi.org/10.1016/j.scitotenv.2023.164385.

[99] J. Hirose, F. Kondo, T. Nakano, T. Kobayashi, N. Hiro, Y. Ando, H. Takenaka, K. Sano, Inactivation of antineoplastics in clinical wastewater by electrolysis, Chemosphere. 60 (2005) 1018–1024.

https://doi.org/10.1016/j.chemosphere.2005.01.024.

[100] T. Kobayashi, J. Hirose, K. Sano, N. Hiro, Y. Ijiri, H. Takiuchi, H. Tamai, H. Takenaka, K. Tanaka, T. Nakano, Evaluation of an electrolysis apparatus for inactivating antineoplastics in clinical wastewater, Chemosphere. 72 (2008) 659–665. https://doi.org/10.1016/j.chemosphere.2008.02.020.

[101] C. Hernández, Y. Ramos, L.A. Fernández, O. Ledea, M. Bataller, E. Véliz, V. Besada, A. Rosado, Ozonation of Cisplatin in Aqueous Solution at pH 9, Ozone Sci. Eng. 30 (2008) 189–196. https://doi.org/10.1080/01919510801907722.

[102] M. Patel, R. Kumar, K. Kishor, T. Mlsna, C.U. Pittman, D. Mohan, Pharmaceuticals of emerging concern in aquatic systems: Chemistry, occurrence, effects, and removal methods, Chem. Rev. 119 (2019) 3510–3673. https://doi.org/10.1021/acs.chemrev.8b00299.

[103] F. OGATA, K. INOUE, H. TOMINAGA, Y. IWATA, A. UEDA, Y. TANAKA, N. KAWASAKI, Use of Calcined Gibbsite to Remove Cisplatin from Aqueous Solutions, J. Water Environ. Technol. 12 (2014) 13–23. https://doi.org/10.2965/jwet.2014.13.

[104] K. Folens, A. Abebe, J. Tang, F. Ronsse, G. Du Laing, Biosorption of residual cisplatin, carboplatin and oxaliplatin antineoplastic drugs in urine after chemotherapy treatment, Environ. Chem. 15 (2018) 506–512. https://doi.org/10.1071/EN18115.

[105] T. Farías, S. Hajizadeh, L. Ye, Cryogels with high cisplatin adsorption capacity: Towards removal of cytotoxic drugs from wastewater, Sep. Purif. Technol. 235 (2020) 116203. https://doi.org/10.1016/j.seppur.2019.116203.

[106] K.D. Lee, Y. Il Jeong, D.H. Kim, G.T. Lim, K.C. Choi, Cisplatin-incorporated nanoparticles of poly(acrylic acid-co-methyl methacrylate) copolymer, Int. J. Nanomedicine. 8 (2013) 2835–2845. https://doi.org/10.2147/IJN.S48367.

[107] B. Singh, N. Chauhan, V. Sharma, Design of molecular imprinted hydrogels for

controlled release of cisplatin: Evaluation of network density of hydrogels, Ind. Eng. Chem. Res. 50 (2011) 13742–13751. https://doi.org/10.1021/ie200758b.

[108] J. Dobrzynska, M. Dabrowska, R. Olchowski, E. Zieba, R. Dobrowolski, Development of a method for removal of platinum from hospital wastewater by novel ion-imprinted mesoporous organosilica, J. Environ. Chem. Eng. 9 (2021). https://doi.org/10.1016/j.jece.2021.105302.

[109] R. Lombana Fraguela, J.A. Ricardo Garcia, M.E. Villanueva Tagle, M.S. Pomares Alfonso, M. Cracchiolo, A. Kovačević, M. Tolazzi, A. Melchior, M. Sanadar, Evaluation of Dithiocarbamate-Modified Silica for Cisplatin Removal from Water, Processes. 11 (2023) 472. https://doi.org/10.3390/pr11020472.

[110] K. Folens, A. Abebe, J. Tang, F. Ronsse, G. Du Laing, G. Du Laing, Biosorption of residual cisplatin, carboplatin and oxaliplatin antineoplastic drugs in urine after chemotherapy treatment, Environ. Chem. 15 (2018) 506–512. https://doi.org/10.1071/EN18115.

Chapter 2

Compilation of articles

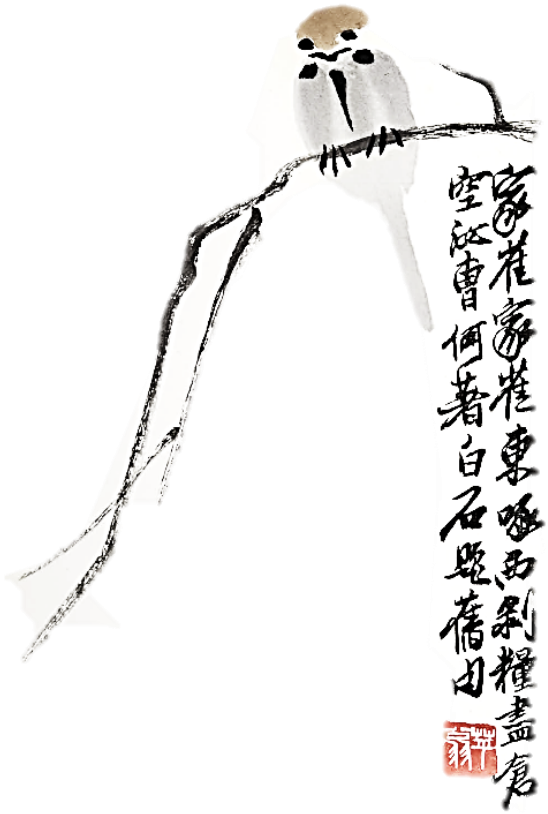

Science may not have all the answers, but it's the only quest where you can wear a lab coat and pretend to be a wizard for real.

2.1 Comparative study on removal of platinum cytostatic drugs at trace level by cysteine, diethylenetriamino functionalized Si-gels and polyethyleneimine functionalized sponge: adsorption performance and mechanisms

Dong Han,[1] Montserrat López-Mesas[(*)],[1] Markel Luaces,[2] Yusleydi Enamorado,[2] Martina Sanadar,[3] Andrea Melchior[3] and Manuel Valiente[1]

[1]*GTS-UAB Research Group, Department of Chemistry, Faculty of Science, Universitat Autònoma de Barcelona, Bellaterra, (Cerdanyola del Vallès), 08193 Barcelona, Spain*

[2]*Faculty of Chemistry, University of Havana, 10400 Havana, Cuba*

[3]*Dipartimento Politecnico di Ingegneria e Architettura, Università di Udine, via del Cotonificio 108, 33100 Udine, Italy*

Journal: Science of The Total Environment

https://doi.org/10.1016/j.scitotenv.2023.164385

Available online 25 May 2023, Version of Record 30 May 2023

Science of the Total Environment 891 (2023) 164385

Contents lists available at ScienceDirect

Science of the Total Environment

journal homepage: www.elsevier.com/locate/scitotenv

Comparative study on removal of platinum cytostatic drugs at trace level by cysteine, diethylenetriamino functionalized Si-gels and polyethyleneimine functionalized sponge: Adsorption performance and mechanisms

Dong Han [a], Montserrat López-Mesas [a,*], Markel Luaces [b], Yusleydi Enamorado [b], Martina Sanadar [c], Andrea Melchior [c], Manuel Valiente [a]

[a] GTS-UAB Research Group, Department of Chemistry, Faculty of Science, Universitat Autònoma de Barcelona, Bellaterra, (Cerdanyola del Vallès), 08193 Barcelona, Spain
[b] Faculty of Chemistry, University of Havana, 10400 Havana, Cuba
[c] Dipartimento Politecnico di Ingegneria e Architettura, Università di Udine, via del Cotonificio 108, 33100 Udine, Italy

HIGHLIGHTS

- Adsorption of emerging contaminants Pt-cytostatics using functionalized materials
- Effective elimination of trace concentrations of cisplatin and carboplatin
- Removal of Pt-cytostatics from hospital wastewater analogs
- Explanation of the adsorption mechanisms of different Pt compounds
- Enhanced adsorption *via* complexation between Pt-cytostatics and thiol groups

GRAPHICAL ABSTRACT

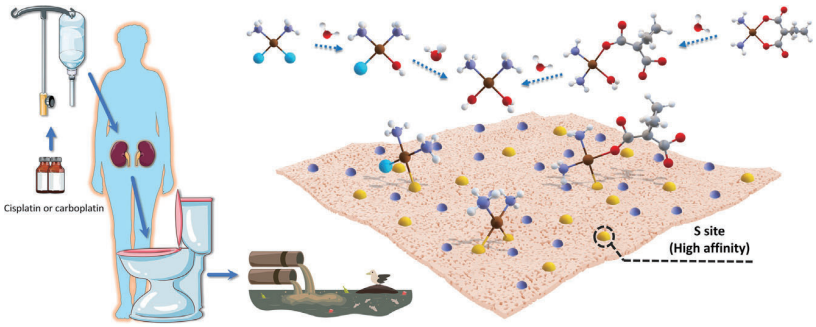

ARTICLE INFO

Editor: Damia Barcelo

Keywords:
Platinum cytostatics
Adsorption
Cisplatin
Carboplatin
Functionalized adsorbents

ABSTRACT

To efficiently remove trace Pt-based cytostatic drugs (Pt-CDs) from aqueous environments, a comparative investigation was conducted on the adsorption behavior of three commercial adsorbents including cysteine-functionalized silica gel (Si-Cys), 3-(diethylenetriamino) propyl-functionalized silica gel (Si-DETA) and open-celled cellulose MetalZorb® sponge (Sponge). The research on the adsorption of cisplatin and carboplatin encompasses investigations of pH dependence, adsorption kinetics, adsorption isotherms, and adsorption thermodynamics. The obtained results were compared with those of $PtCl_4^{2-}$ to better understand the adsorption mechanisms. The adsorption of cisplatin and carboplatin by Si-Cys was significantly better than Si-DETA and Sponge, which suggested that in chelation-dominated chemisorption, thiol groups provided high-affinity sites for Pt(II) complexation. Adsorption of the anion $PtCl_4^{2-}$ was more pH dependent and generally superior to that of cisplatin and carboplatin, benefiting from the contribution of ion association with protonated surfaces. The removal process of aqueous Pt(II) compounds occurred by the hydrolysis of complexes in solution and subsequent adsorption, and the specific adsorption process was explained by the synergistic action of ion association and chelation mechanisms. The rapid adsorption processes involving diffusion and chemisorption were well described by pseudo-second-order kinetic model. The isotherm studies suggested monolayer adsorption, consistent with the Langmuir model. Indicated from the adsorption enthalpy results, the chelation of cisplatin and carboplatin with thiol groups was an endothermic reaction, while the adsorption of $PtCl_4^{2-}$ was exothermic. At 343 K, Si-Cys achieved 98.5 ± 0.1 % (cisplatin) and 94.1 ± 0.1 % (carboplatin) removal. To validate the

* Corresponding author.
E-mail addresses: Dong.Han@uab.cat (D. Han), montserrat.lopez.mesas@uab.cat (M. López-Mesas).

http://dx.doi.org/10.1016/j.scitotenv.2023.164385
Received 21 March 2023; Received in revised form 16 May 2023; Accepted 20 May 2023
Available online 25 May 2023

obtained findings, the described process was applied to urine samples doped with Pt-CDs as analog of hospital wastewaters and the removal was very efficient, ranging from 72 ± 1 % to 95 ± 1 %, when using Si-Cys as adsorbent, although limited matrix effects were observed.

1. Introduction

Cisplatin (*cis*-diamminedichloroplatinum (II)) and carboplatin (1,1-cyclobutanedicarboxylatodiammineplatinum (II)), both well-known cytostatic agents, are administered intravenously to treat various types of cancers, including sarcomas, carcinomas, and germ cell tumors (Loehrer, 1984; Prestayko et al., 1979; Zamble and Lippard, 1995). Pharmacokinetic studies revealed that approximately 10–40 % of total Pt administered is excreted in the urine within 24 h, in the form of intact cisplatin which accounts for the majority of Pt excreted within 1 h of administration, or their metabolites and transformation products (Hann et al., 2003; Hoffmann-La Roche, 2020; Schmidt, 2019). These Pt compounds end up in hospital wastewater. Additionally, as a result of more frequent outpatient treatments, domestic discharge has become another considerable contribution of excreted Pt compounds, which is directly and inevitably discharged into municipal wastewater (Gouveia et al., 2023). Several studies, by means of advanced analytical methods, has shown the emergence of Pt-CDs in different water matrices (Ghafuri et al., 2018; Ghafuria et al., 2018; Isidori et al., 2016; Johnson et al., 2013; Kümmerer et al., 1999; Lenz et al., 2007a; Lenz et al., 2007b; Lenz et al., 2005; Roque-Diaz et al., 2021; Santana-Viera et al., 2020). European-wide investigations have found Pt compounds at concentrations ranging from tens of ng L^{-1} to a few hundred μg L^{-1} in hospital wastewaters (Ghafuria et al., 2018; Isidori et al., 2016; Kümmerer et al., 1999; Lenz et al., 2007a; Lenz et al., 2007b; Lenz et al., 2005; Santana-Viera et al., 2020; Vyas et al., 2014). Also, by analyzing samples from conventional wastewater treatment plants (WWTPs), it has been revealed that Pt concentration of municipal wastewater was one to three orders of magnitude lower than that of hospital wastewater (Ghafuri et al., 2018; Isidori et al., 2016; Santana-Viera et al., 2020). Through extensive dilution, it appears fortuitous that the concentration of Pt in surface waters remains consistently negligible and typically falls below the limit of detection (LODs), making its detection infrequent (Besse et al., 2012; Ghafuri et al., 2018; Isidori et al., 2016; Vyas et al., 2014). Regrettably, the hazardous Pt-CDs also have the potential to damage healthy cells within living organisms. The ecotoxicology and environmental risks of cisplatin or carboplatin have been assessed in recent years, and it can pose serious carcinogenic, teratogenic and mutagenic effects on exposed aquatic organisms (Araújo et al., 2019; Ghafuria et al., 2018; Heath and Isidori, 2020; Jureczko and Kalka, 2020; Li et al., 2021; Mišík et al., 2019; Queirós et al., 2021; Villarini et al., 2016; Yadav et al., 2021). In addition, the consequences of prolonged low-dose exposure might be underestimated and have not been fully characterized. Conventional WWTPs have been shown to be insufficient to effectively deal with this environmental threat due to the great challenges posed by the treatment of low-concentration Pt-CDs contaminated wastewater (Abdulbur-Alfakhoury et al., 2021; Heath and Isidori, 2020; Roque-Diaz et al., 2021).

This urgent environmental issue has raised concerns, and efforts have been made to explore potentially promising laboratory-scale treatments towards Pt-CDs contaminated wastewater (Roque-Diaz et al., 2021), including membrane bioreactor system (MBR) treatment (Lenz et al., 2007b), MBR coupled with adsorption and UV-treatment (Lenz et al., 2007a), and advanced oxidation process techniques (AOPs) (Hernández et al., 2008; Hirose et al., 2005; Kobayashi et al., 2008; Pieczyńska et al., 2017). Although these disposal methods have achieved certain effects, they are often accompanied by some shortcomings such as prolonged treatment time requirements, complicated installation and operation procedures, and high energy demands. Additionally, for example, after AOPs treatment, platinum by-products may still pose an environmental threat as heavy metal ions.

Compared with the aforementioned treatment methods, adsorption shows certain advantages over other technologies when considering the balance between economics, ease of operation and treatment efficiency. Moreover, adsorption demonstrates its applicability even at low concentrations of adsorbates, its capability in both batch and continuous processing modes, as well as the potential for recovery and regeneration of the adsorbent (Patel et al., 2019). Several adsorbent materials have been validated for their potential in the elimination of Pt-CDs (Dobrzynska et al., 2021; Farías et al., 2020; Folens et al., 2018; Fraguela et al., 2023; Lenz et al., 2005; Ogata et al., 2014). However, most of the previous adsorption experiments were carried out based on concentrations far higher than actual concentrations found in environments. For example, the newly reported low-cost adsorbent, Dithiocarbamate-Modified Silica (Fraguela et al., 2023), has achieved the effective removal of cisplatin in physiological conditions, but the study is based in concentration range > 5 mg L^{-1}. However, low Pt-CDs concentration will pose a challenge for efficient and fast adsorption, since small concentration gradients are insufficient to drive Pt compounds at the liquid-solid interface. Secondly, the reported adsorbents often require contact time of up to 24 h to reach equilibrium when adsorbing Pt compounds (Folens et al., 2018; Lenz et al., 2005; Ogata et al., 2014). The slow kinetic performance would not be conducive to scaling up the adsorption system to a column adsorption system and landing on a field application (Farías et al., 2020; Folens et al., 2018; Ogata et al., 2014). Some studies have initiated their adsorption investigations utilizing $PtCl_4^{2-}$ or $PtCl_6^{2-}$ as a preliminary model (Dobrzynska et al., 2021; Folens et al., 2018). However, it should be noted that the adsorption mechanism of these models may differ from that of the intended targets, and this aspect has been disregarded in said studies. For example, when adsorbents as biochar, chitosan, and granular activated carbon were used to adsorb cisplatin, carboplatin and oxaliplatin respectively, substantial differences from template $PtCl_6^{2-}$ in Pt recovery were already observed by authors (Folens et al., 2018). But these differences could not be well explained in detail. Interestingly, another material reported, Pt(II)-imprinted thiocyanato-functionalized SBA-15 (Dobrzynska et al., 2021) showed the similar removal effect as the template $PtCl_4^{2-}$ when adsorbing cisplatin, carboplatin and oxaliplatin but with achieving equilibrium in seven days. In conclusion, to address the above-mentioned issues, subsequent research needs to focus more on the adsorbents with strong affinity and high selectivity for Pt-CDs at trace concentrations in the environment. In turn, to achieve this goal, it is essential to explore and explain possible different adsorption mechanisms, especially in the face of diverse Pt-CDs.

This study first investigated the adsorption of cisplatin and carboplatin from aqueous solutions at trace concentrations typically present in real hospital wastewaters, using three commercially available adsorbents: cysteine-functionalized silica gel (Si-Cys), 3-(diethylenetriamino)propyl-functionalized silica gel (Si-DETA), and a derivatized open-celled MetalZorb® sponge (Sponge). Moreover, the adsorption of $PtCl_4^{2-}$, a compound with a structural similarity to cisplatin that has been widely utilized as a template in prior research, was also investigated for comparative purposes, with the differences in its intrinsic adsorption behavior being firstly elucidated. In detail, the influence of several parameters including pH, contact time, initial concentration, and temperature was studied.

2. Experimental methods

2.1. Materials

Potassium tetrachloroplatinate (II) (K_2PtCl_4, 99.9 %, CAS: 10025–99-7), diamminedichloroplatinum (II) (cisplatin, 99 %, CAS: 15663–27-1) and 1,1-cyclobutanedicarboxylatodiammineplatinum (II) (carboplatin,

99 %, CAS: 41575–94-4) were purchased from STREM Chemicals and were used without further purification. K_2PtCl_4, cisplatin and carboplatin stock solution (Pt concentration 100 mg L^{-1}) was initially prepared in 0.2 mol L^{-1} HCl respectively, and then diluted to the required concentration. Cysteine-functionalized silica gel (Si-Cys) and 3-(diethylenetriamino)propyl-functionalized silica gel (Si-DETA) were purchased from Sigma-Aldrich. MetalZorb® sponge (Sponge) was kindly supplied by CleanWay Environmental Partners, Inc. (Portland, USA). Details of the three commercial adsorbents are shown in Fig. S1(in Supplementary data). Milli-Q water (resistivity of 18.2 MΩ/m) was used throughout the entire experiment.

2.2. Preparation and characterization of adsorbents

Cube-shaped sponge (Fig. S1c, in Supplementary data) is an open-celled cellulose sponge that incorporates a water-insoluble polyamide chelating polymer formed by the reaction of polyethyleneimine and nitrilotriacetic acid. The sponge was claimed to contain free available ethyleneamine and iminodiacetate groups that could interact with heavy metals ions by ion exchange mechanism and chelation (Lou et al., 2022a; Lou et al., 2022b; Muñoz et al., 2002). These cubes were ground in a knife-milling commercial blender and sieved to a particle size of ≤0.5 mm. These fine sponge powders were washed with 1.0 mol L^{-1} HCl and Milli-Q water several times. Then the Sponge was dried at 80 °C for 24 h and stored for further studies.

To identify the functional groups of Si-Cys, Si-DETA, and Sponge, Fourier Transform Infrared Spectroscopy equipped with an Attenuated Total Reflectance module (ATR-FTIR, Tensor 27, Bruker, Germany) was used to record the FTIR spectra. The total content of C, H, N and S of three adsorbents was determined using element analyzer (Flash EA 2000 CHNS, Thermo Fisher, America). Brunauer-Emmett-Teller (BET) analysis results of Si-Cys and Si-DETA were provided by the manufacturer.

2.3. Batch adsorption

The adsorption of $PtCl_4^{2-}$, cisplatin and carboplatin was studied as a function of pH (pH 2–6, controlled by 0.1 mol L^{-1} HCl and/or 0.1 mol L^{-1} NaOH before, during, and after the adsorption, and monitored by pH meter, Crison, Spain), contact time (1–180 min), initial concentration (47 μg L^{-1} -1000 mg L^{-1}, all concentrations of Pt compounds are expressed as Pt), and solution temperature (293, 318 and 343 K). A series of batch adsorption experiments were performed in 10 mL plastic centrifuge tubes containing 10 mL of Pt solution (in form of $PtCl_4^{2-}$, cisplatin or carboplatin). After 50 mg of adsorbent was added, the tubes were agitated mechanically at 300 rpm at 293 K (except for thermodynamic studies). After 24 h (except for kinetic studies), the adsorbent in solution was filtrated using a 0.22 μm filter. The concentration of Pt in solutions was determined by Inductively Coupled Plasma Mass Spectrometry (ICP-MS, Thermo XSeries II, Thermo Scientific, USA).

The adsorption capacity q_e (μg g^{-1}) of Pt at equilibrium was calculated by the Eq. (1):

$$q_e = \frac{(c_0 - c_e)}{m} \times V \quad (1)$$

where c_0 and c_e (μg L^{-1}) are the initial and equilibrium concentrations of Pt solutions, respectively. V (mL) is the volume of solution and m (mg) is the adsorbent dosage. For kinetic studies, the concentration at equilibrium is replaced by the concentration at different contact time, c_t (μg L^{-1}), calculating the adsorption capacity q_t (μg g^{-1}).

Then the removal ratios were calculated according to Eq. (2):

$$\text{Removal ratio} = \frac{(c_0 - c_e)}{c_0} \times 100\% \quad (2)$$

All the experiments were conducted in triplicated, and the average values and the relative standard deviation were calculated.

2.4. Adsorption kinetic and isotherm modeling

To further understand the Pt adsorption behavior, kinetic models including pseudo-first-order model (PFOM) and pseudo-second-order model (PSOM) were used to fit the adsorption data collected at different contact time, while data obtained from different initial concentration were fitted with Langmuir and Freundlich isotherm models. The adsorption kinetic and isotherm equations are described in Supplementary data.

2.5. Experimental validation of the removal of Pt-CDs in wastewater analog samples

To validate the feasibility and efficiency of the Pt-CDs removal, experiments were carried out by using urine samples doped with Pt-CDs as hospital wastewater analogs. To this purpose, and due to the difficulty of obtaining hospital samples, hospital wastewater analogs were prepared from anonymous urine samples obtained from a healthy male spiked with cisplatin and carboplatin at the level of reported excreted in urine of patients undergoing chemotherapy (cisplatin concentration from 312.39 μg L^{-1} to 114.81 mg L^{-1}) (Jantarat et al., 2021). Then, these samples were diluted ten and 100-fold to account for typical conditions in hospital wastewaters. Ion chromatography (Dionex Aquion, Thermo Scientific, America) was employed to determine the concentration of typical anions and cations in urine and two wastewater analogs, and details are described in Supplementary data. Experiments were carried out by contacting the prepared analog samples with the adsorbent Si-Cys in the same conditions as explained when using the synthetic Pt-CDs solutions. Thus, 10 mL of the resulting Pt-spiked urine samples were then respectively mixed with 50 mg of the selected adsorbent (stirred for 24 h, T = 343 K, pH 2) and were collected using sterile plastic bottles after filtration using 0.22 μm filters. The samples were immediately quantified using a standard analytical method described elsewhere (Flores et al., 2011; Gao et al., 2012). In our case, analog samples aliquots (100 μL) were equilibrated to room temperature and digested using 200 μL of nitric acid (69.0–70.0 %, for trace metal analysis) at 363 K for 1 h. The digested samples were then diluted to 10 mL with Milli-Q water to a final concentration of 2 % v/v HNO_3. These solutions were instantly subjected to ICP-MS analysis with external calibration ranging from 1 to 150 μg L^{-1} (Rh and Y as internal standard elements). The calculation of removal ratio was according to Eq. (2).

3. Results and discussion

3.1. Characterization of adsorbents

The FTIR test was performed on Si-Cys, Si-DETA, and Sponge, showing the spectra observed in Fig. 1. The spectra of Si-Cys and Si-DETA are very similar, and the characteristic peaks mainly correspond to the properties of silica. Absorption bands at 1051 cm^{-1} and 795 cm^{-1} arise from asymmetric vibration of Si-O-Si and symmetric vibration of Si-O-Si, respectively (Grumezescu et al., 2014). The peaks at 2973 cm^{-1} and 2900 cm^{-1} represent the C—H stretching vibration of the alkyl groups. The broad band at around 3273 cm^{-1} was assigned to N—H stretching of amine, which was relatively weak due to low load rate of cysteine and 3-(diethylenetriamino) propyl groups. Then, the band appears at 1615 cm^{-1} for Si-Cys representing C═O stretching vibration. For Sponge, the absorbances at 3435, 2891, 1365, 1157, and 1024 cm^{-1} are associated with cellulose substrate (Li et al., 2009). A strong band 3435 cm^{-1} originates from the O—H stretching. The peak at 2891 cm^{-1} is attributed to the stretching vibration of alkane C—H. The absorption at 1365 cm^{-1} is due to O—H bending and that at 1157 cm^{-1} corresponds to C-O-C antisymmetric bridge stretching. The strong peak at 1024 cm^{-1} can be assigned to C-O-C pyranose ring skeletal vibration. Besides, the surface polyamide chelating polymer contributes to the strong band at around 3317 cm^{-1} due to the N—H stretching. The peak at 1637 cm^{-1} is related to the C═O stretching vibration and the rightward shift of the peak coincides with the amide structure (electron-donating property of nitrogen). These findings are consistent with

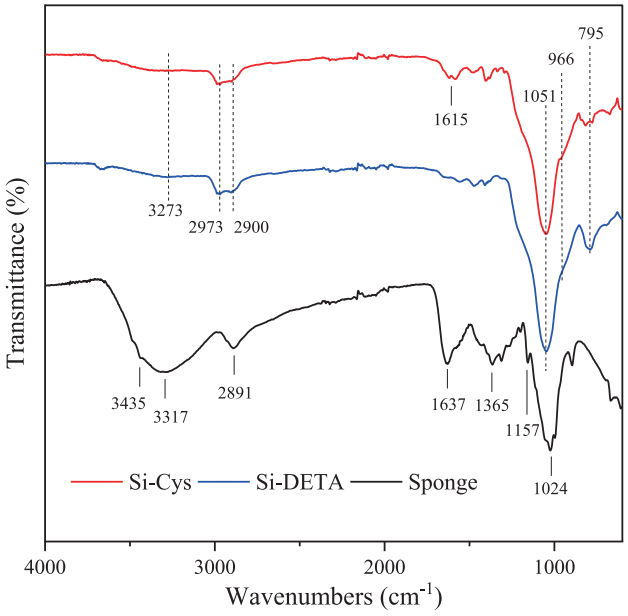

Fig. 1. FTIR spectra of Si-Cys, Si-DETA, and Sponge.

the interpretation of the chemical structure of the different adsorbents, shown in Fig. S1(in Supplementary data).

BET analysis and elemental analysis (EA) results are summarized in Table S1 and Table S2 (in Supplementary data), respectively. The EA analysis conducted confirmed the existence of the respective functional groups in the three adsorbents, which aligns with the FTIR findings and uphold the claims made by the manufacturers.

3.2. Adsorption experiments

3.2.1. Effect of solution pH on adsorption

The pH is one of the key factors that determine the interaction between adsorbate and adsorbent as it can change the protonation state of surface functional groups, thereby changing the surface charge, which in turn affects the adsorption performance. For adsorption of $PtCl_4^{2-}$ (Fig. 2a), the pH dependences of the three materials are very different. The adsorption capacity of Si-Cys decreased considerably from 45 ± 1 to 19 ± 4 μg g^{-1} as pH increased from 2 to 6. As implied in Fig. 3a, after dilution from Pt stock (in 0.2 mol L^{-1} HCl), the Cl ligands are gradually displaced by H_2O to give the aqua complexes (like $PtCl_3(H_2O)^-$). And at low pH values, the amino groups were protonated, which made the adsorbent to be positively charged. The protonation facilitated Si-Cys to attract anionic $PtCl_4^{2-}$ and/or $PtCl_3(H_2O)^-$ through ion association, concomitantly, Pt gradually chelated with the S sites and the N sites (even with low affinity). However, when the pH kept increasing, the carboxyl group, thiol group and protonated amine group sequentially deprotonated, which eventually caused Si-Cys to be negatively charged. Due to electrostatic repulsion, parts of $PtCl_4^{2-}$ and/or $PtCl_3(H_2O)^-$ molecules were repelled, as a result, there was a significant decrease in the adsorption capacity. Meanwhile, however, the changing of adsorption capacity with increasing pH was moderated when Si-DETA was studied, adsorption capacity of Si-DETA dropped slightly from 48 ± 1 to 42 ± 1 μg g^{-1} in the same range of pH. The elevation of pH levels induced deprotonation of amine groups in Si-DETA, resulting in a reduction of its positive charge density. As a consequence, the effectiveness of electrostatic attraction-assisted adsorption was moderately diminished. The effect of pH on the adsorption of $PtCl_4^{2-}$ to Sponge is almost negligible.

For cisplatin (Fig. 2b) and carboplatin (Fig. 2c), the adsorption capacities were overall lower than that of $PtCl_4^{2-}$ and slightly affected by pH changes, since facing cisplatin and carboplatin (neutral molecules) as well as their hydrated complexes (non-anionic molecules) electrostatic attraction did not contribute to the adsorption. Regarding the adsorbents, Si-Cys has higher adsorption capacities of cisplatin and carboplatin than Si-DETA and Sponge due to the presence of thiol groups in Si-Cys. According to HSAB theory (Bugarčić et al., 2012), Pt(II) as a "soft" acid has a high affinity for sulfur donors ("soft" bases) *e.g.* thiols and thioethers. For example, it is assumed that most of Pt-CDs bind to glutathione and L-cysteine in intracellular liquid forming stable compounds before it reaches DNA (Bugarčić et al., 2012; Reedijk, 2009; Reedijk, 1999). This suggests that in chelation-dominated chemisorption (Fig. 3b and c), thiol groups provide more chelation sites for the complexation of cisplatin and carboplatin.

In addition, it is worth mentioning here that the influence of the alkaline environment is not considered, because the chemical structures of $PtCl_4^{2-}$, cisplatin and carboplatin are not stable when the pH exceeds 6. Black precipitation appeared in both stocks prepared by directly dissolving compounds in water at pH > 6, due to the oxidation of Pt.

3.2.2. Adsorption kinetics analysis

Kinetic is an important index to evaluate the removal efficiency and mechanism of the adsorption process, that is a key knowledge to scale up the Pt-CDs removal to industrial application. Fig. 4A and a give the adsorption kinetic curves of $PtCl_4^{2-}$ onto Si-Cys, Si-DETA, and Sponge. It is shown a fast adsorption kinetics for all the three materials. The adsorption capacities rose sharply within the first few minutes, because there are rich effective adsorption sites on the surface of Si-Cys, Si-DETA, and Sponge at the beginning of the adsorption process. Then the growth gradually slowed down until reaching the adsorption equilibrium after approximately 40 min, as the amounts of available active sites gradually decreased, leading to a decrease in the adsorption rate. However, despite of the fast kinetics, the adsorption of cisplatin and carboplatin still exhibited disadvantages if compared to that of $PtCl_4^{2-}$(see in Fig. 4). The removal rate of Si-DETA and Sponge for cisplatin was only 32 ± 2 % and 38 ± 3 % (while 9 ± 1 % and 10 ± 2 % for carboplatin), compared to 90 ± 1 % and 83 ± 3 % for $PtCl_4^{2-}$. This confirmed the inference in the previous section that the adsorption was frustrated due to the lack of thiol groups to provide complexation sites. In addition, carboplatin showed worse adsorption performance, which was caused by its low hydrolysis rate. Meanwhile, the removal rate of Si-Cys also slightly decreased from 92 ± 1 % for $PtCl_4^{2-}$ to 74 ± 1 % for cisplatin and 73 ± 1 % for carboplatin, indicating that electrostatic adsorption probably did not play a role in adsorbing cisplatin and carboplatin molecules.

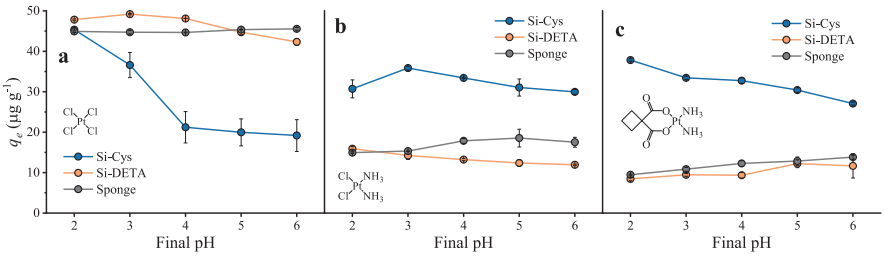

Fig. 2. The effect of solution pH on the adsorption capacity of (a) $PtCl_4^{2-}$, (b) cisplatin and (c) carboplatin [adsorbent dosage: 50 mg, solution volume: 10 mL, Pt concentration: 235 μg L^{-1}, T: 293 K].

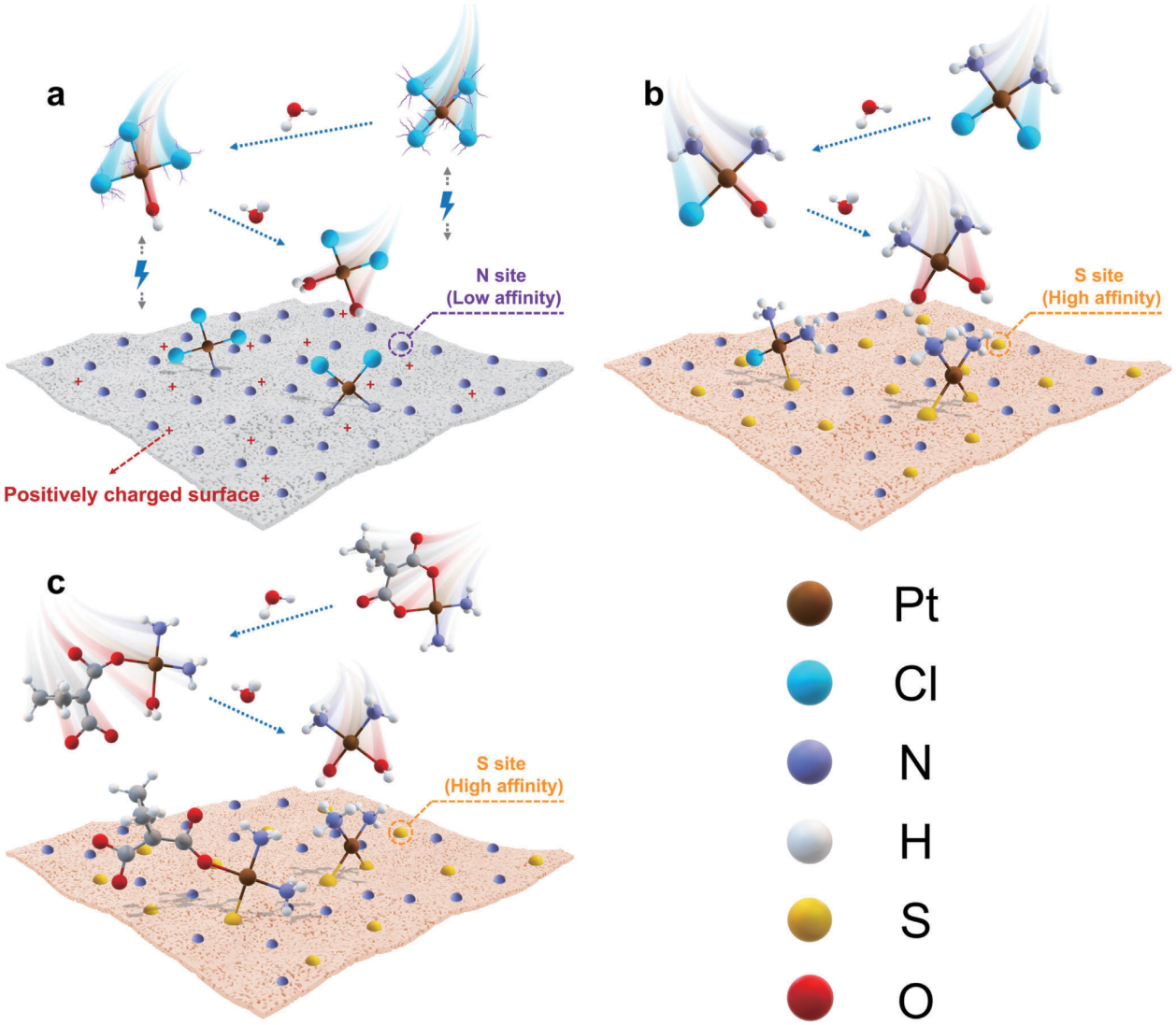

Fig. 3. The difference in adsorption mechanism between (a) $PtCl_4^{2-}$, ion association enhanced adsorption to amino-rich adsorbent surface (adsorption to Si-Cys containing thiol group is omitted here); (b) cisplatin and (c) carboplatin chelation dominant adsorption to thiol-containing Si-Cys surface.

The kinetics fitting curves are also plotted in Fig. 4. As indicated by the correlation coefficients R^2 summarized in Table S3 (in Supplementary data), PSOM fitted better than PFOM. As is known PSOM assumes that the rate-limiting step may be chemisorption involving valance forces through sharing or exchanging electrons between adsorbate and adsorbent (Feiqiang et al., 2018; Mohan et al., 2011; Sen Gupta and Bhattacharyya, 2011). Specifically, this is consistent with the ion-association between the $PtCl_4^{2-}$ anion and the protonated amine group, and the complexation between Pt and surface functional groups such as thiol, amino and carboxyl groups. Furthermore, it has been reported that the PFOM is more suitable for the description of the initial stage in which the external/internal diffusion is the rate controlling step, and the initial concentration of adsorbate is usually high (Feiqiang et al., 2018; Wang and Guo, 2020a). However, the initial concentration of the target Pt compounds here was as low as 235 μg L^{-1}, and the adsorbents are abundant with active sites, therefore, the adsorption kinetics are dominated by the adsorption onto active site as PSOM expected.

3.2.3. Adsorption isotherms analysis

Adsorption isotherm reveals the relationship between the adsorbate concentration in the liquid and solid phases when the adsorption process reaches equilibrium. Adsorption capacities mounted with the increase of the initial concentration of $PtCl_4^{2-}$, cisplatin and carboplatin solution (see in Fig. 5), which may be due to the higher concentration gradient at the solid-liquid interface. The mass transfer of $PtCl_4^{2-}$, cisplatin and carboplatin towards the surface of adsorbents could be driven by the concentration gradient, which satisfied the generalized Fick Law (Chinh et al., 2019; Han et al., 2021). It can be seen from Fig. 5A that the maximum adsorption capacity of Si-DETA (169 ± 6 mg g^{-1}) to $PtCl_4^{2-}$ is greater than that of Si-Cys (131 ± 1 mg g^{-1}), due to the different loading rates of their respective functional groups, -Cys (0.3 mmol g^{-1}) and -DETA (1.3 mmol g^{-1}) (provided by the manufacturer, see Fig. S1a and S1b, in Supplementary data). Moreover, the adsorption of $PtCl_4^{2-}$ surpasses that of the other two Pt compounds, ascribed to the complementary effect of electrostatic adsorption and Van der Waals force, alongside the presence of ligands (Cl) that readily detach from the molecule. Cisplatin and carboplatin contain two inert NH_3 ligands which makes complexation to the adsorbent surface more difficult. This predicament is slightly alleviated when Si-Cys containing thiol functional groups were used to adsorb cisplatin and carboplatin.

The isotherm fitting curves are also plotted in Fig. 5, and parameters derived from models are summarized in Table S4 (in Supplementary data). Langmuir model represents satisfactorily the adsorption process with high

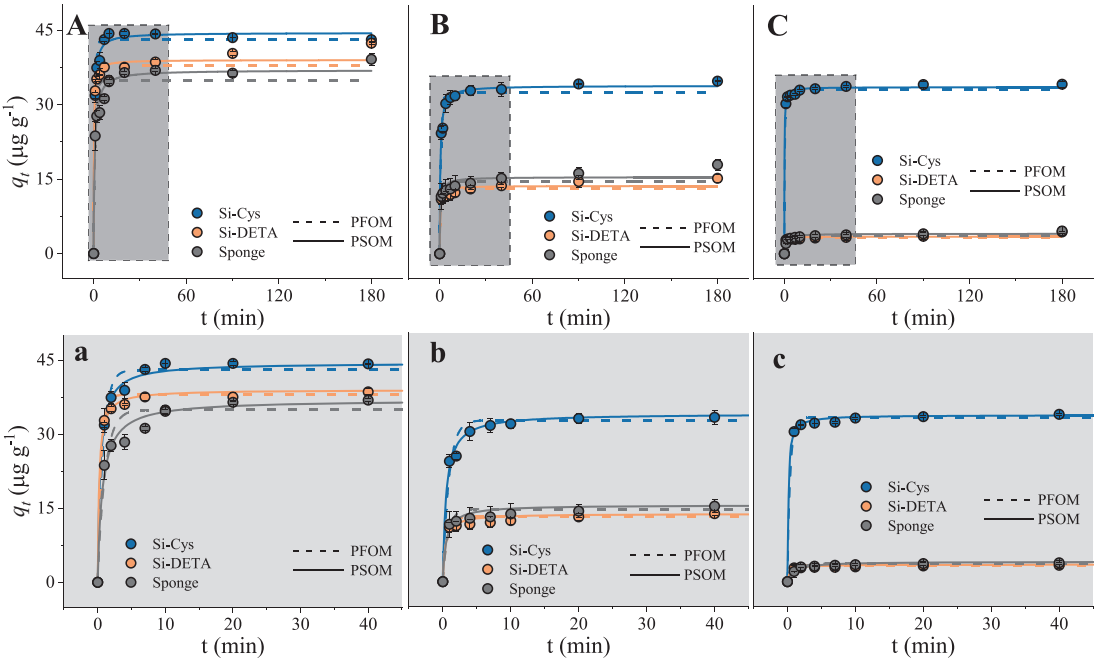

Fig. 4. The effect of contact time on the adsorption capacity of (A) $PtCl_4^{2-}$, (B) cisplatin and (C) carboplatin [adsorbent dosage: 50 mg, solution volume: 10 mL, Solution pH = 2 for Si-Cys and Si-DETA, solution pH = 3 for Sponge, Pt concentration: 235 μg L^{-1}, T: 293 K] and kinetic models fitting. The lowercase figures (gray background) are the enlarged interval (0–40 min).

coefficients of determination ($R^2 > 0.92$) and gives a better fit than Freundlich model only except for Si-Cys adsorption of cisplatin and Si-DETA adsorption of carboplatin (while Freundlich model fit is slightly better). The results indicate that the adsorption of three Pt compounds by all adsorbents takes place in a monolayer adsorption manner. In addition, the adsorption (Fig. 5a-c) in the low concentration range obeys the linear

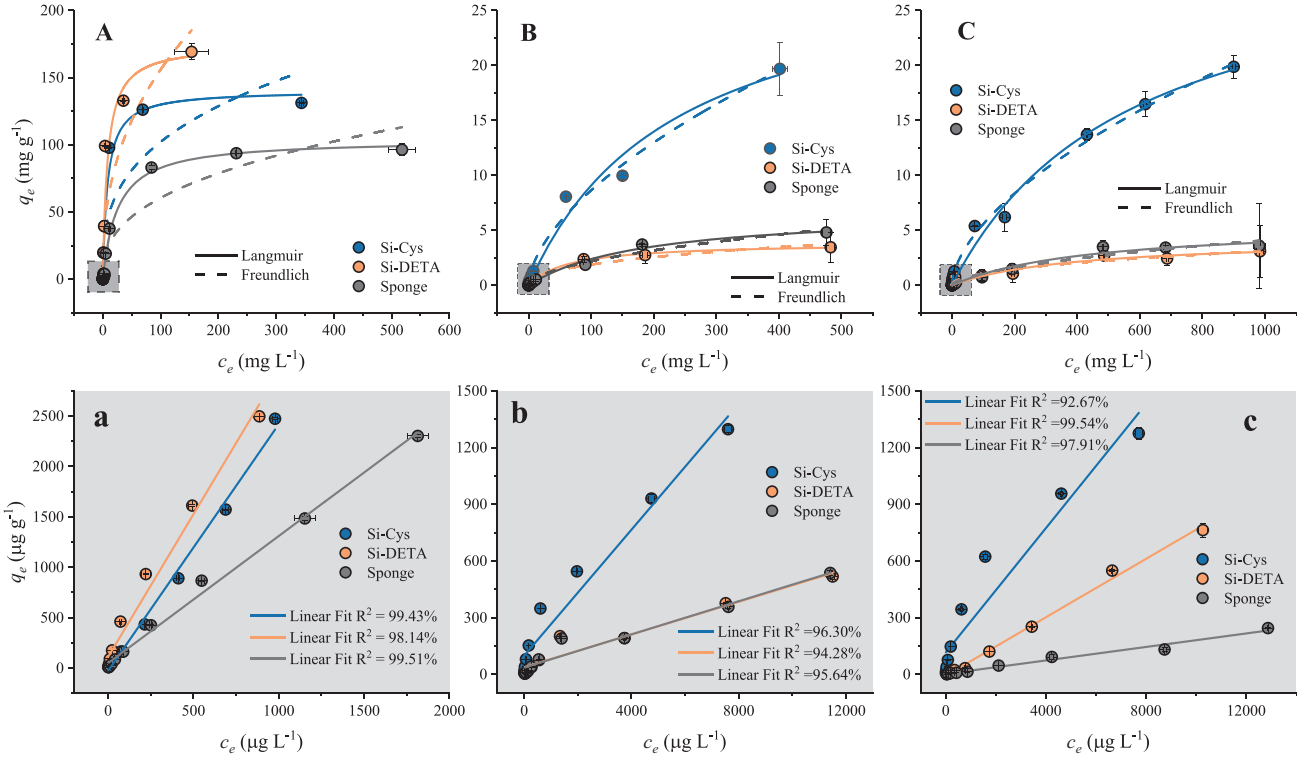

Fig. 5. Adsorption equilibriums of (A) $PtCl_4^{2-}$, (B) cisplatin and (C) carboplatin [adsorbent dosage: 50 mg; solution volume: 10 mL; initial concentration: maximum 1000 mg L^{-1} of $PtCl_4^{2-}$ and carboplatin, 500 mg L^{-1} of cisplatin because of low solubility; solution pH = 2 for Si-Cys and Si-DETA, solution pH = 3 for Sponge; contact time 24 h; T: 293 K] and isotherm models fitting. The lowercase figures (gray background) are the enlarged interval (initial concentration 47–14,100 μg L^{-1}).

model (Henry's law), which also illustrates the monolayer adsorption behavior with low coverage (Wang and Guo, 2020b). From the data listed in Table S4 (in Supplementary data), all the Langmuir separation factor R_L fell into 0 to 1 within the concentration range investigated. It proves that all Pt adsorptions towards three materials are favorable. The theoretical maximum adsorption q_m predicted by the Langmuir model is close to but slightly higher than the actual maximum adsorption capacity obtained in the experiment. Regarding the Freundlich constant, all adsorption processes are favorable as the value of $1/n < 1$.

3.2.4. Thermodynamics of adsorption processes

Experimental thermodynamic analysis was performed under different temperatures to further understand the adsorption behavior. For $PtCl_4^{2-}$ (see in Fig. 6A), with the increase of adsorption temperature (from 293 to 343 K), the adsorption capacities of Si-Cys, Si-DETA, and Sponge all decreased slightly. Then when initial concentrations doubled to 470 μg L^{-1}, the decline was more obvious (see in Fig. 6a). As illustrated in Fig. 3a, the adsorption of anionic $PtCl_4^{2-}$ was dominated by physical adsorption such as electrostatic attraction and Van der Waals forces. Specifically, the weak binding between $PtCl_4^{2-}$ and adsorbents surface caused by Van der Waals interactions, which are always present in adsorption processes (Veclani et al., 2020), were easily undermined as the solutions were heated up to 343 K. In comparison, the adsorption of cisplatin is much more complicated. As shown in Fig. 6B and b, the adsorption capacities of Si-Cys to cisplatin were greatly promoted when temperature was increased, and the removal rates almost reached the theoretical maximum at 343 K (98.5 ± 0.1 % and 97.5 ± 0.5 % for initial concentration of 235 and 470 μg L^{-1}, respectively). The adsorption process of carboplatin also showed a similar pattern. This implied that the chemisorption dominated by chelation was a thermophilic process, and the complexation between Pt and S from the thiol group was facilitated at higher temperatures during the process. However, for the other two adsorbents, Si-DETA and Sponge, the adsorption capacities of them for cisplatin and carboplatin were not only much lower than that of Si-Cys (electrostatic adsorption was ineffective for neutral cisplatin or carboplatin, and the complexation of Pt—N was weaker), they also showed a trend of increasing and then decreasing during the warming process (see in Fig. 6B,C and 6b,c). For instance, when the temperature increased from 293 K to 318 K, adsorption capacities of cisplatin on Si-DETA and Sponge generally increased (except for the adsorption of Si-DETA in Fig. 6b, which adsorption decreased by a very small amount of 1.66 μg L^{-1}), which was due to the high temperature promoting to some extent the complexation of Pt with the amine functional groups on the surface of Si-DETA and Sponge. However, as explained before, this complexation was very limited because of the fact that N is a "hard" base and its bonding with the "soft" acid Pt is not favored. Therefore, when the temperature continued to increase up to 343 K, the decline brought by the frustrated Van der Waals adsorption came to the fore.

Furthermore, three thermodynamic parameters including Gibbs free energy ($\Delta G°$), enthalpy change ($\Delta H°$), and entropy change ($\Delta S°$) were calculated by equations described in Supplementary data. Results are listed in Table S5 (also in Supplementary data).

As seen in Table S5, $PtCl_4^{2-}$ adsorption is a spontaneous process with negative $\Delta G°$. It can be seen from the comparison of $\Delta H°$ that the adsorption of $PtCl_4^{2-}$ by Si-Cys was very different from that of cisplatin or carboplatin. First, as can be determined from the positive value of $\Delta H°$, the adsorption of cisplatin or carboplatin is endothermic reaction (while that of $PtCl_4^{2-}$ is exothermic). Additionally, cisplatin has an enthalpy value ($\Delta H° = 44 \pm 7$ kJ mol^{-1}) approximately twice as high as the $\Delta H°$ of $PtCl_4^{2-}$ ($\Delta H° = -23 \pm 6$ kJ mol^{-1}), which corroborates the dominance of chemisorption in the adsorption of cisplatin by Si-Cys. It can be recognized that temperature promoted bonding of Pt—S, and enthalpy change of this process was incontrovertibly higher than that involved in physisorption. In addition, the entropy changes of Si-Cys in the process of adsorbing $PtCl_4^{2-}$ and other two Pt-CDs are also diametrically opposite. Negative values of $\Delta S°$ indicated an increase in the order of the system during the adsorption process of $PtCl_4^{2-}$ at solid-liquid interface, while positive $\Delta S°$ suggested an increase of the degrees of freedom when cisplatin and carboplatin was adsorbed on Si-Cys.

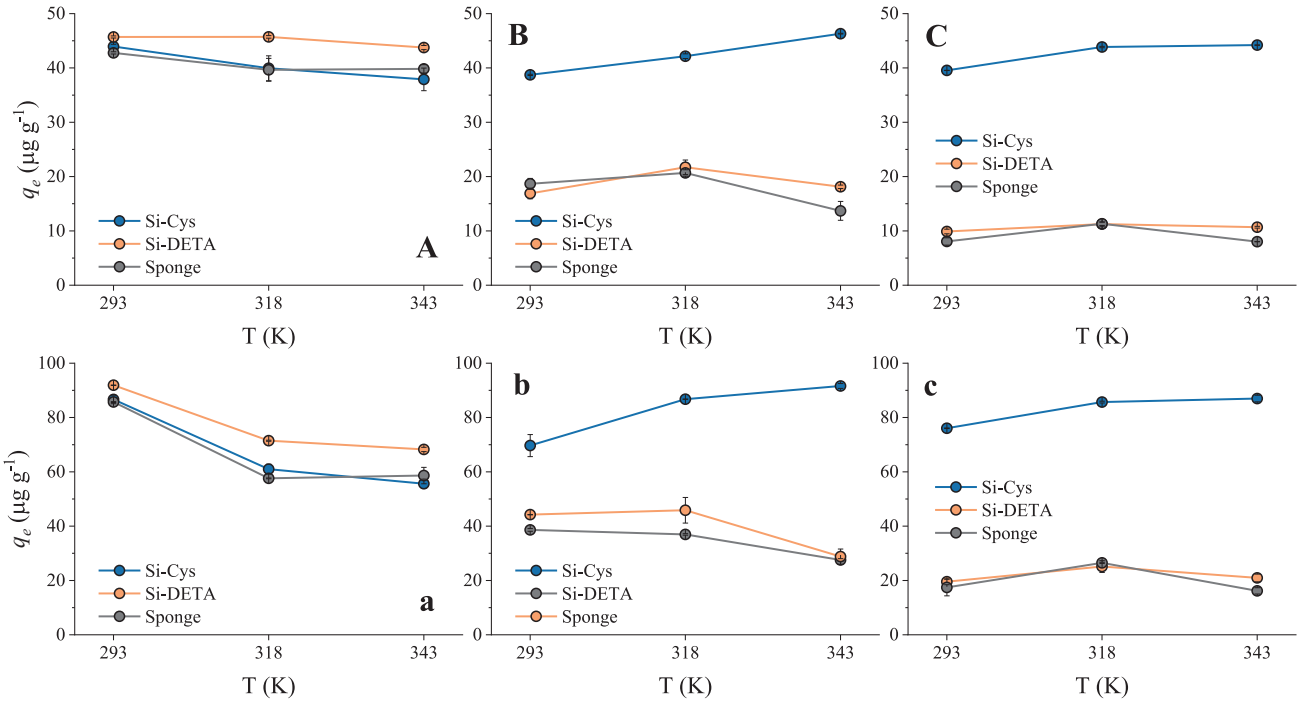

Fig. 6. The effect of temperature on the adsorption capacity of $PtCl_4^{2-}$, Pt concentration: (A) 235 μg L^{-1} and (a) 470 μg L^{-1}; cisplatin, Pt concentration: (B) 235 μg L^{-1} and (b) 470 μg L^{-1}; carboplatin, Pt concentration: (C) 235 μg L^{-1} and (c) 470 μg L^{-1}. [adsorbent dosage: 50 mg, solution volume: 10 mL, contact time: 24 h, Solution pH = 2 for Si-Cys and Si-DETA, solution pH = 3 for Sponge].

3.3. Experimental validation of the removal of Pt-CDs in wastewater analog samples

The results of the removal of Pt-CDs in wastewater analog samples are depicted in Fig. 7, and the characteristics of urine and wastewater analogs are summarized in Table S6 (in Supplementary data). It can be observed by comparing Fig. 7a and b, the Si-Cys adsorption towards the two targets generally achieved similar removal rates, which are from 72 ± 1 % to 95 ± 1 % for cisplatin and from 75 ± 1 % to 95 ± 1 % for carboplatin. The removal was found to be less efficient for low concentrations of cisplatin and carboplatin in undiluted urine samples, likely due to the complexity of the urine matrix (as Table S6 shows). Furthermore, the observed removal of Pt-CDs in simulated wastewaters was consistently lower than that in Milli-Q water. This disparity may be attributed to the matrix effect that arises from the presence of urine and tap water. One of its interferences may be derived from the trace protein contained in urine such as Tamm-Horsfall protein (Aitekenov et al., 2021; Micanovic et al., 2020), which contains cystines sites that pre-chelated part of cisplatin and carboplatin. Secondly, the ligands replacement of cisplatin and carboplatin could be disturbed due to the presence of components such as Cl^- and NH_4^+ in urine matrix, which were significantly more abundant than Pt-CDs as indicated in the Table S6, thus the complexation of Pt to the Si-Cys surface was also affected (Guo et al., 2020). In addition, co-existing ions such as Na^+, K^+, Ca^{2+} and so on (several to thousands of mg L^{-1}) present in urine posed additional competition for active binding therefore slightly inhibited the capture of cisplatin and carboplatin (Curtis et al., 2010). For the undiluted samples, the Pt species had more competitive advantages when the initial concentration was increased to 57 or 115 mg L^{-1}, hence the removal rates increased significantly driven by the high concentration gradients. The interference from matrix effects diminished gradually with more dilution of urine, almost all removals reached the maximum (92 ± 1 % - 95 ± 1 %) when adsorptions were carried out in 100-fold diluted urine samples. The only exception occurred in the adsorption of spiked low-concentration Pt from urine. When the urine samples were further diluted from ten times to 100 times, the removal rate decreased unexpectedly. However, the initial Pt concentration was as low as only 3.12 μg L^{-1}, which may predict the ineffective capture of Pt molecules at such a low concentration. Perhaps longer time or higher temperature can guarantee more Pt—S complexation formed for ideal adsorption.

Then when the mixture of cisplatin and carboplatin was adsorbed from 100-fold diluted urine, as shown in Fig. 7c, around 95 % of Pt was effectively removed. The removal of Pt-CDs from 100-fold diluted urine is comparable to that from Milli-Q water, albeit slightly lower.

3.4. Comparison of the adsorption performance with current knowledge

The adsorption efficiency of Si-Cys for cisplatin and carboplatin was compared with other published adsorbents and listed in Table 1. It is

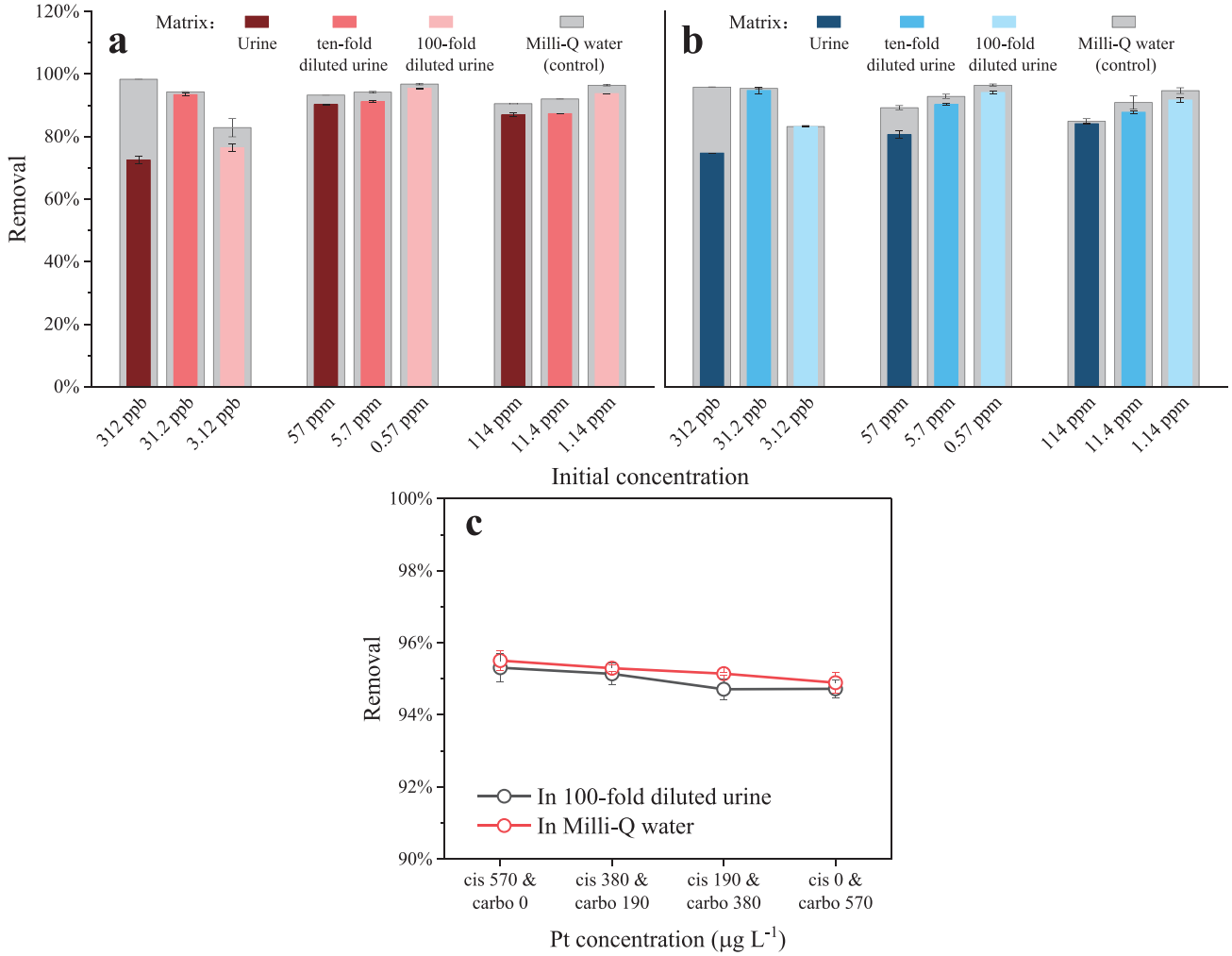

Fig. 7. Removal of (a) cisplatin and (b) carboplatin from spiked urine samples, its ten-fold diluted and 100-fold diluted matrices; (c) mixture of cisplatin and carboplatin from 100-fold diluted urine.

Table 1
Comparison of Pt-CDs removal by Si-Cys to adsorbents previously reported.

Adsorbent	Target Pt compound	Contact time (h)	Dosage (g L^{-1})	Treatment effect	Ref.
Si-Cys	Cisplatin (235 μg L^{-1} Pt) Carboplatin (235 μg L^{-1} Pt)	40 min	5.0	98.5 ± 0.1 % removal 94.1 ± 0.1 % removal	This study
Activated sludge	Cisplatin (6.5 μg L^{-1} Pt) Carboplatin (5.3 μg L^{-1} Pt) Oxaliplatin (4.9 μg L^{-1} Pt)	24	4.2	96 % removal 70 % removal 74 % removal	(Lenz et al., 2005)
Biomass-derived adsorbents (chitosan, biochar, wood ash, activated carbon)	$PtCl_6^{2-}$ as model (1–10 mg L^{-1} Pt)	24	10.0	Adsorption capacity 0.23–0.97 mg g^{-1}	(Folens et al., 2018)
Calcination of gibbsite	Cisplatin (10 mg L^{-1} Pt)	24	6.0	Adsorption capacity 1.5 mg g^{-1}	(Ogata et al., 2014)
Macroporous cryogels (by polymerization of methacrylic acid and 2-hydroxyethyl methacrylate)	Cisplatin (250–2000 mg L^{-1})	1–48	0.5 & 2.0	Adsorption capacity up to 150 mg g^{-1}	(Farías et al., 2020)
Pt (II)-imprinted thiocyanato-functionalized SBA-15 materials	$PtCl_4^{2-}$ as model (100 mg L^{-1} Pt)	5	5.0	Adsorption capacity 76.4 mg g^{-1}	(Dobrzynska et al., 2021)
Dithiocarbamate-Modified Silica	Cisplatin (10 mg L^{-1})	0.25–2	1–10	Adsorption capacity 15.6 mg g^{-1} with 1 mg mL^{-1}. Removal up to 85 % with 10 mg L^{-1}. 1 h contact time	(Fraguela et al., 2023)

evident that Si-Cys achieved maximum removal of 98.5 ± 0.1 % and 94.1 ± 0.1 % for cisplatin and carboplatin, respectively. Moreover, it was achieved at a low concentration of 235 μg L^{-1}, which is close to the environmental concentrations. Although activated sludge (Lenz et al., 2005) also exhibited good removal efficiency at low concentrations, the disadvantage of slow kinetics required a long processing time of up to 24 h. While it is acknowledged that novel adsorbents like macroporous cryogels (Farías et al., 2020) and Pt (II)-imprinted thiocyanato-functionalized SBA-15 (Dobrzynska et al., 2021) demonstrated outstanding adsorption capacity, their adsorption was performed at concentrations far higher than the actual environmental concentrations, and their removal efficiency for trace Pt-CDs remains unknown.

4. Conclusions

This study presents a comparative investigation of the adsorption behavior of trace cisplatin, carboplatin, and $PtCl_4^{2-}$ onto three different adsorbents, including studies on pH effect, adsorption kinetics, adsorption isotherms, and thermodynamic studies. Distinct adsorption mechanisms of each Pt compounds were revealed. The major findings of this study can be summarized as follows: (1) All three adsorbents exhibited a significant removal of anionic $PtCl_4^{2-}$ (>90 %) compared to cisplatin and carboplatin due to the assistance of electrostatic adsorption, however, the adsorption of $PtCl_4^{2-}$ is more pH dependent. Therefore, $PtCl_4^{2-}$ should be cautiously considered as a template for Pt-CDs, despite of structural similarity. (2) Si-Cys, containing thiol groups, exhibited a remarkable removal efficiency of cisplatin (maximum 76 ± 1 %), which is significantly higher than that of Si-DETA (maximum 34 ± 1 %) and Sponge (maximum 40 ± 5 %). And this similar contrast was also shown in the adsorption of carboplatin. It indicates the adsorption of cisplatin and carboplatin highly depends on the complexation with high-affinity thiol sites. (3) All the observed adsorption processes conform to the PSOM and Langmuir model descriptions, indicative of a monolayer chemisorption process. (4) The adsorption of cisplatin and carboplatin onto Si-Cys is an endothermic process (different from exothermic adsorption of $PtCl_4^{2-}$), as Pt—S binding is thermally favored. As a result, the removal of cisplatin and carboplatin onto Si-Cys reached 98.5 ± 0.1 % and 94.1 ± 0.1 %, respectively, when increasing the temperature up to 343 K. (5) The finding of treatment of Pt-spiked urine found that thiol-containing Si-Cys can be used to treat cisplatin and/or carboplatin-contained patient urine and hospital wastewater contaminated by it. In summary, our work provided ideas for the treatment of Pt-CDs contaminated wastewater and offered a strategy for dealing with this emerging and continuously deteriorating environmental threat that has been always neglected.

CRediT authorship contribution statement

Dong Han: Conceptualization, Methodology, Validation, Formal analysis, Investigation, Writing – original draft, Visualization. **Montserrat López-Mesas:** Conceptualization, Methodology, Resources, Writing – review & editing, Supervision, Project administration. **Markel Luaces:** Validation, Investigation, Writing – review & editing. **Yusleydi Enamorado:** Validation, Investigation, Writing – review & editing. **Martina Sanadar:** Methodology, Resources, Writing – review & editing. **Andrea Melchior:** Conceptualization, Methodology, Resources, Supervision, Writing – review & editing. **Manuel Valiente:** Conceptualization, Methodology, Resources, Project administration, Supervision, Funding acquisition.

Data availability

Data will be made available on request.

Declaration of competing interest

The authors declare that they have no known competing financial interests or personal relationships that could have appeared to influence the work reported in this paper.

Acknowledgements

This work has been developed in the framework of the European Community's H2020 Program H2020-MSCA-RISE 2017 under the project RECOPHARMA (grant agreement #778266). D. Han acknowledges COST action 18202, "Network for Equilibria and Chemical Thermodynamics Advanced Research" (NECTAR) for supporting a STSM in Udine and the program of China Scholarships Council (No. 201906450024). The authors would also like to thank Júlia Senyé Lacher, Tania Farías, Ana Rosa Lazo Fraga and Raquel Cantero Rodriguez for supporting in the experiment. Open Access funding provided thanks to the agreement CRUE-CSIC with Elsevier.

Appendix A. Supplementary data

Supplementary data to this article can be found online at https://doi.org/10.1016/j.scitotenv.2023.164385.

References

Abdulbur-Alfakhoury, E., Trommetter, G., Brion, N., Dumoulin, D., Reichstädter, M., Billon, G., Leermakers, M., Baeyens, W., 2021. Distribution of platinum (Pt), palladium (Pd), and rhodium (Rh) in urban tributaries of the Scheldt River assessed by diffusive gradients in thin films technique (DGT). Sci. Total Environ. 784, 147075. https://doi.org/10.1016/j.scitotenv.2021.147075.

Aitekenov, S., Gaipov, A., Bukasov, R., 2021. Review: detection and quantification of proteins in human urine. Talanta 223, 121718. https://doi.org/10.1016/j.talanta.2020.121718.

Araújo, A.P. da C., Mesak, C., Montalvão, M.F., Freitas, Í.N., Chagas, T.Q., Malafaia, G., 2019. Anti-cancer drugs in aquatic environment can cause cancer: insight about mutagenicity in tadpoles. Sci. Total Environ. 650, 2284–2293. https://doi.org/10.1016/J.SCITOTENV.2018.09.373.

Besse, J.P., Latour, J.F., Garric, J., 2012. Anticancer drugs in surface waters. What can we say about the occurrence and environmental significance of cytotoxic, cytostatic and endocrine therapy drugs? Environ. Int. 39, 73–86. https://doi.org/10.1016/j.envint.2011.10.002.

Bugarčić, Ž.D., Bogojeski, J., Petrović, B., Hochreuther, S., van Eldik, R., 2012. Mechanistic studies on the reactions of platinum(ii) complexes with nitrogen- and sulfur-donor biomolecules. Dalton Trans. 41, 12329. https://doi.org/10.1039/c2dt31045g.

Chinh, V.D., Hung, L.X., Di Palma, L., Hanh, V.T.H., Vilardi, G., 2019. Effect of carbon nanotubes and carbon nanotubes/gold nanoparticles composite on the photocatalytic activity of TiO2 and TiO2-SiO2. Chem. Eng. Technol. 42, 308–315. https://doi.org/10.1002/ceat.201800265.

Curtis, L., Turner, A., Vyas, N., Sewell, G., 2010. Speciation and reactivity of cisplatin in river water and seawater. Environ. Sci. Technol. 44, 3345–3350. https://doi.org/10.1021/es903620z.

Dobrzynska, J., Dabrowska, M., Olchowski, R., Zieba, E., Dobrowolski, R., 2021. Development of a method for removal of platinum from hospital wastewater by novel ion-imprinted mesoporous organosilica. J. Environ. Chem. Eng. 9. https://doi.org/10.1016/j.jece.2021.105302.

Farías, T., Hajizadeh, S., Ye, L., 2020. Cryogels with high cisplatin adsorption capacity: towards removal of cytotoxic drugs from wastewater. Sep. Purif. Technol. 235, 116203. https://doi.org/10.1016/j.seppur.2019.116203.

Feiqiang, G., Xiaolei, L., Xiaochen, J., Xingmin, Z., Chenglong, G., Zhonghao, R., 2018. Characteristics and toxic dye adsorption of magnetic activated carbon prepared from biomass waste by modified one-step synthesis. Coll. Surf. A Physicochem. Eng. Asp. 555, 43–54. https://doi.org/10.1016/j.colsurfa.2018.06.061.

Flores, C.R., Puga, M.P., Wrobel, Katarzyna, Garay Sevilla, M.E., Wrobel, Kazimierz, 2011. Trace elements status in diabetes mellitus type 2: possible role of the interaction between molybdenum and copper in the progress of typical complications. Diabetes Res. Clin. Pract. 91, 333–341. https://doi.org/10.1016/j.diabres.2010.12.014.

Folens, K., Abebe, A., Tang, J., Ronsse, F., Laing, G. Du, 2018. Biosorption of residual cisplatin, carboplatin and oxaliplatin antineoplastic drugs in urine after chemotherapy treatment. Environ. Chem. 15, 506–512. https://doi.org/10.1071/EN18115.

Fraguela, R.L., Ricardo, A., Edelia, M., Tagle, V., Sime, M., Alfonso, P., Cracchiolo, M., 2023. Evaluation of Dithiocarbamate-Modified Silica for Cisplatin Removal from Water 1–16.

Gao, Y., Yang, N., Yan, X., Hang, W., Xing, J., Zheng, J., Zhu, E., Huang, B., 2012. Early diagnosis of urinary lithiasis via elementary profile of serum samples. Anal. Methods 4, 693–698. https://doi.org/10.1039/c2ay05705k.

Ghafuri, Y., Yunesian, M., Nabizadeh, R., Mesdaghinia, A., Dehghani, M.H., Alimohammadi, M., 2018. Platinum cytotoxic drugs in the municipal wastewater and drinking water, a validation method and health risk assessment. Hum. Ecol. Risk. Assess. 24, 784–796. https://doi.org/10.1080/10807039.2017.1400372.

Ghafuria, Y., Yunesian, M., Nabizadeh, R., Mesdaghinia, A., Dehghani, M.H., Alimohammadi, M., 2018. Environmental risk assessment of platinum cytotoxic drugs: a focus on toxicity characterization of hospital effluents. Int. J. Environ. Sci. Technol. 15, 1983–1990. https://doi.org/10.1007/s13762-017-1517-6.

Gouveia, T.I.A., Silva, A.M.T., Freire, M.G., Sousa, A.C.A., Alves, A., Santos, M.S.F., 2023. Multi-target analysis of cytostatics in hospital effluents over a 9-month period. J. Hazard. Mater. 448, 130883. https://doi.org/10.1016/j.jhazmat.2023.130883.

Grumezescu, A.M., Ghitulica, C.D., Voicu, G., Huang, K.S., Yang, C.H., Ficai, A., Vasile, B.S., Grumezescu, V., Bleotu, C., Chifiriuc, M.C., 2014. New silica nanostructure for the improved delivery of topical antibiotics used in the treatment of staphylococcal cutaneous infections. Int. J. Pharm. 463, 170–176. https://doi.org/10.1016/j.ijpharm.2013.07.016.

Guo, W., Zhou, Q., Jia, Y., Xu, J., 2020. Cluster and factor analysis of elements in serum and urine of diabetic patients with peripheral neuropathy and healthy people. Biol. Trace Elem. Res. 194, 48–57. https://doi.org/10.1007/s12011-019-01747-x.

Han, D., Li, X., Gong, Z., Jiang, L., Wang, Z., Liu, P., 2021. Hierarchical porous catalytic pyrolysis char derived from oily sludge for enhanced adsorption. ACS Omega 6, 20549–20559. https://doi.org/10.1021/acsomega.1c02575.

Hann, S., Koellensperger, G., Stefánka, Z., Stingeder, G., Fürhacker, M., Buchberger, W., Mader, R.M., 2003. Application of HPLC-ICP-MS to speciation of cisplatin and its degradation products in water containing different chloride concentrations and in human urine. J. Anal. At. Spectrom. 18, 1391–1395. https://doi.org/10.1039/b309028k.

Heath, E., Isidori, M., 2020. Fate and Effects of Anticancer Drugs in the Environment, Fate and Effects of Anticancer Drugs in the Environment. Springer International Publishing, Cham https://doi.org/10.1007/978-3-030-21048-9.

Hernández, C., Ramos, Y., Fernández, L.A., Ledea, O., Bataller, M., Véliz, E., Besada, V., Rosado, A., 2008. Ozonation of cisplatin in aqueous solution at pH 9. Ozone Sci. Eng. 30, 189–196. https://doi.org/10.1080/01919510801907722.

Hirose, J., Kondo, F., Nakano, T., Kobayashi, T., Hiro, N., Ando, Y., Takenaka, H., Sano, K., 2005. Inactivation of antineoplastics in clinical wastewater by electrolysis. Chemosphere 60, 1018–1024. https://doi.org/10.1016/j.chemosphere.2005.01.024.

Hoffmann-La Roche, 2020. Product monograph Esbriet * product monograph [WWW document]. https://www.pfizer.ca/sites/default/files/202004/Cisplatin_PM_E_235278_2020-04-03.pdf.

Isidori, M., Lavorgna, M., Russo, C., Kundi, M., Žegura, B., Novak, M., Filipič, M., Mišík, M., Knasmueller, S., de Alda, M.L., Barceló, D., Žonja, B., Česen, M., Ščančar, J., Kosjek, T., Heath, E., 2016. Chemical and toxicological characterisation of anticancer drugs in hospital and municipal wastewaters from Slovenia and Spain. Environ. Pollut. 219, 275–287. https://doi.org/10.1016/j.envpol.2016.10.039.

Jantarat, T., Chuaychob, S., Thammakhet-Buranachai, C., Thavarungkul, P., Kanatharana, P., Srisintorn, W., Buranachai, C., 2021. A label-free DNA-based fluorescent sensor for cisplatin detection. Sensors Actuators B Chem. 326, 128764. https://doi.org/10.1016/j.snb.2020.128764.

Johnson, A.C., Oldenkamp, R., Dumont, E., Sumpter, J.P., 2013. Predicting concentrations of the cytostatic drugs cyclophosphamide, carboplatin, 5-fluorouracil, and capecitabine throughout the sewage effluents and surface waters of europe. Environ. Toxicol. Chem. 32, 1954–1961. https://doi.org/10.1002/etc.2311.

Jureczko, M., Kalka, J., 2020. Cytostatic pharmaceuticals as water contaminants. Eur. J. Pharmacol. 866, 172816. https://doi.org/10.1016/j.ejphar.2019.172816.

Kobayashi, T., Hirose, J., Sano, K., Hiro, N., Ijiri, Y., Takiuchi, H., Tamai, H., Takenaka, H., Tanaka, K., Nakano, T., 2008. Evaluation of an electrolysis apparatus for inactivating antineoplastics in clinical wastewater. Chemosphere 72, 659–665. https://doi.org/10.1016/j.chemosphere.2008.02.020.

Kümmerer, K., Helmers, E., Hubner, P., Mascart, G., Milandri, M., Reinthaler, F., Zwakenberg, M., 1999. European hospitals as a source for platinum in the environment in comparison with other sources. Sci. Total Environ. 225, 155–165. https://doi.org/10.1016/S0048-9697(98)00341-6.

Lenz, K., Hann, S., Koellensperger, G., Stefanka, Z., Stingeder, G., Weissenbacher, N., Mahnik, S.N., Fuerhacker, M., 2005. Presence of cancerostatic platinum compounds in hospital wastewater and possible elimination by adsorption to activated sludge. Sci. Total Environ. 345, 141–152. https://doi.org/10.1016/j.scitotenv.2004.11.007.

Lenz, K., Mahnik, S.N., Weissenbacher, N., Mader, R.M., Krenn, P., Hann, S., Koellensperger, G., Uhl, M., Knasmüller, S., Ferk, F., Bursch, W., Fuerhacker, M., 2007b. Monitoring, removal and risk assessment of cytostatic drugs in hospital wastewater. Water Sci. Technol. 56, 141–149. https://doi.org/10.2166/wst.2007.828.

Lenz, Katharina, Koellensperger, G., Hann, S., Weissenbacher, N., Mahnik, S.N., Fuerhacker, M., 2007a. Fate of cancerostatic platinum compounds in biological wastewater treatment of hospital effluents. Chemosphere 69, 1765–1774. https://doi.org/10.1016/j.chemosphere.2007.05.062.

Li, D., Chen, H., Liu, H., Schlenk, D., Mu, J., Lacorte, S., Ying, G.G., Xie, L., 2021. Anticancer drugs in the aquatic ecosystem: environmental occurrence, ecotoxicological effect and risk assessment. Environ. Int. 153, 106543. https://doi.org/10.1016/j.envint.2021.106543.

Li, J., Zhang, L.P., Peng, F., Bian, J., Yuan, T.Q., Xu, F., Sun, R.C., 2009. Microwave-assisted solvent-free acetylation of cellulose with acetic anhydride in the presence of iodine as a catalyst. Molecules 14, 3551–3566. https://doi.org/10.3390/molecules14093551.

Loehrer, P.J., 1984. Cisplatin. Ann. Intern. Med. 100, 704. https://doi.org/10.7326/0003-4819-100-5-704.

Lou, X.Y., Boada, R., Simonelli, L., Valiente, M., 2022a. Enhanced arsenite removal by superparamagnetic iron oxide nanoparticles in-situ synthesized on a commercial cube-shape sponge: adsorption-oxidation mechanism. J. Colloid Interface Sci. 614, 460–467. https://doi.org/10.1016/j.jcis.2022.01.119.

Lou, X.-Y., Boada, R., Verdugo, V., Simonelli, L., Pérez, G., Valiente, M., 2022b. Decoupling the adsorption mechanisms of arsenate at molecular level on modified cube-shaped sponge loaded superparamagnetic iron oxide nanoparticles. J. Environ. Sci. 121, 1–12. https://doi.org/10.1016/j.jes.2021.09.001.

Micanovic, R., Lafavers, K., Garimella, P.S., Wu, X.R., El-Achkar, T.M., 2020. Uromodulin (Tamm-Horsfall protein): Guardian of urinary and systemic homeostasis. Nephrol. Dial. Transplant. 35, 33–43. https://doi.org/10.1093/ndt/gfy394.

Mišík, M., Filipic, M., Nersesyan, A., Kundi, M., Isidori, M., Knasmueller, S., 2019. Environmental risk assessment of widely used anticancer drugs (5-fluorouracil, cisplatin, etoposide, imatinib mesylate). Water Res. 164, 114953. https://doi.org/10.1016/j.watres.2019.114953.

Mohan, D., Sarswat, A., Singh, V.K., Alexandre-Franco, M., Pittman, C.U., 2011. Development of magnetic activated carbon from almond shells for trinitrophenol removal from water. Chem. Eng. J. 172, 1111–1125. https://doi.org/10.1016/j.cej.2011.06.054.

Muñoz, J.A., Gonzalo, A., Valiente, M., 2002. Arsenic adsorption by Fe(III)-loaded open-celled cellulose sponge. Thermodynamic and selectivity aspects. Environ. Sci. Technol. 36, 3405–3411. https://doi.org/10.1021/es020017c.

Ogata, F., Inoue, K., Tominaga, H., Iwata, Y., Ueda, A., Tanaka, Y., Kawasaki, N., 2014. Use of calcined gibbsite to remove cisplatin from aqueous solutions. J. Water Environ. Technol. 12, 13–23. https://doi.org/10.2965/jwet.2014.13.

Patel, M., Kumar, R., Kishor, K., Mlsna, T., Pittman, C.U., Mohan, D., 2019. Pharmaceuticals of emerging concern in aquatic systems: chemistry, occurrence, effects, and removal methods. Chem. Rev. 119, 3510–3673. https://doi.org/10.1021/acs.chemrev.8b00299.

Pieczyńska, A., Borzyszkowska, A.F., Ofiarska, A., Siedlecka, E.M., 2017. Removal of cytostatic drugs by AOPs: a review of applied processes in the context of green technology. Crit. Rev. Environ. Sci. Technol. 47, 1282–1335. https://doi.org/10.1080/10643389.2017.1370990.

Prestayko, A.W., D'Aoust, J.C., Issell, B.F., Crooke, S.T., 1979. Cisplatin (cis-diamminedichloroplatinum II). Cancer Treat. Rev. 6, 17–39. https://doi.org/10.1016/S0305-7372(79)80057-2.

Queirós, V., Azeiteiro, U.M., Soares, A.M.V.M., Freitas, R., 2021. The antineoplastic drugs cyclophosphamide and cisplatin in the aquatic environment – review. J. Hazard. Mater. 412. https://doi.org/10.1016/j.jhazmat.2020.125028.

Reedijk, J., 1999. Why does cisplatin reach guanine-N7 with competing S-donor ligands available in the cell? Chem. Rev. 99, 2499–2510. https://doi.org/10.1021/cr980422f.

Reedijk, J., 2009. Platinum anticancer coordination compounds: study of DNA binding inspires new drug design. Eur. J. Inorg. Chem. 1303–1312. https://doi.org/10.1002/ejic.200900054.

Roque-Diaz, Y., Sanadar, M., Han, D., López-Mesas, M., Valiente, M., Tolazzi, M., Melchior, A., Veclani, D., 2021. The dark side of platinum based cytostatic drugs: from detection to removal. Processes 9, 1873. https://doi.org/10.3390/pr9111873.

Santana-Viera, S., Padrón, M.E.T., Sosa-Ferrera, Z., Santana-Rodríguez, J.J., 2020. Quantification of cytostatic platinum compounds in wastewater by inductively coupled plasma mass spectrometry after ion exchange extraction. Microchem. J. 157, 104862. https://doi.org/10.1016/j.microc.2020.104862.

Schmidt, C.W.P., 2019. Pediatric Oncologic Pharmacy. Springer International Publishing, Cham, Pediatric Oncologic Pharmacy https://doi.org/10.1007/978-3-030-10988-2.

Sen Gupta, S., Bhattacharyya, K.G., 2011. Kinetics of adsorption of metal ions on inorganic materials: a review. Adv. Colloid Interf. Sci. 162, 39–58. https://doi.org/10.1016/j.cis.2010.12.004.

Veclani, D., Tolazzi, M., Melchior, A., 2020. Molecular interpretation of pharmaceuticals' adsorption on carbon nanomaterials: theory meets experiments. Processes 8, 1–39. https://doi.org/10.3390/PR8060642.

Villarini, M., Gianfredi, V., Levorato, S., Vannini, S., Salvatori, T., Moretti, M., 2016. Occupational exposure to cytostatic/antineoplastic drugs and cytogenetic damage measured using the lymphocyte cytokinesis-block micronucleus assay: a systematic review of the literature and meta-analysis. Mutat. Res. Rev. Mutat. Res. 770, 35–45. https://doi.org/10.1016/j.mrrev.2016.05.001.

Vyas, N., Turner, A., Sewell, G., 2014. Platinum-based anticancer drugs in waste waters of a major UK hospital and predicted concentrations in recipient surface waters. Sci. Total Environ. 493, 324–329. https://doi.org/10.1016/j.scitotenv.2014.05.127.

Wang, J., Guo, X., 2020a. Adsorption kinetic models: physical meanings, applications, and solving methods. J. Hazard. Mater. 390, 122156. https://doi.org/10.1016/j.jhazmat.2020.122156.

Wang, J., Guo, X., 2020b. Adsorption isotherm models: classification, physical meaning, application and solving method. Chemosphere 258, 127279. https://doi.org/10.1016/j.chemosphere.2020.127279.

Yadav, A., Rene, E.R., Mandal, M.K., Dubey, K.K., 2021. Threat and sustainable technological solution for antineoplastic drugs pollution: review on a persisting global issue. Chemosphere 263, 128285. https://doi.org/10.1016/j.chemosphere.2020.128285.

Zamble, D.B., Lippard, S.J., 1995. Cisplatin and DNA repair in cancer chemotherapy. Trends Biochem. Sci. 20, 435–439. https://doi.org/10.1016/S0968-0004(00)89095-7.

Supplementary data of

Comparative study on removal of platinum cytostatic drugs at trace level by cysteine, diethylenetriamino functionalized Si-gels and polyethyleneimine functionalized sponge: adsorption performance and mechanisms

Dong Han,[1] Montserrat López-Mesas[(*)],[1] Markel Luaces,[2] Yusleydi Enamorado,[2] Martina Sanadar,[3] Andrea Melchior[3] and Manuel Valiente[1]

[1]*GTS-UAB Research Group, Department of Chemistry, Faculty of Science, Universitat Autònoma de Barcelona, Bellaterra, (Cerdanyola del Vallès), 08193 Barcelona, Spain*

[2]*Faculty of Chemistry, University of Havana, 10400 Havana, Cuba*

[3]*Dipartimento Politecnico di Ingegneria e Architettura, Università di Udine, via del Cotonificio 108, 33100 Udine, Italy*

The experimental kinetic data were fitted to the PFOM (eq. 1) and PSOM (eq. 2) (Wang and Guo, 2020):

$$q_t = q_{e.cal}(1-e^{-k_1 t}) \quad (1)$$

$$q_t = \frac{q_{e.cal}^2 k_2 t}{q_{e.cal} k_2 t + 1} \quad (2)$$

where $q_{e.cal}$ and q_t corresponds to adsorption capacities (μg g^{-1}) at equilibrium derived from models and at contact time t (min), respectively. k_1 is the PFOM rate constant (min^{-1}), and k_2 is the PSOM rate constant (min^{-1}).

The adsorption equilibrium data were fitted by Langmuir (eq. 3) and Freundlich (eq. 5) models in this work. Both the two models are expressed as follows

$$q_e = \frac{q_m K_L c_e}{1 + K_L c_e} \quad (3)$$

$$R_L = \frac{1}{1 + K_L c_0} \quad (4)$$

$$q_e = K_F c_e^{1/n} \quad (5)$$

where q_m is the maximum adsorption capacity (μg g^{-1}). K_L is the constant related to the affinity of binding sites (L μg^{-1}). The dimensionless separation factor or equilibrium parameter, R_L (eq. 4) indicates the adsorption nature (irreversible if $R_L = 0$, favorable if $0 < R_L < 1$, linear if $R_L = 1$, unfavorable if $R_L > 1$) (Weber and Chakravorti, 1974). K_F ((μg g^{-1})(L $\mu g^{-1})^{1/n}$) and n are the Freundlich constants related to the adsorption capacity and intensity, respectively. If value of $1/n < 1$, it indicates a normal adsorption, and $1/n > 1$ indicates cooperative adsorption. If $1/n$ lies between one and ten, this indicates a favorable sorption process (Chinh et al., 2019; Furuya et al., 1997; Goldberg, 2018; "Physical chemistry," 1961).

Three thermodynamic parameters including Gibbs free energy ($\Delta G°$), enthalpy

change ($\Delta H°$), and entropy change ($\Delta S°$) were calculated by eq. (6), (7) and (8) and listed in Table S3 (in Supplementary data).

$$\Delta G^o = -\mathrm{R}T \ln K \tag{6}$$

$$\ln K = \frac{\Delta S^o}{\mathrm{R}} - \frac{\Delta H^o}{\mathrm{R}T} \tag{7}$$

$$K = \frac{c_0 - c_e}{c_e} \tag{8}$$

Where R is the ideal gas constant (8.314 J mol^{-1} K^{-1}), T is the absolute temperature (K), K is dimensionless distribution constant. Values of $\Delta H°$ and $\Delta S°$ were obtained via the slope and intercept of linear Van't Hoff plots (ln K versus $1/T$).

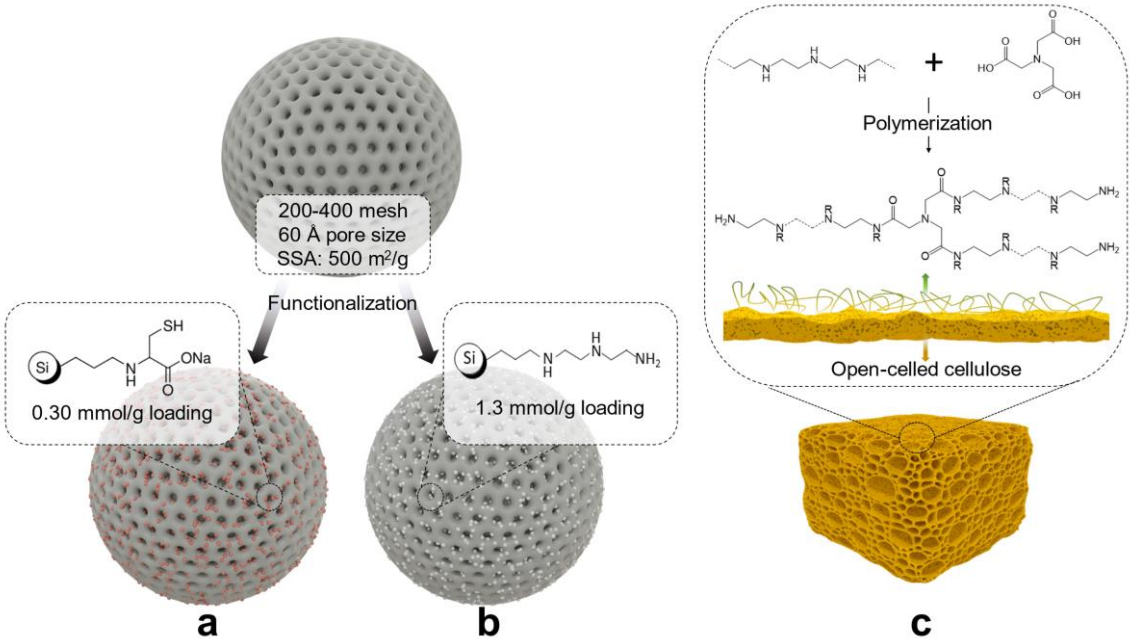

Figure S1. Schematic illustration of (a) Si-Cys, (b) Si-DETA, and (c) Sponge.

Table S1. Brunauer–Emmett–Teller (BET) analysis of Si-Cys and Si-DETA, provided by the manufacturer.

Adsorbents	Si-Cys	Si-DETA
Specific surface area (m^2/g)	480 - 550	480 - 550
Pore diameter (Å)	55 - 65	55 - 65
Pore volume (mL/g)	0.70 - 0.85	0.70 - 0.85

Table S2. Summary of elemental analysis of Si-Cys, Si-DETA and Sponge.

Element (wt%)	Si-Cys	Si-DETA	Sponge
C	11.83 ± 0.02	11.09 ± 0.03	40.2 ± 0.2
H	2.16 ± 0.02	2.64 ± 0.03	6.4 ± 0.1
N	1.86 ± 0.03	4.62 ± 0.07	3.04 ± 0.01
S	1.30 ± 0.02	<0.1	<0.1

Table S3. Kinetic parameters for the adsorption of $PtCl_4^{2-}$, cisplatin and carboplatin by Si-Cys, Si-DETA, and Sponge.

Kinetic model			Pseudo-first-order			Pseudo-second-order		
		$q_{e.exp}$	k_1	$q_{e.cal}$	R^2	k_2	$q_{e.cal}$	R^2
	Adsorbent	μg g^{-1}	min^{-1}	μg g^{-1}		g μg^{-1} min^{-1}	μg g^{-1}	
$PtCl_4^{2-}$	Si-Cys	43.1 ± 0.3	1.2 ± 0.1	43.0 ± 0.7	0.9848	0.06 ± 0.01	44.5 ± 0.5	0.9947
	Si-DETA	42.3 ± 0.5	1.9 ± 0.4	38.0 ± 0.8	0.9675	0.12 ± 0.04	39.0 ± 0.8	0.9795
	Sponge	39 ± 1	0.9 ± 0.2	35 ± 1	0.9312	0.04 ± 0.01	37.0 ± 0.8	0.9786
cisplatin	Si-Cys	34.8 ± 0.1	1.1 ± 0.2	32.5 ± 0.8	0.9656	0.06 ± 0.01	33.8 ± 0.5	0.9920
	Si-DETA	15.2 ± 0.9	1.5 ± 0.5	13.1 ± 0.5	0.9210	0.20 ± 0.07	13.7 ± 0.4	0.9561
	Sponge	18 ± 1	1.3 ± 0.4	14.6 ± 0.6	0.8911	0.13 ± 0.05	15.4 ± 0.6	0.9374
carboplatin	Si-Cys	34.1 ± 0.5	2.4 ± 0.3	33.0 ± 0.3	0.9936	0.24 ± 0.04	33.5 ± 0.2	0.9979
	Si-DETA	4.4 ± 0.2	1.6 ± 0.7	3.3 ± 0.2	0.8430	0.7 ± 0.4	3.5 ± 0.2	0.8826
	Sponge	4.6 ± 0.8	0.7 ± 0.2	3.8 ± 0.2	0.9121	0.25 ± 0.06	4.0 ± 0.1	0.9596

Table S4. Adsorption isotherms parameters of Si-Cys, Si-DETA, and Sponge towards $PtCl_4^{2-}$, cisplatin and carboplatin solutions.

Isotherm model			Langmuir				Freundlich		
		$q_{m.exp}$	$q_{m.cal}$	K_L	R_L	R^2	K_F	$1/n$	R^2
	Adsorbent	mg g^{-1}	mg g^{-1}	10^{-5} L μg^{-1}			($\mu g\ g^{-1}$) (L μg^{-1})$^{1/n}$		
$PtCl_4^{2-}$	Si-Cys	131 ± 1	141 ± 10	12 ± 3	0.008 -0.994	0.9655	2 ± 1 $\times 10^3$	0.33 ± 0.06	0.8074
	Si-DETA	169 ± 6	175 ± 15	12 ± 3	0.008 -0.994	0.9287	2 ± 1 $\times 10^3$	0.40 ± 0.06	0.8499
	Sponge	96 ± 5	104 ± 3	4 ± 1	0.024 -0.998	0.9907	0.8 ± 0.5 $\times 10^3$	0.38 ± 0.05	0.9052
cisplatin	Si-Cys	20 ± 2	30 ± 4	0.4 ± 0.1	0.319 -0.999	0.9811	10 ± 5	0.59 ± 0.04	0.9890
	Si-DETA	3 ± 1	3.9 ± 0.1	1.6 ± 0.2	0.113 -0.999	0.9965	13 ± 8	0.44 ± 0.05	0.9580
	Sponge	5 ± 1	7 ± 1	0.5 ± 0.1	0.270 -0.999	0.9892	5 ± 3	0.54 ± 0.05	0.9764
carboplatin	Si-Cys	20 ± 1	32 ± 3	0.17 ± 0.04	0.365 -0.999	0.9902	7 ± 2	0.59 ± 0.03	0.9951
	Si-DETA	3 ± 2	4.2 ± 0.8	0.26 ± 0.02	0.281 -0.999	0.9331	6 ± 4	0.46 ± 0.05	0.9575
	Sponge	4 ± 3	5.6 ± 0.6	0.23 ± 0.06	0.306 -0.999	0.9807	2 ± 1	0.57 ± 0.07	0.9620

Table S5. Summary of thermodynamic parameters: $\Delta G°$ (kJ mol^{-1}), $\Delta H°$ (kJ mol^{-1}), and $\Delta S°$ (J mol^{-1} K^{-1}).

Adsorbents		Si-Cys			Si-DETA			Sponge		
T(K)		293	318	343	293	318	343	293	318	343
$PtCl_4^{2-}$	$\Delta G°$	-6.2 ± 0.5	-4.2 ± 0.6	-3.4 ± 0.4	-9.1 ± 0.1	-9.0 ± 0.2	-7.2 ± 0.6	-5.8 ± 0.1	-3.5 ± 0.2	-4.1 ± 0.5
	$\Delta H°$	-23 ± 6			-20 ± 3			-16 ± 3		
	$\Delta S°$	-57 ± 19			-36 ± 11			-36 ± 11		
Cisplatin	$\Delta G°$	-2.7 ± 0.5	-6.2 ± 0.2	-10.7 ± 0.7	*	*	*	*	*	*
	$\Delta H°$	44 ± 7			*			*		
	$\Delta S°$	158 ± 24			*			*		
Carboplatin	$\Delta G°$	-3.6 ±0.1	-6.3 ±0.1	-7.3 ±0.3	*	*	*	*	*	*
	$\Delta H°$	19 ±2			*			*		
	$\Delta S°$	76 ± 7								

*Not acceptable values, because the adsorption *vs.* temperature curves were not monotonically increasing or decreasing, poor linear fit.

Table S6. Characteristics of selected urine and wastewater analogs.

Parameters	Urine	Urine diluted tenfold with tap water	Urine diluted 100 times with tap water
pH	5.62 ± 0.02	6.36 ± 0.01	6.90 ± 0.02
Cations and anions (mg L^{-1})			
Sodium Na^+	1972 ± 17	264 ± 1	102 ± 16
Ammonium NH_4^+	982 ± 2	95 ± 4	10 ± 2
Potassium K^+	1530 ± 4	157 ± 5	19.8 ± 0.7
Magnesium Mg^{2+}	8.7 ± 0.8	5.0 ± 0.5	4.0 ± 0.2
Calcium Ca^{2+}	43 ± 7	29 ± 1	26 ± 6
Chloride Cl^-	3606 ± 7	550 ± 8	85 ± 1
Phosphate PO_4^{3-}	6138 ± 19	682 ± 14	66.4 ± 1
Sulfate SO_4^{2-}	8961 ± 14	1004 ± 8	197 ± 6
Oxalate $C_2O_4^{2-}$	251 ± 4	24.9 ± 0.4	2.3 ± 0.1

Ion chromatography (IC, Dionex Aquion, Thermo Scientific, USA) was employed to verify the presence of typical anions and cations in urine and two wastewater simulants. IC was equipped an Dionex 500 Carbonate AERS suppressor (4 mm) for anions and a Dionex 600 CDRS suppressor (4 mm) for cations. Chromeleon 7.2 chromatography management software was used for system control and data processing. A Dionex IonPac AS23 analytical column (4 mm × 250 mm) and a guard column (4 mm × 50 mm) were used for anion separation and a Dionex IonPac CS12A analytical column (4 mm × 250 mm) and a guard column (4 mm × 50 mm) were used for cation separation.

References:

Chinh, V.D., Hung, L.X., Di Palma, L., Hanh, V.T.H., Vilardi, G., 2019. Effect of Carbon Nanotubes and Carbon Nanotubes/Gold Nanoparticles Composite on the Photocatalytic Activity of TiO2 and TiO2-SiO2. Chem. Eng. Technol. 42, 308–315. https://doi.org/10.1002/ceat.201800265

Furuya, E.G., Chang, H.T., Miura, Y., Noll, K.E., 1997. A fundamental analysis of the isotherm for the adsorption of phenolic compounds on activated carbon. Sep. Purif. Technol. 11, 69–78. https://doi.org/10.1016/S1383-5866(96)01001-5

Goldberg, S., 2018. Equations and Models Describing Adsorption Processes in Soils. pp. 489–517. https://doi.org/10.2136/sssabookser8.c10

Physical chemistry, 1961. . J. Franklin Inst. 272, 71. https://doi.org/10.1016/0016-0032(61)90671-8

Wang, J., Guo, X., 2020. Adsorption kinetic models: Physical meanings, applications, and solving methods. J. Hazard. Mater. 390, 122156. https://doi.org/10.1016/j.jhazmat.2020.122156

Weber, T.W., Chakravorti, R.K., 1974. Pore and solid diffusion models for fixed-bed adsorbers. AIChE J. 20, 228–238. https://doi.org/10.1002/aic.690200204

2.2 Trace cisplatin and carboplatin removal by 3-mercaptopropionic acid and L-cysteine functionalized sponges: adsorption behaviour and mechanism

Dong Han,[1] Montserrat López-Mesas[(*)],[1] Roberto Boada,[1] Tania Farías,[2] Ana R. Lazo Fraga,[2] and Manuel Valiente[1]

[1]*GTS-UAB Research Group, Department of Chemistry, Faculty of Science, Universitat Autònoma de Barcelona, Bellaterra, (Cerdanyola del Vallès), 08193, Barcelona, Spain*

[2]*Institute of Materials Science and Technology, University of Havana, 10400, Havana, Cuba*

Journal: Chemical Engineering Journal

https://doi.org/10.1016/j.cej.2023.144894

Available online 17 July 2023, Version of Record 24 July 2023

Chemical Engineering Journal 472 (2023) 144894

Contents lists available at ScienceDirect

Chemical Engineering Journal

journal homepage: www.elsevier.com/locate/cej

Trace cisplatin and carboplatin removal by 3-mercaptopropionic acid and L-cysteine functionalized sponges: Adsorption behaviour and mechanism

Dong Han [a], Montserrat López-Mesas [a,*], Roberto Boada [a], Tania Farías [b], Ana R. Lazo Fraga [b], Manuel Valiente [a]

[a] GTS-UAB Research Group, Department of Chemistry, Faculty of Science, Universitat Autònoma de Barcelona, Bellaterra, (Cerdanyola del Vallès), 08193 Barcelona, Spain

[b] Institute of Materials Science and Technology, University of Havana, 10400 Havana, Cuba

ARTICLE INFO

Keywords:
Adsorption
Cisplatin
Carboplatin
Pt-based cytostatics
Thiol-functionalization
XAS

ABSTRACT

This study presents functionalized open-celled cellulose Metalzorb® sponge (Sponge) with 3-mercaptopropionic acid (MPA) and L-Cysteine (Cys), and the resulting MPA@Sponge and Cys@Sponge showed significantly improved removal efficiency towards trace cisplatin and carboplatin against Sponge. MPA@Sponge achieved maximum removal of 88.9 ± 0.5% for cisplatin and 85.2 ± 0.4% for carboplatin, while Cys@Sponge achieved maximum removal of 75 ± 2% and 59 ± 1%. In contrast, Sponge only achieved removal of 29 ± 4% and 4 ± 1%, respectively. It suggests that thiol groups serve as favourable binding sites for Pt complexation. Carboplatin exhibits lower adsorption compared to cisplatin due to its limited hydration. However, the presence of Cl^- in stock and high temperature facilitate the hydration and the formation of active derivatives of carboplatin, thereby enhancing its adsorption. The rapid adsorption processes of cisplatin and carboplatin are well described by the pseudo-second-order kinetic model involving diffusion and chemisorption. The results from adsorption isotherms revealed a monolayer adsorption that aligns with the principles proposed by the Langmuir model. High temperature significantly enhances the adsorption, and the positive enthalpies indicate that the binding of Pt with thiol groups is endothermic process. X-ray absorption spectroscopy measurements at the Pt L_3-edge revealed a similar coordination environment of the adsorbed Pt on both functionalized adsorbents, which can be attributed to the formation of four Pt-S bonds during the adsorption. To assess the validity of the adsorption results under realistic medium conditions, an adsorption study was carried out by using diluted urine spiked with trace platinum cytostatic drugs to simulate hospital wastewater. 90.2 ± 0.3% of cisplatin and 77.0 ± 0.2% of carboplatin was effectively removed by MPA@Sponge from diluted urine.

1. Introduction

Cisplatin and carboplatin, well-known platinum cytostatic drugs (Pt-CDs), are widely utilized in cancer therapy and characterized for possessing genotoxicity, mutagenicity, carcinogenicity, and teratogenicity as they attack not only cancer cells but also healthy cells [1]. The presence of these substances in aquatic environments has been identified as a significant hazard to both humans and aquatic organisms that are exposed to them, thereby posing a serious threat [2,3]. Pharmacokinetic investigations provide substantiation that approximately 10–40% of Pt-CDs administered to patients are excreted via urine, either in their original form or as metabolites [4]. These compounds are ultimately released into the environment through the discharge of hospital or domestic wastewaters (the latter contaminated by ambulatory patients), as has been proved by many researchers over the last two decades, with concentrations varying between $ng{\cdot}L^{-1}$ to 250 $\mu g{\cdot}L^{-1}$ [5]. Furthermore, several investigations have verified the harmful impacts of cisplatin and carboplatin on certain aquatic invertebrates, even at low levels, in both freshwater and marine ecosystems [6–12]. Limited efforts have been taken to investigate the viability of efficient wastewater remediation methods for Pt-CDs, utilizing diverse techniques such as adsorption [13–17], membrane separation [18,19], ozonation [20] and electrolysis [21,22]. Among them, adsorption, a well-established technology, is frequently considered a favorable approach due to its inherent simplicity of operation, low cost, easy scalability, and significant treatment efficiency. In fact, some pioneering studies on the adsorption of Pt-

* Corresponding author.
E-mail address: montserrat.lopez.mesas@uab.cat (M. López-Mesas).

https://doi.org/10.1016/j.cej.2023.144894
Received 9 June 2023; Received in revised form 14 July 2023; Accepted 16 July 2023
Available online 17 July 2023

CDs using various materials have already been conducted. As early as 2005, Lenz et al., evaluated the adsorption of three cancerostatic platinum compounds (concentrations ranging from 4.7 to 145 μg·L^{-1}) by activated sludge, and after 24 h of incubation time, the removal rates reached 96%, 70% and 74% for cisplatin, carboplatin and oxaliplatin respectively [15]. Ogata et al., prepared calcined gibbsite for the adsorption of cisplatin (initial concentration of 10 mg·L^{-1}) and achieved a removal efficiency of about 90% [14]. Biomass-derived materials such as activated carbon, biochar, chitosan, and wood ash were proposed for adsorption of inorganic $PtCl_6^{2-}$ as a model of Pt-CDs (initial concentration of Pt within the range of 1 to 10 mg·L^{-1}), with adsorption capacities ranging from 0.23 to 0.97 mg·g^{-1} of Pt at an adsorbent dose of 10 g·L^{-1} [16]. Cryogels were synthesized to adsorb cisplatin (250 to 2000 mg·L^{-1}), and the maximum adsorption capacity was discovered to be 150 mg·g^{-1}, attributed to the formation of a stable complex between Pt and the carboxyl group on methacrylic acid [13], where similar strategies were previously used to synthesize carriers for cisplatin drug delivery [23,24]. Recently, a study proposed ion-imprinted mesoporous organosilica for adsorption of $PtCl_4^{2-}$ as a model of Pt-CDs and a maximum adsorption capacity of 76.4 mg·g^{-1} was attained [17]. Another recent study reported the synthesis of dithiocarbamate-modified silica for the removal of cisplatin at varying concentrations (ranging from 5 to 150 mg·L^{-1} Pt in NaCl 0.9% w/v). The maximum adsorption capacity of the adsorbent was determined to be 15.6 mg·g^{-1}, and removal efficiency of up to 85% was observed at a dose of 10 g·L^{-1} of adsorbent and contact time of 1 h [25].

Upon reviewing the aforementioned studies, it becomes evident that the majority of the adsorption experiments predominantly occurred within the mg·L^{-1} concentration range. The establishment of adsorption systems and the elucidation of adsorption mechanisms were based on concentrations that surpassed those observed in actual environmental scenarios. However, the performance assessment of these approaches in the actual treatment of low-concentration Pt-CDs remains unclear. In view of the trace concentration (less than 1 mg·L^{-1}) of Pt-CDs, a notable challenge exists in establishing an efficient and rapid adsorption system, owing to the limited concentration gradient at the interface between the liquid and solid phases. Hence, further research efforts ought to be directed towards developing adsorbents that exhibit high selectivity and strong affinity. To attain this goal, exploring and interpreting the adsorption mechanism assumes critical significance. Additionally, it is imperative to consider the economic and operational convenience aspects, to strike a balance between efficiency and cost-effectiveness.

In our previous study, we conducted a comparative analysis of three commercially available materials, namely 3-(diethylenetriamino)propyl-functionalized silica gel, cysteine-functionalized silica gel, and open-celled cellulose MetalZorb® sponge (Sponge), for their adsorption capabilities towards trace amounts of cisplatin and carboplatin [26]. Our results suggest that the presence of thiol groups as affinity sites offered the potential for complexation of the target Pt species [26]. Moreover, following intravenous administration of Pt-CDs, investigations have demonstrated their interaction with diverse constituents of the blood, like human serum albumin (HSA). HSA, being the predominant protein in human blood, comprises cysteine residues that can interact with administered Pt complexes [27–30]. In addition, according to Hard-Soft Acid-Base (HSAB) theory [31], Pt(II) as a "soft" acid has a high affinity for sulfur donors ("soft" bases) *e.g.* thiols and thioethers. Inspired by these findings, the current study sought to improve the adsorption properties of cheap and commercially available Sponge through functionalization with thiol-containing compounds, as 3-mercaptopropionic acid (MPA) and L-Cysteine (Cys). The resulting materials, namely MPA@Sponge and Cys@Sponge, respectively, were then evaluated for their capacity to remove trace cisplatin and carboplatin from aqueous solutions, and compared to raw Sponge. Moreover, the adsorption mechanisms have been explained by the results obtained from synchrotron X-ray absorption spectroscopy (XAS) technique.

2. Materials and methods

2.1. Reagents and materials

Cisplatin (99%, CAS: 15663–27–1) and carboplatin (99%, CAS: 41575–94–4) were acquired from STREM Chemicals. The compounds were utilized in their as-received form without undergoing any further purification. Stock solutions of cisplatin and carboplatin (Pt 100 mg·L^{-1}), were firstly prepared in 0.2 mol·L^{-1} HCl and Milli-Q water respectively and were subsequently diluted to the required concentration. MetalZorb® Sponge (Sponge) was generously provided by CleanWay Environmental Partners, Inc. (Portland, USA). Acetic anhydride (Ac_2O, ≥ 99%), 3-mercaptopropionic acid (MPA, ≥ 99%) and L-Cysteine (Cys, 97%) were acquired from Sigma-Aldrich. Throughout the experimental procedure, Milli-Q water with a resistivity of 18.2 MΩ·m^{-1} was utilized, unless explicitly stated otherwise.

2.2. Preparation of thiol-functionalized sponges

The original Sponge utilized in this study has a cube-shaped structure composed of an open-celled cellulose substrate. The dimensions of the cubes were measured to be 13 ± 2 (L) × 10 ± 1 (W) × 7 ± 1 (H) mm on average, with an average weight of 0.20 ± 0.02 g per cube. In order to minimize the usage of expensive and toxic Pt-CDs in the adsorption experiments, sponges were employed in powdered form to reduce scale. The cubes underwent mechanical grinding in a commercial blender using knife milling, followed by sieving to achieve the desired particle size of ≤ 0.5 mm. The resulting fine sponge powders were washed once with 1.0 mol·L^{-1} HCl and three times with Milli-Q water. After the washing process, the Sponge powders were dried at 353 K for a duration of 24 h and subsequently stored for further use. As illustrated in Fig. 1, the process of thiol-functionalization of Sponge was carried out through esterification, utilizing a modified version of the procedure described in previous studies [32–35]. In a glass tube with screw cap, 10 mL of MPA (114.8 mmol) or 2.5 g of Cys (20.6 mmol) was mixed with 10 mL of Ac_2O and 50 μL of concentrated sulfuric acid. Ac_2O serves as a reaction medium, simultaneously consuming the water generated during the esterification reaction. When cooled to room temperature, 0.5 g of sponge powder was added, and the mixture was stirred in an oven at 338 K for 4 days. The two products generated, namely MPA@Sponge and Cys@Sponge, were subjected to sequential washing with acetone, alcohol, and Milli-Q water, and subsequently dried at 353 K overnight.

2.3. Characterization of sponges

To obtain the Fourier Transform Infrared Spectroscopy (FTIR) spectra and identify the functional groups present in Sponge, MPA@Sponge, and Cys@Sponge; FTIR equipped with Attenuated Total Reflectance (ATR) module (ATR-FTIR, Tensor 27, Bruker, Germany) was utilized. The quantification of sulfur content was performed utilizing an element analyzer (Flash EA 2000 CHNS, Thermo Fisher, America). The point of zero charge (pH_{pzc}) of sponges were measured using pH drift method [36]. Specifically, pH_{pzc} was determined using 0.1 mol·L^{-1} NaCl solutions spanning pH 2–9. pH adjustments were achieved using either 0.1 mol·L^{-1} HCl or 0.1 mol·L^{-1} NaOH solutions. A total of 20 mL of each solution was brought into contact with 0.1 g of the sample, followed by 24 h of stirring. Subsequently, the sponge was separated via filtration, and the pH of the filtrate was measured. The pH_{pzc} value was obtained by plotting the initial pH of solution against the difference in pH values. The morphological analysis of the sponges was performed using a Field Emission-Scanning Electron Microscope (FE-SEM, MERLIN, Zeiss) with a resolution of 1.4 nm at 1 kV. The probe current ranges from 4 pA to 100 nA, while the accelerating voltage varies from 0.2 to 30 kV. The specific surface areas of sponges were determined using N_2 adsorption–desorption experiments conducted on a Micromeritics ASAP 2460 analyzer at a temperature of 77 K. All sponges were degassed 12 h under

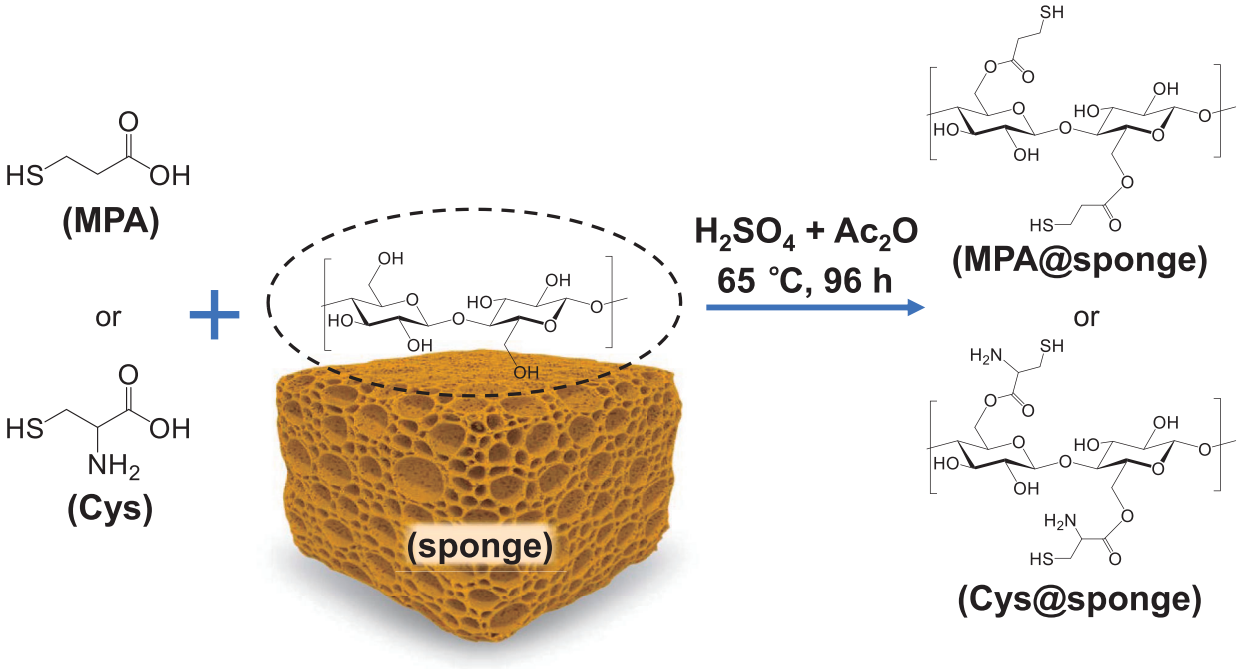

Fig. 1. Schematic illustration of the preparation procedure for MPA@Sponge and Cys@Sponge.

a vacuum at 423 K before the measurement. The specific surface area was calculated utilizing the Brunauer-Emmett-Teller (BET) method.

2.4. Batch adsorption Pt-CDs

The adsorption behavior of cisplatin and carboplatin was investigated under different experimental conditions, including pH (ranging from 2 to 6), contact time (from 1 min to 24 h), initial concentration (varying from 47 $\mu g{\cdot}L^{-1}$ to 500 $mg{\cdot}L^{-1}$, expressed as Pt for both Pt-CDs), and solution temperature (293, 318, and 343 K). The pH of the solution was controlled by using 0.1 $mol{\cdot}L^{-1}$ NaOH and/or 0.1 $mol{\cdot}L^{-1}$ HCl to achieve the desired pH, which was monitored using a pH meter (Crison, Spain) prior to, during, and after the adsorption. Batch adsorption experiments were conducted by adding 10 mg of the adsorbent to 2 mL of Pt solution (either cisplatin or carboplatin) in a plastic centrifuge tube. The mixture was subjected to mechanical agitation at 300 rpm at a specific temperature. Following a predetermined duration, typically 24 h (except in the case of kinetic studies), the adsorbent was separated from the solution by a 0.22 μm membrane filter. The remaining Pt concentration of the filtrate was quantified by means of Inductively Coupled Plasma Mass Spectrometry (ICP-MS, Thermo XSeries II, Thermo Scientific, USA).

The equilibrium adsorption capacity q_e ($\mu g{\cdot}g^{-1}$) of Pt was determined by applying Eq. (1):

$$q_e = \frac{(c_0 - c_e)}{m} \times V \tag{1}$$

where c_0 and c_e represent the initial and equilibrium Pt concentrations ($\mu g{\cdot}L^{-1}$), respectively, V indicates the volume of solution (mL), and m denotes the adsorbent dosage (mg). In the case of kinetic studies, c_e is substituted by the remaining Pt concentration at time t, c_t ($\mu g{\cdot}L^{-1}$), to calculate the corresponding adsorption capacity (q_t, $\mu g{\cdot}g^{-1}$).

Subsequently, the removal ratios were determined by Eq. (2):

$$\text{Removal ratio} = \frac{(c_0 - c_e)}{c_0} \times 100\% \tag{2}$$

All adsorption experiments were performed in triplicate, and the average along with the corresponding relative standard deviations were computed.

To fully comprehend the adsorption behaviour of Pt-CDs, fitting analysis was conducted on the adsorption data collected at different contact time using pseudo-first-order (PFO) and pseudo-second-order (PSO) kinetic models. Additionally, isotherm models such as Langmuir and Freundlich were employed to fit the data derived from diverse initial concentrations. All chosen model formulations are described in Supplementary data.

2.5. Synchrotron X-ray absorption spectroscopy (XAS)

X-ray absorption spectroscopy (XAS) experiment was carried out at BL22 CLÆSS beamline of ALBA CELLS synchrotron [37]. Pt L_3-edge XAS measurements were conducted to investigate the chemical state and coordination environment of adsorbed cisplatin and carboplatin. The measurements were collected on adsorbents that had been exposed to an initial concentration of 235 $\mu g{\cdot}L^{-1}$ Pt. Samples were pressed into a 13 mm pellet to facilitate handling. A Si(311) double crystal monochromator was employed for the measurements. The measurements were performed at a temperature of liquid nitrogen to mitigate potential radiation-induced damage. Given the relatively low Pt concentration in the samples, the measurements were conducted in fluorescence mode utilizing a multi-element silicon drift detector equipped with Xspress3 electronics.

Solid Pt references (K_2PtCl_4, cisplatin, carboplatin) were measured in transmission mode at room temperature, and their solutions in different mediums (cisplatin in 0.2 $mol{\cdot}L^{-1}$ HCl, carboplatin in 0.2 $mol{\cdot}L^{-1}$ HCl and Milli-Q water, Pt concentration of 100 $mg{\cdot}L^{-1}$) were loaded into the in-house designed 3D-printed liquid cell [38] and then collected in fluorescence mode at room temperature.

The X-ray absorption near edge structure (XANES) data were subjected to normalization and background subtraction procedures utilizing the Athena software, while the extended X-ray Absorption fine structure (EXAFS) data were processed through the Artemis software [39]. The pseudoradial distribution functions presented as the module of the Fourier transform of the EXAFS signal are not phase-shift corrected.

2.6. Removal of Pt-CDs from urine and diluted urine

The study intended to assess the feasibility and effectiveness of thiol functionalized sponge in eliminating cisplatin and carboplatin from urine. Experiments were conducted using spiked urine samples obtained from a healthy male, as collecting urine samples from patients undergoing Pt cytostatic treatment proved challenging. The spiked samples used in the study consisted of cisplatin, carboplatin, and their mixtures. Each sample had an initial total Pt concentration of 235 $\mu g \cdot L^{-1}$, which closely resembled the concentrations typically found in hospital wastewaters. Additionally, to assess the matrix effect and simulate possible dilution in hospital wastewater, the same procedure was applied to urine samples diluted ten-time and 100-time using tap water. Ion chromatography (Dionex Aquion, Thermo Scientific, America) was chosen as the analytical technique for quantifying the levels of commonly occurring cations and anions in urine samples as well as two synthetic analogues of hospital wastewater, and further information can be found in the Table S6 in Supplementary data.

Subsequently, 10 mg of the chosen adsorbent was added to 2 mL of the Pt-spiked urine samples, and the mixture was continuously stirred for 24 h at 343 K. The resultant samples were then filtered via 0.22 μm filters before being collected using sterile plastic bottles. The Pt concentration of the samples was subsequently determined using a standardized analytical technique that has been detailed in previous literature [40,41]. In detail, a 100 μL sample was subjected to equilibration at room temperature and then was digested with 200 μL of HNO_3 (69.0–70.0%, for trace metal analysis), at a temperature of 363 K for 1 h. The resultant digested samples were then diluted to a final concentration of 2% v/v HNO_3 by diluting to 10 mL with Milli-Q water. The concentration of Pt was immediately determined by ICP-MS, with external calibration over a concentration range of 1 to 150 $\mu g \cdot L^{-1}$. Indium (In) and Rhodium (Rh) were employed as internal standard elements. Then the removal ratio was determined by Eq. (2).

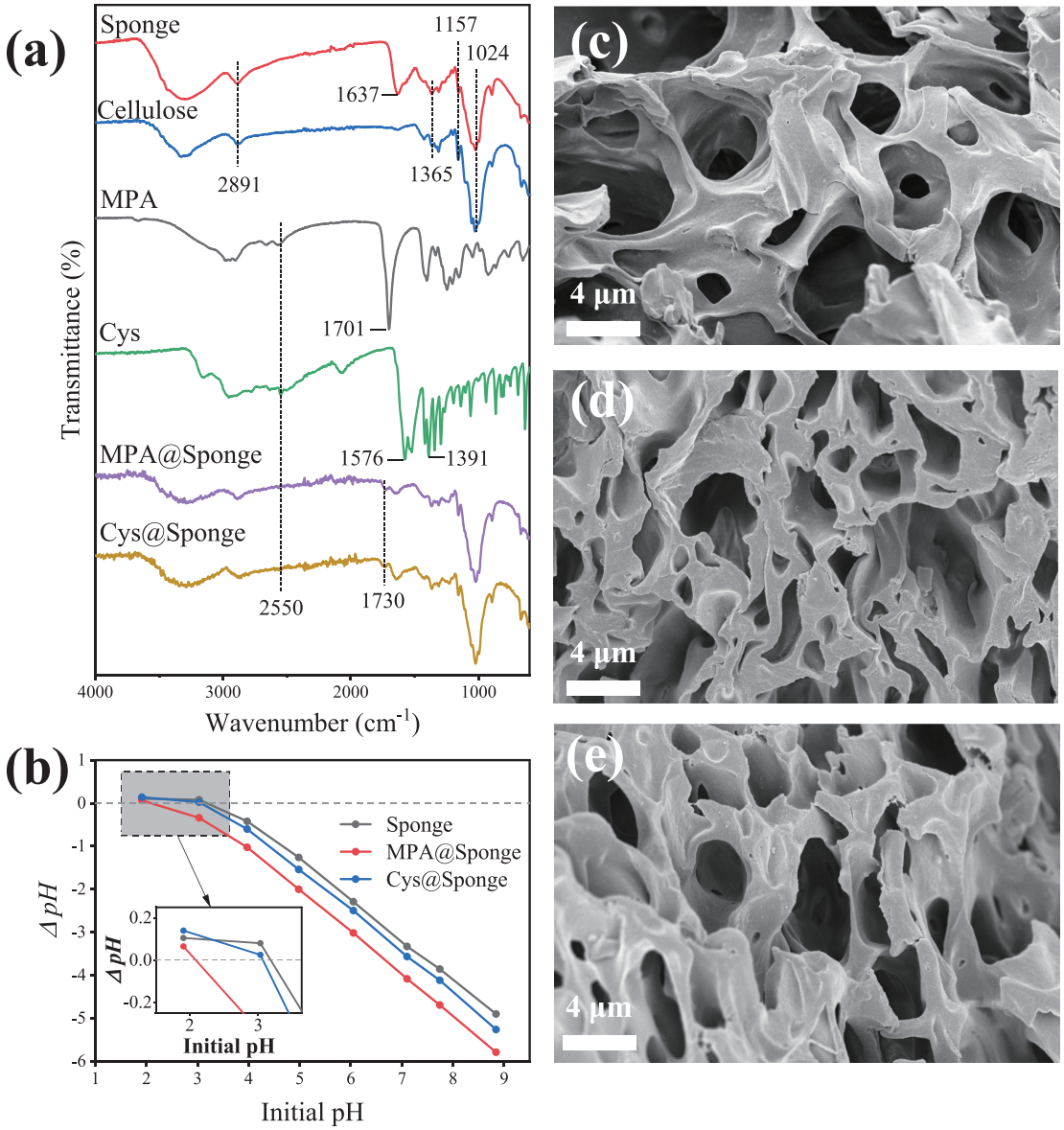

Fig. 2. (a) FTIR spectra of Sponge, cellulose, MPA, Cys, MPA@Sponge, and Cys@Sponge; (b) pH_{pzc} determination of Sponge, MPA@Sponge, and Cys@Sponge by pH drift method; SEM images of (c) Sponge, (d) MPA@Sponge, and (e) Cys@Sponge.

3. Results and discussion

3.1. Characterization of sponges

Fig. 2a presents the spectra resulting from the FTIR analysis of Sponge, cellulose, MPA, Cys, MPA@Sponge and Cys@Sponge. Relevant patents and studies [42–47] suggest that the porous cellulose sponge is composed of a thermally induced amide-forming, insoluble, water-swellable polymer, polyethyleneimine, physically bound to the sponge (see in Fig. S1). This polymer product is claimed to exhibit high affinity for the adsorption of transition metal ions [42–47]. Regarding Sponge, compared to pure cellulose, the FTIR analysis revealed absorbances at 3435, 2891, 1365, 1157, and 1024 cm^{-1}, which can be attributed to the cellulose substrate [48]. The notable absorption band observed at a wavenumber of 3435 cm^{-1} can be ascribed to the stretching vibration of the O-H bond. This band is broader in Sponge than in cellulose, which is attributed to the overlap of the band corresponding to N-H stretching vibrations. This feature is ascribed to the polyethyleneimine on the surface of the Sponge. Alkanes C-H bond stretching vibration is responsible for the peak with a center value of 2891 cm^{-1}. The absorption band observed at a wavenumber of 1365 cm^{-1} is assigned to the bending of the O-H bond, whereas the peak observed at 1157 cm^{-1} corresponds to the antisymmetric stretching of the C-O-C bridge. The prominent peak recorded at a wavenumber of 1024 cm^{-1} arises due to the skeletal vibration of the C-O-C pyranose ring [48]. Moreover, the absorption spectrum of Sponge exhibits an additional peak at 1637 cm^{-1}, in contrast to cellulose, and can be assigned to the stretching vibration of the C = O bond. Additionally, the peak experiences a shift towards higher wavenumbers (due to the electron-donating characteristics of nitrogen), indicating the presence of an amide structure in the polymer formed through the reaction between nitrilotriacetic acid and polyethyleneimine.

Both functionalization reagents exhibit a modest absorption peak of around 2550 cm^{-1}, which is associated with the S-H bond stretching vibration. In addition, MPA also exhibits an absorption peak at 1701 cm^{-1}, which is due to the stretching vibration of the C = O bond in the carboxyl group [49]. In contrast, the spectrum of Cys exhibits two distinct peaks at 1576 and 1391 cm^{-1}, which are attributed to the asymmetric and symmetric stretching vibrations of carboxyl (–COO-) groups, respectively [50–53]. The limited loading of the functionalized sponges resulted in the almost negligible presence of the characteristic peaks of thiols at 2550 cm^{-1}. However, the detection of a new peak at 1730 cm^{-1} in MPA@Sponge and Cys@Sponge spectra, which is attributed to the C = O stretching vibration of the ester group, serves as evidence for successful esterification. Stated differently, the anchoring of MPA and Cys on the substrate was accomplished successfully. And, similar FTIR spectral characteristics were also presented in different studies on thiol-functionalized cellulose materials [34,35,54–56].

As listed in Table S1, elemental analysis (EA) measurements showed that 1.23 ± 0.07 and 0.59 ± 0.03 wt% of sulfur were present in MPA@Sponge and Cys@Sponge after functionalization, respectively. These results also validate the successful anchoring of MPA and Cys on the substrate, as the sulfur content in the original sponge is negligible. The lower sulfur content observed in Cys@Sponge after functionalization is attributed to the necessity of employing less Cys compared to MPA, due to the low solubility of Cys in Ac_2O medium. According to Fig. 2b, the pH_{pzc} values of Sponge, MPA@Sponge, and Cys@Sponge are approximately 3.2, 2.1, and 3.1, respectively. Therefore, when the solution pH is lower than these values, the surface of the sponges will become positively charged, primarily due to the protonation of amino groups [57]. As depicted in Fig. 2c-e, all sponges demonstrate a porous structure featuring an intricate network of interconnected channels with diameters ranging approximately from 1 to 5 μm. Furthermore, after modification, these pore characteristics are retained. The N_2 adsorption–desorption isotherms are illustrated in Fig. S2, and the BET specific surface areas of Sponge, MPA@Sponge, and Cys@Sponge were determined to be 1.55, 1.66, and 1.65 $m^2 \cdot g^{-1}$, respectively.

3.2. Adsorption of Pt-CDs

3.2.1. Effect of pH values

The pH value is a crucial parameter governing the interaction between adsorbate and adsorbent. Through protonation or deprotonation processes, it can induce changes in surface charge, thereby affecting the adsorption efficiency. Additionally, in the case of Pt-CDs, the pH also impacts the hydration of Pt complexes.

Upon comparing the adsorption capacity of the sponge before and after functionalization shown in Fig. 3, it becomes apparent that the adsorption of the two Pt-CDs was enhanced when MPA and Cys were introduced. According to HSAB theory [31], Pt (II) exhibits characteristics of a “soft” acid, displaying a pronounced propensity for forming stable complexes with sulfur donors, which are classified as “soft” bases. Notably, the improvement observed in the case of MPA@Sponge is markedly superior to that observed in the case of Cys@Sponge. This is because MPA@Sponge has a higher sulfur loading rate than Cys@Sponge, as shown by EA (1.23 ± 0.07 and 0.59 ± 0.03 wt% of sulfur content in MPA@Sponge and Cys@Sponge, respectively), providing more adsorption sites. Moreover, it has been proposed that the three sponge materials demonstrated superior capabilities in the adsorption of cisplatin compared to carboplatin. This distinction can be attributed to the inherent tendency of cisplatin to undergo hydration. The dissimilarity arises from the differences between the chloride ligands of cisplatin and the bidentate chelated ligand 1,1-cyclobutanedicarboxylato (CBDCA) of carboplatin. Specifically, the chloride ligands of cisplatin are more prone to hydration, while the CBDCA ligand of carboplatin exhibits lesser susceptibility to hydration [58–63]. Consequently, the hydration-resistant nature of carboplatin impedes the substitution by the thiol group, leading to the observed disadvantage in adsorption capacity.

The impact of pH on the adsorption of cisplatin onto the three sponges is evident from the findings illustrated in Fig. 3a. As the pH value rises, a slight increase in cisplatin adsorption can be observed. This observation can be attributed to the favourable influence of high pH levels and low Cl^- concentration on the hydration of cisplatin, thereby enhancing its reactivity and facilitating complexation with the sponges [28,64–68]. The impact of pH variation on carboplatin adsorption is negligible (see Fig. 3b), except for pH 2, wherein MPA@Sponge exhibits a higher adsorption capacity compared to the values obtained at other pH values. The observed phenomenon is attributed to the introduction of additional HCl at a pH of 2, resulting in partial displacement of CBDCA ligand on carboplatin, and rendering its molecular conformation more similar to that of cisplatin, and this transformation has been already detected by chromatography [61] and XAS techniques [69].

3.2.2. Adsorption kinetics

The kinetic parameter plays a pivotal role in assessing the efficiency and mechanism of adsorption processes, which is a critical aspect to consider when scaling up Pt-CDs removal for industrial applications. The adsorption kinetic curves for cisplatin and carboplatin onto Sponge, MPA@Sponge, and Cys@Sponge are presented in Fig. 4. The results demonstrate rapid adsorption kinetics for all materials. During the initial few minutes, there is a notable rise in adsorption capacity as a result of the ample presence of active adsorption sites on the surfaces of sponges. However, as the adsorption proceeds, the growth rate progressively decelerates until it reaches equilibrium after approximately 3 h. This is primarily due to the decrease in available active sites, resulting in a reduction in the rate of adsorption. Despite its fast kinetics, the adsorption of carboplatin exhibits certain limitations when compared to that of cisplatin. As depicted in Fig. 4, the adsorption capacities (at 24 h) of MPA@Sponge and Cys@Sponge for carboplatin were merely 6.3 ± 0.8 and 5.7 ± 0.1 $\mu g \cdot g^{-1}$, respectively, compared to 29.8 ± 0.1 and 21.4 ± 0.3 $\mu g \cdot g^{-1}$ for cisplatin. Similar behavior was also observed in the

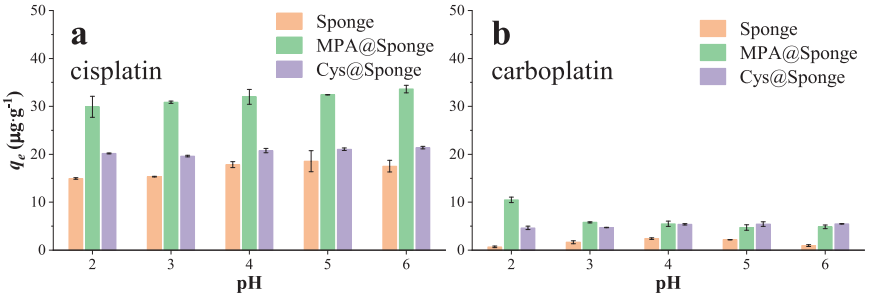

Fig. 3. pH effect on adsorption capacities of sponges on (a) cisplatin and (b) carboplatin.

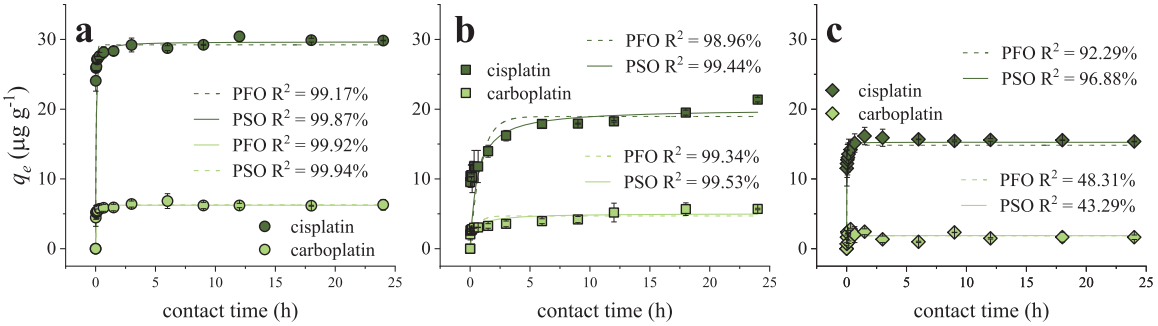

Fig. 4. Adsorption capacities of (a) MPA@Sponge, (b) Cys@Sponge, and (c) Sponge on cisplatin and carboplatin at different contact time.

adsorption on Sponge (Fig. 4c). As previously explained, this can be attributed to the low hydration rate of carboplatin.

It can be concluded that the PSO model was more suitable for fitting the data than the PFO model based on the coefficients of determination R^2 shown in Table S2 (see Supplementary data). The PSO model postulates that the rate-limiting step entails chemisorption, involving valence forces that result from the electrons sharing or exchanging between the adsorbent and adsorbate [36,70,71]. On the other hand, the PFO model is suitable for characterizing the early phase of adsorption, wherein the rate-controlling step is external/internal diffusion, and the adsorbate typically exhibits a high initial concentration [70,72]. On the contrary, the present study involved a low initial concentration (235 μg·L^{-1}) of the target Pt-CDs and an abundance of active sites in the adsorbents. This scenario signifies that the adsorption is primarily governed by the bonding process of the adsorbate to the active sites, thus aligning with assumptions of the PSO model.

3.2.3. *Adsorption isotherms*

Adsorption isotherm characterizes the equilibrium relationship between the adsorbate present in the liquid phase and the adsorbate adsorbed on solid adsorbent at constant temperature [73]. Fig. 5 illustrates an increase in adsorption capacity as the initial concentration increases. This phenomenon can be accounted for by the presence of a higher concentration gradient occurring at the interface between the solid and liquid phases, which drives the mass transfer of Pt-CDs towards the adsorbent surface, which satisfies the generalized Fick Law [74,75].

By comparing the adsorption isotherms at varying temperatures, a discernible increase in adsorption can be observed with rising temperature. Nevertheless, distinct patterns can be observed in the impact of temperature on the adsorption processes of cisplatin and carboplatin. It has been observed that the adsorption of cisplatin proportionally increases with the temperature rise (left column in Fig. 5). The observed phenomenon is ascribed to the temperature-favoured complexation of the center Pt of cisplatin with thiol groups present on the surfaces of the MPA@Sponge and Cys@Sponge, and the same explanation also applies to the adsorption of carboplatin. In contrast, as illustrated in the right column of Fig. 5, a slight increase in the adsorption capacity of carboplatin was observed as the temperature was elevated from 293 K to 318 K. However, an appreciable enhancement in the adsorption capacity was noted upon further raising the temperature to 343 K, particularly within the lower concentration regime, as depicted in Fig. 5d and h. As shown in another study [76], comparable distinctions were also noted during an investigation of the impact of temperature on the interplay between cisplatin and carboplatin with cellular DNA [76]. It can be explained that the influence of temperature on the adsorption of carboplatin is not only reflected in the promotion of complexation of Pt-S, but it also has a notable effect on the hydration of carboplatin [77], which is crucial to the complexation process that follows. It can be inferred that when the temperature rose to 318 K, the bidentate-chelated CBDCA of carboplatin, hindered the subsequent ligand replacement conferring carboplatin resistance to hydration. However, at 343 K, the CBDCA ring was opened and hydrated [77], resulting in derivatives with greater activity. Consequently, the adsorption of carboplatin was significantly enhanced, to a degree comparable to that of cisplatin (as evidenced by the comparison displayed in Fig. 5c and d at 343 K).

Fig. 5 also depicts the fitting curves for the adsorption processes, while Table S3 (Supplementary data) summarizes the parameters derived from the isotherm models used. By comparison, the coefficient of determination for the Langmuir model ($R^2 > 0.96$) typically surpasses that of the Freundlich model, thereby suggesting a superior fit of the Langmuir isotherm model to the experimental data, except for adsorption of cisplatin on MPA@Sponge at 318 K, where the Freundlich model shows slightly better fitting. These findings suggest that the adsorption of two Pt-CDs by MPA@Sponge and Cys@Sponge occurs via monolayer adsorption. Furthermore, in the low concentration range (Fig. 5c, d, g and h), the adsorption isotherms exhibit linear characteristics, consistent with the description of Henry's law, thereby indicating a monolayer adsorption as well [78]. The Langmuir separation factor R_L values for both Pt-CDs adsorptions on the two materials, within the concentration range investigated, range from 0 to 1, demonstrating favourable adsorption. The theoretical maximum adsorption capacities (q_m) estimated by the Langmuir model closely approximates, albeit slightly

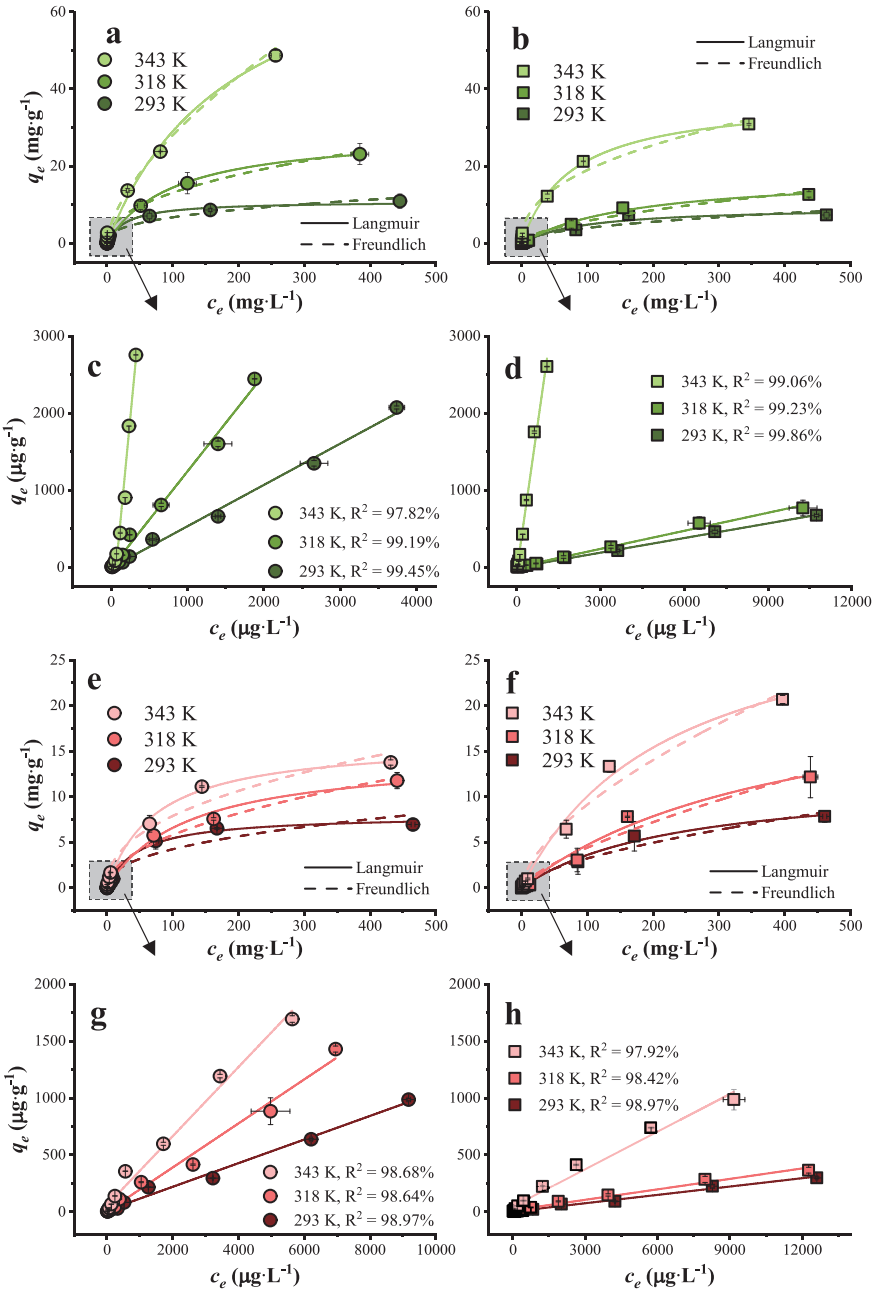

Fig. 5. Adsorption equilibriums of (a) cisplatin on MPA@Sponge, (b) carboplatin on MPA@Sponge, (e) cisplatin on Cys@Sponge and (f) carboplatin on Cys@Sponge and isotherm models fitting. Fig. (c), (d), (g) and (h) below each depict the magnified interval (with an initial concentration range of 47–14100 μg·L^{-1}).

exceeds, the experimentally obtained actual maximum adsorption capacities. The favourable nature of all adsorption processes is indicated by the Freundlich constant, as the value of $1/n$ is less than 1.

3.2.4. *Adsorption thermodynamics*

To further understand adsorption characteristics, experimental thermodynamic studies were carried out at various temperatures. The impact of temperature on the adsorption efficacy of unfunctionalized and functionalized sponges is divergent. The experimental findings presented in Fig. 6 show that the thiol-modified sponges display a temperature-favoured behaviour. Conversely, the original sponge exhibits an adsorption trend that initially increases with temperature, but subsequently decreases. It can be readily comprehended that the chemisorption processes of Pt-CDs on MPA@Sponge and Cys@Sponge were primarily governed by chelation, which exhibited a thermophilic nature. Thus, it was observed that high temperatures promoted the complexation reaction between Pt and S originating from the thiol group. However, the adsorption capacities of Pt-CDs on Sponge were only found to increase with an increase in temperature from 293 K to 318 K. This limited increase was attributed to the promotion of complexation between Pt and the amine groups on Sponge surface at 318 K. However, it is worth noting that the complexation was limited d due to the inherent "hard" basic character of N and its relatively lower bonding affinity with the "soft" acid Pt, as compared to S [31,79,80]. The adverse effects of reduced van der Waals adsorption become more pronounced when the temperature is further elevated to 343 K, resulting

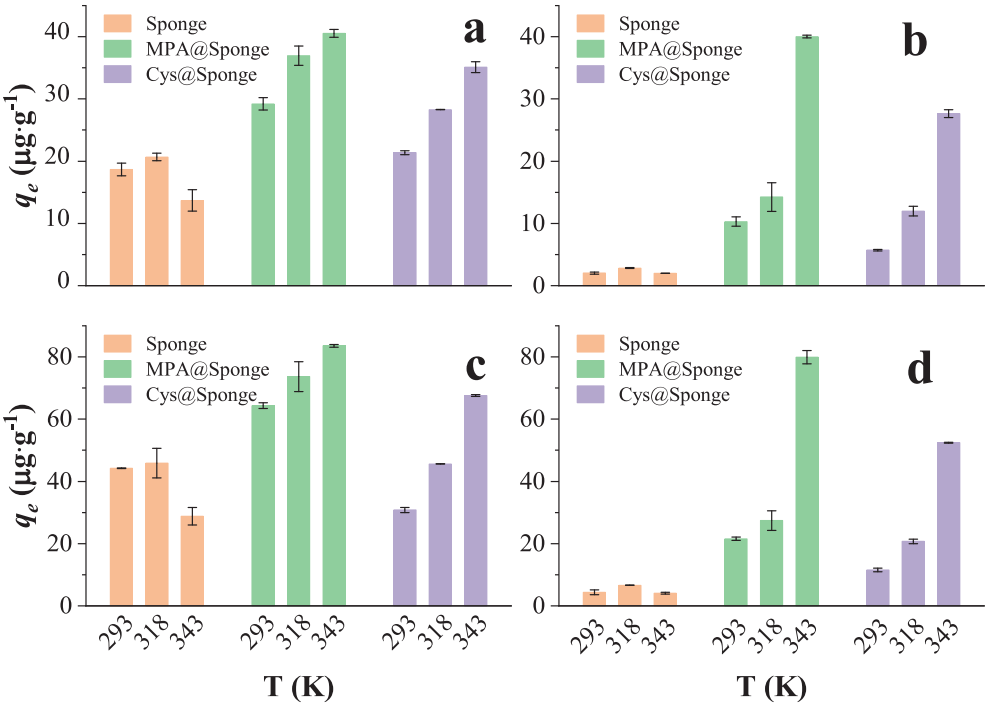

Fig. 6. Effect of temperature on the adsorption capacity of cisplatin and carboplatin. Initial Pt concentration of cisplatin: (a) 235 μg·L^{-1} and (c) 470 μg·L^{-1}; of carboplatin: (b) 235 μg·L^{-1} and (d) 470 μg·L^{-1}.

in a decline in adsorption capacity. [81]. Moreover, upon comparing the adsorption of cisplatin and carboplatin on functionalized sponges, it is noteworthy that the role of temperature in enhancing the process manifests itself in distinct manners. Specifically, while the adsorption of cisplatin exhibits a gradual increase with each increment in temperature, the adsorption of carboplatin experiences a substantial surge only when the temperature surpasses the threshold of 318 K. This observation suggests that the impact of temperature on carboplatin extends beyond the complexation reaction to other associated processes. For instance, the promotion of hydration due to an increase in temperature, as previously described, facilitates the pre-morphological transformation of carboplatin.

Furthermore, the determination of three fundamental thermodynamic parameters, namely ΔG° (Gibbs free energy), ΔH° (enthalpy change), and ΔS° (entropy change), was carried out using the equations detailed in the Supplementary data.

The values of ΔG° presented in Table S4 indicate that the adsorption process of cisplatin onto the two modified sponges was predominantly spontaneous, except for Cys@Sponge at a temperature of 293 K. Conversely, the adsorption of carboplatin was found to be non-spontaneous, only except at highest 343 K, where the system exhibited an energy gain from the surroundings [82–85]. Moreover, the ΔG° values exhibited a decrease as the temperature increased, suggesting that higher temperatures promote the spontaneity of adsorption [86]. The adsorption of cisplatin or carboplatin is an endothermic process based on positive ΔH° values. Additionally, a comparison of the ΔH° of cisplatin and carboplatin reveals a significant difference between the two compounds. Specifically, the adsorption of cisplatin is generally characterized by a lower energy requirement, which is consistent with previous explanations. On the other hand, the adsorption of carboplatin is hindered by a higher heat threshold, necessitating the promotion of carboplatin hydration to facilitate its activation for subsequent adsorption processes.

The positive value of the change in standard entropy (ΔS°) suggests an enhanced inclination towards disorder at the interface between the solid and solution phases during the adsorption process of Pt-CDs onto MPA@Sponge and Cys@Sponge. The process of binding Pt-CDs onto a sponge surface should be associated with a decrease in entropy due to the restriction on their conformational space, which consequently resulted in a negative contribution to the ΔS°. However, the restricted degree of freedom of Pt-CDs in solution implies that their entropy change upon adsorption is comparatively low when compared to that of water. Evidently, the positive contribution to ΔS° is a result of water molecules being excluded from the hydration layers of both the sponges and Pt-CDs upon adsorption. The exchange of molecules between the Pt-CDs and functional groups on the sponge surface facilitates the liberation of water molecules, resulting in an increase in disorderliness at the solid/fluid interface [83]. Similar results were also found in other studies using cellulose [87] or lignocellulosic waste [88] as adsorbents.

3.3. X-ray absorption spectroscopy of adsorbed Pt-CDs

The findings derived from the batch adsorption experiments conducted at the macro scale reveal that the adsorption behaviour of trace Pt-CDs follows a chemisorption mechanism, which dependents on the formation of Pt-S bonds. However, to gain deeper insights into the molecular-level adsorption process regarding the coordination environment and the chemical state of Pt in the adsorbed Pt-CDs, Pt L_3-edge XAS measurements were performed.

Fig. 7a presents Pt L_3-edge XANES spectra of Pt-CDs adsorbed on the different sponges, along with Pt(II) reference compounds (K_2PtCl_4, cisplatin, and carboplatin). Generally, the XANES spectra of the adsorbed Pt resemble those of the Pt(II) standards, albeit with slight deviations in the configuration of the white line, demonstrating the unchanged Pt valence. Consequently, unaltered Pt valence indicated the adsorption of Pt-CDs onto sponges did not entail any oxidation or redox reaction. The spectral profiles of cisplatin and carboplatin absorbed by functionalized sponges are very similar. The temperature of adsorption only affects the intensity of the white-line in the case of MPA@Sponge. However, the adsorbed Pt-CDs at low temperature manifests more noise

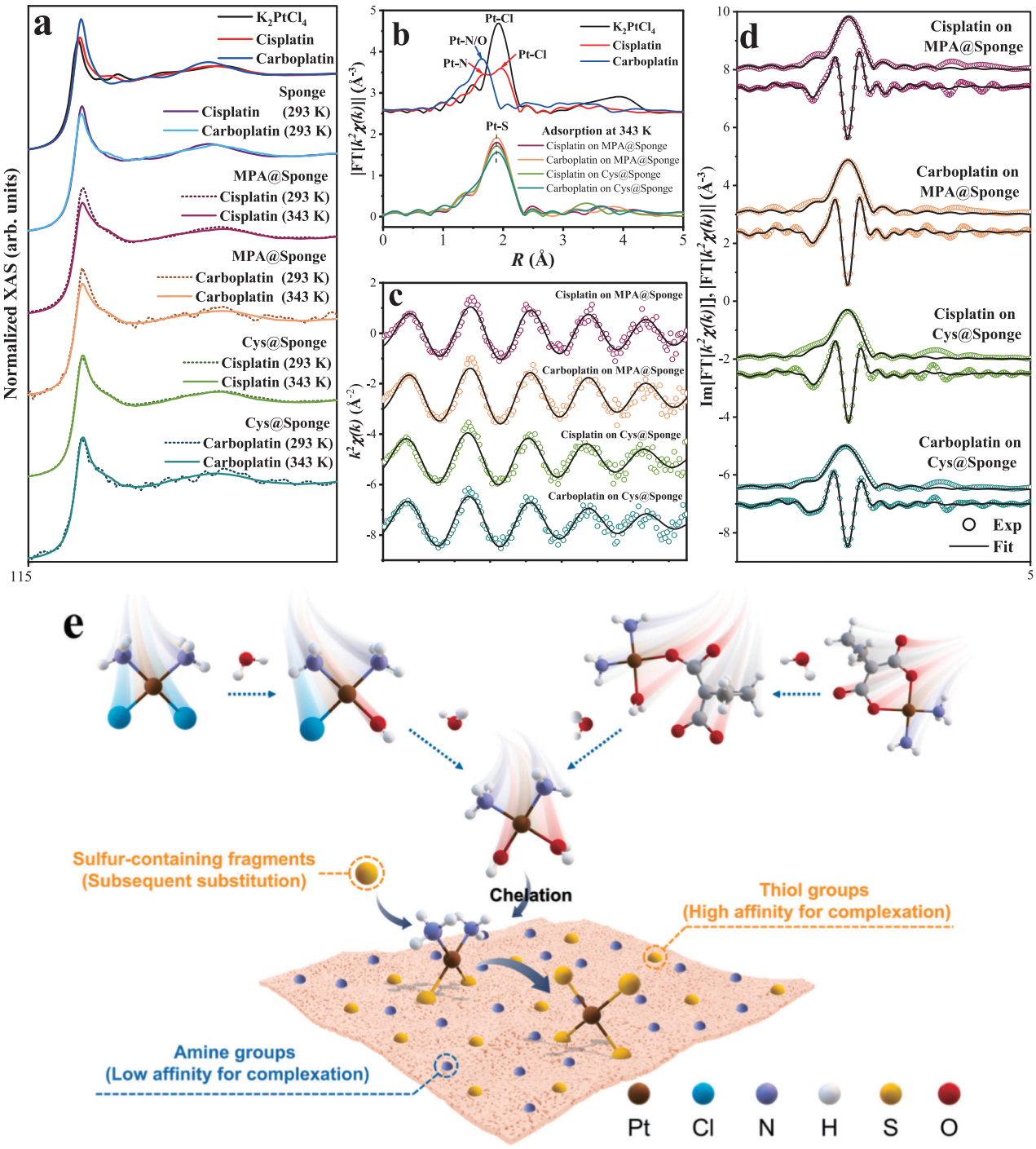

Fig. 7. Pt L_3-edge (a) XANES spectra, (b) module of the Fourier transformed EXAFS signal of Pt references (K_2PtCl_4, cisplatin and carboplatin in solid) and Pt-CDs adsorbed on sponges, (c) EXAFS signals, (d) imaginary part and module of the Fourier transformed EXAFS of Pt-CDs adsorbed on sponges at 343 K (the line represents the best fit), (e) schematic representation of Pt-CDs adsorption mechanisms by thiol-functionalized sponges.

due to the low adsorption capacities. The presence of inherent noise in low Pt-loaded samples posed a challenge for the identification of oscillations, thus EXAFS fitting analysis was feasible only on samples obtained at high-temperature adsorption. Fig. 7b depicts the module of the Fourier transformed (FT) EXAFS signal, which offers valuable insights into the coordination environment of adsorbed Pt. The dominant shell of Pt-loaded on MPA@Sponge and Cys@Sponge appears at a distance and amplitude which is like the Pt-Cl contribution in the K_2PtCl_4. In our case, this can be attributed to Pt-S bond. In order to establish the Pt coordination structure, EXAFS fitting analysis was conducted. The findings revealed that, on average, each Pt atom was coordinated by approximately four sulfur atoms within the first coordination shell at ~ 2.30 Å (as illustrated in Fig. 7c and d, and presented in Table S5). These results suggest the cisplatin and carboplatin adsorption process at low

concentrations proceeds in a manner depicted by Fig. 7e. The initial stage involves hydration of both Pt-CDs, followed by complexation with the thiol groups present on the surface of functionalized sponge by activated Pt aqua-derivatives. With prolonged heating, a portion of MPA and Cys undergoes thermal decomposition (confirmed by EA, S content of MPA@Sponge and Cys@Sponge decreased about 47% and 39%, respectively, after stirring in 343 K solution without Pt for 24 h), giving rise to sulfur-containing fragments in solution, such as sulfides [89–92], which subsequently displace the ammonia ligand despite its inertness.

3.4. Effect of Cl^- presence in stock solution on carboplatin adsorption

As elaborated previously, the derivatives of cisplatin and carboplatin demonstrated a facile complexation behaviour attributed to the Pt-S bond formation after hydration activation. However, it is noteworthy that the adsorption capacity of cisplatin always surpassed that of carboplatin. The observed contrast can be attributed to the influence of distinct ligands on the hydration rate. In particular, relative to the Cl ligand present in cisplatin, the CBDCA ligand found in carboplatin demonstrated higher resistance to hydration. Consequently, CBDCA tended to remain bound, thus resulting in more pronounced steric hindrance during subsequent complexation reactions.

In order to verify the proposed hypothesis, chloride ions (at a concentration of 0.2 $mol{\cdot}L^{-1}$ in either the form of HCl or NaCl) were introduced into the stock solution of carboplatin (Pt 100 $mg{\cdot}L^{-1}$) to expedite the hydration process of carboplatin. The adsorption experiment was conducted under identical conditions to those of the carboplatin Cl-free stock solution (initial Pt concentration of 235 $\mu g{\cdot}L^{-1}$ obtained through dilution of the stock solution with Milli-Q water, adsorbent dosage of 10 mg, solution volume of 2 mL, pH 3, 24 h, and 293 K). Their adsorption capacities were determined and compared, as depicted in Fig. 8a.

Upon introduction of HCl to the stored solution, there was a notable improvement in the adsorption of carboplatin by both adsorbents. Specifically, the adsorption capacity of MPA@Sponge and Cys@Sponge increased significantly from 5.8 ± 0.1 and 4.7 ± 0.1 to 13.9 ± 0.9 and 9.4 ± 0.2 $\mu g{\cdot}g^{-1}$, respectively. By analyzing XANES spectra of carboplatin stocks in the presence and absence of HCl, as illustrated in Fig. 8b, it is observed that carboplatin manifests distinct spectral features compared to carboplatin in H_2O stock solution, but shares similarities with cisplatin when exposed to HCl. The mechanism of the carboplatin transformation was proposed by Curis et al., [69] to explain their XAS results on carboplatin decomposition in chloride medium. And it was also previously corroborated by chromatographic techniques [61]. It can be inferred that the stability of carboplatin was affected by this transformation (Fig. 8c), which resulted in the formation of an open-ring structure that demonstrated enhanced adsorption activity. Nonetheless, the introduction of an equivalent concentration of Cl ions in the form of NaCl to the original solution did not result in the anticipated increase in adsorption. Although a slight increase was observed with ageing of the stock up to 40 days, it suggested that acidity and Cl jointly played a crucial role in the conversion process. Similarly, Curis et al., did not find that carboplatin had the same transformation in neutral NaCl solution as in HCl solution [69].

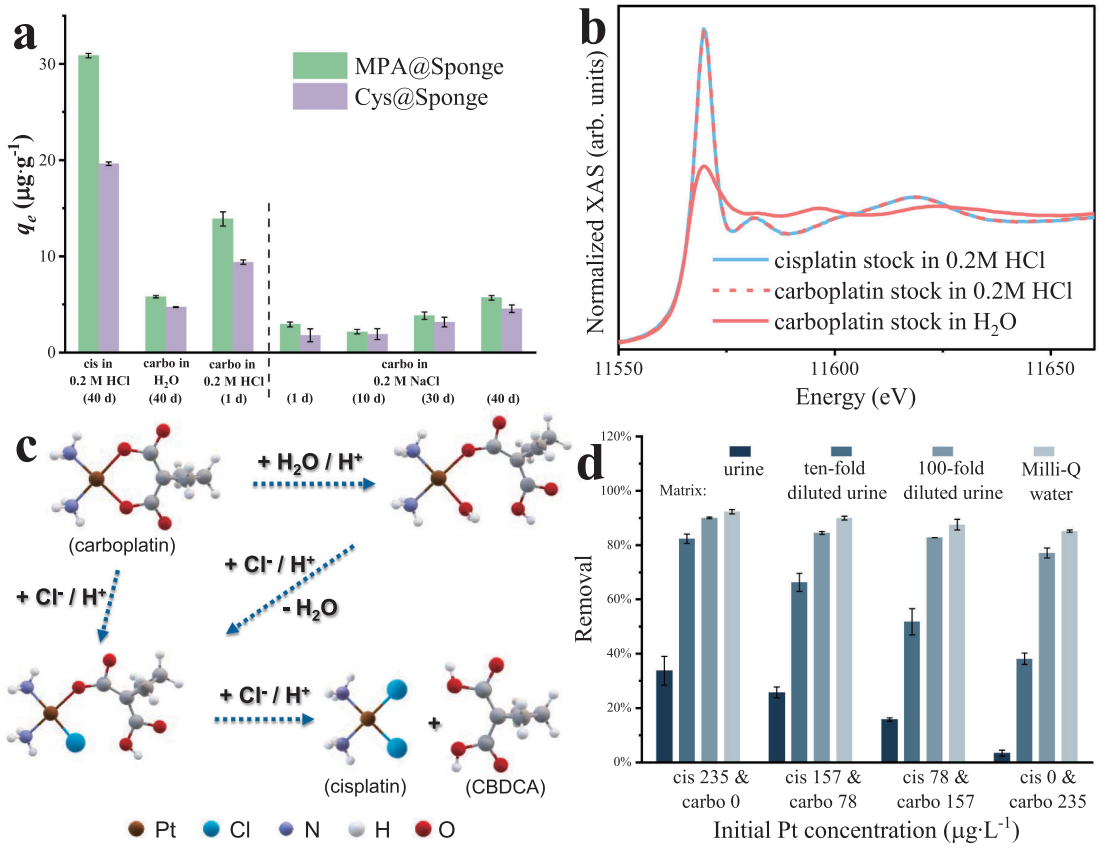

Fig. 8. (a) Effect of Cl ions in the stock solution on the adsorption capacity of carboplatin; (b) XANES spectra of cisplatin stock solution in 0.2 $mol{\cdot}L^{-1}$ HCl, carboplatin stock solution in H_2O, and cisplatin stock solution in 0.2 $mol{\cdot}L^{-1}$ HCl; (c) the transformation of carboplatin to cisplatin within an HCl-containing medium; (d) removal of cisplatin, carboplatin, and their mixtures from spiked urine samples by MPA@Sponge.

3.5. Experimental verification of Pt-CDs removal from urine and diluted urine

As present in Fig. 8d, there is a noteworthy augmentation in the adsorption capacity of MPA@Sponge towards Pt with the dilution of the urine matrix. This effect signifies a considerable reduction in the interference intensity of the matrix effect. The matrix effect observed in the experiment is unequivocally attributed to the intricate nature of the urine composition (listed in Table S6). One of the potential factors that may impede the removal of cisplatin and carboplatin is the presence of trace proteins like Tamm-Horsfall protein in urine [93,94], which contains cysteine residues that may pre-chelate a portion of these drugs. Furthermore, the presence of components like NH_4^+ and Cl^- in the urine matrix may interfere with the substitution of cisplatin and carboplatin ligands., thereby adversely affecting their complexation with the MPA@Sponge surface [40]. In addition, the coexistence of ions such as Na^+, K^+, Mg^{2+}, and Ca^{2+} in urine results in competitive adsorption, thereby slightly impeding the adsorption of cisplatin and carboplatin [95].

Additionally, the results reveal that the rise in mixed carboplatin leads to a notable reduction in the Pt adsorption capacity. Nonetheless, this declining pattern appears to mitigate in 100-fold diluted urine, whereby the reduction decreases from 90.0 ± 0.3% to 77.0 ± 0.2% while the values decrease from 34 ± 5% to 3 ± 1% in non-diluted urine and from 82 ± 2% to 38 ± 2% in ten-fold diluted urine, respectively. The present finding demonstrates that the matrix effect may exert a greater influence on the pre-hydration activation of carboplatin, in comparison to aforementioned interference factors like protein complexation and competitive adsorption which are expected to impede the adsorption of the two Pt-CDs to a similar degree. In essence, the impurities in the urine maintained the rigidity of the carboplatin structure.

3.6. Comparison of thiol-functionalized sponges with commercial adsorbents

The efficacy of MPA@Sponge and Cys@Sponge for cisplatin removal was compared with that of two commercially available adsorbents, namely 3-Mercaptopropyl-functionalized silica gel (Si-SH) and cysteine-functionalized silica gel (Si-Cys), and results were summarized in Table S7. MPA@Sponge exhibits significant efficiency in the removal process (71.5 ± 0.2%), which is comparable to Si-Cys (76.3 ± 0.2%), but noticeably lower than Si-SH (98.7 ± 0.1%). This disparity can be attributed to the much higher sulfur loading of Si-SH (4.97 ± 0.07 wt%) than that of MPA@Sponge (1.23 ± 0.07 wt%) and Si-Cys (1.30 ± 0.02 wt%). While the performance of functionalized sponges is slightly inferior to commercial adsorbents, cost considerations must be taken into account. From a cost perspective, our proposed materials offer considerable advantages. Furthermore, the removal efficiency of Si-Cys on Pt-CDs, in comparison with other reported adsorbents, has been previously published in prior research study [26].

4. Conclusions

The coupling of MPA and Cys with Sponge via a simple one-step esterification reaction has been demonstrated as a feasible and successful process. The presence of an implanted high-affinity thiol group has been demonstrated to significantly enhance the adsorption of both cisplatin and carboplatin, suggesting that Pt-S complexation plays a pivotal role in chelation-dominated chemical adsorption. Then the utilization of synchrotron XAS has enabled the investigation of the coordination environment of Pt-CDs loaded at extremely low concentrations. In particular, EXAFS analysis provides insight into the formation of Pt-S bonds after adsorption, allowing for a persuasive explanation of the molecular-level adsorption mechanism. Besides complexation, the process of removing Pt-CDs also involves a hydration process for both Pt-CDs. Pre-displacing ligands in an aqueous solution can result in the production of more active derivatives, which in turn facilitate subsequent complexation. Therefore, the distinct hydration patterns of cisplatin and carboplatin lead to the preferential adsorption of cisplatin over carboplatin. The higher hydration resistance of CBDCA ligand from carboplatin accounts for the adsorption disadvantages observed. Further elevating the temperature to 343 K promoted the adsorption of Pt-CDs by MPA@Sponge, resulting in the removal of 88.9 ± 0.5% and 85.2 ± 0.4%, respectively (while 75 ± 2% and 59 ± 1% for Cys@Sponge). This was due to the temperature-enhanced chelation reaction of Pt-S. Adsorption thermodynamic studies also confirmed that adsorption is a thermally favoured endothermic reaction. Moreover, the adsorption of both Pt-CDs conforms to the Pseudo-second-order kinetic model and the Langmuir isotherm model. In summary, the elimination of Pt-CDs at trace concentrations is associated with a hydration process and a chelation-dominant chemisorption. Significantly, the examination of the Pt-spiked urine treatment has demonstrated the potential utilization of MPA@Sponge for the purpose of treating urine samples from patients that contain cisplatin and/or carboplatin, as well as hospital wastewater contaminated with these substances. To summarize, our study has introduced innovative methods for effectively managing wastewater polluted with Pt-CDs, thereby offering a practical strategy to tackle this emerging environmental threat that has been persistently overlooked.

Declaration of Competing Interest

The authors declare that they have no known competing financial interests or personal relationships that could have appeared to influence the work reported in this paper.

Data availability

Data will be made available on request.

Acknowledgements

This study was conducted within the scope of the RECOPHARMA project (grant agreement #778266) under the European Community's H2020 Program H2020-MSCA-RISE 2017. D. Han acknowledges the support from the China Scholarships Council (No. 201906450024). The authors would like to express their gratitude to the ALBA synchrotron facility for providing beamtime (No. 2022085922) at the BL22-CLÆSS beamline, and to Carlo Marini for his assistance as the scientific local contact. The authors would like to thank Cristina Navarro Senent from the Servei de Microscòpia of Universitat Autònoma de Barcelona (UAB). All the authors are grateful to the Servei d'Anàlisi Química of the UAB for the analysis. All authors thank Yunhui Yang for his help on BET analysis. Additionally, the authors extend their appreciation to Markel Luaces, Yusleydi Enamorado, and Alejandro Barragán Beltri for their assistance during the experiment. Open Access funding provided thanks to the agreement CRUE- CSIC with Elsevier.

Appendix A. Supplementary data

Supplementary data to this article can be found online at https://doi.org/10.1016/j.cej.2023.144894.

References

[1] E. Heath, M. Isidori, T. Kosjek, M. Filipič (Eds.), Fate and Effects of Anticancer Drugs in the Environment, Springer International Publishing, Cham, 2020.
[2] T.I.A. Gouveia, A.M.T. Silva, M.G. Freire, A.C.A. Sousa, A. Alves, M.S.F. Santos, Multi-target analysis of cytostatics in hospital effluents over a 9-month period, J. Hazard. Mater. 448 (2023), 130883, https://doi.org/10.1016/j.jhazmat.2023.130883.
[3] D. Li, H. Chen, H. Liu, D. Schlenk, J. Mu, S. Lacorte, G.G. Ying, L. Xie, Anticancer drugs in the aquatic ecosystem: environmental occurrence, ecotoxicological effect

and risk assessment, Environ. Int. 153 (2021), 106543, https://doi.org/10.1016/j.envint.2021.106543.
[4] C.W.P. Schmidt, Pediatric oncologic pharmacy, springer international publishing, Cham (2019), https://doi.org/10.1007/978-3-030-10988-2.
[5] V. Queirós, U.M. Azeiteiro, A.M.V.M. Soares, R. Freitas, The antineoplastic drugs cyclophosphamide and cisplatin in the aquatic environment – review, J. Hazard. Mater. 412 (2021) 125028.
[6] M. Kundi, A. Parrella, M. Lavorgna, E. Criscuolo, C. Russo, M. Isidori, Prediction and assessment of ecogenotoxicity of antineoplastic drugs in binary mixtures, Environ. Sci. Pollut. Res. 23 (2016) 14771–14779, https://doi.org/10.1007/s11356-015-4884-x.
[7] C. Russo, M. Isidori, J.A. Deaver, H.C. Poynton, Toxicogenomic responses of low level anticancer drug exposures in Daphnia magna, Aquat. Toxicol. 203 (2018) 40–50, https://doi.org/10.1016/j.aquatox.2018.07.010.
[8] S. Kolarević, Z. Gačić, J. Kostić, K. Sunjog, M. Kračun-Kolarević, M. Paunović, J. Knežević-Vukčević, B. Vuković-Gačić, Impact of common cytostatics on DNA damage in freshwater mussels unio pictorum and unio tumidus, Clean - Soil, Air, Water. 44 (2016) 1471–1476, https://doi.org/10.1002/clen.201500482.
[9] C. Trombini, T. Garcia da Fonseca, M. Morais, T.L. Rocha, J. Blasco, M.J. Bebianno, Toxic effects of cisplatin cytostatic drug in mussel Mytilus galloprovincialis, Mar. Environ. Res. 119 (2016) 12–21, https://doi.org/10.1016/j.marenvres.2016.05.004.
[10] T.G. Fonseca, M.B. Morais, T. Rocha, D.M.S. Abessa, M. Aureliano, M.J. Bebianno, Ecotoxicological assessment of the anticancer drug cisplatin in the polychaete Nereis diversicolor, Sci. Total Environ. 575 (2017) 162–172, https://doi.org/10.1016/j.scitotenv.2016.09.185.
[11] T.G. da Fonseca, D.M.S. Abessa, M.J. Bebianno, Effects of mixtures of anticancer drugs in the benthic polychaete Nereis diversicolor, Environ. Pollut. 252 (2019) 1180–1192, https://doi.org/10.1016/j.envpol.2019.05.095.
[12] M. Jureczko, J. Kalka, Cytostatic pharmaceuticals as water contaminants, Eur. J. Pharmacol. 866 (2020), 172816, https://doi.org/10.1016/j.ejphar.2019.172816.
[13] T. Farías, S. Hajizadeh, L. Ye, Cryogels with high cisplatin adsorption capacity: Towards removal of cytotoxic drugs from wastewater, Sep. Purif. Technol. 235 (2020), 116203, https://doi.org/10.1016/j.seppur.2019.116203.
[14] F. Ogata, K. Inoue, H. Tominaga, Y. Iwata, A. Ueda, Y. Tanaka, N. Kawasaki, Use of calcined gibbsite to remove cisplatin from aqueous solutions, J. Water Environ. Technol. 12 (2014) 13–23, https://doi.org/10.2965/jwet.2014.13.
[15] K. Lenz, S. Hann, G. Koellensperger, Z. Stefanka, G. Stingeder, N. Weissenbacher, S. N. Mahnik, M. Fuerhacker, Presence of cancerostatic platinum compounds in hospital wastewater and possible elimination by adsorption to activated sludge, Sci. Total Environ. 345 (2005) 141–152, https://doi.org/10.1016/j.scitotenv.2004.11.007.
[16] K. Folens, A. Abebe, J. Tang, F. Ronsse, G. Du Laing, Biosorption of residual cisplatin, carboplatin and oxaliplatin antineoplastic drugs in urine after chemotherapy treatment, Environ. Chem. 15 (2018) 506–512, https://doi.org/10.1071/EN18115.
[17] J. Dobrzyńska, M. Dąbrowska, R. Olchowski, E. Zięba, R. Dobrowolski, Development of a method for removal of platinum from hospital wastewater by novel ion-imprinted mesoporous organosilica, J. Environ. Chem. Eng. 9 (4) (2021) 105302.
[18] K. Lenz, G. Koellensperger, S. Hann, N. Weissenbacher, S.N. Mahnik, M. Fuerhacker, Fate of cancerostatic platinum compounds in biological wastewater treatment of hospital effluents, Chemosphere 69 (2007) 1765–1774, https://doi.org/10.1016/j.chemosphere.2007.05.062.
[19] K. Lenz, S.N. Mahnik, N. Weissenbacher, R.M. Mader, P. Krenn, S. Hann, G. Koellensperger, M. Uhl, S. Knasmüller, F. Ferk, W. Bursch, M. Fuerhacker, Monitoring, removal and risk assessment of cytostatic drugs in hospital wastewater, Water Sci. Technol. 56 (2007) 141–149, https://doi.org/10.2166/wst.2007.828.
[20] C. Hernández, Y. Ramos, L.A. Fernández, O. Ledea, M. Bataller, E. Véliz, V. Besada, A. Rosado, Ozonation of cisplatin in aqueous solution at pH 9, Ozone Sci. Eng. 30 (2008) 189–196, https://doi.org/10.1080/01919510801907722.
[21] T. Kobayashi, J. Hirose, K. Sano, N. Hiro, Y. Ijiri, H. Takiuchi, H. Tamai, H. Takenaka, K. Tanaka, T. Nakano, Evaluation of an electrolysis apparatus for inactivating antineoplastics in clinical wastewater, Chemosphere 72 (2008) 659–665, https://doi.org/10.1016/j.chemosphere.2008.02.020.
[22] J. Hirose, F. Kondo, T. Nakano, T. Kobayashi, N. Hiro, Y. Ando, H. Takenaka, K. Sano, Inactivation of antineoplastics in clinical wastewater by electrolysis, Chemosphere 60 (2005) 1018–1024, https://doi.org/10.1016/j.chemosphere.2005.01.024.
[23] K.D. Lee, Y. Il Jeong, D.H. Kim, G.T. Lim, K.C. Choi, Cisplatin-incorporated nanoparticles of poly(acrylic acid-co-methyl methacrylate) copolymer, Int. J. Nanomedicine. 8 (2013) 2835–2845, https://doi.org/10.2147/IJN.S48367.
[24] B. Singh, N. Chauhan, V. Sharma, Design of molecular imprinted hydrogels for controlled release of cisplatin: evaluation of network density of hydrogels, Ind. Eng. Chem. Res. 50 (2011) 13742–13751, https://doi.org/10.1021/ie200758b.
[25] R. Lombana Fraguela, J.A. Ricardo Garcia, M.E. Villanueva Tagle, M.S. Pomares Alfonso, M. Cracchiolo, A. Kovačević, M. Tolazzi, A. Melchior, M. Sanadar, Evaluation of Dithiocarbamate-Modified Silica for Cisplatin Removal from Water, Processes. 11 (2023) 472. https://doi.org/10.3390/pr11020472.
[26] D. Han, M. López-Mesas, M. Luaces, Y. Enamorado, M. Sanadar, A. Melchior, M. Valiente, Comparative study on removal of platinum cytostatic drugs at trace level by cysteine, diethylenetriamino functionalized Si-gels and polyethyleneimine functionalized sponge: adsorption performance and mechanisms, Sci. Total Environ. 891 (2023), 164385, https://doi.org/10.1016/j.scitotenv.2023.164385.
[27] T.C. Johnstone, K. Suntharalingam, S.J. Lippard, The next generation of platinum drugs: targeted Pt(II) agents, nanoparticle delivery, and Pt(IV) prodrugs, Chem. Rev. 116 (2016) 3436–3486, https://doi.org/10.1021/acs.chemrev.5b00597.
[28] L. Kelland, The resurgence of platinum-based cancer chemotherapy, Nat. Rev. Cancer. 7 (2007) 573–584, https://doi.org/10.1038/nrc2167.
[29] B.P. Espósito, R. Najjar, Interactions of antitumoral platinum-group metallodrugs with albumin, Coord. Chem. Rev. 232 (2002) 137–149, https://doi.org/10.1016/S0010-8545(02)00049-8.
[30] A.I. Ivanov, J. Christodoulou, J.A. Parkinson, K.J. Barnham, A. Tucker, J. Woodrow, P.J. Sadler, Cisplatin binding sites on human albumin, J. Biol. Chem. 273 (1998) 14721–14730, https://doi.org/10.1074/jbc.273.24.14721.
[31] Ž.D. Bugarčić, J. Bogojeski, B. Petrović, S. Hochreuther, R. van Eldik, Mechanistic studies on the reactions of platinum(ii) complexes with nitrogen- and sulfur-donor biomolecules, Dalt. Trans. 41 (2012) 12329, https://doi.org/10.1039/c2dt31045g.
[32] Z. Wu, Z. Cheng, W. Ma, Adsorption of Pb(II) from glucose solution on thiol-functionalized cellulosic biomass, Bioresour. Technol. 104 (2012) 807–809, https://doi.org/10.1016/j.biortech.2011.10.100.
[33] Z. Li, L. Wu, H. Liu, H. Lan, J. Qu, Improvement of aqueous mercury adsorption on activated coke by thiol-functionalization, Chem. Eng. J. 228 (2013) 925–934, https://doi.org/10.1016/j.cej.2013.05.063.
[34] B. Parambath Kanoth, M. Claudino, M. Johansson, L.A. Berglund, Q. Zhou, Biocomposites from natural rubber: synergistic effects of functionalized cellulose nanocrystals as both reinforcing and cross-linking agents via free-radical thiol-ene chemistry, ACS Appl. Mater. Interfaces. 7 (2015) 16303–16310, https://doi.org/10.1021/acsami.5b03115.
[35] S.Y. Park, J.W. Chung, R.D. Priestley, S.Y. Kwak, Covalent assembly of metal nanoparticles on cellulose fabric and its antimicrobial activity, Cellul. 19 (2012) 2141–2151, https://doi.org/10.1007/s10570-012-9773-6.
[36] D. Mohan, A. Sarswat, V.K. Singh, M. Alexandre-Franco, C.U. Pittman, Development of magnetic activated carbon from almond shells for trinitrophenol removal from water, Chem. Eng. J. 172 (2-3) (2011) 1111–1125.
[37] L. Simonelli, C. Marini, W. Olszewski, M. Ávila Pérez, N. Ramanan, G. Guilera, V. Cuartero, K. Klementiev, Clæss,, The hard X-ray absorption beamline of the ALBA CELLS synchrotron, Cogent Phys. 3 (2016), https://doi.org/10.1080/23311940.2016.1231987.
[38] C. Marini, R. Boada, J. Prieto Burgos, N. Ramanan, I. García Domínguez, J. Zhao, T. T. Xiao, L. Simonelli, Low-cost vacuum compatible liquid cell for hard X-ray absorption spectroscopy, Nucl. Instruments Methods Phys. Res. Sect. A Accel. Spectrometers, Detect. Assoc. Equip. 908 (2018) 333–337, https://doi.org/10.1016/j.nima.2018.08.036.
[39] B. Ravel, M. Newville, Athena, Artemis, Hephaestus: data analysis for X-ray absorption spectroscopy using IFEFFIT, J. Synchrotron Radiat. 12 (2005) 537–541, https://doi.org/10.1107/S0909049505012719.
[40] W. Guo, Q. Zhou, Y. Jia, J. Xu, Cluster and factor analysis of elements in serum and urine of diabetic patients with peripheral neuropathy and healthy people, Biol. Trace Elem. Res. 194 (2020) 48–57, https://doi.org/10.1007/s12011-019-01747-x.
[41] Y. Gao, N. Yang, X. Yan, W. Hang, J. Xing, J. Zheng, E. Zhu, B. Huang, Early diagnosis of urinary lithiasis via elementary profile of serum samples, Anal. Methods. 4 (2012) 693–698, https://doi.org/10.1039/c2ay05705k.
[42] X.-Y. Lou, R. Boada, V. Verdugo, L. Simonelli, G. Pérez, M. Valiente, Decoupling the adsorption mechanisms of arsenate at molecular level on modified cube-shaped sponge loaded superparamagnetic iron oxide nanoparticles, J. Environ. Sci. 121 (2022) 1–12, https://doi.org/10.1016/j.jes.2021.09.001.
[43] A. Politzer, J.C. H Teng, T.T. Singh, T.J.C. H, T.T. Singh, The method of producing a regenerated cellulose sponge, 1963. https://lens.org/073-184-824-742-697.
[44] P.E.L. Kyle, T.B. P, Ion exchange polymers on improved porous substrates, 1982. https://lens.org/080-517-023-858-186.
[45] X.Y. Lou, R. Boada, L. Simonelli, M. Valiente, Enhanced arsenite removal by superparamagnetic iron oxide nanoparticles in-situ synthesized on a commercial cube-shape sponge: adsorption-oxidation mechanism, J. Colloid Interface Sci. 614 (2022) 460–467, https://doi.org/10.1016/j.jcis.2022.01.119.
[46] N.B. Rainer, R.N. B, Polymer product for the selective absorption of dissolved ions, 1992. https://lens.org/018-286-240-697-194.
[47] J.A. Muñoz, A. Gonzalo, M. Valiente, J. O S E Ä A N T O N I O M U N˜ O Z, A N N A G O N Z A L O, A N D M A N U E L V A L I E N T E, J.A. Muñoz, A. Gonzalo, M. Valiente, Arsenic Adsorption by Fe(III)-Loaded Open-Celled Cellulose Sponge. Thermodynamic and Selectivity Aspects, Environ. Sci. Technol. 36 (2002) 3405–3411. https://doi.org/10.1021/es020017c.
[48] J. Li, L.P. Zhang, F. Peng, J. Bian, T.Q. Yuan, F. Xu, R.C. Sun, Microwave-assisted solvent-free acetylation of cellulose with acetic anhydride in the presence of iodine as a catalyst, Molecules 14 (2009) 3551–3566, https://doi.org/10.3390/molecules14093551.
[49] T. Burks, M. Avila, F. Akhtar, M. Göthelid, P.C. Lansåker, M.S. Toprak, M. Muhammed, A. Uheida, Studies on the adsorption of chromium(VI) onto 3-Mercaptopropionic acid coated superparamagnetic iron oxide nanoparticles, J. Colloid Interface Sci. 425 (2014) 36–43, https://doi.org/10.1016/j.jcis.2014.03.025.
[50] C. Han, K. Xu, Q. Liu, X. Liu, J. Li, Colorimetric sensing of cysteine using label-free silver nanoparticles, Sensors Actuators, B Chem. 202 (2014) 574–582, https://doi.org/10.1016/j.snb.2014.05.139.
[51] K.H. Glover, H. Tsubomura, Compounds with zinc (II), cadmium (II), mercury (II), J. Am. Chem. Soc. 87 (1965) 1904–1909.
[52] S. Aryal, B.K.C. Remant, N. Dharmaraj, N. Bhattarai, C.H. Kim, H.Y. Kim, Spectroscopic identification of SAu interaction in cysteine capped gold

nanoparticles, Spectrochim. Acta - Part A Mol. Biomol. Spectrosc. 63 (2006) 160–163, https://doi.org/10.1016/j.saa.2005.04.048.
[53] A. Ihs, B. Liedberg, Chemisorption of l-cysteine and 3-mercaptopropionic acid on gold and copper surfaces: an infrared reflection-absorption study, J. Colloid Interface Sci. 144 (1991) 282–292, https://doi.org/10.1016/0021-9797(91)90259-B.
[54] R. Alimohammadzadeh, A.A. Rafi, L. Goclik, C.W. Tai, A. Cordova, Direct organocatalytic thioglycolic acid esterification of cellulose nanocrystals: a simple entry to click chemistry on the surface of nanocellulose, Carbohydr. Polym. Technol. Appl. 3 (2022), 100205, https://doi.org/10.1016/j.carpta.2022.100205.
[55] H.Y. Choi, J.H. Bae, Y. Hasegawa, S. An, I.S. Kim, H. Lee, M. Kim, Thiol-functionalized cellulose nanofiber membranes for the effective adsorption of heavy metal ions in water, Carbohydr. Polym. 234 (2020), 115881, https://doi.org/10.1016/j.carbpol.2020.115881.
[56] K. Pramanik, P. Sarkar, D. Bhattacharyay, 3-Mercapto-propanoic acid modified cellulose filter paper for quick removal of arsenate from drinking water, Int. J. Biol. Macromol. 122 (2019) 185–194, https://doi.org/10.1016/j.ijbiomac.2018.10.065.
[57] G.H. Gao, M.J. Park, Y. Li, G.H. Im, J.H. Kim, H.N. Kim, J.W. Lee, P. Jeon, O. Y. Bang, J.H. Lee, D.S. Lee, The use of pH-sensitive positively charged polymeric micelles for protein delivery, Biomaterials 33 (2012) 9157–9164, https://doi.org/10.1016/j.biomaterials.2012.09.016.
[58] M. Pavelka, M.F.A. Lucas, N. Russo, On the hydrolysis mechanism of the second-generation anticancer drug carboplatin, Chem. - A Eur. J. 13 (2007) 10108–10116, https://doi.org/10.1002/chem.200700887.
[59] M. Sooriyaarachchi, A. Narendran, J. Gailer, Comparative hydrolysis and plasma protein binding of cis-platin and carboplatin in human plasma in vitro, Metallomics 3 (2011) 49–55, https://doi.org/10.1039/c0mt00058b.
[60] X.L. Yang, A.H.J. Wang, Structural studies of atom-specific anticancer drugs acting on, DNA (1999), https://doi.org/10.1016/S0163-7258(99)00020-0.
[61] W.J.F. van der Vijgh, Clinical pharmacokinetics of carboplatin, Clin. Pharmacokinet. 21 (1991) 242–261, https://doi.org/10.2165/00003088-199121040-00002.
[62] A.J. Di Pasqua, J. Goodisman, J.C. Dabrowiak, Understanding how the platinum anticancer drug carboplatin works: from the bottle to the cell, Inorganica Chim. Acta. 389 (2012) 29–35, https://doi.org/10.1016/j.ica.2012.01.028.
[63] J. Wang, J. Tao, S. Jia, M. Wang, H. Jiang, Z. Du, The protein-binding behavior of platinum anticancer drugs in blood revealed by mass spectrometry, Pharmaceuticals. 14 (2021) 1–17, https://doi.org/10.3390/ph14020104.
[64] D. Wang, S.J. Lippard, Cellular processing of platinum anticancer drugs, Nat. Rev. Drug Discov. 4 (2005) 307–320, https://doi.org/10.1038/nrd1691.
[65] K.U. Maheswari, T. Ramachandran, D. Rajaji, Interaction of cisplatin with planar model membranes - dose dependent change in electrical characteristics, Biochim. Biophys. Acta - Biomembr. 1463 (2000) 230–240, https://doi.org/10.1016/S0005-2736(99)00189-3.
[66] G. Speelmans, W.H.H.M. Sips, R.J.H. Grisel, R.W.H.M. Staffhorst, A.M. J. Fichtinger-Schepman, J. Reedijk, B. De Kruijff, The interaction of the anti-cancer drug cisplatin with phospholipids is specific for negatively charged phospholipids and takes place at low chloride ion concentration, Biochim. Biophys. Acta - Biomembr. 1283 (1996) 60–66, https://doi.org/10.1016/0005-2736(96)00080-6.
[67] T. Zimmermann, F. Šebesta, J.V. Burda, A new grand-canonical potential for the thermodynamic description of the reactions in solutions with constant pH, J. Mol. Liq. 335 (2021) 115979.
[68] J.R. Yachnin, I. Wallin, R. Lewensohn, F. Sirzén, H. Ehrsson, The kinetics and cytotoxicity of cisplatin and its monohydrated complex, Cancer Lett. 132 (1998) 175–180, https://doi.org/10.1016/S0304-3835(98)00175-X.
[69] E. Curis, K. Provost, D. Bouvet, I. Nicolis, S. De Crauste-Manciet, D. De Brossard, S. Bénazeth, Carboplatin and oxaliplatin decomposition in chloride medium, monitored by XAS, J. Synchrotron Radiat. 8 (2001) 716–718, https://doi.org/10.1107/S0909049500017775.
[70] G. Feiqiang, L. Xiaolei, J. Xiaochen, Z. Xingmin, G. Chenglong, R. Zhonghao, Characteristics and toxic dye adsorption of magnetic activated carbon prepared from biomass waste by modified one-step synthesis, Colloids Surfaces A Physicochem. Eng. Asp. 555 (2018) 43–54, https://doi.org/10.1016/j.colsurfa.2018.06.061.
[71] S. Sen Gupta, K.G. Bhattacharyya, Kinetics of adsorption of metal ions on inorganic materials: a review, Adv. Colloid Interface Sci. 162 (2011) 39–58, https://doi.org/10.1016/j.cis.2010.12.004.
[72] J. Wang, X. Guo, Adsorption kinetic models: physical meanings, applications, and solving methods, J. Hazard. Mater. 390 (2020), 122156, https://doi.org/10.1016/j.jhazmat.2020.122156.
[73] M. Mourabet, H. El Boujaady, A. El Rhilassi, H. Ramdane, M. Bennani-Ziatni, R. El Hamri, A. Taitai, Defluoridation of water using brushite: equilibrium, kinetic and thermodynamic studies, Desalination 278 (2011) 1–9, https://doi.org/10.1016/j.desal.2011.05.068.
[74] D. Han, X. Li, Z. Gong, L. Jiang, Z. Wang, P. Liu, Hierarchical porous catalytic pyrolysis char derived from oily sludge for enhanced adsorption, ACS Omega 6 (2021) 20549–20559, https://doi.org/10.1021/acsomega.1c02575.
[75] V.D. Chinh, L.X. Hung, L. Di Palma, V.T.H. Hanh, G. Vilardi, Effect of carbon nanotubes and carbon nanotubes/gold nanoparticles composite on the photocatalytic activity of TiO2 and TiO2-SiO2, Chem. Eng. Technol. 42 (2019) 308–315, https://doi.org/10.1002/ceat.201800265.
[76] G. Los, M.J.H. Van Vugt, L. Den Engelse, H.M. Pinedo, Effects of temperature on the interaction of cisplatin and carboplatin with cellular DNA, Biochem. Pharmacol. 46 (1993) 1229–1237, https://doi.org/10.1016/0006-2952(93)90472-9.
[77] M.A. Allsopp, G.J. Sewell, C.G. Rowland, C.M. Riley, R.L. Schowen, The degradation of carboplatin in aqueous solutions containing chloride or other selected nucleophiles, Int. J. Pharm. 69 (1991) 197–210, https://doi.org/10.1016/0378-5173(91)90362-R.
[78] J. Wang, X. Guo, Adsorption isotherm models: classification, physical meaning, application and solving method, Chemosphere 258 (2020), 127279, https://doi.org/10.1016/j.chemosphere.2020.127279.
[79] R.D. Hancock, A.E. Martell, Ligand design for selective complexation of metal ions in aqueous solution, Chem. Rev. 89 (1989) 1875–1914, https://doi.org/10.1021/cr00098a011.
[80] A. Alfarra, E. Frackowiak, F. Béguin, The HSAB concept as a means to interpret the adsorption of metal ions onto activated carbons, Appl. Surf. Sci. 228 (2004) 84–92, https://doi.org/10.1016/j.apsusc.2003.12.033.
[81] P. Pourhakkak, A. Taghizadeh, M. Taghizadeh, M. Ghaedi, S. Haghdoust, Fundamentals of adsorption technology, 1st ed., Elsevier Ltd., 2021. https://doi.org/10.1016/B978-0-12-818805-7.00001-1.
[82] M. Sun, Y. Yang, M. Huang, S. Fu, Y. Hao, S. Hu, D. Lai, L. Zhao, Adsorption behaviors and mechanisms of antibiotic norfloxacin on degradable and nondegradable microplastics, Sci. Total Environ. 807 (2022), 151042, https://doi.org/10.1016/j.scitotenv.2021.151042.
[83] R.M. Schneider, C.F. Cavalin, M.A.S.D. Barros, C.R.G. Tavares, Adsorption of chromium ions in activated carbon, Chem. Eng. J. 132 (2007) 355–362, https://doi.org/10.1016/j.cej.2007.01.031.
[84] S. Guo, M. Gao, T. Shen, Y. Xiang, G. Cao, Effective adsorption of sulfamethoxazole by novel organo-Vts and their mechanistic insights, Microporous Mesoporous Mater. 286 (2019) 36–44, https://doi.org/10.1016/j.micromeso.2019.05.032.
[85] Z. Gu, M. Gao, Z. Luo, L. Lu, Y. Ye, Y. Liu, Bis-pyridinium dibromides modified organo-bentonite for the removal of aniline from wastewater: a positive role of π-π Polar interaction, Appl. Surf. Sci. 290 (2014) 107–115, https://doi.org/10.1016/j.apsusc.2013.11.008.
[86] S.F. Soares, J. Nogueira, T. Trindade, A.L. Daniel-da-Silva, Towards efficient ciprofloxacin adsorption using magnetic hybrid nanoparticles prepared with κ-, ι-, and λ-carrageenan, J. Nanostructure Chem. 13 (2022) 283–302, https://doi.org/10.1007/s40097-022-00498-x.
[87] S. Kishani, T. Benselfelt, L. Wågberg, J. Wohlert, Entropy drives the adsorption of xyloglucan to cellulose surfaces – a molecular dynamics study, J. Colloid Interface Sci. 588 (2021) 485–493, https://doi.org/10.1016/j.jcis.2020.12.113.
[88] G.D. Değermenci, N. Değermenci, V. Ayvaoğlu, E. Durmaz, D. Çakır, E. Akan, Adsorption of reactive dyes on lignocellulosic waste; characterization, equilibrium, kinetic and thermodynamic studies, J. Clean. Prod. 225 (2019) 1220–1229, https://doi.org/10.1016/j.jclepro.2019.03.260.
[89] T. Yoshinaga, Y. Iso, T. Isobe, Optimizing the microwave-assisted hydrothermal synthesis of blue-emitting L-cysteine-derived carbon dots, J. Lumin. 213 (2019) 6–14, https://doi.org/10.1016/j.jlumin.2019.05.003.
[90] V. Sharma, P. Ilaiyaraja, A.C. Dakshinamurthy, C. Sudakar, One step thermolysis of Sb-Mercaptopropionic acid complex in ambient air atmosphere for growing Sb2S3 thin films with controlled microstructure, Mater. Sci. Semicond. Process. 121 (2021), 105330, https://doi.org/10.1016/j.mssp.2020.105330.
[91] M. Mrad, T. Ben Chaabane, H. Rinnert, B. Lavinia, J. Jasniewski, G. Medjahdi, R. Schneider, Aqueous synthesis for highly emissive 3-mercaptopropionic acid-capped AIZS quantum dots, Inorg. Chem. 59 (2020) 6220–6231, https://doi.org/10.1021/acs.inorgchem.0c00347.
[92] W. Jian, S. Liu, J. Li, W. Yang, Decomposition reaction of Zn-MPA(3-mercaptopropionic acid) complex under microwave irradiation, Chem. Res. Chinese Univ. 24 (3) (2008) 353–356.
[93] R. Micanovic, K. Lafavers, P.S. Garimella, X.R. Wu, T.M. El-Achkar, Uromodulin (Tamm-Horsfall protein): guardian of urinary and systemic homeostasis, Nephrol. Dial. Transplant. 35 (2020) 33–43, https://doi.org/10.1093/ndt/gfy394.
[94] S. Aitekenov, A. Gaipov, R. Bukasov, Review: detection and quantification of proteins in human urine, Talanta 223 (2021), 121718, https://doi.org/10.1016/j.talanta.2020.121718.
[95] L. Curtis, A. Turner, N. Vyas, G. Sewell, Speciation and reactivity of cisplatin in river water and seawater, Environ. Sci. Technol. 44 (2010) 3345–3350, https://doi.org/10.1021/es903620z.

Supplementary data of

Trace cisplatin and carboplatin removal by 3-mercaptopropionic acid and L-cysteine functionalized sponges: adsorption behavior and mechanism

Dong Han,[1] Montserrat López-Mesas(*),[1] Roberto Boada,[1] Tania Farías,[2] Ana R. Lazo Fraga,[2] and Manuel Valiente[1]

[1]*GTS-UAB Research Group, Department of Chemistry, Faculty of Science, Universitat Autònoma de Barcelona, Bellaterra, (Cerdanyola del Vallès), 08193 Barcelona, Spain*

[2]*Institute of Materials Science and Technology, University of Havana, 10400, Havana, Cuba*

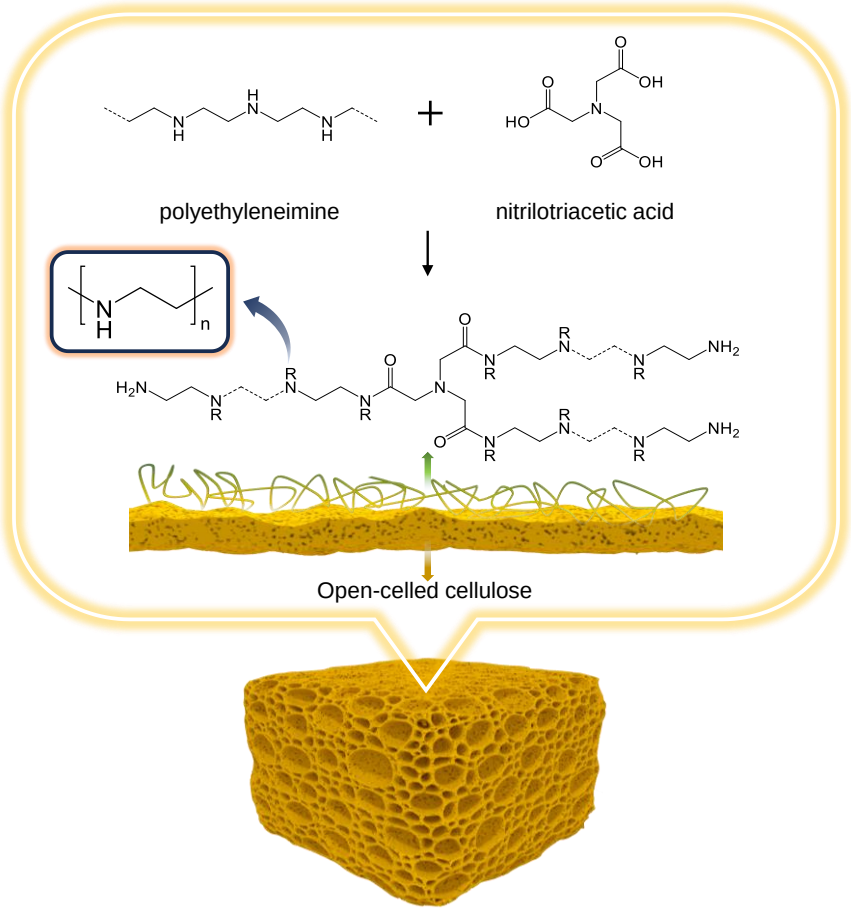

Fig. S1. Schematic illustration of Sponge.

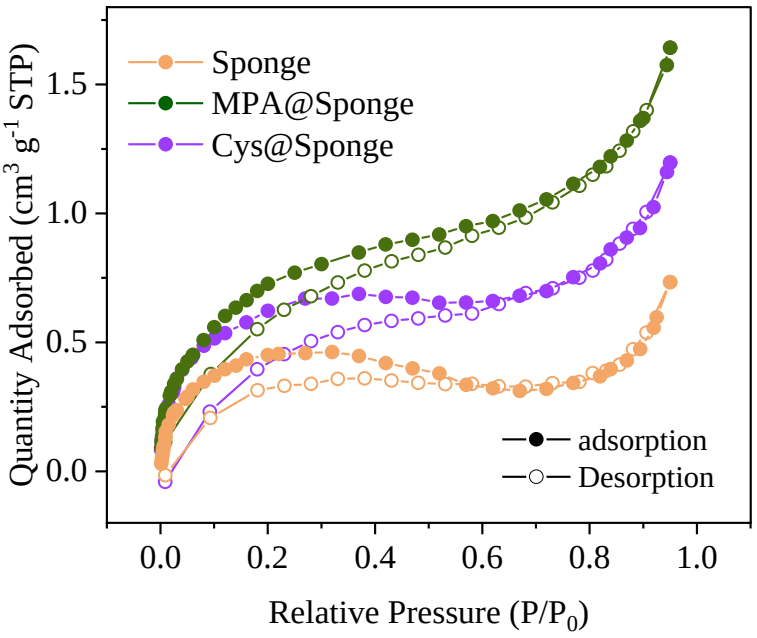

Fig. S2. N_2 adsorption-desorption isotherms of Sponge, MPA@Sponge, and Cys@Sponge.

The experimental kinetic data were fitted to the PFO model (eq. 1) and PSO model (eq. 2)[1]:

$$q_t = q_{e.cal}(1-e^{-k_1 t}) \quad (1)$$

$$q_t = \frac{q_{e.cal}^2 k_2 t}{q_{e.cal} k_2 t + 1} \quad (2)$$

The variables $q_{e.cal}$ and q_t represent adsorption capacities (μg g^{-1}) at equilibrium derived from models and at a given contact time t (h), respectively. The rate constant for PFO is denoted as k_1 (h^{-1}), while the rate constant for PSO is denoted as k_2 (h^{-1}).

In the present study, the adsorption equilibrium data was fitted using Langmuir (eq. 3) and Freundlich (eq. 5) models. These models are formulated as follows:

$$q_e = \frac{q_m K_L c_e}{1 + K_L c_e} \quad (3)$$

$$R_L = \frac{1}{1 + K_L c_0} \quad (4)$$

$$q_e = K_F c_e^{1/n} \quad (5)$$

where q_m represents the maximum adsorption capacity (μg g^{-1}). K_L is the constant indicative of the affinity of binding sites (L μg^{-1}). The dimensionless parameter known as the equilibrium parameter or separation factor, denoted R_L (eq. 4), serves to characterize the nature of the adsorption process. Specifically, values of R_L falling within the ranges of 0, $0 < R_L < 1$, 1, and >1 correspond to irreversible, favorable, linear, and unfavorable adsorption behaviors, respectively[2]. K_F ((μg g^{-1})(L $\mu g^{-1})^{1/n}$) and n are the Freundlich constants related to the adsorption capacity and intensity, respectively. Value of $1/n < 1$, it indicates a normal adsorption, and $1/n > 1$ indicates cooperative adsorption. If $1/n$ lies between one and ten, this indicates a favorable sorption process [3–6].

Three key thermodynamic parameters, specifically the Gibbs free energy ($\Delta G°$),

enthalpy change ($\Delta H°$), and entropy change ($\Delta S°$), were determined using eq. (6), (7), and (8), respectively.

$$\Delta G^o = -\mathrm{R}T \ln K \tag{6}$$

$$\ln K = \frac{\Delta S^o}{\mathrm{R}} - \frac{\Delta H^o}{\mathrm{R}T} \tag{7}$$

$$K = \frac{C_0 - C_e}{C_e} \tag{8}$$

Where R is the ideal gas constant (8.314 J mol^{-1} K^{-1}), T is the absolute temperature (K), K is dimensionless distribution constant. Values of $\Delta H°$ and $\Delta S°$ were obtained via the slope and intercept of linear Van't Hoff plots (ln K versus $1/T$).

Table S1. Summary of elemental analysis of MPA@Sponge, Cys@Sponge and Sponge.

Element (wt%)	MPA@Sponge	Cys@Sponge	Sponge
C	41.5 ± 0.1	40.2 ± 0.7	40.2 ± 0.2
H	6.35 ± 0.09	6.32 ± 0.09	6.4 ± 0.1
N	4.2 ± 0.1	5.6 ± 0.2	3.04 ± 0.01
S	1.23 ± 0.07	0.59 ± 0.03	<0.1

Table S2. Kinetic parameters for the adsorption of cisplatin and carboplatin by MPA@Sponge and Cys@Sponge.

Kinetic model			Pseudo-first-order			Pseudo-second-order		
		$q_{e.exp}$	k_1	$q_{e.cal}$	R^2	k_2	$q_{e.cal}$	R^2
Adsorbent		µg g^{-1}	h^{-1}	µg g^{-1}		h^{-1}	µg g^{-1}	
MPA@ Sponge	Cisplatin	29.8 ± 0.1	17 ± 30	29.2 ± 0.2	0.9917	0.9 ± 0.3	29.7 ± 0.2	0.9987
	Carboplatin	6.3 ± 0.8	14 ± 9	6.2 ± 0.1	0.9992	5 ± 2	6.3 ± 0.1	0.9994
Cys@ Sponge	Cisplatin	21.4 ± 0.3	1.1 ± 0.4	19.0 ± 0.4	0.9896	0.08 ± 0.03	20.0 ± 0.5	0.9944
	Carboplatin	5.7 ± 0.1	1.9 ± 0.9	4.7 ± 0.3	0.9934	0.4 ± 0.2	5.1 ± 0.3	0.9953
Sponge	Cisplatin	15.4 ± 0.1	74 ± 15	14.8 ± 0.3	0.9229	8 ± 2	15.3 ± 0.2	0.9688
	Carboplatin	1.7 ± 0.3	50 ± 33	1.8 ± 0.2	0.4831	61 ± 74	1.8 ± 0.2	0.4329

Table S3. Adsorption isotherms parameters of MPA@Sponge and Cys@Sponge towards cisplatin and carboplatin solutions.

Isotherm model				Langmuir				Freundlich		
		T	$q_{m.exp}$	$q_{m.cal}$	K_L	R_L	R^2	K_F	$1/n$	R^2
Adsorbent		K	mg g^{-1}	mg g^{-1}	10^{-5} L μg^{-1}			($\mu g\ g^{-1}$) (L μg^{-1})$^{1/n}$		
MPA@	Cis	293	11 ± 2	10.9 ± 0.5	3.4 ± 0.8	0.055-0.998	0.9885	91 ± 39	0.37 ± 0.03	0.9708
Sponge		318	23 ± 3	29 ±2	1.0 ± 0.2	0.168-0.999	0.9910	81 ± 21	0.44 ± 0.02	0.9942
		343	49 ± 1	85 ± 7	0.5 ± 0.1	0.277-0.999	0.9935	20 ± 1	0.62 ± 0.01	0.9928
	Carbo	293	7.3 ± 0.7	10 ± 1	1.0 ± 0.4	0.089-0.999	0.9617	15 ±16	0.49 ± 0.09	0.9047
		318	12.7 ± 0.7	18.0 ± 0.9	0.6 ± 0.1	0.148-0.999	0.9954	8 ± 6	0.57 ± 0.05	0.9732
		343	30.9 ± 0.2	38 ± 2	1.3 ± 0.2	0.071-0.999	0.9935	146 ± 49	0.42 ± 0.03	0.9884
Cys@	Cis	293	7.0 ± 0.6	8.0 ± 0.3	2.1 ± 0.3	0.086-0.999	0.9941	36 ± 29	0.41 ± 0.06	0.9180
Sponge		318	11.8 ± 0.9	14.6 ± 0.9	0.8 ± 0.1	0.196-0.999	0.9915	20 ± 7	0.49 ± 0.03	0.9890
		343	13.8 ± 0.3	16.2 ±0.6	1.4 ± 0.2	0.128-0.999	0.9959	55 ± 27	0.43 ± 0.04	0.9734
	Carbo	293	7.8 ± 0.7	12.1 ± 0.9	0.43 ± 0.07	0.190-0.999	0.9916	3 ± 2	0.62 ± 0.06	0.9695
		318	12 ± 2	24 ± 4	0.25 ± 0.07	0.288-0.999	0.9859	1 ± 1	0.71 ± 0.07	0.9746
		343	20.7 ± 0.4	33 ± 2	0.44 ± 0.06	0.185-0.999	0.9942	7 ± 5	0.62 ±0.05	0.9812

Table S4. Summary of thermodynamic parameters: $\Delta G°$ (kJ mol^{-1}), $\Delta H°$ (kJ mol^{-1}), and $\Delta S°$ (J mol^{-1} K^{-1}).

Adsorbents		MPA@Sponge			Cys@Sponge		
T(K)		293	318	343	293	318	343
Cisplatin	$\Delta G°$	-2.3 ± 0.1	-4.1 ± 0.4	-6.59 ± 0.06	0.78 ± 0.02	-0.8 ± 0.1	-2.97 ± 0.05
	$\Delta H°$	22.5 ± 0.1			22.6 ± 0.5		
	$\Delta S°$	84 ± 3			74 ± 2		
Carboplatin	$\Delta G°$	3.0 ± 0.2	2.5 ± 0.4	-5.5 ± 0.2	4.90 ± 0.06	3.43 ± 0.04	-0.3 ± 0.1
	$\Delta H°$	51.4 ± 0.1			34.1 ± 0.1		
	$\Delta S°$	161.3 ± 0.5			102 ± 3		

Table S5. EXAFS fitting parameters at the Pt L_3-edge for Pt foil, Pt(II) standards, and Pt-CDs adsorbed on sponges.

Sample	**Path**	**S_0^2** [a]	**CN** [b]	***R*** **(Å)** [c]	**σ^2 (Å^2)** [d]	**ΔE_0 (eV)** [e]	***R*-factor**
Pt foil	Pt–Pt	0.82 ± 0.04	12*	2.742 ± 0.002	0.005 ± 0.001	5.9 ± 0.5	0.005
K_2PtCl_4	Pt–Cl	0.83 ± 0.09	4*	2.305 ± 0.006	0.002 ± 0.001	9.2 ± 1.3	0.016
cisplatin	Pt–Cl Pt–N	0.82 ± 0.02	2* 2*	2.36 ± 0.02 1.96 ± 0.01	0.003 ± 0.002 0.002 ± 0.001	6.1 ± 1.6	0.012
carboplatin	Pt–O/N	0.81 ± 0.05	4*	1.99 ± 0.05	0.003 ± 0.001	4.1 ± 2.3	0.032
cisplatin on MPA@Sponge	Pt–S	0.82*	3.8 ± 0.4	2.305 ± 0.008	0.002 ± 0.001	5.3 ± 1.2	0.011
carboplatin on MPA@Sponge	Pt–S	0.82*	4.1 ± 0.3	2.298 ± 0.006	0.002 ± 0.001	4.0 ± 0.9	0.015
cisplatin on Cys@Sponge	Pt–S	0.82*	4.2 ± 0.1	2.31 ± 0.01	0.004 ± 0.001	2.5 ± 1.4	0.022
carboplatin on Cys@Sponge	Pt–S	0.82*	4.2 ± 0.1	2.305 ± 0.009	0.004 ± 0.001	2.4 ± 1.2	0.012

(a) Amplitude reduction factor, (b) coordination number, (c) interatomic distance, (d) EXAFS Debye-Waller factor, (e) the inner potential correction, R-factor is a measure of the mean square sum of the misfit at each data point which gives an indication of the goodness of fit. It is defined as: R-factor $= \frac{\sum(data-fit)^2}{\sum data^2}$, where the sums are over the data points in the fitting region, * fixed.

Table S6. Characteristics of selected urine and wastewater analogs [7]. Concentrations of cations and anions determined by Ion chromatography (IC, Dionex Aquion, Thermo Scientific, USA).

Samples	Urine in tap water (1:100)	Urine in tap water (1:10)	Urine
pH	6.90 ± 0.02	6.36 ± 0.01	5.62 ± 0.02
Cations (mg L^{-1})			
Na^+	102 ± 16	264 ± 1	1972 ± 17
K^+	19.8 ± 0.7	157 ± 5	1530 ± 4
Ca^{2+}	26 ± 6	29 ± 1	43 ± 7
Mg^{2+}	4.0 ± 0.2	5.0 ± 0.5	8.7 ± 0.8
NH_4^+	10 ± 2	95 ± 4	982 ± 2
Anions (mg L^{-1})			
Cl^-	85 ± 1	550 ± 8	3606 ± 7
SO_4^{2-}	197 ± 6	1004 ± 8	8961 ± 14
PO_4^{3-}	66.4 ± 1	682 ± 14	6138 ± 19
$C_2O_4^{2-}$	2.3 ± 0.1	24.9 ± 0.4	251 ± 4

Table S7. Comparison of cost, sulfur content, and removal efficiency between the thiol-functionalized sponges (MPA@Sponge and Cys@Sponge) and the commercially available adsorbents (Si-SH and Si-Cys).

Adsorbents	Reagents [€ per g]	Sulfur content [a] wt%	Removal [b] %	Ref.
MPA@Sponge	5.5 [d]	1.23 ± 0.07	71.5 ± 0.2	This work
Cys@Sponge	6.3 [d]	0.59 ± 0.03	45.5 ± 0.6	This work
Si-SH [c]	39.4 [e]	4.97 ± 0.07	98.7 ± 0.1	This work
Si-Cys [c]	22.3 [e]	1.30 ± 0.02	76.3 ± 0.2	[7]

(a) Determined by using element analyzer (Flash EA 2000 CHNS, Thermo Fisher, America); (b) adsorption of cisplatin, initial concentration of 235 μg L^{-1}, volume 10 mL, dosage 50 mg, temperature 293 K; (c) commercial adsorbents purchased from Sigma-Aldrich; (d) sum of calculated synthetic reagent costs; (e) finished product price.

References:

[1] J. Wang, X. Guo, Adsorption kinetic models: Physical meanings, applications, and solving methods, J. Hazard. Mater. 390 (2020) 122156. https://doi.org/10.1016/j.jhazmat.2020.122156.

[2] T.W. Weber, R.K. Chakravorti, Pore and solid diffusion models for fixed-bed adsorbers, AIChE J. 20 (1974) 228–238. https://doi.org/10.1002/aic.690200204.

[3] S. Goldberg, Equations and Models Describing Adsorption Processes in Soils, in: 2018: pp. 489–517. https://doi.org/10.2136/sssabookser8.c10.

[4] E.G. Furuya, H.T. Chang, Y. Miura, K.E. Noll, A fundamental analysis of the isotherm for the adsorption of phenolic compounds on activated carbon, Sep. Purif. Technol. 11 (1997) 69–78. https://doi.org/10.1016/S1383-5866(96)01001-5.

[5] Physical chemistry, J. Franklin Inst. 272 (1961) 71. https://doi.org/10.1016/0016-0032(61)90671-8.

[6] V.D. Chinh, L.X. Hung, L. Di Palma, V.T.H. Hanh, G. Vilardi, Effect of Carbon Nanotubes and Carbon Nanotubes/Gold Nanoparticles Composite on the Photocatalytic Activity of TiO2 and TiO2-SiO2, Chem. Eng. Technol. 42 (2019) 308–315. https://doi.org/10.1002/ceat.201800265.

[7] D. Han, M. López-Mesas, M. Luaces, Y. Enamorado, M. Sanadar, A. Melchior, M. Valiente, Comparative study on removal of platinum cytostatic drugs at trace level by cysteine, diethylenetriamino functionalized Si-gels and polyethyleneimine functionalized sponge: Adsorption performance and mechanisms, Sci. Total Environ. 891 (2023) 164385. https://doi.org/10.1016/j.scitotenv.2023.164385.

Chapter 3

Further insight

If you ever feel insignificant, remember, every atom in your body was once forged in the fiery heart of a star. You're literally stardust with shoes!

Trace cisplatin adsorption by thiol-functionalized sponge (TFS) and Sn/SnO_2-coated TFS: adsorption study and mechanism investigation

Dong Han [a], Margarita Edelia Villanueva Tagle [b], Mirella Peña Icart [c], Montserrat López-Mesas [a,*], and Manuel Valiente [a]

[a] *GTS-UAB Research Group, Department of Chemistry, Faculty of Science, Universitat Autònoma de Barcelona, Bellaterra, (Cerdanyola del Vallès), 08193 Barcelona, Spain*

[b] *Faculty of Chemistry, University of Havana, Havana 10400, Cuba*

[c] *Institute of Materials Science and Technology, University of Havana, Havana 10400, Cuba*

To be submitted

Abstract

Trace cisplatin (235 μg L^{-1}) were efficiently removed by thiol-functionalized sponges (TFSs) derived from cellulose-based Metalzorb® sponge (Sponge) that was functionalized with 3-mercaptopropionic acid (3-MPA). Additionally, the functionalization process involves the reduction of TFS through $Na_2S·9H_2O$ or $SnCl_2·2H_2O$, resulting in TFS_1 and Sn/SnO_2-coated TFS_2, respectively. TFS_1 and TFS_2 exhibited maximum removal efficiencies of 95.5 ± 0.8% and 99.5 ± 0.1% for cisplatin, respectively, while the non-functionalized Sponge achieved removal of only 29 ± 4%. FTIR, elemental analysis, SEM-EDS, and XPS characterization substantiated the porous morphology of TFSs and the successful grafting of thiol groups, which serve as affinity sites for Pt−S complexation, thereby enhancing the adsorption. During adsorption, aqua-derivatives of cisplatin, formed through hydration, complexed with thiol sites via ligand displacement. Additionally, the presence of blister-like Sn/SnO_2 coating on TFS_2 further improved the adsorption. The rapid adsorption process fitted to a pseudo-second-order kinetic model, involving diffusion and chemisorption. Generally, the Langmuir isotherm model can adequately describe the monolayer adsorption behavior of cisplatin. However, the aggregation of Sn/SnO_2 loaded onto TFS_2 at 343 K introduced surface heterogeneity, thereby rendering adsorption isotherm to exhibit a better fit to the Freundlich model. Furthermore, despite Pt−S complexation being crucial for the adsorption of cisplatin, the differential pH dependence observed in the adsorption by the two TFSs and the assessment of mean free energy derived from Dubinin-Radushkevich isotherm model, suggest that the adsorption of cisplatin onto TFS_1 also involves physisorption such as electrostatic attraction, whereas for TFS_2, chemisorption predominates. Increasing temperature facilitates the thermal-favored formation of Pt−S bonds, thereby significantly promoting the adsorption. However, for TFS_2, the highest temperature (343 K) leads to aggregation of Sn/SnO_2, which consequently compromises the adsorption.

Keywords: cisplatin; cytostatics; adsorption; functionalized materials; emerging pharmaceutical pollutants

1. Introduction

Cisplatin, a widely employed platinum-based cytostatic drug (Pt-CDs), has exhibited remarkable efficacy in the field of cancer therapy [1–3]. The cytotoxic effects and antitumor activity of cisplatin can be attributed to its preferential binding to guanine-N7, which subsequently triggers DNA damage responses and apoptosis [4]. However, despite its potent anticancer properties, cisplatin is accompanied by a spectrum of adverse effects resulting from its non-selective impact on normal cells, in particular nephrotoxicity [5]. Kidney damage emerges as one of the most prevalent side effects observed, because the kidneys serve as the primary excretory organs for cisplatin [6]. Pharmacokinetic investigations have provided evidence indicating that roughly 10-40% of the cisplatin is excreted through urine of patients in 24 h after administration, either in its unmodified state or as metabolites [7]. Many studies have demonstrated over the past two decades that these cytostatic substances were eventually emitted into the ecosystem via the release of hospital or household wastewaters, with the latter being polluted by outpatients. The concentrations of these compounds range from ng L^{-1} to several hundred of μg L^{-1} [8–18]. Once in water bodies, cisplatin can persist and accumulate, leading to long-term exposure for aquatic organisms [19]. Studies have shown that cisplatin can have toxic effects on aquatic organisms. It can disrupt the physiological processes and biochemical pathways of aquatic species, like invertebrates [20]. The drug has been found to cause DNA damage, interfere with cell division, and induce oxidative stress in exposed organisms. These adverse effects can ultimately impact the survival, growth, reproduction, and overall ecological balance of affected both marine and freshwater aquatic ecosystems [21]. In summary, cisplatin poses environmental hazards due to its potential contamination of water bodies and its toxicity towards aquatic organisms [22]. Efforts should be made to minimize the release of cisplatin into the environment and develop appropriate wastewater treatment methods to mitigate its ecological impact.

There has been a relatively limited amount of research focused on exploring the

feasibility and effectiveness of wastewater remediation techniques for cisplatin [13]. Several different approaches have been investigated in this regard, including adsorption [16,23–28], membrane bioreactor system [15], ozonation [29], and electrolysis [30,31]. Among them, adsorption exhibits distinct advantages compared to alternative technologies, particularly in terms of economic feasibility, operational simplicity, and treatment effectiveness. Adsorption demonstrates notable applicability even in scenarios involving low concentrations of adsorbates. Additionally, its versatility is evident through its compatibility with both continuous processing and batch modes. Furthermore, adsorption exhibits promising prospects for the adsorbates recovery and the adsorbents regeneration, enhancing its sustainability and resource efficiency [32]. For instance, several pioneering studies have investigated the adsorption of cisplatin employing various materials [13]. In 2005, activated sludge was used to adsorb cisplatin. Following a 24-hour treatment period, 96% of cisplatin (initial concentration ranging from 4.7 to 145 μg L^{-1}) was effectively removed [16]. Ogata et al. employed calcined gibbsite to adsorb 10 mg L^{-1} of cisplatin, resulting in an observed efficient removal of about 90% of cisplatin [24]. Different adsorbents derived from biomass, including wood ash, biochar, chitosan and activated carbon, were prepared to remove inorganic $PtCl_6^{2-}$ as a template of cisplatin (with initial Pt concentrations ranging from 1 to 10 mg L^{-1}). It was observed that at an adsorbent dosage of 10 g L^{-1}, the adsorption capacities ranged from 0.23 to 0.97 mg g^{-1}. [26]. In 2020, Carboxyl-functionalized cryogels designed for the adsorption of cisplatin (initial concentration range: 0.25 to 2 g L^{-1}) were synthesized. It is reported that due to the potential formation of stable complexes between Pt and carboxyl groups, the maximum adsorption capacity for cisplatin reached 150 mg g^{-1} [27]. A recent study proposed the synthesis of Pt(II)-imprinted mesoporous thiocyanato-functionalized silica, and this material demonstrated a maximum static adsorption capacity of 76.4 mg g^{-1} for $PtCl_4^{2-}$ (as a template for cisplatin) [25]. Similarly, another recent investigation reported the modification of silica using dithiocarbamate. When the dithiocarbamate-modified

silica was employed to adsorb cisplatin (initial Pt concentration 5-150 mg L^{-1} in saline solution), a removal rate of 85% was achieved under conditions of 10 g L^{-1} adsorbent dosage and one hour contact. And the maximum attainable adsorption capacity reached 15.6 mg g^{-1} [28]. After conducting a thorough examination of the aforementioned studies, future investigations concerning the adsorption of Pt-CDs should prioritize the adsorption at low concentration levels that closely resemble those found in the environment. This emphasis is justified due to the predominant controlled laboratory experiments in the existing literature that not covered environmentally relevant concentrations. In addition, the adsorption mechanism of Pt-CDs needs to be well explained, which is beneficial to provide guidance for the preparation of high affinity and strong selectivity adsorption materials in future.

In our previous investigation, a comparative analysis was conducted on three commercially accessible materials, specifically cysteine-functionalized silica gel, 3-(diethylenetriamino)propyl-functionalized silica gel, and open-celled cellulose MetalZorb® sponge (Sponge), to evaluate their respective abilities in adsorbing trace cisplatin and carboplatin [33]. From the conclusions, the existence of thiol groups, serving as sites of affinity, showed promise in forming complexes with the targeted Pt species. Subsequently, guided by these findings, we achieved successful enhancement of the adsorption capacity for Pt-CDs on inexpensive Sponge in another study by employing functionalization with 3-mercaptopropionic acid (3-MPA) [34]. Nevertheless, there is some evidence indicating that thiols (−SH) may undergo oxidation to form disulfides (−S−S− bonds) induced by diverse oxidizing agents or enzymatic processes [35–42]. This inevitable oxidation has the potential to exert a discernible influence on following Pt−S bonding. Therefore, to further enhance the adsorption of cisplatin by thiol-functionalized sponges, in this study, following the functionalization of Sponge with 3-MPA, two reducing agents, $Na_2S·9H_2O$ and $SnCl_2·2H_2O$, were employed to reduce disulfides to thiols. The synthesized adsorbents were characterized by SEM-EDS, ATR-FTIR, XPS,

and elemental analyzer (EA). And a comprehensive investigation was conducted to examine the fundamental variables that influence the adsorption capacity of cisplatin onto synthesized materials. The parameters under scrutiny included the pH of the solution, contact time, initial concentration, and temperature.

2. Materials and methods

2.1 Reagents and materials

Cisplatin (diamminedichloroplatinum(II), CAS: 15663-27-1, purity: 99%) was acquired from STREM Chemicals and used as received. A stock solution of cisplatin (Pt concentration 500 mg L^{-1}) was initially formulated in 0.2 mol L^{-1} HCl and subsequently diluted with Milli-Q water to desired concentrations. 3-mercaptopropionic acid (3-MPA, ≥ 99%), *N,N*-dimethylformamide (DMF, 99.8%), Sodium hydrogen sulfate monohydrate ($NaHSO_4 \cdot H_2O$, ≥ 99%), Sodium sulfide nonahydrate ($Na_2S \cdot 9H_2O$, ≥ 98%) and Tin(II) chloride dihydrate ($SnCl_2 \cdot 2H_2O$, 98%) were acquired from Sigma-Aldrich. Ethanol (96% v/v) was purchased from Scharlab. MetalZorb® Sponge (Sponge) was generously supplied by CleanWay Environmental Partners, Inc. (Portland, USA). Unless otherwise specified, Milli-Q water (with a resistivity of 18.2 MΩ m^{-1}) was utilized for the duration of the experimental procedure.

2.2 Thiol-functionalization of Sponge

Relevant published patents and studies [34,43–48] propose that the porous cube-shaped cellulose sponge comprises a water-swellable polymer, polyethyleneimine, formed through thermally induced amide formation, and is physically coated on the sponge backbones (illustrated in Fig. 1a). The polymer product is claimed to possess a strong affinity for the adsorption of transition metal ions [34,43–48]. Initially, the Sponge cubes were mechanically ground to achieve fine powders with particle sizes of ≤ 0.5 mm. Subsequently, the powdered Sponge was subjected to washing using 1.0 mol L^{-1} HCl (once) and Milli-Q water (three times). Lastly, it was dried overnight at a temperature of

343 K.

The thiol-functionalization process of the Sponge was conducted via esterification, employing a modified methodology derived from a prior investigation [49]. As depicted in Fig. 1b, 1.0 g of Sponge was mixed with 5 mL of 3-MPA, 2.5 mL of DMF, and 25 mg of $NaHSO_4 \cdot H_2O$ in a round bottom flask. The resulting mixture was stirred and heated in an oil bath at 120 °C for 4 h. Throughout this time, a portion of the thiol groups present in the resulting product inevitably underwent oxidation. Thus, the resultant products were subsequently reduced to free −SH groups using 6.0 g of $Na_2S \cdot 9H_2O$ as a reductant in 25 mL of ethanol (95%) for a period of 1 hour. The resulting thiol-functionalized Sponge (TFS) was designated as TFS_1. Additionally, an alternative approach was employed using $SnCl_2 \cdot 2H_2O$ (5.65 g in 25 mL ethanol) instead of $Na_2S \cdot 9H_2O$ to reduce the −SH groups. Simultaneously, the resulting Sn/SnO_2 species became embedded onto the surface of the Sponge resulting in a Sn/SnO_2-coated thiol-functionalized Sponge designated as TFS_2.

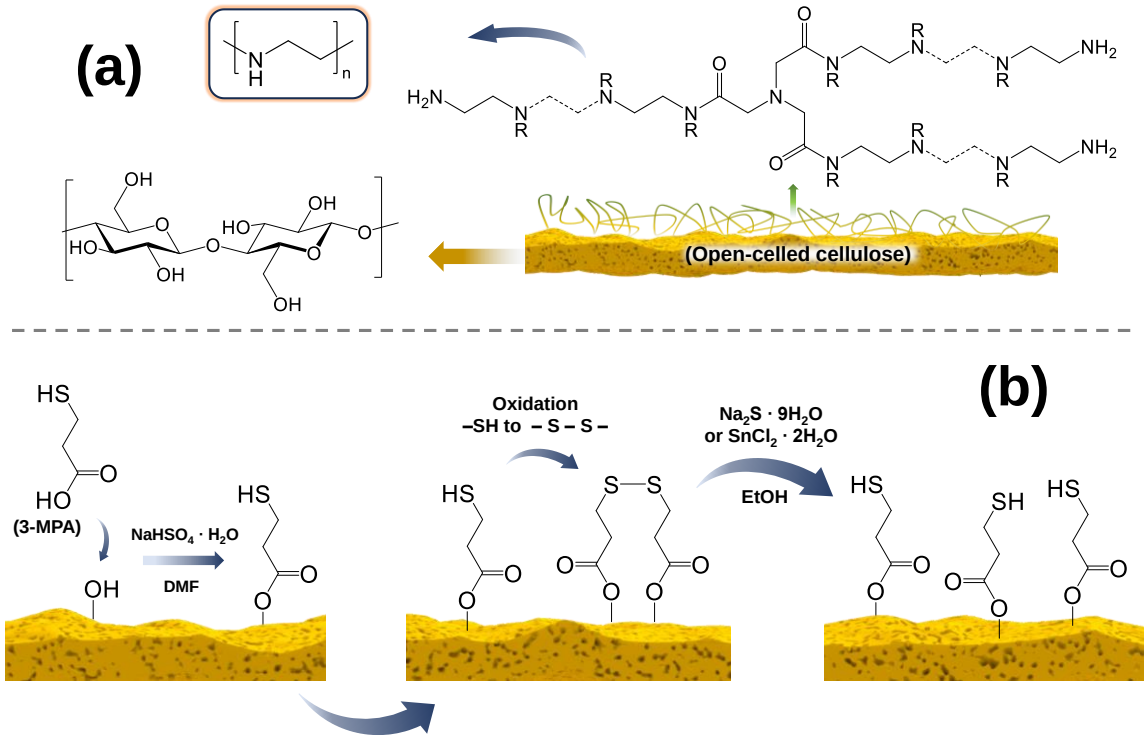

Fig. 1 Schematic illustration of (a) Sponge and (b) the preparation procedure for TFSs.

2.3 Characterization of Sponge, TFS_1, and TFS_2.

Fourier Transform Infrared Spectroscopy (FTIR) was utilized, equipped with an Attenuated Total Reflectance (ATR) module (Tensor 27, Bruker, Germany), to obtain the FTIR spectra and identify the functional groups present in Sponge. The elemental analysis (EA, Flash EA 2000 CHNS, Thermo Fisher, America) was conducted to determine the content of C, H, N, and S. The point of zero charge (pH_{pzc}) of sponges were determined employing pH drift method [50]. In particular, pH_{pzc} was determined using 0.03 mol L^{-1} KNO_3 solution (with a pH range of 2-10). The pH values were adjusted using 0.1 mol L^{-1} HCl and/or NaOH solutions and measured by a pH meter (Crison, Spain). After the addition of 30 mg of sponges, each solution (30 mL) was stirred for 24 hours. Then following the removal of the sponge by filtration, the final pH of the solution was re-measured. The pH_{pzc} value was determined by plotting the initial pH against the pH difference. X-ray photoelectron spectroscopy (XPS) analysis was conducted using a Phoibos 150 analyzer (SPECS GmbH, Berlin, Germany) under ultra-high vacuum conditions (base pressure of 4×10^{-10} mbar). The XPS measurements employed a monochromatic aluminum Kα X-ray source operating at an energy of 1486.74 eV. The morphology of the sponges was studied by Field Emission-Scanning Electron Microscope MERLIN (FE-SEM, Zeiss, 1.4 nm resolution, 1 kV, 4 pA–100 nA probe current, 0.2–30 kV accelerating voltage). The surface chemical compositions of sponges before and after adsorption were analyzed on an energy dispersive X-ray (EDS) detector (Oxford LINCA X-Max).

2.4 Batch adsorption

All adsorption experiments were conducted within plastic centrifuge tubes, placed in an incubator, and subjected to mechanical agitation at 90 rpm. Adsorption capacities were investigated based on the influence of pH, kinetics, isotherms, and thermodynamic analysis by dispersing 10 mg of adsorbent powder into 2 mL of cisplatin solution of

known initial Pt concentration (from 47 μg L^{-1} to 500 mg L^{-1}), followed by 24-hour agitation (except for kinetic studies) at a certain temperature (296, 318, and 343 K). The influence of pH on the adsorption was investigated within the pH range of 2 to 7. To manipulate pH to the desired levels, 0.1 mol L^{-1} NaOH and/or HCl were employed for pH adjustment. Immediately after adsorption, the solution was sampled and filtered through a 0.22 μm membrane filter. Subsequently, all the filtrates were analyzed by using Inductively Coupled Plasma Mass Spectrometry (ICP-MS, Thermo XSeries II, Thermo Scientific, USA) to determine the residual Pt content. All the adsorption experiments were performed in duplicate, and presented data encompassed mean values accompanied by their respective relative standard deviations. The amount of Pt adsorbed on the sponges and the removal ratios were calculated using eq. 1 and eq. 2, respectively:

$$q_e = \frac{(c_0 - c_e)}{m} \times V \quad (1)$$

$$\text{Removal ratio} = \frac{(c_0 - c_e)}{c_0} \times 100\% \quad (2)$$

Where q_e (μg g^{-1}) is the equilibrium adsorption capacity; c_0 and c_e (μg L^{-1}) represent the initial and equilibrium Pt concentrations, respectively; m (mg) denotes the mass of sponges and V (mL) indicates the volume of solution. In kinetic investigations, c_e is replaced by the concentrations at various contact times, denoted as c_t (μg L^{-1}), to calculate the adsorption capacity, q_t (μg g^{-1}).

To obtain a comprehensive understanding of the adsorption characteristics of Pt, the adsorption data collected at different contact time were subjected to fitting analysis using pseudo-first-order (PFO) and pseudo-second-order (PSO) kinetic models. Additionally, the data obtained from adsorption at varied initial concentrations were subjected to fitting using the Langmuir, Freundlich, Sips, and Dubinin-Radushkevich (D-R) isotherm models. All selected model equations applied are explained in Supplementary Data.

3. Results and discussion

3.1 Characterization of sponges

3.1.1 FTIR, EA, pH_{pzc}

Fig. 2a presents the FTIR spectra of TFS_1 and TFS_2, along with a comparison to Sponge, cellulose, and 3-MPA. In the case of TFS_1, TFS_2, and Sponge, evidently due to their cellulose-based substrates, they exhibit FTIR spectra similar to pure cellulose, manifesting characteristic absorption peaks at 1024, 1157, 1365, 2891, and 3435 cm^{-1}. [51]. In detail, the stretching vibration of O−H bonds is manifest as a prominent absorption band observed at the 3435 cm^{-1}. However, it is worth noting that due to the presence of polyethyleneimine on the surface of the Sponge (Fig. 1a), the band resulting from N−H stretching vibrations overlaps with the O−H band. Consequently, the band between 3300-3500 cm^{-1} in Sponge appears slightly broader than in cellulose. Moreover, when contrasted with cellulose, the absorption spectra of TFS_1, TFS_2, and Sponge reveal an additional peak at 1637 cm^{-1}, ascribed to the stretching vibration of the amide C=O bond of the polymer (Fig. 1a), originating from the reaction between polyethyleneimine and nitrilotriacetic acid. However, probably due to the partial dissolution of polyethyleneimine in DMF during the functionalization process, a noticeable decrease in band intensity was observed in the range of 3300-3500 cm^{-1} and 1637 cm^{-1} for both TFSs. The results from EA, depicted in Fig. 2b, also showed a noticeable reduction in the nitrogen content can be observed upon functionalization, decreasing from 3.04 ± 0.01 wt% (Sponge) to 0.84 ± 0.02 wt% (TFS_1) and 0.78 ± 0.02 wt% (TFS_2), respectively. The peak observed at 2891 cm^{-1} can be allocated to the stretching vibration of alkanes C−H bonds. The recorded absorption peak at 1365 cm^{-1} is attributed to the bending motion of O−H bonds, while the peak situated at 1157 cm^{-1} originates from the C−O−C bridge anti-symmetric stretching. The noticeable peak located at 1024 cm^{-1} is referred to the skeletal vibration of the C−O−C pyranose ring [51]. For 3-

MPA, a distinctive absorption peak is observed at 1701 cm^{-1}, arising from the stretching vibration of the carboxyl C=O bond [52]. Moreover, at around 2550 cm^{-1}, 3-MPA exhibits an absorption peak corresponding to the stretching vibration of the S−H bond. But the constrained sulfur loading of TFSs leads to the nearly imperceptible presence of the inherently weak S−H peak at the same wavenumber. However, in the spectra of TFS_1 and TFS_2, a new peak can be observed at 1726 cm^{-1}, which is due to the stretching vibration of the ester C=O bond, confirming the successful esterification. In other words, 3-MPA has been anchored onto the substrate. Similar FTIR spectra features were also observed in various studies involving thiol-functionalized cellulose materials [53–57]. Consistently, as indicated in Fig. 2b, EA revealed sulfur content of 1.04 ± 0.04 wt% for TFS_1 and 1.31 ± 0.05 wt% for TFS_2 subsequent to the functionalization. These findings further corroborate the effective immobilization of 3-MPA onto the Sponge substrate, given the negligible sulfur content in the unmodified Sponge.

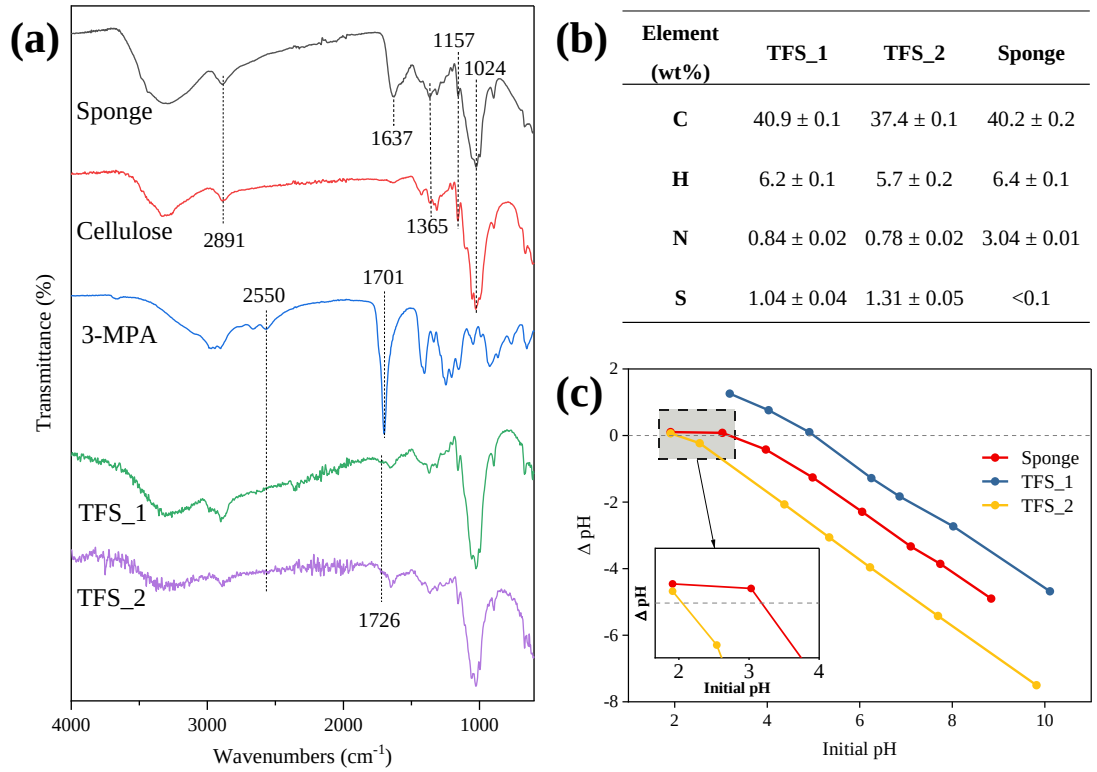

Element (wt%)	TFS_1	TFS_2	Sponge
C	40.9 ± 0.1	37.4 ± 0.1	40.2 ± 0.2
H	6.2 ± 0.1	5.7 ± 0.2	6.4 ± 0.1
N	0.84 ± 0.02	0.78 ± 0.02	3.04 ± 0.01
S	1.04 ± 0.04	1.31 ± 0.05	<0.1

Fig. 2 (a) FTIR spectra of Sponge, pure cellulose, 3-MPA, TFS_1, and TFS_2; (b) summary of EA of TFS_1, TFS_2 and Sponge; and (c) pH_{pzc} determination of Sponge, TFS_1, and TFS_2.

As illustrated in Figure 2c, the pH_{pzc} values of TFS_1, TFS_2 and Sponge are determined to be around 4.8, 2.2, and 3.2, respectively. Therefore, in cases where the solution pH falls below these values, the surface charge of the sponges will become positive, which is most likely caused by the protonation of amino groups [58].

3.1.2 SEM-EDS analysis

As illustrated in Fig. 3a-h, all sponges exhibit a porous architecture characterized by a complex interwoven framework of channels, with diameters spanning approximately 1 to 5 μm. Notably, subsequent to the modification process, these inherent pore attributes remain unaltered. However, in contrast to TFS_1 (Fig. 3b), the surface of TFS_2 (Fig. 3c and d) is coated with blister-like or bubble-like Sn compounds, uniformly dispersed on the sponge surface. The dimensions of these blister-like deposits are not consistent, with a maximum diameter reaching up to around 500 nm. Then, following cisplatin adsorption at 343 K for 24 h, significant morphological alteration of these surface-coated Sn compounds can be observed in Fig. 3h. These changes manifest themselves as uniformly sized spheres with an approximate diameter of 100 nm, which aggregate and exhibit a cauliflower-like pattern.

Fig.3i-k present a comparative representation of EDS spectra, illustrating the surface elemental distribution of the Sponge before and after functionalization, as well as the distinct sponges before and after the adsorption of cisplatin. Initially, both TFS_1 (Fig. 7j) and TFS_2 (Fig. 7k) exhibit S peaks, indicating that −SH groups were anchored on the surface of Sponge. The EDS spectrum of TFS_1 before adsorption reveal the presence of Na element, which may stem from incomplete rinsing leading to residual Na_2S. However, after adsorption, these remnants solubilized into the solution, resulting in the disappearance of the Na element peak.

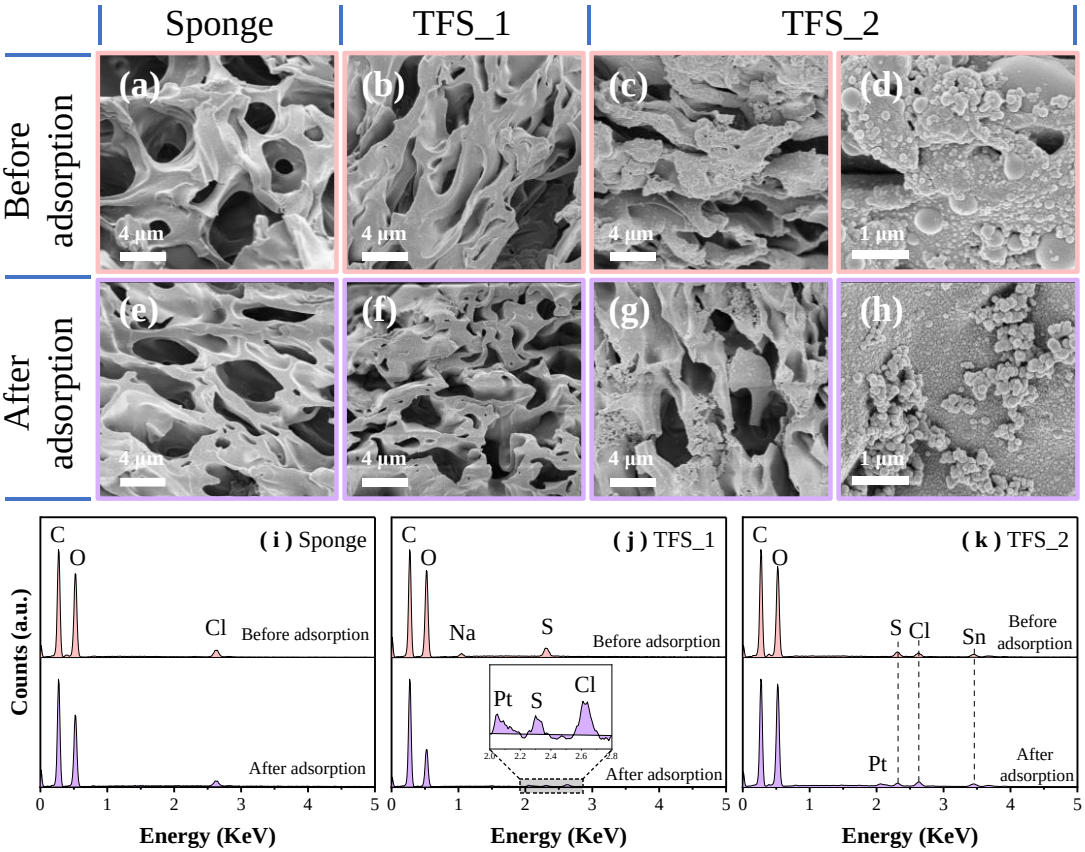

Fig. 3 SEM images (a-h) and EDS spectra (i-k) for Sponge, TFS_1, and TFS_2, before and after adsorption of cisplatin [adsorbent dosage: 200 mg, solution volume: 40 mL, initial concentration of Pt: 100 mg L^{-1}, T: 343 K, contact time: 24 h].

Concerning TFS_2, in accordance with the previously mentioned information, the presence of Sn compounds on the TFS_2 surface (as illustrated in SEM images Fig. 7d and h) is responsible for the discernible peaks corresponding to the Sn element observed in Fig. 7k. Both the EDS spectra of TFS_1 and TFS_2 after adsorption exhibit the presence of Pt elements, whereas Pt is absent in the Sponge. This observation signifies that the functionalized sponges, compared with original Sponge, demonstrates enhanced adsorption capability towards cisplatin. Furthermore, it is more evident that under these conditions, the respective adsorption capacity q_e values for TFS_1 and TFS_2 are 16.2 ± 0.5 and 20.6 ± 0.6 mg g^{-1}, while Sponge exhibits a q_e of 1.9 ± 0.1 mg g^{-1}.

3.1.3 XPS analysis

The utilization of XPS aims to further investigate the surface chemical composition as well as the interactions between cisplatin and TFS_1 and TFS_2. The XPS survey spectra for Sponge, TFS_1, and TFS_2 are presented in Fig. S1, with a comparison between these adsorbents before and after cisplatin adsorption. Obviously, the surface elemental distribution revealed by the XPS survey spectra aligns closely with the findings obtained from the EDS spectra (Fig. 3i-k). Then, in order to comprehend the chemical states of the surface elements S, Pt, and Sn, as well as their alterations before and after adsorption for elucidating the adsorption mechanism, fine XPS spectra of S 2p, Pt 4f, and Sn 3d were acquired and presented in Fig. 4. As seen in Fig. 4a, binding energy centered at 161.79 eV (S $2p_{3/2}$) and 163.09 eV (S $2p_{1/2}$) in the S 2p spectrum could be attributed to S^{2-} of residual Na_2S on TFS_1 [59]. And the observed peaks at 163.87 and 164.97 eV are indicative of the presence of thiol functional groups [60]. Following adsorption, the binding energy of S 2p exhibits a minor shift to higher value (seen in Fig. 4b), which could potentially arise from electron donation originating from sulfur atoms within thiol groups to Pt species [60]. In contrast, with regard to TFS_2 (Fig. 4c), owing to its higher sulfur content (1.31 ± 0.05 wt% compared to 1.04 ± 0.04 wt% for TFS_1), the S 2p spectrum exhibits a notably enhanced signal-to-noise ratio. Furthermore, the deconvolution peaks S 2p are situated at 163.63 and 164.93 eV, primarily originating from the R−SH [61]. And after adsorption, similar to TFS_1, this pair of S 2p peaks exhibits a slight shift towards higher binding energy (Fig. 4d). Concurrently, the presence of two spin-orbit peaks at 162.66 and 163.76 eV in the after-adsorption spectrum provides evidence for the formation of Pt−S bonds [62,63]. Additionally, regarding TFS_2, as shown in Fig. 4e, the Sn 3d spectrum can be predominantly deconvoluted into two sets of spin-orbit split doublet peaks. The prominent peaks at 486.68 eV ($3d_{5/2}$) and 495.11 eV ($3d_{3/2}$) primarily correspond to Sn^{4+} within SnO_2 [64], while the doublet peaks at 485.01 eV and 493.51 eV represent Sn^0 [65].

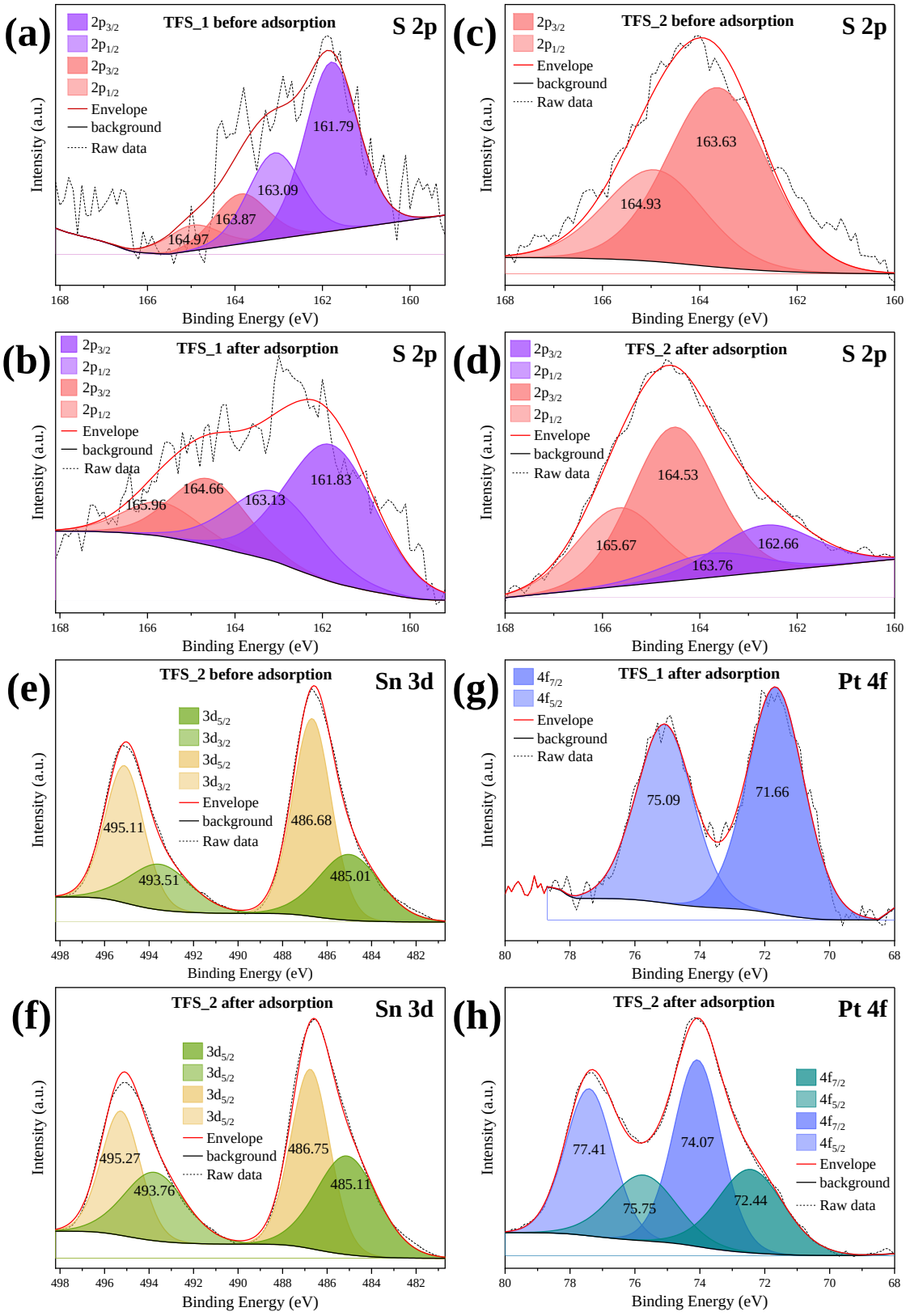

Fig. 4 High-resolution XPS spectra S 2p (a-d), Sn 3d (e and f), and Pt 4f (g and h) of TFS_1 and TFS_2 before and after adsorption of cisplatin.

It can be inferred that $SnCl_2$ compounds, following the reduction of disulfide, were oxidized to tetravalent SnO_2. Simultaneously, a portion of them were reduced to Sn^0. Two types of Sn compounds doping led to the formation of Sn/SnO_2, a similar composite to those reported in other studies [64–70]. Following adsorption, the XPS spectra characteristics of Sn remain unchanged (by comparing Fig. 4e and f), indicating that despite morphological alterations observed in the SEM images (by comparing Fig. 2d and h), the chemical state of Sn remains basically consistent with that prior to adsorption.

The different Pt chemical states subsequent to the adsorption of cisplatin onto TFS_1 and TFS_2 are illustrated through the fine XPS Pt 4f spectra presented in Fig. 4g and h, respectively. Regarding the Pt adsorbed on TFS_1 (Fig. 4g), the $4f_{7/2}$ and $4f_{5/2}$ doublet peaks at 71.66 and 75.09 eV suggest the predominant presence of Pt in an unaltered divalent state [71,72]. However, concerning the Pt adsorption on TFS_2 (Fig. 4h), the peaks located at 74.07 and 77.41 eV indicate the presence of Pt^{4+}, suggesting that the adsorbed Pt may be embedded in the form of PtS_2 or PtO_2 on Sn/SnO_2 [73]. Similar chemical states have also been observed in other Pt/Sn or Pt/SnO_2 synthetic catalyst systems [67,73–76].

3.2 Adsorption experiments

3.2.1 Effect of solution pH on adsorption

Fig. 5 illustrates the adsorption capacities of cisplatin onto Sponge, TFS_1, and TFS_2 at various pH levels. Firstly, it is evident that both thiol-functionalization schemes have significantly enhanced the adsorption levels of low-concentration cisplatin as expected. The enhancement arises from the high affinity of thiols towards Pt. Based on the Hard and Soft Acids and Bases (HSAB) Principle [77], Pt is categorized as a "soft" Lewis acid, readily forming bonds with S, which are regarded as "soft" Lewis base. The covalent nature of Pt−S bonds enables electron sharing and imparts stability to compounds or molecules containing such bonds. For instance, in the clinical utilization

of cisplatin, subsequent to intravenous administration, numerous investigations have substantiated that a considerable proportion of cisplatin can associate with various constituents present in the plasma prior to its interaction with intracellular DNA. Notably, human serum albumin, the predominant protein in human blood, has been identified as one such constituent, and it comprises thiol groups capable of engaging in interactions with the administered cisplatin [78–81]. Furthermore, in our previous study concerning the adsorption of trace cisplatin by thiol-functionalized sponges, the analysis of the coordinated environment of the adsorbed Pt was conducted using synchrotron X-ray absorption spectroscopy, confirming that the enhanced adsorption was dependent on the Pt−S bonding [34]. Meanwhile, higher adsorption capacities of TFS_2 in comparison to TFS_1 are also observed in Fig. 5. The differences can be ascribed, in part, to the higher sulfur content of TFS_2 (1.31 ± 0.05 wt% compared to 1.04 ± 0.04 wt% for TFS_1, Fig. 2b). Additionally, as confirmed by prior XPS analysis, a portion of cisplatin tends to undergo oxidation and adhere onto Sn/SnO_2 coated on TFS_2.

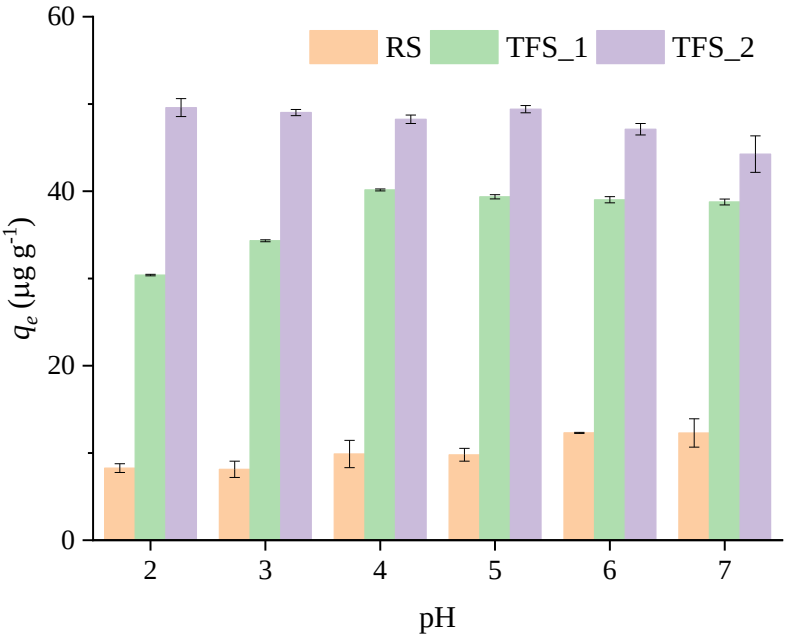

Fig. 5 The pH effect on adsorption of cisplatin by Sponge, TFS_1, and TFS_2 [adsorbent dosage: 10 mg, solution volume: 2 mL, initial concentration of Pt: 235 μg L^{-1}, T: 296 K, contact time: 24 h].

The influence of pH on the adsorption capacities of cisplatin onto Sponge, TFS_1, and TFS_2 is generally moderate. As depicted in Fig. 5, the adsorption capacity of Sponge increases from 8.3 ± 0.5 to 12 ± 2 μg g^{-1} as the pH rises from 2 to 7. Similarly, the adsorption capacity of TFS_1 increases from 30.4 ± 0.1 to 40.2 ± 0.1 as the pH rises from 2 to 4, subsequently maintaining a constant level. This phenomenon is attributed to the alteration of surface charge of both adsorbents due to changes in pH, thereby influencing electrostatic adsorption. The adsorption mechanism of cisplatin resembles its complexation process with DNA or proteins involving a hydration step [13,33,34,79]. As shown in Fig. 6a, the two chloride ligands are sequentially substituted by water molecules, leading to the formation of active aqua-intermediates. Then, in the subsequent complexation process, ligand substitution occurs with H_2O ligands, resulting in cisplatin binding to the target site through either monodentate (blue square in Fig 6a) or bidentate chelation (orange square in Fig 6a).

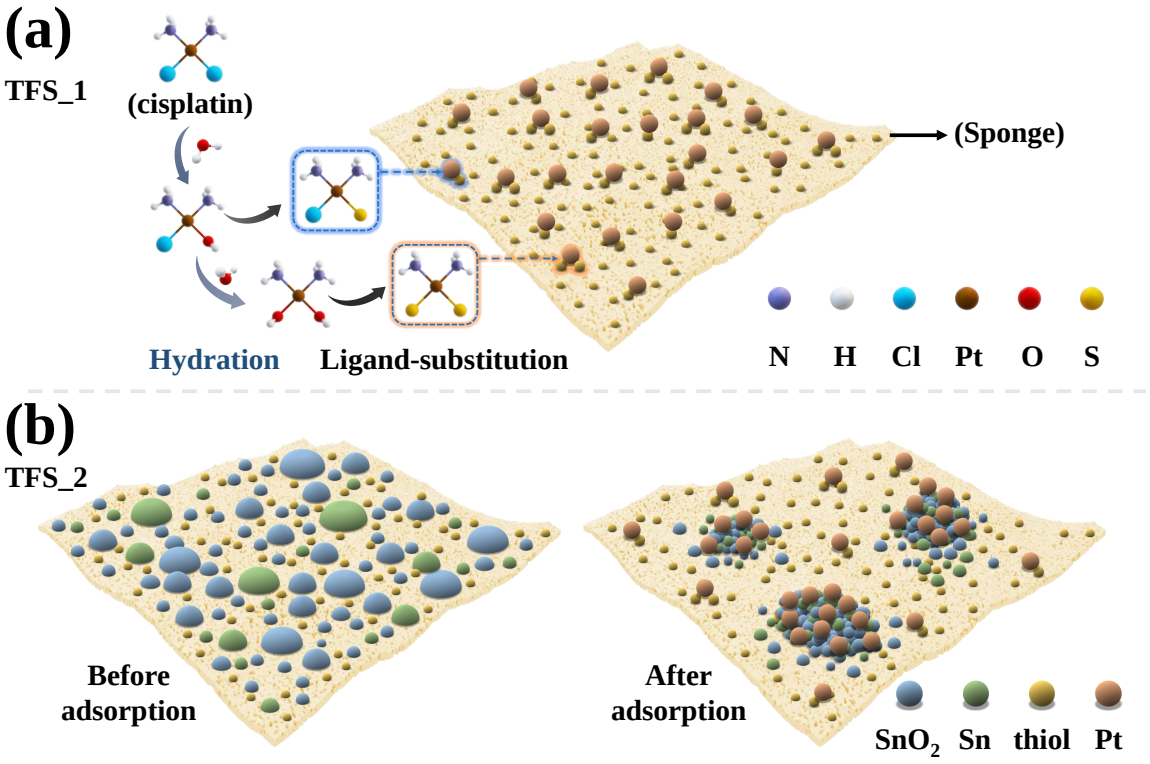

Fig. 6 Schematic depictions of the adsorption mechanisms of cisplatin by TFS_1 (a) and TFS_2 (b).

Hence, under low pH level, such as at a pH of 2, Both the surfaces of Sponge and TFS_1 will attain a positive charge as a consequence of the protonation of amino groups (Fig. 2c). Consequently, this leads to the repulsion of aqua complexes formed during the hydration process, specifically the cis-$[PtCl(H_2O)(NH_3)_2]^+$ and cis-$[Pt(H2O)_2(NH3)_2]^{2+}$ cations. Conversely, low pH results in a positively charged surface for both sponges, thereby assisting electrostatically in the attraction of aqua-cisplatin to the adsorbent surface, facilitating subsequent complexation processes. However, the influence of pH on the adsorption of cisplatin by TFS_2 differs; as the pH increases from 2 to 7, the adsorption capacity decreases slightly from 50 ± 1 to 44 ± 2 μg g^{-1}. This observation highlights the constrained dependence of TFS_2 on physical adsorption mechanisms, including the previously mentioned electrostatic interactions.

3.2.2 Adsorption kinetics analysis

The analysis of adsorption kinetics holds significant importance in the evaluation of both the adsorption rate and the mechanism governing the adsorption process. And it is a crucial consideration in the upscaling of cisplatin removal from hospital wastewater in future industrial applications. Fig.7 presents the adsorption kinetic plots of cisplatin onto TFS_1 and TFS_2. The steep upward trends in the curves indicate fast adsorption behavior for both TFSs. In the initial minutes, the adsorption capacity significantly increases due to the abundant active adsorption sites on the surface of TFS_1 or TFS_2. However, with the extension of contact duration, the rate of adsorption progressively diminishes, reaching equilibrium (q_e of 37 ± 2 and 47.2 ± 0.3 μg g^{-1} for TFS_1 and TFS_2 respectively) after approximately 40 minutes. The deceleration of adsorption is predominantly ascribed to the reduction of accessible adsorption sites, leading to a decrease in the rate of adsorption.

Based on the determination coefficients R^2 as presented in Table S1 and the fitting curves depicted in Fig. 7, it can be concluded that both models yield satisfactory fitting

results. However, the PSO model appears to slightly better suit the data fitting compared to the PFO model. The PSO model assumes a chemisorption mechanism for the rate-limiting step. Chemisorption entails covalent bonding forces that arise from sharing electrons between the adsorbate and the adsorbent. [50,82,83]. In contrast, the PFO model is appropriate for describing the initial phases of adsorption, in which the governing step of the process is associated with either external or internal diffusion. Additionally, adsorbates in this context commonly manifest higher initial concentrations [82,84]. Conversely, the current investigation is concerned with the adsorption of the target cisplatin at 235 μg L^{-1}, which is comparatively low. Hence, it can be inferred that the adsorption is primarily controlled by the chemical bonding interactions occurring between cisplatin and thiol groups, thereby aligning more closely with the postulations of the PSO model.

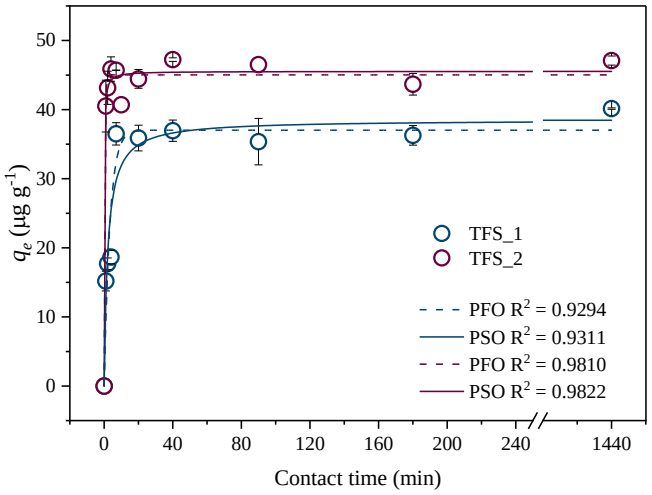

Fig. 7 The adsorption capacities of cisplatin onto TFS_1 and TFS_2 at various contact times, along with the fitted curves using the PFO and PSO models [adsorbent dosage: 10 mg, solution volume: 2 mL, initial concentration of Pt: 235 μg L^{-1}, T: 296 K].

3.2.3 Adsorption isotherms analysis

As depicted in Fig. 8, both TFSs exhibit a marked increase in adsorption capacity of cisplatin with escalating initial concentrations. This enhancement is attributed to the heightened concentration gradient generated at the solid-liquid interface which can

compel cisplatin and hydrated cisplatin to diffuse toward the surfaces of TFSs, according to the Fick's laws of diffusion [85,86].

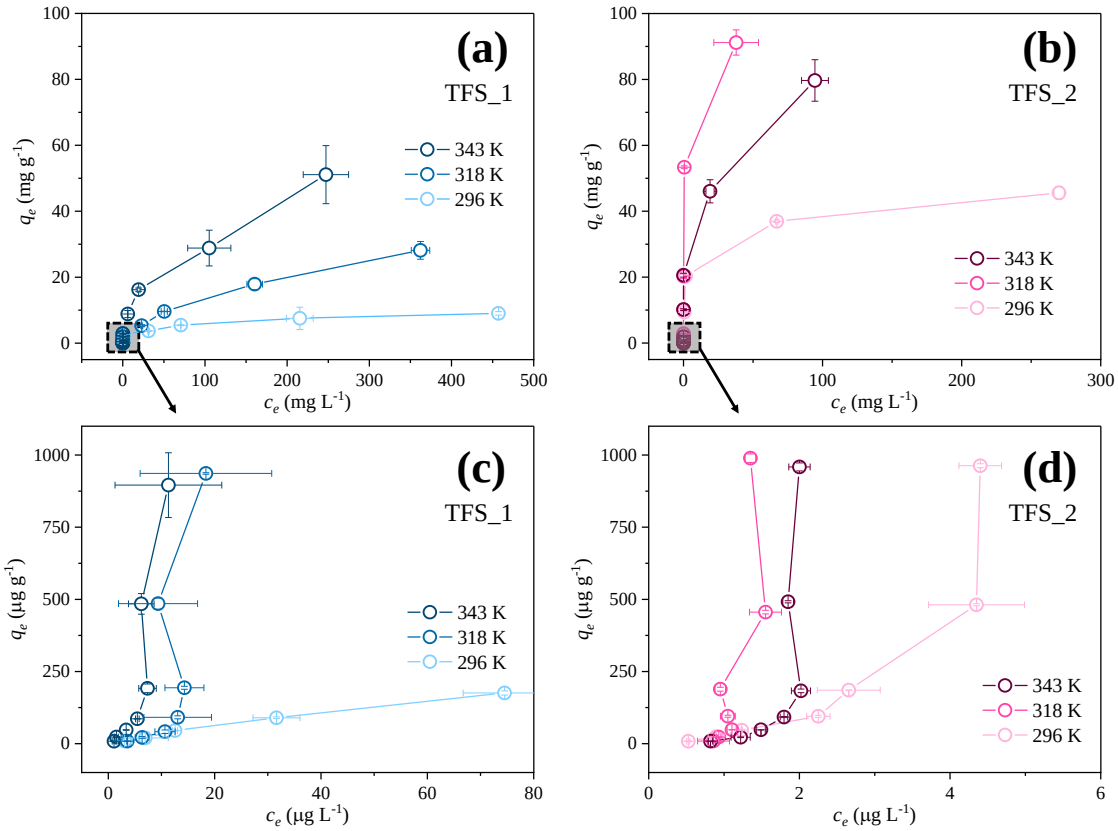

Fig. 8 Cisplatin adsorption isotherms of (a) TFS_1 and (b) and TFS_2 at different temperatures, (c) and (d) depict the magnified interval of low initial concentration range [adsorbent dosage: 10 mg, solution volume: 2 mL, initial concentration of Pt: 47 µg L^{-1} - 500 mg L^{-1}, contact time: 24 h].

However, of notable interest is that, as discerned from Fig. 8c and d, under the conditions of low concentration, the isotherms exhibit an S-shaped profile, with the adsorption capacity displaying gradual growth as initial concentration increase. Other investigations have corroborated that a portion of 3-MPA can undergo decomposition, yielding sulfur-containing fragments such as sulfides within the solution [34,87–90]. The release of these sulfur-containing fragments enhanced the formation of stable soluble Pt complexes, thereby resulting in reduced adsorption of cisplatin by TFS_1 and TFS_2 [91]. Because, at low concentrations of Pt, the adsorption process is influenced by the presence of ligands containing sulfur. Adsorption becomes prominent only after ligand saturation.

The point of inflection signifies the concentration at which Pt adsorption prevails over the complexation of free sulfur species [91]. Subsequently, as the initial concentration continues to increase, nearly all adsorption capacities exhibit a rapid augmentation, which gradually mitigates and transitions into adsorption saturation.

Temperature exerted varying influences on the adsorption of cisplatin onto TFS_1 and TFS_2. Analysis of the adsorption isotherms (Fig. 8a and c) for TFS_1 at different temperatures reveals a noticeable increase in adsorption as the temperature rises. This enhancement arises from the thermo-favored complexation between Pt and S. However, in the case of TFS_2 (Fig. 8b and d), increasing the temperature from 296 to 318 K results in a corresponding increase of the adsorption capacities, but then followed by a decline in adsorption capacity as the temperature further elevates to 343 K. Although increasing the temperature appropriately facilitates the Pt−S complexation in chemical adsorption, temperatures as high as 343 K should be avoided. At this temperature, as depicted in the SEM image (Fig. 3h) and the adsorption mechanism illustration (Fig. 6b), aggregation occurs in the coated-Sn/SnO_2 structure, thereby influencing the deposition of Pt.

The parameters derived from the four isotherm models chosen are summarized in Table S2. Overall, the provided determination coefficients R^2 values range from 0.9618 to 0.9908, indicating a good fit of the Langmuir model (only except for the adsorption onto TFS_1 at 296 K and TFS_2 at 343 K). This implies that the adsorption of cisplatin onto sponges follows monolayer adsorption behavior [34]. Concerning TFS_1, the adsorption isotherm at 296 K demonstrates a better fit by the Freundlich model (R^2=0.9747) as compared to the Langmuir model (R^2=0.8748). This observation indicates that the adsorption of cisplatin on TFS_1 at low temperatures involves a multi-layer adsorption behavior [92], encompassing a synergistic interplay of electrostatic adsorption arising from cationic hydrated Pt derivatives and protonated amino groups, or van der Waals interactions, in addition to Pt−S complexation. At this juncture, the distribution of energetically disparate adsorption sites constitutes a heterogeneous surface of TFS_1. As

the temperature increases, the fit of the Langmuir model to the isotherms improves progressively, albeit still slightly lower than the Freundlich model. This observation indicates that, with rising temperature, the adsorption of cisplatin becomes increasingly reliant on complexation with surface thiol groups, manifesting a more pronounced monolayer adsorption pattern. For TFS_2, upon elevating the temperature to 343 K, it becomes obvious that the Freundlich model (R^2=0.9628) exhibits a superior level of fitting accuracy compared to the Langmuir model (R^2=0.9166) in describing the adsorption isotherm. Incorporating the preceding analysis, it is evident that the aggregation of Sn/SnO_2 at this temperature results in surface heterogeneity of TFS_2. All adsorptions are characterized as favorable, as evidenced by the Langmuir model-derived separation factor R_L values ranging from 0 to 1 within the investigated concentration range. The predicted values for the theoretical maximum adsorption capacities (q_{mL}) based on the Langmuir model closely correspond to, slightly surpassing, the experimentally derived actual maximum adsorption capacities. Furthermore, the Sips model is a hybrid model that integrates both the Langmuir and Freundlich models, capable of characterizing both homogeneous and heterogeneous systems. Moreover, it exhibits similarity to the Freundlich model under conditions of low c_0 [92]. Determined by R^2 (0.9410 - 0.9990) , the Sips model seems to exhibit favorable fitting results for all adsorption isotherms. However, during the process of nonlinear fitting, the parameters prove challenging to converge, leading to significantly higher predicted maximum adsorption capacities than observed experimentally. In addition, the derived values of mean free energy (E) from the D-R model are also calculated and listed in Table S2. The E values of TFS_1 at three temperatures are 8.17, 9.68 and 9.71 kJ mol^{-1} respectively. These values exceed 8 kJ mol^{-1} and fall within the range of 8-16 kJ mol^{-1}, yet they are less than the corresponding E values for TFS_2, which are 10.59, 13.22, and 13.98 kJ mol^{-1}. These findings indicate that both materials exhibited chemisorption dominance in the adsorption process, but notably, chemisorption played a more prominent role in the

adsorption process for TFS_2 [92]. This conclusion also aligns with the discussion in section 3.2.1, where the adsorption process of cisplatin by TFS_1 is observed to involve electrostatic adsorption to some extent.

3.2.4 Adsorption thermodynamics analysis

In order to gain deeper insights into the adsorption characteristics, the thermodynamics of adsorption were investigated. Utilizing the adsorption isotherms data acquired at various temperatures, three pivotal thermodynamic parameters, namely Gibbs free energy ($\Delta G°$, kJ mol^{-1}), the changes in enthalpy ($\Delta H°$, kJ mol^{-1}) and entropy ($\Delta S°$, J mol^{-1} K^{-1}) were calculated by the equations provided in the Supplementary data. $\Delta H°$ and $\Delta S°$ were determined from the slope and intercept of Van't Hoff plots (ln K vs. 1/T) respectively, as illustrated in Fig. S2, and all parameters are summarized in Table S3.

The presented $\Delta G°$ values (from -5.9 ± 0.3 to -16.3 ± 0.1 kJ mol^{-1}) in Table S3 indicate the spontaneous nature of the adsorption process of cisplatin onto both TFS_1 and TFS_2. And, the cisplatin adsorption onto TFS_1 is endothermic, with a $\Delta H°$ of 39 ± 3 kJ mol^{-1}. Simultaneously, the observed positive $\Delta S°$ of 152 ± 11 J mol^{-1} K^{-1} indicates an increase in disorder at the solid-liquid interface following adsorption. The binding process of cisplatin onto the TFS_1 surface would conventionally be linked to a reduction in entropy due to conformational space limitations, thereby leading to a negative $\Delta S°$. However, the contribution to the $\Delta S°$ induced by the restriction of degrees of freedom upon cisplatin adsorption appears to be relatively modest compared to the desorption of water molecules. Notably, the positive $\Delta S°$ arises from the exclusion of water molecules from the hydration layers encompassing both the TFS_1 and cisplatin during the adsorption. The complexation between cisplatin and thiol groups on TFS_1 surface promoted the release of water molecules, consequently fostering an escalation in disorder at the liquid-solid interface [93]. Similar findings have been also reported in other investigations employing lignocellulosic waste [94] or cellulose [95] as adsorbents.

Additionally, in the Van't Hoff plots presented in Fig. S2, TFS_2 exhibits a suboptimal linear fit. This is attributed to the significant alteration of TFS_2 morphology at higher temperatures, consequently affecting the adsorption system. This change is manifested by a trend in its impact on cisplatin adsorption, showing an initial increase followed by a subsequent decrease, with the maximum adsorption capacity observed at the intermediate temperature of 318 K.

3.3 Comparison of cisplatin removal with adsorbents reported in the literature

The removal efficiency of cisplatin by TFS_1 and TFS_2 was compared with that of other previously reported adsorbents, as listed in Table S4. Clearly, through comparison, TFS_1 and TFS_2 achieved excellent removal efficiencies of trace cisplatin (235 μg L^{-1}) under optimal conditions, with removal rates of 95.5 ± 0.8% and 99.5 ± 0.1%, respectively. Notably, TFS_2 demonstrates a removal efficiency surpassing that of all previously reported materials, including even costly commercially available counterparts. Moreover, the rapid kinetic characteristics exhibited by TFS_1 and TFS_2 enhance their prospects for scalability in future industrial applications. Additionally, the removal efficiency of TFS_1 and TFS_2, synthesized with additional reduction steps, was notably superior to that of previously reported non-reduced counterpart of 3-mercaptopropionic acid functionalized sponge (88.9 ± 0.5%) [34]. This substantiates that the reduction steps, as anticipated, ensure a greater abundance of effective thiol adsorption sites. Furthermore, the employed strategy of coating with Sn/SnO_2 has also been demonstrated to be effective in further enhancing the adsorption capacity of TFS. The commercially available adsorbent, 3-mercaptopropyl-functionalized silica gel, demonstrated comparable excellence, achieving a removal efficiency of 98.7 ± 0.1% [34]. However, its high price (40 € g^{-1}) undermines its cost-effectiveness advantage. In comparison, Sponge, being a cheap substrate material, holds industrial applicability potential and is poised to garner market favor.

4. Conclusions

The facile functionalization of 3-MPA on Sponge through esterification, followed by the reduction of oxidized thiol groups, has been proved as a viable and successful process. Characterizations including FTIR, EA, SEM-EDS, and XPS have proved the successful immobilization of thiol groups. The introduction of thiol groups exhibiting strong binding affinity has been observed to markedly improve the adsorption capacity for trace cisplatin. This observation underscores the crucial involvement of Pt−S complexation in facilitating chelation-dominant chemisorption. In addition to complexation, the process of cisplatin removal also includes a hydration step. Pre-substituting ligands with water can lead to the formation of active aqua-derivatives, thereby facilitating subsequent complexation processes. Hence, during the cisplatin adsorption on TFS_1, the cationic derivatives resulting from hydration can migrate towards the negatively charged surface of the adsorbent due to electrostatic attraction, thereby facilitating the subsequent complexation. In the case of TFS_2, different from TFS_1, the surface-doped Sn/SnO_2 also contributes to the adsorption of cisplatin. XPS analysis reveals that the adsorption process involves Pt−S complexation, as well as the partial oxidation of cisplatin and its subsequent adsorption onto Sn compounds. The adsorption of cisplatin conforms to the PSO kinetic model, involving diffusion process followed by chemical adsorption. The Langmuir model adequately describes adsorption isotherms, conforming to monolayer adsorption. Increasing the temperature further enhances the adsorption of cisplatin onto TFSs, as the chemisorption predominantly governed by Pt−S complexation has been substantiated to be an endothermic process. However, caution should be exercised to prevent aggregation also induced by high temperatures, such as 343 K, on the surface coverage of Sn/SnO_2 in TFS_2, as this morphological alteration diminishes the adsorption of cisplatin. In comparison with adsorbents reported in the literature, TFSs exhibit advantages in terms of their adsorption performance, adsorption kinetic characteristics, and cost-effectiveness. In summary, TFSs show potential for the treatment of hospital wastewater contaminated

with Pt-CDs and offer prospects for upscale implementation in industrial applications. Moreover, this work provide inspiration for the development of highly selective and affinity adsorbents for Pt-CDs in future, such as utilizing other cost-effective and readily available cellulose materials (biomass, agricultural waste).

Acknowledgements

This work was carried out within the scope of the RECOPHARMA project (grant agreement #778266) under the European Community's H2020 Program H2020-MSCA-RISE 2017. The authors express their gratitude to Cristina Navarro Senent from the Servei de Microscòpia at Universitat Autònoma de Barcelona (UAB). The authors also acknowledge the Servei d'Anàlisi Química of the UAB for their analytical support. D. Han acknowledges support from the China Scholarship Council (No. 201906450024).

Conflicts of Interest

The authors declare no conflict of interest.

Reference

[1] A.W. Prestayko, J.C. D'Aoust, B.F. Issell, S.T. Crooke, Cisplatin (cis-diamminedichloroplatinum II), Cancer Treat. Rev. 6 (1979) 17–39. https://doi.org/10.1016/S0305-7372(79)80057-2.

[2] D.B. Zamble, S.J. Lippard, Cisplatin and DNA repair in cancer chemotherapy, Trends Biochem. Sci. 20 (1995) 435–439. https://doi.org/10.1016/S0968-0004(00)89095-7.

[3] P.J. LOEHRER, Cisplatin, Ann. Intern. Med. 100 (1984) 704. https://doi.org/10.7326/0003-4819-100-5-704.

[4] J. Reedijk, Why does cisplatin reach guanine-N7 with competing S-donor ligands available in the cell?, Chem. Rev. 99 (1999) 2499–2510. https://doi.org/10.1021/cr980422f.

[5] M.R. Trendowski, O. El Charif, P.C. Dinh, L.B. Travis, M.E. Dolan, Genetic and Modifiable Risk Factors Contributing to Cisplatin-induced Toxicities, Clin. Cancer Res. 25 (2019) 1147–1155. https://doi.org/10.1158/1078-0432.CCR-18-2244.

[6] C. Tang, M.J. Livingston, R. Safirstein, Z. Dong, Cisplatin nephrotoxicity: new insights and therapeutic implications, Nat. Rev. Nephrol. 19 (2023) 53–72. https://doi.org/10.1038/s41581-022-00631-7.

[7] C.W.P. Schmidt, Pediatric Oncologic Pharmacy, Springer International Publishing, Cham, 2019. https://doi.org/10.1007/978-3-030-10988-2.

[8] M. Isidori, M. Lavorgna, C. Russo, M. Kundi, B. Žegura, M. Novak, M. Filipič, M. Mišík, S. Knasmueller, M.L. de Alda, D. Barceló, B. Žonja, M. Česen, J. Ščančar, T. Kosjek, E. Heath, Chemical and toxicological characterisation of anticancer drugs in hospital and municipal wastewaters from Slovenia and Spain, Environ. Pollut. 219 (2016) 275–287. https://doi.org/10.1016/j.envpol.2016.10.039.

[9] S. Santana-Viera, M.E.T. Padrón, Z. Sosa-Ferrera, J.J. Santana-Rodríguez,

Quantification of cytostatic platinum compounds in wastewater by inductively coupled plasma mass spectrometry after ion exchange extraction, Microchem. J. 157 (2020) 104862. https://doi.org/10.1016/j.microc.2020.104862.

[10] Y. Ghafuri, M. Yunesian, R. Nabizadeh, A. Mesdaghinia, M.H. Dehghani, M. Alimohammadi, Platinum cytotoxic drugs in the municipal wastewater and drinking water, a validation method and health risk assessment, Hum. Ecol. Risk Assess. 24 (2018) 784–796. https://doi.org/10.1080/10807039.2017.1400372.

[11] A.C. Johnson, R. Oldenkamp, E. Dumont, J.P. Sumpter, Predicting concentrations of the cytostatic drugs cyclophosphamide, carboplatin, 5-fluorouracil, and capecitabine throughout the sewage effluents and surface waters of europe, Environ. Toxicol. Chem. 32 (2013) 1954–1961. https://doi.org/10.1002/etc.2311.

[12] N. Vyas, A. Turner, G. Sewell, Platinum-based anticancer drugs in waste waters of a major UK hospital and predicted concentrations in recipient surface waters, Sci. Total Environ. 493 (2014) 324–329. https://doi.org/10.1016/j.scitotenv.2014.05.127.

[13] Y. Roque-Diaz, M. Sanadar, D. Han, M. López-Mesas, M. Valiente, M. Tolazzi, A. Melchior, D. Veclani, The Dark Side of Platinum Based Cytostatic Drugs: From Detection to Removal, Processes. 9 (2021) 1873. https://doi.org/10.3390/pr9111873.

[14] Y. Ghafuria, M. Yunesian, R. Nabizadeh, A. Mesdaghinia, M.H. Dehghani, M. Alimohammadi, Environmental risk assessment of platinum cytotoxic drugs: a focus on toxicity characterization of hospital effluents, Int. J. Environ. Sci. Technol. 15 (2018) 1983–1990. https://doi.org/10.1007/s13762-017-1517-6.

[15] K. Lenz, G. Koellensperger, S. Hann, N. Weissenbacher, S.N. Mahnik, M. Fuerhacker, Fate of cancerostatic platinum compounds in biological wastewater treatment of hospital effluents, Chemosphere. 69 (2007) 1765–1774. https://doi.org/10.1016/j.chemosphere.2007.05.062.

[16] K. Lenz, S. Hann, G. Koellensperger, Z. Stefanka, G. Stingeder, N.

Weissenbacher, S.N. Mahnik, M. Fuerhacker, Presence of cancerostatic platinum compounds in hospital wastewater and possible elimination by adsorption to activated sludge, Sci. Total Environ. 345 (2005) 141–152. https://doi.org/10.1016/j.scitotenv.2004.11.007.

[17] K. Kümmerer, E. Helmers, P. Hubner, G. Mascart, M. Milandri, F. Reinthaler, M. Zwakenberg, European hospitals as a source for platinum in the environment in comparison with other sources, Sci. Total Environ. 225 (1999) 155–165. https://doi.org/10.1016/S0048-9697(98)00341-6.

[18] K. Lenz, S.N. Mahnik, N. Weissenbacher, R.M. Mader, P. Krenn, S. Hann, G. Koellensperger, M. Uhl, S. Knasmüller, F. Ferk, W. Bursch, M. Fuerhacker, Monitoring, removal and risk assessment of cytostatic drugs in hospital wastewater, Water Sci. Technol. 56 (2007) 141–149. https://doi.org/10.2166/wst.2007.828.

[19] M. Mišík, M. Filipic, A. Nersesyan, M. Kundi, M. Isidori, S. Knasmueller, Environmental risk assessment of widely used anticancer drugs (5-fluorouracil, cisplatin, etoposide, imatinib mesylate), Water Res. 164 (2019) 114953. https://doi.org/10.1016/j.watres.2019.114953.

[20] J.L. Wilkinson, P.S. Hooda, J. Barker, S. Barton, J. Swinden, Ecotoxic pharmaceuticals, personal care products, and other emerging contaminants: A review of environmental, receptor-mediated, developmental, and epigenetic toxicity with discussion of proposed toxicity to humans, Crit. Rev. Environ. Sci. Technol. 46 (2016) 336–381. https://doi.org/10.1080/10643389.2015.1096876.

[21] V. Queirós, U.M. Azeiteiro, A.M.V.M. Soares, R. Freitas, The antineoplastic drugs cyclophosphamide and cisplatin in the aquatic environment – Review, J. Hazard. Mater. 412 (2021). https://doi.org/10.1016/j.jhazmat.2020.125028.

[22] A. Castellano-Hinojosa, M.J. Gallardo-Altamirano, J. González-López, A. González-Martínez, Anticancer drugs in wastewater and natural environments: A review on their occurrence, environmental persistence, treatment, and ecological

risks, J. Hazard. Mater. 447 (2023) 130818. https://doi.org/10.1016/j.jhazmat.2023.130818.

[23] K. Folens, A. Abebe, J. Tang, F. Ronsse, G. Du Laing, Biosorption of residual cisplatin, carboplatin and oxaliplatin antineoplastic drugs in urine after chemotherapy treatment, Environ. Chem. 15 (2018) 506–512. https://doi.org/10.1071/EN18115.

[24] F. OGATA, K. INOUE, H. TOMINAGA, Y. IWATA, A. UEDA, Y. TANAKA, N. KAWASAKI, Use of Calcined Gibbsite to Remove Cisplatin from Aqueous Solutions, J. Water Environ. Technol. 12 (2014) 13–23. https://doi.org/10.2965/jwet.2014.13.

[25] J. Dobrzynska, M. Dabrowska, R. Olchowski, E. Zieba, R. Dobrowolski, Development of a method for removal of platinum from hospital wastewater by novel ion-imprinted mesoporous organosilica, J. Environ. Chem. Eng. 9 (2021). https://doi.org/10.1016/j.jece.2021.105302.

[26] K. Folens, A. Abebe, J. Tang, F. Ronsse, G. Du Laing, G. Du Laing, Biosorption of residual cisplatin, carboplatin and oxaliplatin antineoplastic drugs in urine after chemotherapy treatment, Environ. Chem. 15 (2018) 506–512. https://doi.org/10.1071/EN18115.

[27] T. Farías, S. Hajizadeh, L. Ye, Cryogels with high cisplatin adsorption capacity: Towards removal of cytotoxic drugs from wastewater, Sep. Purif. Technol. 235 (2020) 116203. https://doi.org/10.1016/j.seppur.2019.116203.

[28] R. Lombana Fraguela, J.A. Ricardo Garcia, M.E. Villanueva Tagle, M.S. Pomares Alfonso, M. Cracchiolo, A. Kovačević, M. Tolazzi, A. Melchior, M. Sanadar, Evaluation of Dithiocarbamate-Modified Silica for Cisplatin Removal from Water, Processes. 11 (2023) 472. https://doi.org/10.3390/pr11020472.

[29] C. Hernández, Y. Ramos, L.A. Fernández, O. Ledea, M. Bataller, E. Véliz, V. Besada, A. Rosado, Ozonation of Cisplatin in Aqueous Solution at pH 9, Ozone Sci. Eng. 30 (2008) 189–196. https://doi.org/10.1080/01919510801907722.

[30] T. Kobayashi, J. Hirose, K. Sano, N. Hiro, Y. Ijiri, H. Takiuchi, H. Tamai, H. Takenaka, K. Tanaka, T. Nakano, Evaluation of an electrolysis apparatus for inactivating antineoplastics in clinical wastewater, Chemosphere. 72 (2008) 659–665. https://doi.org/10.1016/j.chemosphere.2008.02.020.

[31] J. Hirose, F. Kondo, T. Nakano, T. Kobayashi, N. Hiro, Y. Ando, H. Takenaka, K. Sano, Inactivation of antineoplastics in clinical wastewater by electrolysis, Chemosphere. 60 (2005) 1018–1024. https://doi.org/10.1016/j.chemosphere.2005.01.024.

[32] M. Patel, R. Kumar, K. Kishor, T. Mlsna, C.U. Pittman, D. Mohan, Pharmaceuticals of emerging concern in aquatic systems: Chemistry, occurrence, effects, and removal methods, Chem. Rev. 119 (2019) 3510–3673. https://doi.org/10.1021/acs.chemrev.8b00299.

[33] D. Han, M. López-Mesas, M. Luaces, Y. Enamorado, M. Sanadar, A. Melchior, M. Valiente, Comparative study on removal of platinum cytostatic drugs at trace level by cysteine, diethylenetriamino functionalized Si-gels and polyethyleneimine functionalized sponge: Adsorption performance and mechanisms, Sci. Total Environ. 891 (2023) 164385. https://doi.org/10.1016/j.scitotenv.2023.164385.

[34] D. Han, M. López-Mesas, R. Boada, T. Farías, A.R. Lazo Fraga, M. Valiente, Trace cisplatin and carboplatin removal by 3-mercaptopropionic acid and l-cysteine functionalized sponges: adsorption behaviour and mechanism, Chem. Eng. J. 472 (2023) 144894. https://doi.org/10.1016/j.cej.2023.144894.

[35] Y. Cao, Y. Yao, Y. Li, X. Yang, Z. Cao, G. Yang, Tunable keratin hydrogel based on disulfide shuffling strategy for drug delivery and tissue engineering, J. Colloid Interface Sci. 544 (2019) 121–129. https://doi.org/10.1016/j.jcis.2019.02.049.

[36] E. Gross, D.B. Kastner, C.A. Kaiser, D. Fass, Structure of Ero1p, source of disulfide bonds for oxidative protein folding in the cell, Cell. 117 (2004) 601–610. https://doi.org/10.1016/S0092-8674(04)00418-0.

[37] D. Schilter, Thiol oxidation: A slippery slope, Nat. Rev. Chem. 1 (2017) 1–2. https://doi.org/10.1038/s41570-016-0013.

[38] M. Arisawa, K. Fukumoto, M. Yamaguchi, Rhodium-catalyzed oxidation of unprotected peptide thiols to disulfides with oxygen in water, ACS Catal. 10 (2020) 15060–15064. https://doi.org/10.1021/acscatal.0c04799.

[39] V. Rathore, A. Upadhyay, S. Kumar, An Organodiselenide with Dual Mimic Function of Sulfhydryl Oxidases and Glutathione Peroxidases: Aerial Oxidation of Organothiols to Organodisulfides, Org. Lett. 20 (2018) 6274–6278. https://doi.org/10.1021/acs.orglett.8b02756.

[40] A. Khazaei, M.A. Zolfigol, A. Rostami, 1,3-Dibromo-5,5-dimethylhydantoin [DBDMH] as an efficient and selective agent for the oxidation of thiols to Disulfides in solution or under solvent-free conditions, Synthesis (Stuttg). (2004) 2959–2961. https://doi.org/10.1055/s-2004-834919.

[41] R. Sanz, R. Aguado, M.R. Pedrosa, F.J. Arnáiz, Simple and selective oxidation of thiols to disulfides with dimethylsulfoxide catalyzed by dichlorodioxomolybdenum(VI), Synthesis (Stuttg). (2002) 856–858. https://doi.org/10.1055/s-2002-28520.

[42] M. Kirihara, Y. Asai, S. Ogawa, T. Noguchi, A. Hatano, Y. Hirai, A mild and environmentally benign oxidation of thiols to disulfides, Synthesis (Stuttg). (2007) 3286–3289. https://doi.org/10.1055/s-2007-990800.

[43] X.-Y. Lou, R. Boada, V. Verdugo, L. Simonelli, G. Pérez, M. Valiente, Decoupling the adsorption mechanisms of arsenate at molecular level on modified cube-shaped sponge loaded superparamagnetic iron oxide nanoparticles, J. Environ. Sci. 121 (2022) 1–12. https://doi.org/10.1016/j.jes.2021.09.001.

[44] A. POLITZER, J.C. H Teng, T.T. SINGH, T.J.C. H, T.T. SINGH, The method of producing a regenerated cellulose sponge, 1963. https://lens.org/073-184-824-742-697.

[45] P.E.L. Kyle, T.B. P, Ion exchange polymers on improved porous substrates, 1982.

https://lens.org/080-517-023-858-186.

[46] X.Y. Lou, R. Boada, L. Simonelli, M. Valiente, Enhanced arsenite removal by superparamagnetic iron oxide nanoparticles in-situ synthesized on a commercial cube-shape sponge: adsorption-oxidation mechanism, J. Colloid Interface Sci. 614 (2022) 460–467. https://doi.org/10.1016/j.jcis.2022.01.119.

[47] N.B. Rainer, R.N. B, Polymer product for the selective absorption of dissolved ions, 1992. https://lens.org/018-286-240-697-194.

[48] J.A. Muñoz, A. Gonzalo, M. Valiente, Arsenic Adsorption by Fe(III)-Loaded Open-Celled Cellulose Sponge. Thermodynamic and Selectivity Aspects, Environ. Sci. Technol. 36 (2002) 3405–3411. https://doi.org/10.1021/es020017c.

[49] L. Chai, Q. Li, Y. Zhu, Z. Zhang, Q. Wang, Y. Wang, Z. Yang, Synthesis of thiol-functionalized spent grain as a novel adsorbent for divalent metal ions, Bioresour. Technol. 101 (2010) 6269–6272. https://doi.org/10.1016/j.biortech.2010.03.009.

[50] D. Mohan, A. Sarswat, V.K. Singh, M. Alexandre-Franco, C.U. Pittman, Development of magnetic activated carbon from almond shells for trinitrophenol removal from water, Chem. Eng. J. 172 (2011) 1111–1125. https://doi.org/10.1016/j.cej.2011.06.054.

[51] J. Li, L.P. Zhang, F. Peng, J. Bian, T.Q. Yuan, F. Xu, R.C. Sun, Microwave-assisted solvent-free acetylation of cellulose with acetic anhydride in the presence of iodine as a catalyst, Molecules. 14 (2009) 3551–3566. https://doi.org/10.3390/molecules14093551.

[52] T. Burks, M. Avila, F. Akhtar, M. Göthelid, P.C. Lansåker, M.S. Toprak, M. Muhammed, A. Uheida, Studies on the adsorption of chromium(VI) onto 3-Mercaptopropionic acid coated superparamagnetic iron oxide nanoparticles, J. Colloid Interface Sci. 425 (2014) 36–43. https://doi.org/10.1016/j.jcis.2014.03.025.

[53] B. Parambath Kanoth, M. Claudino, M. Johansson, L.A. Berglund, Q. Zhou, Biocomposites from Natural Rubber: Synergistic Effects of Functionalized

Cellulose Nanocrystals as Both Reinforcing and Cross-Linking Agents via Free-Radical Thiol-ene Chemistry, ACS Appl. Mater. Interfaces. 7 (2015) 16303–16310. https://doi.org/10.1021/acsami.5b03115.

[54] S.Y. Park, J.W. Chung, R.D. Priestley, S.Y. Kwak, Covalent assembly of metal nanoparticles on cellulose fabric and its antimicrobial activity, Cellulose. 19 (2012) 2141–2151. https://doi.org/10.1007/s10570-012-9773-6.

[55] R. Alimohammadzadeh, A.A. Rafi, L. Goclik, C.W. Tai, A. Cordova, Direct organocatalytic thioglycolic acid esterification of cellulose nanocrystals: A simple entry to click chemistry on the surface of nanocellulose, Carbohydr. Polym. Technol. Appl. 3 (2022) 100205. https://doi.org/10.1016/j.carpta.2022.100205.

[56] H.Y. Choi, J.H. Bae, Y. Hasegawa, S. An, I.S. Kim, H. Lee, M. Kim, Thiol-functionalized cellulose nanofiber membranes for the effective adsorption of heavy metal ions in water, Carbohydr. Polym. 234 (2020) 115881. https://doi.org/10.1016/j.carbpol.2020.115881.

[57] K. Pramanik, P. Sarkar, D. Bhattacharyay, 3-Mercapto-propanoic acid modified cellulose filter paper for quick removal of arsenate from drinking water, Int. J. Biol. Macromol. 122 (2019) 185–194. https://doi.org/10.1016/j.ijbiomac.2018.10.065.

[58] G.H. Gao, M.J. Park, Y. Li, G.H. Im, J.H. Kim, H.N. Kim, J.W. Lee, P. Jeon, O.Y. Bang, J.H. Lee, D.S. Lee, The use of pH-sensitive positively charged polymeric micelles for protein delivery, Biomaterials. 33 (2012) 9157–9164. https://doi.org/10.1016/j.biomaterials.2012.09.016.

[59] L. Fan, R. Ma, Y. Yang, S. Chen, B. Lu, Covalent sulfur for advanced room temperature sodium-sulfur batteries, Nano Energy. 28 (2016) 304–310. https://doi.org/10.1016/j.nanoen.2016.08.056.

[60] S. Zhang, Y. Zhang, J. Liu, Q. Xu, H. Xiao, X. Wang, H. Xu, J. Zhou, Thiol modified Fe3O4@SiO2 as a robust, high effective, and recycling magnetic sorbent for mercury removal, Chem. Eng. J. 226 (2013) 30–38.

https://doi.org/10.1016/j.cej.2013.04.060.

[61] D.Q. Yang, B. Hennequin, E. Sacher, XPS demonstration of π-π interaction between benzyl mercaptan and multiwalled carbon nanotubes and their use in the adhesion of Pt nanoparticles, Chem. Mater. 18 (2006) 5033–5038. https://doi.org/10.1021/cm061256s.

[62] D. Chen, S. Gao, F. Ur Rehman, H. Jiang, X. Wang, In-situ green synthesis of highly active GSH-capped Pt-Au-Ag-hybrid nanoclusters, Sci. China Chem. 57 (2014) 1532–1537. https://doi.org/10.1007/s11426-014-5208-6.

[63] C. Zhang, L. Gao, Q. Yuan, L. Zhao, W. Niu, P. Cai, J. Li, X. Han, Z. He, F. Gao, Y. Wang, H. Jiang, Z. Chai, X. Gao, Is GSH Chelated Pt Molecule Inactive in Anti-Cancer Treatment? A Case Study of Pt6GS4, Small. 16 (2020) 1–10. https://doi.org/10.1002/smll.202002044.

[64] Y. Kim, Y. Yoon, D. Shin, Fabrication of Sn/SnO2 composite powder for anode of lithium ion battery by aerosol flame deposition, J. Anal. Appl. Pyrolysis. 85 (2009) 557–560. https://doi.org/10.1016/j.jaap.2008.06.005.

[65] H. Ma, K. Teng, Y. Fu, Y. Song, Y. Wang, X. Dong, Synthesis of visible-light responsive Sn-SnO 2/C photocatalyst by simple carbothermal reduction, Energy Environ. Sci. 4 (2011) 3067–3073. https://doi.org/10.1039/c1ee01095f.

[66] A.K. Sinha, M. Pradhan, S. Sarkar, T. Pal, Large-scale solid-state synthesis of Sn-SnO2 nanoparticles from layered SnO by sunlight: A material for dye degradation in water by photocatalytic reaction, Environ. Sci. Technol. 47 (2013) 2339–2345. https://doi.org/10.1021/es303413q.

[67] F.M. Hassan, Z. Chen, A. Yu, Z. Chen, X. Xiao, Sn/SnO2 embedded in mesoporous carbon nanocomposites as negative electrode for lithium ion batteries, Electrochim. Acta. 87 (2013) 844–852. https://doi.org/10.1016/j.electacta.2012.09.015.

[68] K. Kravchyk, L. Protesescu, M.I. Bodnarchuk, F. Krumeich, M. Yarema, M. Walter, C. Guntlin, M. V. Kovalenko, Monodisperse and inorganically capped Sn

and Sn/SnO2 nanocrystals for high-performance Li-ion battery anodes, J. Am. Chem. Soc. 135 (2013) 4199–4202. https://doi.org/10.1021/ja312604r.

[69] A.M. Al-Enizi, M. Naushad, A.H. Al-Muhtaseb, Ruksana, S.M. Alshehri, Z.A. Alothman, T. Ahamad, Synthesis and characterization of highly selective and sensitive Sn/SnO2/N-doped carbon nanocomposite (Sn/SnO2@NGC) for sensing toxic NH3 gas, Chem. Eng. J. 345 (2018) 58–66. https://doi.org/10.1016/j.cej.2018.03.138.

[70] S. Gao, N. Wang, S. Li, D. Li, Z. Cui, G. Yue, J. Liu, X. Zhao, L. Jiang, Y. Zhao, A Multi-Wall Sn/SnO2@Carbon Hollow Nanofiber Anode Material for High-Rate and Long-Life Lithium-Ion Batteries, Angew. Chemie - Int. Ed. 59 (2020) 2465–2472. https://doi.org/10.1002/anie.201913170.

[71] L. Zhang, Z. Zhu, W. Tan, J. Ji, Y. Cai, Q. Tong, Y. Xiong, H. Wan, L. Dong, Thermal-Driven Optimization of the Strong Metal-Support Interaction of a Platinum-Manganese Oxide Octahedral Molecular Sieve to Promote Toluene Oxidation: Effect of the Interface Pt2+-Ov-Mnδ+, ACS Appl. Mater. Interfaces. (2022). https://doi.org/10.1021/acsami.2c16923.

[72] L. Huang, Y. Su, R. Qi, D. Dang, Y. Qin, S. Xi, S. Zaman, B. You, S. Ding, B.Y. Xia, Boosting Oxygen Reduction via Integrated Construction and Synergistic Catalysis of Porous Platinum Alloy and Defective Graphitic Carbon, Angew. Chemie. 133 (2021) 25734–25741. https://doi.org/10.1002/ange.202111426.

[73] J.M. Jacob, P.G. Corradini, E. Antolini, N.A. Santos, J. Perez, Electro-oxidation of ethanol on ternary Pt-Sn-Ce/C catalysts, Appl. Catal. B Environ. 165 (2015) 176–184. https://doi.org/10.1016/j.apcatb.2014.10.012.

[74] I. Marić, G. Dražić, E. Radin, R. Peter, M. Škrabić, T. Jurkin, A. Pustak, N. Baran, L. Mikac, M. Ivanda, M. Petravić, G. Štefanić, M. Gotić, Impact of platinum loading and dispersion on the catalytic activity of Pt/SnO2 and Pt/α-Fe2O3, Appl. Surf. Sci. 607 (2023). https://doi.org/10.1016/j.apsusc.2022.155073.

[75] R. Rizo, D. Sebastián, M.J. Lázaro, E. Pastor, On the design of Pt-Sn efficient

catalyst for carbon monoxide and ethanol oxidation in acid and alkaline media, Appl. Catal. B Environ. 200 (2017) 246–254. https://doi.org/10.1016/j.apcatb.2016.07.011.

[76] L. Wang, W. Wu, Z. Lei, T. Zeng, Y. Tan, N. Cheng, X. Sun, High-performance alcohol electrooxidation on Pt3Sn-SnO2 nanocatalysts synthesized through the transformation of Pt-Sn nanoparticles, J. Mater. Chem. A. 8 (2020) 592–598. https://doi.org/10.1039/c9ta10886f.

[77] Ž.D. Bugarčić, J. Bogojeski, B. Petrović, S. Hochreuther, R. van Eldik, Mechanistic studies on the reactions of platinum(ii) complexes with nitrogen- and sulfur-donor biomolecules, Dalt. Trans. 41 (2012) 12329. https://doi.org/10.1039/c2dt31045g.

[78] T.C. Johnstone, K. Suntharalingam, S.J. Lippard, The Next Generation of Platinum Drugs: Targeted Pt(II) Agents, Nanoparticle Delivery, and Pt(IV) Prodrugs, Chem. Rev. 116 (2016) 3436–3486. https://doi.org/10.1021/acs.chemrev.5b00597.

[79] L. Kelland, The resurgence of platinum-based cancer chemotherapy, Nat. Rev. Cancer. 7 (2007) 573–584. https://doi.org/10.1038/nrc2167.

[80] B.P. Espósito, R. Najjar, Interactions of antitumoral platinum-group metallodrugs with albumin, Coord. Chem. Rev. 232 (2002) 137–149. https://doi.org/10.1016/S0010-8545(02)00049-8.

[81] A.I. Ivanov, J. Christodoulou, J.A. Parkinson, K.J. Barnham, A. Tucker, J. Woodrow, P.J. Sadler, Cisplatin binding sites on human albumin, J. Biol. Chem. 273 (1998) 14721–14730. https://doi.org/10.1074/jbc.273.24.14721.

[82] G. Feiqiang, L. Xiaolei, J. Xiaochen, Z. Xingmin, G. Chenglong, R. Zhonghao, Characteristics and toxic dye adsorption of magnetic activated carbon prepared from biomass waste by modified one-step synthesis, Colloids Surfaces A Physicochem. Eng. Asp. 555 (2018) 43–54. https://doi.org/10.1016/j.colsurfa.2018.06.061.

[83] S. Sen Gupta, K.G. Bhattacharyya, Kinetics of adsorption of metal ions on inorganic materials: A review, Adv. Colloid Interface Sci. 162 (2011) 39–58. https://doi.org/10.1016/j.cis.2010.12.004.

[84] J. Wang, X. Guo, Adsorption kinetic models: Physical meanings, applications, and solving methods, J. Hazard. Mater. 390 (2020) 122156. https://doi.org/10.1016/j.jhazmat.2020.122156.

[85] D. Han, X. Li, Z. Gong, L. Jiang, Z. Wang, P. Liu, Hierarchical Porous Catalytic Pyrolysis Char Derived from Oily Sludge for Enhanced Adsorption, ACS Omega. 6 (2021) 20549–20559. https://doi.org/10.1021/acsomega.1c02575.

[86] V.D. Chinh, L.X. Hung, L. Di Palma, V.T.H. Hanh, G. Vilardi, Effect of Carbon Nanotubes and Carbon Nanotubes/Gold Nanoparticles Composite on the Photocatalytic Activity of TiO2 and TiO2-SiO2, Chem. Eng. Technol. 42 (2019) 308–315. https://doi.org/10.1002/ceat.201800265.

[87] T. Yoshinaga, Y. Iso, T. Isobe, Optimizing the microwave-assisted hydrothermal synthesis of blue-emitting L-cysteine-derived carbon dots, J. Lumin. 213 (2019) 6–14. https://doi.org/10.1016/j.jlumin.2019.05.003.

[88] V. Sharma, P. Ilaiyaraja, A.C. Dakshinamurthy, C. Sudakar, One step thermolysis of Sb-Mercaptopropionic acid complex in ambient air atmosphere for growing Sb2S3 thin films with controlled microstructure, Mater. Sci. Semicond. Process. 121 (2021) 105330. https://doi.org/10.1016/j.mssp.2020.105330.

[89] M. Mrad, T. Ben Chaabane, H. Rinnert, B. Lavinia, J. Jasniewski, G. Medjahdi, R. Schneider, Aqueous Synthesis for Highly Emissive 3-Mercaptopropionic Acid-Capped AIZS Quantum Dots, Inorg. Chem. 59 (2020) 6220–6231. https://doi.org/10.1021/acs.inorgchem.0c00347.

[90] W. JIAN, S. LIU, J. LI, W. YANG, Decomposition Reaction of Zn-MPA(3-Mercaptopropionic Acid) Complex Under Microwave Irradiation, Chem. Res. Chinese Univ. 24 (2008) 353–356. https://doi.org/10.1016/S1005-9040(08)60074-4.

[91] J. Laurent, M. Casellas, C. Dagot, Heavy metals biosorption on disintegrated activated sludge: Description of a new equilibrium model, Chem. Eng. J. 164 (2010) 63–69. https://doi.org/10.1016/j.cej.2010.08.023.

[92] J. Wang, X. Guo, Adsorption isotherm models: Classification, physical meaning, application and solving method, Chemosphere. 258 (2020) 127279. https://doi.org/10.1016/j.chemosphere.2020.127279.

[93] R.M. Schneider, C.F. Cavalin, M.A.S.D. Barros, C.R.G. Tavares, Adsorption of chromium ions in activated carbon, Chem. Eng. J. 132 (2007) 355–362. https://doi.org/10.1016/j.cej.2007.01.031.

[94] G.D. Değermenci, N. Değermenci, V. Ayvaoğlu, E. Durmaz, D. Çakır, E. Akan, Adsorption of reactive dyes on lignocellulosic waste; characterization, equilibrium, kinetic and thermodynamic studies, J. Clean. Prod. 225 (2019) 1220–1229. https://doi.org/10.1016/j.jclepro.2019.03.260.

[95] S. Kishani, T. Benselfelt, L. Wågberg, J. Wohlert, Entropy drives the adsorption of xyloglucan to cellulose surfaces – A molecular dynamics study, J. Colloid Interface Sci. 588 (2021) 485–493. https://doi.org/10.1016/j.jcis.2020.12.113.

Supplementary data of the manuscript:

Trace cisplatin adsorption by thiol-functionalized sponge (TFS) and Sn/SnO_2-coated TFS: adsorption study and mechanism investigation

Dong Han [a], Margarita Edelia Villanueva Tagle [b], Mirella Peña Icart [c], Montserrat López-Mesas [a,*], and Manuel Valiente [a]

[a] *GTS-UAB Research Group, Department of Chemistry, Faculty of Science, Universitat Autònoma de Barcelona, Bellaterra, (Cerdanyola del Vallès), 08193 Barcelona, Spain*

[b]*Faculty of Chemistry, University of Havana, Havana 10400, Cuba*

[c]*Institute of Materials Science and Technology, University of Havana, Havana 10400, Cuba*

The experimental kinetic data were fitted to the PFO model (eq. 1) and PSO model (eq. 2)[1]:

$$q_t = q_{e.cal}(1-e^{-k_1 t}) \quad (1)$$

$$q_t = \frac{q_{e.cal}^2 k_2 t}{q_{e.cal} k_2 t + 1} \quad (2)$$

The variables $q_{e.cal}$ and q_t represent adsorption capacities (μg g^{-1}) at equilibrium derived from models and at a given contact time t (h), respectively. The rate constant for PFO is denoted as k_1 (h^{-1}), while the rate constant for PSO is denoted as k_2 (h^{-1}).

In the present study, the adsorption equilibrium data was fitted using different isotherm models, which are formulated as follows:

Langmuir model (eq. 3):

$$q_e = \frac{q_{mL} K_L c_e}{1 + K_L c_e} \quad (3)$$

$$R_L = \frac{1}{1 + K_L c_0} \quad (4)$$

where q_{mL} represents the maximum adsorption capacity (μg/g). K_L is the constant indicative of the affinity of binding sites (L μg^{-1}). The dimensionless parameter known as the equilibrium parameter or separation factor, denoted R_L (eq. 4), serves to characterize the nature of the adsorption process. Specifically, values of R_L falling within the ranges of 0, $0 < R_L < 1$, 1, and >1 correspond to irreversible, favorable, linear, and unfavorable adsorption behaviors, respectively [2].

Freundlich model (eq. 5):

$$q_e = K_F c_e^{1/n} \quad (5)$$

K_F ((μg g^{-1})(L μg^{-1})$^{1/n}$) and n are the Freundlich constants related to the adsorption capacity and intensity, respectively. Value of $1/n < 1$, it indicates a normal adsorption, and

$1/n > 1$ indicates cooperative adsorption. If $1/n$ lies between one and ten, this indicates a favorable sorption process [3–6].

Sips model (eq. 6):

The Sips model represents a hybrid model that integrates the Langmuir and Freundlich models [7]. Saadi et al. [8] have asserted that the Sips model is the most suitable 3-parameter isotherm model for monolayer adsorption. This model is capable of characterizing both homogeneous and heterogeneous systems. The non-linear Sips isotherm model is mathematically expressed by eq 6.

$$q_e = \frac{q_{mS} K_S c_e^{n_s}}{1 + K_S c_e^{n_s}} \tag{6}$$

where q_{mS} (μg g^{-1}) is the maximum adsorbed amount, K_S ((L μg^{-1})^{ns}) and n_S are the Sips constants. The Sips model is equivalent to the Langmuir model when n_S equals 1 and resembles the Freundlich model under conditions of low c_0. Nevertheless, it fails to comply with Henry's law at low c_0 [9].

Dubinin-Radushkevich (D-R) model (eq. 7):

The D-R model considers the adsorption process as occurring in a heterogeneous adsorbent with different adsorption energies. The model assumes a uniform distribution of these energies and relies on the Polanyi potential [10] to account for the variation in adsorption energy with coverage [11,12].

$$q_e = q_{mDR} e^{-K_{DR}\varepsilon^2} \tag{7}$$

$$\varepsilon = RT \ln \frac{c_s}{c_e} \tag{8}$$

where $q_{mD\text{-}R}$ (μg g^{-1}) refers to the maximum adsorption capacity, K_{DR} (mol^2 kJ^{-2}) represents the model constant, ε (kJ mol^{-1}) is the adsorption potential based on the Polanyi's potential theory [10], c_s (μg L^{-1}) denotes the solubility of adsorbates. The mean

free energy (E, kJ mol^{-1}) can be determined using eq. 9, and it is commonly used to assess whether the adsorption process is predominantly governed by physical interactions (E < 8 kJ mol^{-1}) or chemical interactions (8 < E < 16 kJ mol^{-1}) [13].

$$E = \frac{1}{\sqrt{2K_{DR}}} \tag{9}$$

Three key thermodynamic parameters, specifically the Gibbs free energy ($\Delta G°$), enthalpy change ($\Delta H°$), and entropy change ($\Delta S°$), were determined using equations (10), (11), and (12), respectively.

$$\Delta G^o = -\mathrm{R}T \ln K \tag{10}$$

$$\ln K = \frac{\Delta S^0}{\mathrm{R}} - \frac{\Delta H^0}{\mathrm{R}T} \tag{11}$$

$$K = \frac{C_0 - C_e}{C_e} \tag{12}$$

Where R is the ideal gas constant (8.314 J mol^{-1} K^{-1}), T is the absolute temperature (K), K is dimensionless distribution constant. Values of $\Delta H°$ and $\Delta S°$ were obtained via the slope and intercept of linear Van't Hoff plots (ln K versus 1/T).

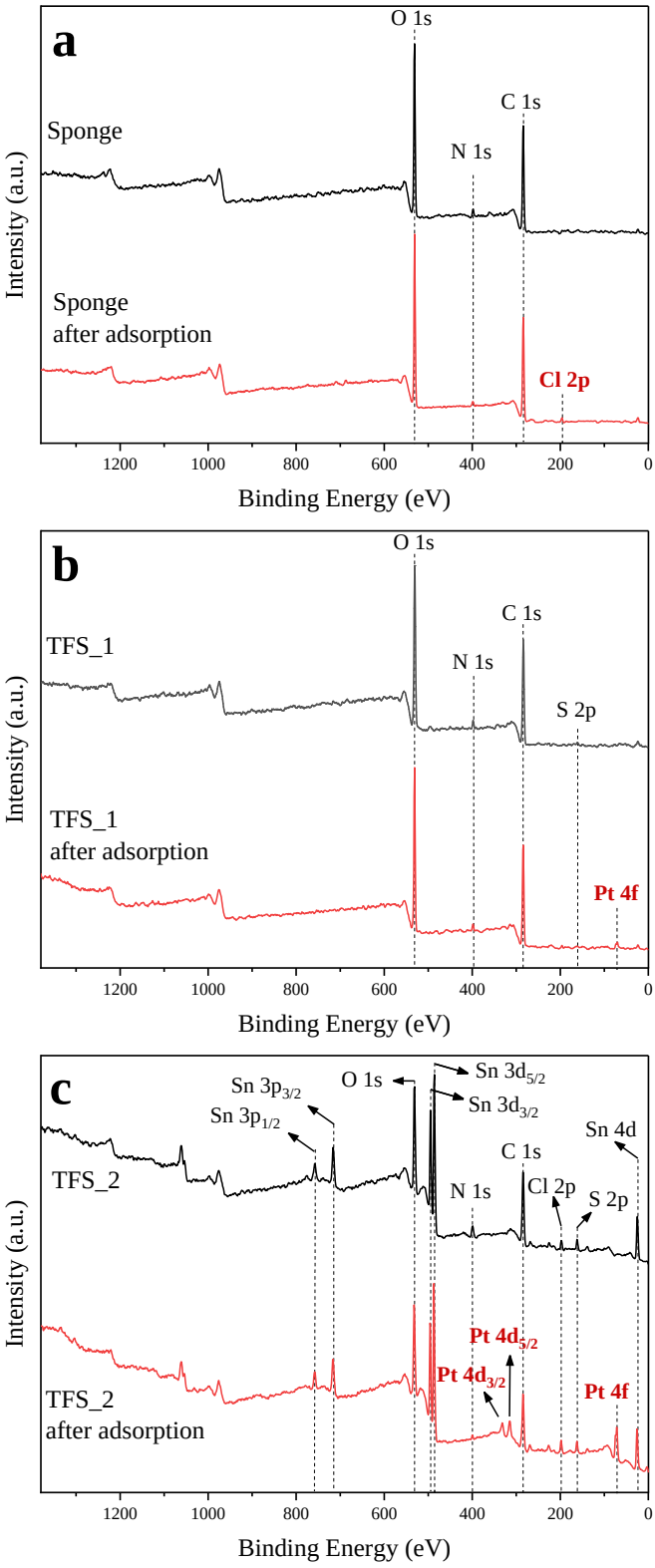

Fig. S1 XPS survey spectra of (a) Sponge, (b) TFS_1, and (c) TFS_2, before and after adsorption of cisplatin [adsorbent dosage: 200 mg, solution volume: 40 mL, initial concentration of Pt: 100 mg L^{-1}, T: 343 K, contact time: 24 h].

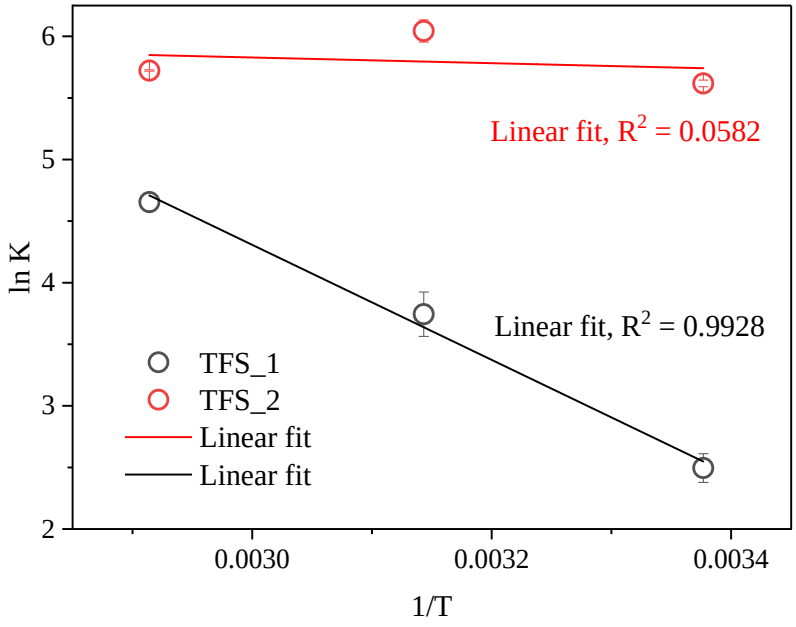

Fig. S2 Van't Hoff plots to determine the thermodynamic parameters of adsorption.

Table S1. Kinetic parameters for the adsorption of cisplatin by TFS_1 and TFS_2.

Kinetic model		**Pseudo-first-order**			**Pseudo-second-order**		
	$q_{e.exp}$	k_1	$q_{e.cal}$	R^2	k_2	$q_{e.cal}$	R^2
Adsorbent	μg g^{-1}	min^{-1}	μg g^{-1}		min^{-1}	μg g^{-1}	
TFS_1	40.2 ± 0.1	0.30 ± 0.06	37 ± 2	0.9294	0.013 ± 0.004	39 ± 2	0.9311
TFS_2	47.1 ± 0.7	2.2 ± 0.4	45.0 ± 0.7	0.9810	0.19 ± 0.09	45.5 ± 0.8	0.9822

Table S2. Adsorption isotherms parameters of TFS_1 and TFS_2 towards cisplatin solutions.

Models		**Adsorbents**	**TFS_1**			**TFS_2**		
Parameters		**T (K)**	**296**	**318**	**343**	**296**	**318**	**343**
	q_m	mg g^{-1}	*9.0 ±0.5*	*28 ± 3*	51 ± 9	46 ± 2	91 ± 4	80 ± 6
Langmuir	q_{mL}	mg g^{-1}	6.7 ± 0.6	42 ± 5	66 ± 9	42 ± 1	90 ± 3	63 ± 5
	K_L	x10^{-4} L μg^{-1}	5 ± 3	0.05 ± 0.01	0.11 ± 0.04	6 ± 1	29 ± 1	132 ± 6
	R_L		0.004 -0.979	0.275 -0.999	0.154 -0.999	0.004 -0.974	0.001 -0.880	0.001 -0.618
	R^2		0.8748	0.9813	0.9618	0.9860	0.9908	0.9166
Freundlich	K_F	$(\mu g\ g^{-1})(L\ \mu g^{-1})^{1/n}$	*191 ± 60*	23 ± 12	118 ± 48	2.0 ± 0.6	6 ± 2	3 ± 1
	$1/n$		0.30 ± 0.02	0.55 ± 0.04	0.49 ± 0.03	0.25 ± 0.03	0.27 ± 0.03	0.29 ± 0.04
	R^2		0.9747	0.9867	0.9891	0.9614	0.9183	0.9628
Sips	q_{mS}	mg g^{-1}	39*	92*	100*	48 ± 4	94 ± 1	90*
	K_S	x10^{-4} $(L\ \mu g^{-1})^{ns}$	38 ± 44	0.7 ± 0.4	3 ± 2	0.009 ± 0.004	0.011 ± 0.002	0.03 ± 0.02
	n_s		0.33 ± 0.07	0.69 ± 0.05	0.66 ± 0.07	0.56 ± 0.09	0.73 ± 0.03	0.42 ± 0.06
	R^2		0.9756	0.9856	0.9799	0.9908	0.9990	0.9410
D-R	q_{mDR}	mg g^{-1}	6.2 ± 0.4	19 ± 2	40 ± 3	45 ± 1	111 ± 6	76 ± 6
	K_{DR}	$mol^2\ kJ^{-2}$	0.007 ±0.001	0.005 ±0.001	0.005 ±0.001	0.0045 ±0.0003	0.0029 ±0.0002	0.0026 ±0.0005
	E	kJ mol^{-1}	8.17	9.68	9.71	10.59	13.22	13.98
	R^2		0.9493	0.8048	0.8931	0.9906	0.9766	0.9416

*Not acceptable values, because fitting iterations do not converge easily.

Table S3. Summary of thermodynamic parameters: $\Delta G°$ (kJ mol^{-1}), $\Delta H°$ (kJ mol^{-1}), and $\Delta S°$ (J mol^{-1} K^{-1}).

Adsorbents		TFS_1			TFS_2		
T(K)		296	318	343	296	318	343
Cisplatin	$\Delta G°$	-5.9 ± 0.3	-9.9 ± 0.5	-13.3 ± 0.2	-13.8 ± 0.1	-16.0 ± 0.2	-16.3 ± 0.1
	$\Delta H°$	39 ± 3			*		
	$\Delta S°$	152 ± 11			*		

*Not acceptable values, because the adsorption *vs.* temperature curves were not monotonically increasing or decreasing, poor linear fit.

Table S4. Comparison of cisplatin removal by TFS_1 and TFS_2 to commercially available and synthetically prepared adsorbents previously reported.

Adsorbent	**Initial concentration (Pt, µg L^{-1})**	**Contact time**	***T*** **(K)**	**Removal (%)**	**Ref.**
TFS_1	235	40 min	343	95.5 ± 0.8	**This study**
TFS_2			318	99.5 ± 0.1	
3-mercaptopropionic acid functionalized sponge (no reduction step)	235	3 h	343	88.9 ± 0.5	[14]
L-cysteine functionalized sponge (no reduction step)			343	75 ± 2	
3-Mercaptopropyl-functionalized silica gel *			293	98.7 ± 0.1	
Cysteine-functionalized silica gel *	235	40 min	343	98.5 ± 0.1	[15]
3-(diethylenetriamino)propyl-functionalized silica gel *		24 h	318	46 ± 3	
Pt(II)-imprinted thiocyanato-functionalized SBA-15	206	7 d	298	98.4	[16]
Dithiocarbamate-Modified Silica	10000	1 h	RT	85	[17]
Biomass-derived adsorbents (activated carbon, biochar, chitosan, wood ash)	100	24 h	RT	63 ± 7	[18]

* Commercial adsorbents purchased from Sigma-Aldrich.

References:

[1] J. Wang, X. Guo, Adsorption kinetic models: Physical meanings, applications, and solving methods, J. Hazard. Mater. 390 (2020) 122156. https://doi.org/10.1016/j.jhazmat.2020.122156.

[2] T.W. Weber, R.K. Chakravorti, Pore and solid diffusion models for fixed-bed adsorbers, AIChE J. 20 (1974) 228–238. https://doi.org/10.1002/aic.690200204.

[3] S. Goldberg, Equations and Models Describing Adsorption Processes in Soils, in: 2018: pp. 489–517. https://doi.org/10.2136/sssabookser8.c10.

[4] E.G. Furuya, H.T. Chang, Y. Miura, K.E. Noll, A fundamental analysis of the isotherm for the adsorption of phenolic compounds on activated carbon, Sep. Purif. Technol. 11 (1997) 69–78. https://doi.org/10.1016/S1383-5866(96)01001-5.

[5] Physical chemistry, J. Franklin Inst. 272 (1961) 71. https://doi.org/10.1016/0016-0032(61)90671-8.

[6] V.D. Chinh, L.X. Hung, L. Di Palma, V.T.H. Hanh, G. Vilardi, Effect of Carbon Nanotubes and Carbon Nanotubes/Gold Nanoparticles Composite on the Photocatalytic Activity of TiO2 and TiO2-SiO2, Chem. Eng. Technol. 42 (2019) 308–315. https://doi.org/10.1002/ceat.201800265.

[7] R. Sips, On the structure of a catalyst surface, J. Chem. Phys. 16 (1948) 490–495. https://doi.org/10.1063/1.1746922.

[8] R. Saadi, Z. Saadi, R. Fazaeli, N.E. Fard, Monolayer and multilayer adsorption isotherm models for sorption from aqueous media, Korean J. Chem. Eng. 32 (2015) 787–799. https://doi.org/10.1007/s11814-015-0053-7.

[9] J. Wang, X. Guo, Adsorption isotherm models: Classification, physical meaning, application and solving method, Chemosphere. 258 (2020) 127279. https://doi.org/10.1016/j.chemosphere.2020.127279.

[10] M. Polanyi, Theories of the Adsorption of gases. A general Survey and some

additional remarks, Trans. Faraday Soc. 28 (1932) 1–18. https://pubs-rsc-org.ezproxy.is.ed.ac.uk/en/content/articlepdf/1932/tf/tf9322800316.

[11] L. Dolatyari, M.R. Yaftian, S. Rostamnia, Removal of uranium(VI) ions from aqueous solutions using Schiff base functionalized SBA-15 mesoporous silica materials, J. Environ. Manage. 169 (2016) 8–17. https://doi.org/10.1016/j.jenvman.2015.12.005.

[12] Y. Zhou, Y. Li, D. Liu, D. Liu, L. Xu, C. Liu, Adsorption optimization of uranium(VI) onto polydopamine and sodium titanate co-functionalized MWCNTs using response surface methodology and a modeling approach, Colloids Surfaces A Physicochem. Eng. Asp. 627 (2021). https://doi.org/10.1016/j.colsurfa.2021.127145.

[13] M. Chabani, A. Amrane, A. Bensmaili, Kinetic modelling of the adsorption of nitrates by ion exchange resin, Chem. Eng. J. 125 (2006) 111–117. https://doi.org/10.1016/j.cej.2006.08.014.

[14] D. Han, M. López-Mesas, R. Boada, T. Farías, A.R. Lazo Fraga, M. Valiente, Trace cisplatin and carboplatin removal by 3-mercaptopropionic acid and l-cysteine functionalized sponges: adsorption behaviour and mechanism, Chem. Eng. J. 472 (2023) 144894. https://doi.org/10.1016/j.cej.2023.144894.

[15] D. Han, M. López-Mesas, M. Luaces, Y. Enamorado, M. Sanadar, A. Melchior, M. Valiente, Comparative study on removal of platinum cytostatic drugs at trace level by cysteine, diethylenetriamino functionalized Si-gels and polyethyleneimine functionalized sponge: Adsorption performance and mechanisms, Sci. Total Environ. 891 (2023) 164385. https://doi.org/10.1016/j.scitotenv.2023.164385.

[16] J. Dobrzynska, M. Dabrowska, R. Olchowski, E. Zieba, R. Dobrowolski, Development of a method for removal of platinum from hospital wastewater by novel ion-imprinted mesoporous organosilica, J. Environ. Chem. Eng. 9 (2021).

https://doi.org/10.1016/j.jece.2021.105302.

[17] R. Lombana Fraguela, J.A. Ricardo Garcia, M.E. Villanueva Tagle, M.S. Pomares Alfonso, M. Cracchiolo, A. Kovačević, M. Tolazzi, A. Melchior, M. Sanadar, Evaluation of Dithiocarbamate-Modified Silica for Cisplatin Removal from Water, Processes. 11 (2023) 472. https://doi.org/10.3390/pr11020472.

[18] K. Folens, A. Abebe, J. Tang, F. Ronsse, G. Du Laing, G. Du Laing, Biosorption of residual cisplatin, carboplatin and oxaliplatin antineoplastic drugs in urine after chemotherapy treatment, Environ. Chem. 15 (2018) 506–512. https://doi.org/10.1071/EN18115.

Chapter 4

General discussion of the results

In the alchemist's dream, atoms dance in cosmic gleam.

The research carried out in this thesis focuses on the removal of trace amounts of Pt-CDs from aqueous solutions using adsorption processes. Previous chapters have described the specific studies developed. Basically, the studies develop novel methodologies to remove Pt-CDs at very low concentrations. On the other hand, the studies also aim not only to project feasible applications to Pt-CDs polluted waters where the problem is the low content of these pollutants, but also to have an industrially proven and economically effective adsorption system. Taking into account this scenario conditions, the conducted study can be categorized into three distinct endeavors including (1) the investigation and comparison of the adsorption of Pt-CDs by three commercially available materials, (2) the enhancement of sponge adsorption capabilities through thiol functionalization, and (3) the optimization of thiol functionalization through reduction reactions. Now, considering the obtained results, the general discussion is categorized into three sections.

4.1 A comparative study on removal of Pt-CDs at trace level by commercial adsorbents

Here, we will include the main results of the specific studies. This will include both the adsorption capacities, the process kinetics and the application to model samples.

4.1.1 Comparative analysis of the adsorption behavior of $PtCl_4^{2-}$, cisplatin, and carboplatin on Si-Cys, Si-DETA, and Sponge

The adsorption behavior of $PtCl_4^{2-}$ (as a model of cisplatin) onto Si-Cys, Si-DETA, and Sponge was influenced by pH in distinct manners. Lowering the pH of the solution resulted in the protonation of amino groups on the surface of Si-Cys, thereby inducing a positive surface charge, thus enhancing the electrostatic attraction to anionic $PtCl_4^{2-}$. Hence a marked increase in adsorption capacity from 19 ± 4 to 45 ± 1 μg g^{-1} was observed as the pH decreased from 6 to 2. However, a comparable pH variation resulted in a slight enhancement in adsorption by Si-DETA and Sponge. This is hypothesized to stem from

the primarily amine-rich surfaces of Si-DETA and Sponge, where protonation contributes only to the increase in surface positive charge density, thereby reinforcing electrostatic attractions. Unlike Si-Cys, which can experience a shift to negative charge due to deprotonation of thiol and carboxyl groups at higher pH values, thereby repelling $PtCl_4^{2-}$. However, in the case of cisplatin and carboplatin adsorption, their overall adsorption capacities are lower than that of $PtCl_4^{2-}$, and the influence of pH is not pronounced. Additionally, both Si-DETA and Sponge exhibited suboptimal adsorption capacities, compared to Si-Cys. Unlike $PtCl_4^{2-}$ (with four labile Cl ligands), cisplatin (with two labile Cl ligands and two inert NH_3 ligands) and carboplatin (with a bidentate CDDCA ligand and two inert NH_3 ligands) pose greater challenges in complexing with the adsorbent due to ligand substitution. And for non-anionic cisplatin and carboplatin, electrostatic interactions contributes minimally; their adsorption primarily relies on complexation within the chemical adsorption mode, wherein Pt−S coordination is prominent. In summary, the adsorption pathways of both cisplatin and carboplatin differ from that of the template $PtCl_4^{2-}$, with their adsorption predominantly governed by Pt−S complexation. Conversely, the adsorption of $PtCl_4^{2-}$ is relatively favorable due to the potential assistance of physical adsorption mechanisms such as electrostatic forces.

4.1.2 Analysis of adsorption kinetics, isotherms, and thermodynamics

Rapid adsorption kinetics were observed for all Pt compounds. The initial phase exhibited a swift increase in adsorption capacities during the initial few minutes due to the abundant active adsorption sites on the surfaces of three adsorbents. Subsequently, the rate of growth progressively decelerated, culminating in the attainment of adsorption equilibrium at approximately 40 minutes. The PSO model demonstrated superior fitting performance compared to the PFO model. The PSO model postulates that adsorption is primarily driven by chemisorption, involving complexation between Pt and surface functional groups such as thiol, carboxyl, and amino groups. Contrastingly, the PFO model is better suited for characterizing the initial external/internal diffusion stage,

typically observed when the initial concentration of adsorbate is relatively high. The target Pt complexes studied in adsorption kinetics exhibited exceedingly low initial concentrations (235 μg L^{-1}), and the adsorbent possessed abundant active binding sites. This scenario aligns more closely with the context described by the PSO model, wherein chemisorption predominantly governs the adsorption process.

In the investigation of adsorption isotherms, it is observed that within the low concentration range, the adsorption capacities exhibit a rapid linear increase in response to elevated initial concentrations of $PtCl_4^{2-}$, cisplatin, and carboplatin solutions. This phenomenon is likely attributable to the high concentration gradient generated at the solid-liquid interface which can force Pt compounds to diffuse towards the surface of adsorbents, according to the Fick's laws of diffusion. Then, as the initial concentration gradually increases to several hundred mg L^{-1}, the growth in adsorption capacity slows down due to nearing adsorption saturation. Based on the higher coefficients of determination ($R^2 > 0.92$), it can be inferred that the Langmuir model provides a superior fit compared to the Freundlich model, with the exception of the cisplatin adsorption by Si-Cys and carboplatin adsorption by Si-DETA (where the Freundlich model demonstrates slight superiority). The findings indicate a monolayer adsorption behavior for all adsorbents concerning the adsorption of the three Pt complexes. And the adsorption behavior within the range of low concentrations follows a linear pattern, also confirming monolayer adsorption within a limited coverage in accordance with Henry's law.

For the $PtCl_4^{2-}$ adsorption, increasing temperature (from 293 to 343 K) resulted in a slight reduction in adsorption capacities onto three adsorbents. The adsorption mechanism for anionic $PtCl_4^{2-}$ primarily involved physical adsorption forces, encompassing Van der Waals interactions and electrostatic attraction. Particularly, Van der Waals force, inherently present in adsorption processes, exhibited diminished effects as temperatures reached 343 K, due to its susceptibility to thermal disruption. In contrast, the adsorption of cisplatin exhibited distinct a different pattern, wherein high

temperatures notably increased the adsorption of cisplatin (initial Pt concentration: 235 μg L^{-1}) on Si-Cys, with maximum removal efficiency of 98.5 ± 0.1% at 343 K. Similar trends were observed for the adsorption of carboplatin. These findings indicate that high temperatures are conducive to chelation-driven chemisorption, wherein high temperatures promote Pt−S complexation. For Sponge and Si-DETA, their adsorption capacities exhibited a characteristic pattern of initial increase followed by subsequent decrease as the temperature was raised. Notably, the adsorption capabilities of cisplatin on Sponge and Si-DETA were generally improved as the temperature was raised from 293 to 318 K. This enhancement was primarily attributed to the temperature-driven facilitation of Pt−N complexation. However, this complexation process was constrained due to the inherent unfavorable interaction between the "hard" base N and the "soft" acid Pt. Subsequently, the further temperature increase to 343 K accentuated the influence of diminished Van der Waals adsorption, culminating in a reduction of the adsorption capacities for both Sponge and Si-DETA.

First, the adsorption of the three Pt complexes occurs spontaneously with a negative $\Delta G°$. A comparison of $\Delta H°$ values reveals distinct differences in the adsorption of $PtCl_4^{2-}$ when contrasted with cisplatin or carboplatin. Specifically, the positive $\Delta H°$ value denotes an endothermic process in the cisplatin or carboplatin adsorption, in contrast to the exothermic nature of $PtCl_4^{2-}$ adsorption. Furthermore, the absolute value of $\Delta H°$ for cisplatin (44 ± 7 kJ mol^{-1}) is approximately twice that for $PtCl_4^{2-}$ (-23 ± 6 kJ mol^{-1}), demonstrating that the cisplatin adsorption by Si-Cys is more prone to chemisorption. This observation implies a temperature-enhanced formation of Pt−S bonds, with an enthalpy change surpassing that associated with physisorption. Moreover, the entropy changes ($\Delta S°$) during the adsorption process of $PtCl_4^{2-}$ and the other two Pt-CDs on Si-Cys exhibit opposing trends. Negative $\Delta S°$ values indicate greater order at the liquid-solid interface during $PtCl_4^{2-}$adsorption, whereas positive $\Delta S°$ values suggest a rise in degrees of freedom during the adsorption of cisplatin and carboplatin onto Si-Cys.

4.1.3 Adsorption of Pt-CDs from model samples of hospital wastewater

Si-Cys demonstrates comparable removal efficiencies for cisplatin and carboplatin, with removal rates ranging from 72 ± 1% to 95 ± 1% for cisplatin and from 75 ± 1% to 95 ± 1% for carboplatin. In undiluted urine samples, lower removal efficiencies were observed; additionally, the removal of cisplatin and carboplatin from analogous samples of hospital wastewater was lower than their removal from Milli-Q water, because of the complicated constituents of the urine samples. Potential interference arises from trace proteins present in urine. These proteins contain cystine sites capable of pre-chelating a fraction of Pt-CDs. Moreover, the existence of abundant components such as Cl^- and NH_4^+ in the urine matrix could potentially disrupt ligand replacement processes for cisplatin and carboplatin, influencing Pt complexation on the Si-Cys surface. Additionally, coexisting cations like Na^+, K^+, and Ca^{2+} in urine at concentrations spanning from several to thousands of mg L^{-1} contribute to increased competition for accessible adsorption sites, causing a minor hindrance in capturing cisplatin and carboplatin. As urine dilution increased, the diminishing influence of matrix effects became evident, with nearly all removal efficiencies reaching maximum (92 ± 1% - 95 ± 1%) from 100-time diluted urine. Exception was observed in the adsorption of spiked Pt-CDs (3.12 μg L^{-1}) from 100-time diluted urine. After further dilution of urine samples from 10-time to 100-time, an unexpected reduction in removal rates was noted. However, given the exceptionally low initial Pt concentration (merely 3.12 μg L^{-1}), limited efficiency in capturing Pt species at such minute concentrations is foreseeable.

4.2 **Improving the adsorption efficiency of industrially proven adsorbents for Pt-CDs**

The preceding discussion in Section 4.1 has confirmed the pivotal role of thiol groups as high-affinity binding sites in the adsorption of Pt-CDs. Inspired by this, the cheap industrially proven Sponge material was chosen and functionalized to enhance its

Pt-CDs adsorption capacity. Specifically, functionalization was achieved through esterification reactions by grafting MPA and Cys onto the cellulose substrate. Here, we also incorporated a novel methodology to elucidate the adsorption mechanisms on the improved industrial adsorbent by applying synchrotron-based techniques to determine the Pt species.

4.2.1 Characterization of functionalized MPA@Sponge and Cys@Sponge

In the FTIR spectra, the functional reagent MPA exhibits a peak at 1701 cm^{-1} attributed to the carboxyl C=O stretching. Conversely, Cys presents distinct bands at 1391 and 1576 cm^{-1}, ascribable to the symmetric and asymmetric stretching vibrations of the −COO− in carboxyl group. However, the characteristic peaks representing the carboxyl group in both MPA and Cys experience a noticeable shift upon functionalization, resulting in the emergence of a new absorption band at 1730 cm^{-1} in the spectra of both functionalized sponges. This is assigned to the ester C=O stretching, confirming the successful esterification. However, due to the low sulfur loading on the MPA@Sponge and Cys@Sponge, the characteristic peak of thiol groups at 2550 cm^{-1} is nearly absent, as the characteristic peak resulting from S−H stretching is inherently weak. Nonetheless, EA measurements indicated the presence of sulfur in both functionalized sponges after functionalization, with sulfur contents of 1.23 ± 0.07 wt% and 0.59 ± 0.03 wt%, respectively. These findings corroborate the effective immobilization of MPA and Cys on the Sponge, considering the negligible sulfur present in the unmodified Sponge.

4.2.2 Studies on the batch adsorption process of cisplatin and carboplatin onto MPA@Sponge and Cys@Sponge

It becomes clear that the introduction of MPA and Cys enhanced the adsorption of both Pt-CDs, by comparing their adsorption by Sponge. It is noteworthy that the adsorption enhancement in MPA@Sponge surpasses that observed in Cys@Sponge. This discrepancy arises from the higher sulfur content of MPA@Sponge than Cys@Sponge

(1.23 ± 0.07 vs. 0.59 ± 0.03 wt%, determined by EA), thereby providing a greater number of adsorption sites. Additionally, when compared to carboplatin, both functionalized sponges performed better in cisplatin adsorption. This differentiation can be due to the fact that cisplatin is more easily hydrated. Specifically, the Cl ligands of cisplatin, distinct from bidentate chelating ligand CBDCA of carboplatin, are more prone to displacement by water molecules. In contrast, the CBDCA ligand of carboplatin shows more resistance to hydration. Therefore, the resistance to hydration hinders subsequent complexation to thiol groups, leading to worse adsorption of carboplatin.

All observed adsorption behaviors exhibited rapid kinetics, well fitted by the PSO kinetic model. Specifically, during the initial minutes, cisplatin rapidly diffused to the surfaces of both functionalized sponges, followed by subsequent complexation with thiol groups. The PSO model assumes that adsorption is dominated by chemisorption, such as the bonding process between target adsorbates and active binding sites. In terms of adsorption isotherms, based on the higher coefficients of determination ($R^2 > 0.96$), it can be inferred that the Langmuir model provides a superior fit compared to the Freundlich model, with the exception of the cisplatin adsorption by MPA@Sponge at 318 K (where the Freundlich model demonstrates slight superiority). The findings indicate a monolayer adsorption behavior for both sponges concerning the adsorption of the both Pt-CDs. And the adsorption behavior within the range of low concentrations follows a linear pattern, also confirming monolayer adsorption within a limited coverage in accordance with Henry's law.

The influence of temperature on the adsorption of Pt-CDs by functionalized sponges manifests distinct behavior compared to non-functionalized sponge. Thiol-modified sponge exhibits a temperature-favorable adsorption behavior. The adsorption process of Pt-CDs on both functionalized sponges is mainly dominated by Pt−S complexation and exhibits a pronounced thermophilic feature. Hence, increasing temperature can promote more Pt to be chelated by thiol groups. Moreover, it is noteworthy that the effect of

temperature manifests differently in the enhancement of cisplatin and carboplatin adsorption. In particular, the cisplatin adsorption steadily increases with each temperature increment, whereas the carboplatin adsorption only shows a significant increase beyond 318 K. This phenomenon indicates that the influence of temperature on the adsorption of carboplatin extends beyond its impact on complexation and may potentially affect other processes, such as the aforementioned hydration process. Temperatures exceeding 318 K notably enhance the formation of aqua-derived carboplatin species.

4.2.3 Adsorption mechanism elucidation by synchrotron XAS

Results obtained from macro-scale batch adsorption experiments indicate that the adsorption of trace cisplatin and carboplatin depends on the presence of thiol groups. Then, in order to acquire a more profound molecular-level insight into the coordination environment of adsorbed Pt, Pt L_3-edge XAS measurements were carried out. The distances and amplitudes of the primary shells containing loaded Pt on MPA@Sponge and Cys@Sponge exhibit similarities to the Pt−Cl contributions in K_2PtCl_4, which can be contributed by the Pt−S bonds. EXAFS fitting analysis was performed to understand the Pt coordination structure. The results suggest that every Pt atom is coordinated by around four sulfur atoms in the first coordination sphere at a distance of approximately 2.30 Å. These outcomes indicate that after hydration, both Pt-CDs chelated with thiol groups present on the functionalized sponge surface. But upon prolonged heating, partial thermal decomposition of MPA and Cys occurs (quantified by EA, the sulfur reduction rates for MPA@Sponge and Cys@Sponge were approximately 47% and 39%, respectively), generating sulfur-containing fragments such as sulfides in solution, that subsequently replace the ammonia ligands, despite their inertness.

4.3 Further enhancing adsorption capacity of TFS through the introduction of a reduction process based on promising results

As anticipated, the results in Section 4.2 validate a significant enhancement in the

adsorption of Pt-CDs by thiol-functionalized sponges (MPA@Sponge and Cys@Sponge). However, it is evident that this functionalization process can still be optimized. The strategy employed involves the introduction of $Na_2S·9H_2O$ or $SnCl_2·2H_2O$ as reducing agents to convert oxidized disulfides into free thiol groups, maximizing effective adsorption sites. This section will specifically discuss the adsorption of cisplatin by reduced thiol-functionalized sponges.

4.3.1 Characterization of functionalized TFS_1 and TFS_2 before and after cisplatin adsorption

FTIR analysis revealed that 3-MPA exhibited an absorption peak near 2550 cm^{-1} due to the stretching vibration of the S−H bond. However, upon loading onto TFSs, the presence of the inherently weak thiol feature peak at 2550 cm^{-1} became almost negligible due to the limited loading. Additionally, the absorption peak was observed at 1701 cm^{-1} for 3-MPA, attributed to the stretching vibration of the C=O bond of carboxyl group. Notably, shifted peaks corresponding to the C=O bond at 1726 cm^{-1} were observed in the spectra of TFS_1 and TFS_2, attributed to the stretching vibration of the ester C=O bond, serving as evidence of successful esterification.

In addition, EA determined sulfur contents of 1.04 ± 0.04 wt% for functionalized TFS_1 and 1.31 ± 0.05 wt% for TFS_2. Given the negligible sulfur content in the unmodified sponge, these findings further corroborate the successful immobilization of 3-mercaptopropionic acid (3-MPA) onto the sponge substrate. Similarly, SEM-EDS and XPS survey spectra also qualitatively confirmed the presence of sulfur elements on TFS_1 and TFS_2. SEM images indicate that all sponges display a porous morphology distinguished by an intricate interlaced structure of interconnected channels, with diameters ranging from approximately 1 to 5 μm. Regarding TFS_2, its surface is coated with evenly distributed blister-like or bubble-like Sn compounds on the sponge substrate. Then, following cisplatin adsorption at 343 K for 24 h, significant morphological

alteration of these surface-coated Sn compounds can be observed in Fig. 3h. These changes manifest as uniformly sized spheres with an approximate diameter of 100 nm, which aggregate and exhibit a cauliflower-like pattern.

Inference from the Sn 3d fine XPS spectra reveals that the pronounced peaks at 486.68 eV ($3d_{5/2}$) and 495.11 eV ($3d_{3/2}$) predominantly correspond to Sn^{4+} species within the SnO_2, while the doublet peaks observed at 485.01 eV and 493.51 eV are indicative of Sn^0. Therefore, Sn compounds were doped onto TFS_2 in the form of Sn/SnO_2. In the S 2p spectra, deconvolution peaks were identified at 163.87 and 164.97 eV for TFS_1, and at 163.63 and 164.93 eV for TFS_2, confirming the existence of thiol functional groups. Upon adsorption, a marginal upward shift in the binding energy was observed, likely attributable to electron donation originating from sulfur atoms within thiol groups towards Pt species. The distinct Pt chemical states resulting from the adsorption of cisplatin onto TFS_1 and TFS_2 are elucidated through Pt 4f spectra. In the case of Pt adsorbed on TFS_1, the presence of the $4f_{7/2}$ and $4f_{5/2}$ doublet peaks at 71.66 and 75.09 eV, respectively, signifies the predominant existence of Pt in an unmodified divalent state. Conversely, for Pt adsorption on TFS_2, the discernible peaks at binding energies of 74.07 and 77.41 eV imply the presence of Pt^{4+}, suggesting that the adsorbed Pt species may adopt forms such as PtS_2 or PtO_2 within the Sn/SnO_2 substrate.

4.3.2 Investigation of the batch adsorption process of cisplatin onto TFS_1 and TFS_2

As anticipated, both thiol-functionalization strategies have markedly enhanced the adsorption capacities for low-concentration cisplatin. Increasing the solution pH leads to a marginal enhancement in the adsorption capacity of Sponge and TFS_1 for cisplatin. This can be attributed to the resulting negatively charged surface of the adsorbents, facilitating electrostatic attraction towards the aqua-derivatives of cisplatin formed through hydration. Conversely, the influence of pH variations on cisplatin adsorption by

TFS_2 remains negligible, suggesting a minor role of electrostatic interactions in influencing the adsorption onto TFS_2. Instead, the predominant mode of adsorption for TFS_2 is reliant on chemical complexation.

The adsorption of cisplatin onto TFS_1 and TFS_2 conforms to the PSO kinetic model, indicating that cisplatin rapidly diffused from the liquid phase to the adsorbent, followed by subsequent chemical binding with adsorption sites. In addition, the adsorption isotherms of TFS_1 and TFS_2 conform primarily to the monolayer adsorption behavior described by the Langmuir model.

Temperature exerts distinct effects on the adsorption of cisplatin on the two TFSs. Analysis of the adsorption isotherms for TFS_1 at various temperatures reveals a pronounced enhancement in adsorption capacity with increasing temperature. This observed behavior is attributed to thermal-favored complexation between the Pt center in cisplatin and the surface thiol groups of TFS_1. Conversely, for TFS_2, elevating the temperature from 296 K to 318 K leads to a corresponding increase in adsorption capacity, followed by a decline as temperature further rises to 343 K. While elevating the temperature appropriately favors Pt−S complexation in chemical adsorption, caution should be exercised in avoiding temperatures as high as 343 K. At this temperature, aggregation occurs within the coated Sn/SnO_2 structure, consequently affecting the deposition of Pt.

4.3.3 Comparison of cisplatin removal with adsorbents reported in the literature

The removal efficacy of cisplatin by TFS_1 and TFS_2 was subjected to comparative assessment against other previously reported adsorbents. Notably, under optimized conditions, TFS_1 and TFS_2 manifest exceptional removal efficiencies for trace cisplatin (235 μg L^{-1}), achieving removal rates of 95.5 ± 0.8% and 99.5 ± 0.1%, respectively. Remarkably, TFS_2 notably surpasses the removal efficiency of all hitherto reported materials, including expensive commercial materials. Furthermore, the rapid

adsorption kinetics observed in TFS_1 and TFS_2 suggest promising prospects for their prospective scalability in industrial applications. Additionally, the enhanced removal efficiency of TFS_1 and TFS_2, synthesized through additional reduction step, significantly outperformed the previously reported non-reduced counterpart, MPA@Sponge (88.9 ± 0.5%). This emphasizes the significant influence of reduction steps, ensuring a higher number of effective thiol adsorption sites. Furthermore, the utilization of Sn/SnO_2 coating strategy has been demonstrated to exhibit significant efficacy in further enhancing the adsorption capacity of TFS. 3-mercaptopropyl-functionalized silica gel, a commercial adsorbent, has also exhibited excellent adsorption, with a removal efficiency of 98.7 ± 0.1%. However, its high cost (39.4 euros/gram) undermines its cost-effectiveness advantage. In comparison, Sponge, being a cheap substrate material, holds industrial applicability potential.

4.4 Comparison of all studied adsorbents

In conclusion, the three key parameters of all investigated adsorbents, namely sulfur content, adsorption capacity, and maximum removal rate, are compared in the table below. It is evident from the table that the adsorption capacity of the adsorbents with respect to Pt-CDs is highly correlated with their sulfur content. The introduction of thiol groups into the Sponge, as anticipated, enhances its adsorption capabilities towards Pt-CDs. The adsorption capacity of TFSs has reached a level comparable to that of the commercial adsorbent Si-Cys. Furthermore, the incorporation of a reduction step to liberate more active thiol sites will further enhance the adsorption levels of TFSs, despite the sulfur content of TFS_1 and TFS_2 remaining consistent with that of unreduced MPA@Sponge. The removal of trace Pt-CDs (235 $\mu g\ L^{-1}$) by functionalized sponges was also investigated and is presented in the table. The highest removal efficiency was observed during the adsorption of cisplatin on TFS_2, with a rate of 99.5 ± 0.1%.

Table. Comparison of parameters of all studied adsorbents.

Adsorbents	Sulfur (wt%)	Targets	q_e (mg g^{-1})	Removal* (%)	Kinetic	Isotherm	$\Delta G°$ kJ mol^{-1} (from RT to 343 K)	$\Delta H°$ kJ mol^{-1}	Adsorption evaluation
Commercial adsorbents									
Si-Cys	1.30 ± 0.02	cisplatin	20 ± 2	98.5 ± 0.1	PSO	L/F**	-2.7 ± 0.5 to -10.7 ± 0.7	44 ± 7	thermophilic chemisorption-dominated
		carboplatin	20 ± 1	94.1 ± 0.1	PSO	L/F	-3.6 ± 0.1 to -7.3 ± 0.3	19 ±2	thermophilic chemisorption-dominated
Si-DETA	<0.1	cisplatin	3 ± 1	32 ± 2	PSO	L			poor adsorption
		carboplatin	3 ± 2	17.8 ± 0.9	PSO	L/F			poor adsorption
Sponge	<0.1	cisplatin	5 ± 1	38 ± 3	PSO	L			poor adsorption
		carboplatin	4 ± 3	19.9 ± 0.4	PSO	L			poor adsorption
Thiol-functionalized sponges (without reduction)									
MPA@Sponge	1.23 ± 0.07	cisplatin	49 ± 1	88.9 ± 0.5	PSO	L/F	-2.3 ± 0.1 to -6.59 ± 0.06	22.5 ± 0.1	thermophilic chemisorption-dominated
		carboplatin	30.9 ± 0.2	85.2 ± 0.4	PSO	L	3.0 ± 0.2 to -5.5 ± 0.2	51.4 ± 0.1	thermophilic chemisorption-dominated favored adsorption over 318 K
Cys@Sponge	0.59 ± 0.03	cisplatin	13.8 ± 0.3	75 ± 2	PSO	L	0.78 ± 0.02 to -2.97 ± 0.05	22.6 ± 0.5	thermophilic chemisorption-dominated
		carboplatin	20.7 ± 0.4	59 ± 1	PSO	L	4.90 ± 0.06 to -0.3 ± 0.1	34.1 ± 0.1	thermophilic chemisorption-dominated favored adsorption over 318 K
Thiol-functionalized sponges (with reduction)									
TFS_1	1.04 ± 0.04	cisplatin	51 ± 9	95.5 ± 0.8	PSO	F at 296 K, L/F at high T	-5.9 ± 0.3 to -13.3 ± 0.2	39 ± 3	thermophilic chemisorption-dominated
TFS_2	1.31 ± 0.05	cisplatin	91 ± 4	99.5 ± 0.1	PSO	L at Low T, F at 343 K	-13.8 ± 0.1 to -16.3 ± 0.1		thermophilic chemisorption-dominated (But Sn/SnO_2 aggregated at 343 K)

* The maximum removal rate obtained under the respective optimal conditions, initial Pt concentration of 235 µg L^{-1}.
** L: Langmuir isotherm model, F: Freundlich isotherm model, L/F: Indicates that both models exhibit a high degree of fitting with minimal discernible distinction.

Chapter 5

Conclusions

In the lab, mad scientists scheme and plot,
seeking inventions that time forgot.

The ensuing key points summarize the main conclusions drawn from the results detailed in present thesis work:

General conclusion:

The obtained results describe a very promising adsorption system to remove Pt-CDs from polluted waters at the very low concentrations found in hospital wastewaters and also in some municipal wastewaters. The proven benefits of the sponge adsorbent, already commercialized for treatment of industrial wastewaters assure for an easy scale-up of the improved adsorbent developed in the present thesis.

Other more specific conclusions follow:

Adsorption of $PtCl_4^{2-}$, cisplatin and carboplatin onto three commercial adsorbents

- ✧ Assisted by electrostatic adsorption, all Si-Cys, Si-DETA, and Sponge materials exhibit substantial removal of the anionic species $PtCl_4^{2-}$ (>90%), higher than that of cisplatin and carboplatin. Nonetheless, the adsorption of $PtCl_4^{2-}$ is notably pH-dependent. Consequently, despite their structural similarities, the utilization of $PtCl_4^{2-}$ as a template for Pt-CDs should be cautiously considered.
- ✧ Si-Cys, bearing thiol functional groups, exhibits notable removal efficiencies for cisplatin and carboplatin, significantly surpassing those of Si-DETA and Sponge. This observation underscores the pronounced dependence of cisplatin and carboplatin adsorption on Pt−S complexation.
- ✧ All adsorption phenomena observed adhere to the PSO kinetic model and Langmuir isotherm model, signifying the monolayer chemisorption processes.
- ✧ The adsorption of cisplatin and carboplatin on Si-Cys is characterized by an

endothermic process (in contrast to the exothermic adsorption of $PtCl_4^{2-}$). This can be due to the thermophilic nature of Pt−S binding. Consequently, upon elevation to 343 K, the removal efficiencies of cisplatin and carboplatin on Si-Cys reached 98.5 ± 0.1% and 94.1 ± 0.1%, respectively.

✧ The treatment of spiked Pt-containing urine revealed the suitability of sulfur-containing Si-Cys for treatment of Pt-CDs contained urine from patients, and wastewaters contaminated by it.

Cisplatin and carboplatin adsorption onto MPA@Sponge and Cys@Sponge

✧ Incorporating high-affinity thiol groups onto Sponge through esterification reactions to immobilize MPA and Cys has been proved to substantially improve the adsorption of cisplatin and carboplatin. This observation underscores the pivotal role of Pt−S complexation in chelation-dominant chemisorption process.

✧ The application of synchrotron XAS facilitated the exploration of the coordination environment of trace Pt adsorbed. EXAFS analysis demonstrated the formation of Pt−S bonds after Pt-CDs adsorption.

✧ In addition to complexation, the removal process of Pt-CDs also involved hydration processes. The different hydration patterns of cisplatin and carboplatin result in better adsorption of cisplatin than that of carboplatin. The CBDCA ligand in carboplatin exhibits greater hydration resistance, accounting for the observed adsorption discrepancy.

✧ Increasing the temperature to 343 K facilitated the Pt-CDs adsorption by MPA@Sponge and Cys@Sponge, attributed to the thermo-favored Pt−S complexation. Thermodynamic investigations also substantiated that the adsorption process is an endothermic process.

✧ The validation of MPA@Sponge for the treatment of Pt-CDs spiked urine samples

indicates its potential utility in disposing Pt-CDs contained urine from patients, and wastewaters contaminated by it.

Adsorption of trace cisplatin by reduced TFSs

- ✧ TFS_1 and TFS_2, synthesized through 3-MPA functionalization and reduction by $Na_2S·9H_2O$ or $SnCl_2·2H_2O$, demonstrated maximum removal efficiencies of 95.5 ± 0.8% and 99.5 ± 0.1%, respectively, for trace cisplatin (235 μg L^{-1}).
- ✧ Characterizations including FTIR, EA, SEM-EDS, and XPS have proved the successful immobilization of thiol groups. The introduction of thiol groups exhibiting strong binding affinity has been observed to markedly improve the adsorption capacity for trace cisplatin.
- ✧ Pre-substituting ligands within solutions can lead to the formation of active aqua-derivatives, thereby facilitating subsequent complexation processes. Hence, during the cisplatin adsorption on TFS_1, the cationic derivatives resulting from hydration can migrate towards the negatively charged surface of the adsorbent due to electrostatic attraction, thereby facilitating the subsequent complexation.
- ✧ In the case of TFS_2, different from TFS_1, the surface-doped Sn/SnO_2 also contributes to the adsorption of cisplatin. XPS analysis reveals that the adsorption process involves Pt−S complexation, as well as the partial oxidation of cisplatin and its subsequent adsorption onto Sn compounds.
- ✧ The adsorption of cisplatin conforms to the PSO kinetic model, involving diffusion process followed by chemical adsorption. The Langmuir model adequately describes adsorption isotherms, conforming to monolayer adsorption.
- ✧ Increasing the temperature further enhances the adsorption of cisplatin onto TFSs, as the chemisorption predominantly governed by Pt−S complexation has been substantiated to be an endothermic process. However, caution should be exercised to

prevent aggregation also induced by high temperatures, such as 343 K, on the surface coverage of Sn/SnO2 in TFS_2, as this morphological alteration diminishes the adsorption of cisplatin.

Chapter 6

Future perspectives

Every 'Oops' is just another opportunity to exclaim 'Wow'!

Given the findings presented in this work, future perspectives could encompass the following aspects:

- ✧ Apart from cisplatin and carboplatin, the scope of treatment can extend to encompass other Pt-CDs, such as Oxaliplatin. Additionally, considering that chemotherapy often employs “cocktail” therapies, the residuals of cytostatics are commonly excreted as mixtures, contributing to the contamination of hospital wastewater. Future investigations could focus on addressing the treatment of multi-target, multi-component systems in such scenarios.
- ✧ Design and prepare selective adsorbents to achieve specific adsorption and separation of target Pt-CDs, providing a pathway for the recovery of Pt-CDs, thereby establishing a comprehensive separation-removal-recovery system.
- ✧ Designing selective adsorbents to achieve specific adsorption and separation of target Pt-CDs offers a pathway for the recovery of Pt-CDs and thus establishes a comprehensive separation-removal-recovery system.
- ✧ Given the intricate composition of real hospital wastewater, where feasible, it is advisable to directly sample wastewaters contaminated with Pt-CDs for treatment validation using the synthesized adsorbents presented in this thesis.
- ✧ Although the Pt-CDs of interest are present in hospital wastewater at exceedingly low concentrations, the recovery of Pt, as a noble metal, warrants consideration. This entails investigation into the desorption process, thereby concurrently substantiating the reusability of the adsorbents.
- ✧ For reasons of cost and safety, Sponge has been employed in powdered form throughout the scope of this thesis research to reduce experimental scale. With experience gained, future investigations could contemplate scaling up and employing its original, unground, cube form for functionalization and adsorption experiments.

In comparison to powders, the primary advantage of cubic sponges lies in their reduced flow impedance, consequently enhancing hydraulic permeability. When employed as column packing material, this attribute facilitates rapid passage of substantial volumes of wastewater without necessitating supplementary hydraulic driving forces. At the same time, the cube-shaped sponge will not be easily flushed away by the flow. So, the loss of material is controllable.

- ✧ With the results of the batch adsorption experiment, consideration could be given to expanding the experimental scale to validate the efficacy of the adsorbents in the treatment of continuous Pt-CDs-contaminated wastewater through fixed-bed column adsorption.

- ✧ While the Sponge adsorbent employed in this thesis proves to be an economical and well-established commercial option, the functionalization strategy on its cellulose-based matrix has indeed yielded the intended adsorption outcomes. However, exploring alternative sources of cellulose as substrates could be considered as well, given the widespread availability and accessibility of cellulose materials, such as biomass. This avenue may encompass the valorization of agricultural waste for resourceful utilization.